Institut für Wärmetechnik

TU Graz
Graz University of Technology

Investigation of in-situ desulfurization as process step for sulfur removal from synthesis gas derived from thermal gasification of biomass

---

Performed for the purpose of attainment of the academic degree of a Doctor of Engineering Sciences by

Dipl.-Ing. Moritz Husmann

Submitted at the Graz University of Technology
Faculty of Mechanical Engineering and Economic Sciences

Graz, May 2017

This dissertation has been approved by:

Univ.-Prof. Dr. Christoph Hochenauer, Institute of Thermal Engineering, Graz University of Technology

Univ.-Prof. Dr. Thomas Kienberger, Chair of Energy Network Technology, University of Mining Leoben

Affidavit

I declare that I have authored this thesis independently, that I have not used other than the declared sources/resources, and that I have explicitly indicated all material which has been quoted either literally or by content from the sources used. The text document uploaded to TUGRAZonline is identical to the present PhD thesis.

Date	Signature

Danksagung

Die vorliegende Arbeit entstand während meiner Tätigkeit als wissenschaftlicher Mitarbeiter am Institut für Wärmetechnik an der Technischen Universität Graz im Rahmen des FFG-Projektes „InnoGasClean“ (FFG Projekt Nr. 838730) mit einer Projektlaufzeit von März 2013 bis Mai 2016.

Bei Herrn Prof. Hochenauer, Vorstand des Instituts für Wärmetechnik an der Technischen Universität Graz, möchte ich mich für die Bereitstellung der Infrastruktur des Instituts und die Möglichkeit zur Mitarbeit in dem Projekt bedanken. Die Betreuung aus einer Kombination aus dem Gewähren von Freiheit auf der einen und ein „auf Spur bringen“ auf der anderen Seite, haben mir sehr geholfen meine eigenen Ziele zu setzen aber dann auch einzuhalten. Dafür bin ich Ihnen dankbar!

Bei Prof. Thomas Kienberger, Vorstand des Lehrstuhls für Energieverbundtechnik an der Montanuniversität Leoben, möchte ich mich für den großen Einsatz bereits im Vorfeld meiner Arbeit bedanken. Dies schließt das Verfassen des Antrags für das zugrunde liegende Projekt sowie das Wecken meiner Begeisterung für das Themenfeld der thermischen Vergasung mit ein. Die Entscheidung eine Dissertation zu beginnen - und das auch noch in Graz - wäre ohne dein Zutun sicher nicht gefallen und ich habe es nie bereut mich auf dieses Abenteuer einzulassen. Darüber hinaus sind wesentliche Weichenstellungen für das fachliche und methodische Vorgehen durch deine Anregungen zustande gekommen. Auch nach deiner Zeit in Graz warst du stets für Fragen verfügbar und hast weiterhin den Verlauf meiner Arbeit durch Diskussionen und Rat begleitet und geprägt. Für diese umfassende Unterstützung gilt Dir mein herzlicher Dank!

Bei Herrn Dr. Müller möchte ich mich für die gute Zusammenarbeit und für das Bereitstellen des „CaBa“ Adsorbentiums, sowie für die Durchführung der Analysen bedanken. Durch Ihren Beitrag wurden meiner Arbeit ganz neue Möglichkeiten eröffnet und wesentliche Teile der relevanten Erkenntnisse bauen darauf auf. Vielen Dank, dass Sie mir diese Möglichkeit gegeben haben!

Meinen externen Kollegen von der Highterm Research GesmbH, besonders Christian Zuber und Gerald Binder, danke ich für alle kritischen Fragen und guten Ideen, Anregungen und Schmäh’s. Das hat mir gerade in schwierigen Zeiten sehr geholfen. Meinen internen Kollegen vom IWT danke ich für die lustigen Runden zu später Stunde bei „Fackelbier“ und „Ungeheuer füttern“, das hat die teilweise zähen Versuchstage wesentlich erheitert. Bei meiner Diplomandin Viktoria Maitz möchte ich mich für die tatkräftige Unterstützung und Einsatzbereitschaft bedanken.

Ein weiterer Dank geht auch an die lieben Kollegen der Werkstatt vom Institut, die auch bei mitunter kurzfristiger Planung oder Bedarf an Ersatzteilen zur Stelle waren oder sich zumindest mit Leberkäse haben bestechen lassen. Es hat Spaß gemacht mit Euch zusammen zu arbeiten!

Meiner Familie, besonders meinen Eltern und meinem Bruder, möchte ich danken für die Unterstützung meiner Ausbildung, Bildung und Erziehung. Als kleines aber starkes Team haben wir noch jede Schwierigkeit gemeistert. Danke!

Abstract

The utilization of biomass as part of a renewable energy supply is useful due to the flexibility and reliability of this technology for energy conversion. A process yielding highest energy efficiency and flexibility for further application is the allothermal steam gasification of biomass in a fluidized bed. This process converts solid biomass into a nitrogen lean gas with high heating value, suitable for direct energetic or further substantial use as for example the production of substitute natural gas (SNG) or biofuels. Despite its high efficiency, biomass gasification suffers from cost competition with fossil fuels which, especially for the use of woody fuels, is presently out of reach. The use of waste fuels can be an alternative however, besides technological challenges due to ash agglomeration during gasification, it commonly yields relevantly high amounts of sulfur, chlorine and alkaline loads in the produced gas. Once a catalytic conversion of the produced gas is pursued, the sulfur, with H_2S as the dominant species, acts as a poison on the catalyst surface and thus has to be removed upstream. For the use of alternative fuels, the higher content of sulfur might easily negate the benefit of a cheaper fuel by an increased consumption of desulfurization sorbent. In small and medium-scale biomass applications fixed bed chemisorption over ZnO is commonly deployed for desulfurization.

In order to achieve low sulfur contents in the produced synthesis gas (syngas), independent of the gasification fuel, the concept of in-situ desulfurization has been investigated in the course of the presented work. This concept aims at the removal of sulfur inside the fluidized bed gasification reactor by addition of suitable sorbents that allow the reduction of sulfur at lower costs as compared to ZnO fixed bed desulfurization.

In a simulative assessment different sorbent materials for in-situ desulfurization of biomass derived syngas were evaluated according to the thermodynamic equilibrium of their desulfurization reaction. Results of phase equilibrium calculations were obtained with respect to the H_2S equilibrium concentration under a variation of different parameters. The use of copper-based sorbent material turned out to be promising due to a predicted positive impact of high steam conditions for sorption equilibria. Results for the application of a mixed phase BaO-based sorbent “CaBa” were confirmed. The BaO is stabilized against the formation of carbonate, qualifying this material combination as a promising candidate for in-situ desulfurization. Equilibrium calculations predict the removal of sulfur to a level of 2.1 ppm_v H_2S at a steam content of about 40 vol% and 820 °C. This content is sufficient for further catalytic gas processing applications.

The results obtained by equilibrium calculations were then verified under real process conditions of a fluidized bed gasifier. Gasification experiments were performed using wood pellets as fuel with addition of a defined amount of CS_2 such as to raise the content of sulfur without significantly changing the composition of permanent gases. The conversion of CS_2 to H_2S under gasification conditions ensures a high sulfur content in the produced gas in the range of 1400 ppm_v, representing a syngas derived from gasification of low grade residual biomass like for example sewage sludge. This type of gas is suitable for investigating the equilibrium of desulfurization reaction under real process conditions, as the initial sulfur content is high enough to observe a desulfurization effect upon addition of potentially suitable sorbents.

Experimental results were obtained for the application of lime, limestone, calcined and uncalcined dolomite regarding their properties as in-situ desulfurization sorbents in biomass gasification. Besides the determination of the steady state equilibrium, several parameters of gasification have been varied consecutively in order to distinguish the differences between the CaO-based sorbents and elucidate the influence of gasification conditions on the steady state desulfurization results. The parameters include gasification temperature, gas residence time, steam content of the syngas, and particle size of the sorbents. The conversion of sorbents has been determined to evaluate the necessary amount of sorbent required for the reduction of the residual H_2S content to a steady state equilibrium value. For lime, limestone and dolomite a steady state value of 500 ppm_v H_2S was determined which is in accordance with the simulated equilibrium calculation. Dolomite showed a higher residual H_2S content of 600 ppm_v under steady state conditions. Results further show that the variation of temperature in the range of 700 to 825 °C has no influence on the residual H_2S content. The variation of steam content from 30 to 42 vol% in the syngas showed a rather significant change of residual H_2S for lime increasing from 330 to 786 ppm_v and a less considerable rise of 410 to 578 ppm_v H_2S for dolomite under steady state conditions. A clear difference between the different CaO-based sorbents has been observed for the conversion of CaO to CaS in fully calcined dolomite as compared to the other sorbents tested. The conversion is clearly higher in lime, limestone and dolomite with an average of 35% as compared to fully calcined dolomite with an average of 15%. The application of copper-based sorbents wasn't persecuted in gasification experiments due to their tendency of sintering at elevated temperatures.

Instead, the novel BaO-based sorbent "CaBa", developed by Forschungszentrum Jülich, was tested for the first time as desulfurization agent for in-situ application in an allothermal biomass gasification process. In real process application, sintering of the sorbent occurred and had to be prevented by the addition of lime as separating agent. Furthermore a kinetic limitation of the desulfurization with BaO was shown for the in-bed sorption of sulfur. An increase of gasification temperature from 760 to 810 °C significantly improved the desulfurization performance. With the novel BaO-based sorbent, a desulfurization from 85 down to 35 ppm_v residual H_2S is shown upon addition of the sorbent to the gasifier. Particle analysis via SEM-EDX, XRD, ICP-OES and BET complement the results of in-situ desulfurization. SEM-EDX results indicate the stabilization of BaO in sintering bridges and a certain depletion of Barium from the sorbent after in-bed application. In experiments with a combined desulfurization of CaO and BaO a release of H_2S from CaS was shown once the H_2S content in the gas drops below the CaO-based steady state equilibrium of desulfurization. Therefore the application in a countercurrent FICFB gasifier is suggested which enables the separation of the different levels of desulfurization.

In an economic assessment the different scenarios for the application of in-situ desulfurization were evaluated. The results of this analysis qualify a combined application of limestone and „CaBa" as in-situ desulfurization sorbents and ZnO-based fixed bed desulfurization as the economically most viable option under the given conditions. Under consideration of a benchmark of costs below 1 ct/kWh_{SNG} for the desulfurization of a syngas with 1400 ppm_v to below 1 ppm_v H_2S, such a combined concept was evaluated. The benchmark of 1 ct/kWh_{SNG} can be met once the CaBa is available at 0.5 €/kg. The concept of in-situ desulfurization therefore offers the possibility of a significant economic improvement for the use of high sulfur fuels, compared to alternative technologies for gas cleaning at the investigated size scale of gasification technology.

Kurzfassung

Die Nutzung von Biomasse als Teil einer erneuerbaren Energieversorgung ist vorteilhaft im Hinblick auf die bedarfsgerechte Verfügbarkeit für die Energiebereitstellung. Höchste Energieeffizienz und Flexibilität für die weitere Anwendung erreicht dabei das Verfahren der allothermen Wasserdampfvergasung von Biomasse in einer Wirbelschicht, da feste Biomasse in ein wasserstoffreiches, stickstoffarmes Synthesegas überführt wird. Dieses ist sowohl für eine direkte energetische als auch eine stoffliche Nutzung wie die Synthese von Ergassubstitut (SNG) geeignet. Insbesondere im Falle der Nutzung holzartiger Brennstoffe kann jedoch die Biomassevergasung den Kostenwettbewerb mit fossilen Brennstoffen, derzeit nicht bestehen. Die Verwendung von Abfallbrennstoffen wäre eine Alternative. Neben technologischen Herausforderungen aufgrund der Agglomeration von Asche bei der Vergasung, werden hierbei jedoch deutlich erhöhte Mengen an Schwefel, Chlor und Alkalisalzen freigesetzt. Wird eine katalytische Umsetzung des erzeugten Gases angestrebt, muss der Schwefel, mit H_2S als dominierender Spezies, vorher entfernt werden, da dieser auf der Katalysatoroberfläche als Gift wirken würde. Für den Einsatz von alternativen Brennstoffen könnte der höhere Gehalt an Schwefel somit schnell den Vorteil eines günstigeren Brennstoffs durch erhöhte Kosten der Entschwefelung zunichtemachen. In kleinen und mittelgroßen Biomasseanwendungen wird gemeinhin ZnO als Adsorbens zur Entschwefelung eingesetzt.

Um unabhängig von dem eingesetzten Brennstoff niedrige Schwefelgehalte im Produktgas zu erreichen, wurde im Rahmen der vorliegenden Arbeit das Konzept der in-situ Entschwefelung untersucht. Dieses Konzept zielt auf die Entfernung von Schwefel innerhalb der Wirbelschicht des Vergasungsreaktors durch Zugabe geeigneter Sorbentien ab. Ziel ist die Reduktion von Schwefel zu geringeren Kosten im Vergleich zu einer ausschließlich externen Entschwefelung mittels ZnO Festbettschüttung in einem nachgeschalteten Apparat.

In einer simulativen Beurteilung wurden verschiedene Adsorbentien für die in-situ Entschwefelung von Synthesegas aus Biomassevergasung nach dem thermodynamischen Gleichgewicht ihrer Entschwefelungsreaktion bewertet. Die H_2S-Gleichgewichtskonzentration wurde unter Variation verschiedener Parameter berechnet. Entsprechend der Phasengleichgewichte erweist sich die Verwendung von Kupfer basierten Adsorbentien als vorteilhaft da eine positive Auswirkung des hohen Dampfgehaltes im Synthesegas aus Biomassevergasung gezeigt werden kann. Für die Anwendung eines BaO-basierten Adsorbens "CaBa" wurden die positiven Ergebnisse aus vorangegangenen Studien bestätigt. Für die in-situ Entschwefelung konnte dieses Material als vielversprechender Kandidat qualifiziert werden. Gleichgewichtsberechnungen prognostizieren die Entschwefelung auf ein Niveau von 2,1 ppm_v H_2S bei einem Dampfgehalt von etwa 40 vol% und 820 °C. Dies wäre für weitere katalytische Gasanwendungen ausreichend.

Die aus Gleichgewichtsberechnungen erhaltenen Ergebnisse wurden unter realen Prozessbedingungen eines Wirbelschichtvergasers verifiziert. Vergasungsexperimente wurden mit Holzpellets als Brennstoff unter Zugabe einer definierten Menge CS_2 durchgeführt. Dies dient dazu den Gehalt an Schwefel zu erhöhen, ohne die Zusammensetzung der Permanentgase zu verändern. Die Umwandlung von CS_2 zu H_2S unter Vergasungsbedingungen, gewährleistet einen hohen Schwefelgehalt in dem erzeugten Gas im Bereich von 1400 ppm_v, was ein Synthesegas aus der Vergasung minderwertiger Reststoffe, wie zum Beispiel Klärschlamm, darstellt. Das so erzeugte Gas ist geeignet das Gleichgewicht der Entschwefelungsreaktion verschiedener potentiell geeigneter

Adsorbentien unter realen Prozessbedingungen zu untersuchen, da der anfängliche Schwefelgehalt hoch genug ist, um eine Entschwefelungswirkung bei Additivzugabe zu beobachten.

Experimentelle Untersuchungen wurden unter Anwendung von Kalk, Kalkstein sowie kalziniertem und nicht kalziniertem Dolomit in Bezug auf ihre Eigenschaften als Adsorbentien für die in-situ Entschwefelung durchgeführt. Neben der Bestimmung des Gleichgewichts im stationären Zustand wurden verschiedene Parameter der Vergasung variiert, um die Unterschiede zwischen den CaO basierenden Adsorbentien zu ermitteln und den Einfluss von Vergasungsbedingungen auf den stationären Zustand der Entschwefelung zu klären. Die Parameter umfassen Vergasungstemperatur, Verweilzeit, Dampfgehalt des Synthesegases und die Partikelgröße der Adsorbentien. Zudem wurde der Umsatz der Adsorbentien ermittelt um die minimal erforderliche Menge an Adsorbens zur Reduktion des H_2S-Gehaltes abzuschätzen. Für Kalk, Kalkstein und Dolomit wurde im stationären Zustand ein Restwert von 500 ppm_v H_2S im Gas ermittelt, was eine gute Übereinstimmung mit den simulierten Ergebnissen darstellt. Kalzinierter Dolomit zeigte einen höheren Restschwefelgehalt von 600 ppm_v H_2S unter stationären Bedingungen. Die Ergebnisse zeigen ferner, dass die Variation der Temperatur im Bereich von 700 bis 825 °C keinen Einfluss auf den Restschwefelgehalt aufweist. Die Variation des Wasserdampfgehaltes von 30 bis 42 Vol% im Synthesegas zeigte eine erhebliche Änderung des Restgehaltes an H_2S von 330-786 ppm_v unter Anwendung von Kalk und einen weniger deutlichen Anstieg von 410 auf 578 ppm_v H_2S für Dolomit. Ein klarer Unterschied zwischen den verschiedenen CaO-basierten Adsorbentien wurde für den Umsatz von CaO zu CaS beobachtet. Der Umsatz ist dabei deutlich höher bei Kalk, Kalkstein und Dolomit mit einem Durchschnitt von 35%, im Vergleich zu kalziniertem Dolomit mit einem Durchschnitt von 15%.

Aufgrund einer zu vermutenden thermischen Instabilitiät wurde von der experimentellen Untersuchung kupferbasierter Adsorbentien abgesehen. Stattdessen wurde das neuartige BaO-basierte Adsorbens "CaBa", welches vom Forschungszentrum Jülich entwickelt wurde, zum ersten Mal als in-situ Adsorbens für den Einsatz in einem allothermen Biomassevergasungsprozess getestet. Die reale Prozessanwendung zeigt ein Sintern des Adsorbens was durch die Zugabe von Kalk als Trennmittel zu verhindern ist. Weiterhin wurde eine kinetische Limitierung der Entschwefelung mit BaO unter in-situ Anwendung gezeigt. Eine Erhöhung der Vergasungstemperatur von 760 auf 810 °C konnte die Entschwefelungswirkung deutlich verbessern. Mit dem neuartigen „CaBa“ Adsorbens wurde eine in-situ Entschwefelung von 85 auf 35 ppm_v Restgehalt an H_2S bei der Zugabe des Sorptionsmittels in den Vergaser erreicht. Partikelanalysen mittels REM-EDX, XRD, ICP-OES und BET ergänzen die Ergebnisse der in-situ Entschwefelung. REM-EDX Ergebnisse zeigen die Stabilisierung von BaO in Sinterbrücken und eine gewisse Verarmung an Barium im Adsorbens nach der in-situ Anwendung. In Experimenten mit einer kombinierten Entschwefelung von CaO und BaO wurde eine Freisetzung von H_2S aus CaS gezeigt, sobald der H_2S-Gehalt im Gas unter den CaO bezogen Gleichgewichtswert der Entschwefelung fällt. Daher wird die Anwendung in einem neuartigen Gegenstromvergaser entsprechend dem FICFB-Konzept vorgeschlagen, welcher die Trennung der verschiedenen Gleichgewichtsebenen der Entschwefelung ermöglichen würde.

In einer wirtschaftlichen Bewertung wurden verschiedenen Szenarien für die Anwendung von in-situ Entschwefelung im gegeben Kontext ausgewertet. Die Ergebnisse dieser Analyse zeigen, dass eine kombinierte Anwendung von Kalkstein, „CaBa“ und ZnO das aus wirtschaftlicher Sicht vielversprechendste Szenario ist. Unter Berücksichtigung eines Zielwertes von 1 ct/kWh_{SNG} für die Kosten der Entschwefelung eines Gases von 1400 ppm_v auf unter 1 ppm_v H_2S wurden die erforderlichen Kriterien für ein kombiniertes Enschwefelungskonzept untersucht. Dies ergab

maximale Kosten des CaBa-Adsorbens von 0.5 €/kg als Voraussetzung für ein Erreichen des Zielwertes. Für die untersuchte Größenskala der Vergasungstechnologie bietet die Einführung von in-situ Entschwefelung das Potential einer Kostenreduktion bei Einsatz schwefelreicher Alternativbrennstoffe im Vergleich zu alternativen Gasreinigungstechnologien.

Content

Affidavit III
Danksagung V
Abstract VII
Kurzfassung IX
Directory of Figures XVII
Directory of Tables XXI
Nomenclature XXIII
1 Introduction 1
2 Fundamentals and state of the art 3
2.1 Biomass potential 3
2.2 Biomass gasification 5
2.3 Gasifier types and process variations 9
2.3.1 Autothermal gasifiers 11
2.3.2 Allothermal gasifiers 11
2.4 Gas cleaning 16
2.4.1 Cold gas cleaning 18
2.4.2 Hot gas cleaning 20
2.5 In-situ desulfurization 23
2.5.1 Thermodynamic considerations 23
2.5.2 Results in literature 27
3 Motivation and Approach 31
4 Thermodynamic assessment of sorbent materials 33
4.1 Simulative conditions & assumptions 33
4.2 Results of thermodynamic assessment 36
4.2.1 Influencing parameters 37
4.2.2 Suitable sorbent materials 46
5 Experimental setup and analytical methods 51
5.1 Design of experimental test rig 51
5.1.1 Gasifier 51
5.1.2 Improvements in gasifier setup 55
5.1.3 Gas manifold 61

5.2 Analytical setup and methods 64
5.2.1 Gas analysis 66
5.2.2 Gas chromatography 68
5.2.3 Particle characterization 73
6 Experimental results and discussion 75
6.1 Characterization and conditions of experimental setup 75
6.1.1 System characterization and boundary conditions 75
6.1.2 Experimental procedure 76
6.1.3 Experimental conditions of in-situ desulfurization 77
6.2 Calcium-based in-situ desulfurization 81
6.2.1 Sorbent characterization and preparation 81
6.2.2 Experiments on CaO-based in-situ desulfurization 84
6.2.3 Effect of CaO-based sorbents on the gas composition 87
6.2.4 Desulfurization steady states of different CaO-based sorbents 90
6.2.5 Influence of particle size 92
6.2.6 Influence of sorbent stoichiometry 93
6.2.7 Influence of residence time 96
6.2.8 Influence of temperature 96
6.2.9 Influence of steam content 98
6.2.10 Determination of sorbent conversion 100
6.3 Barium based in-situ desulfurization 103
6.3.1 Sorbent materials and preparation 103
6.3.2 Sorbent characterization 105
6.3.3 Experimental procedure 112
6.3.4 Application of original CaBa 115
6.3.5 Influence of sorbent treatment 117
6.3.6 Influence of sorbent amount and sulfur content 118
6.3.7 Influence of temperature 121
6.4 Combined desulfurization with CaBa and lime 126
6.4.1 Experimental application of CaBa and lime 126
6.4.2 Options for process setup 130
6.4.3 Consideration of legal restrictions 134
6.5 Discussion of possible sources of error 135
6.5.1 Systematic errors 135
6.5.2 Statistical errors 136

7 Assessment of economics 137
7.1 Background for economic evaluation 137
7.2 Economic model and fundamentals 139
7.3 Conditions and assumptions 140
7.3.1 Technical conditions 140
7.3.2 Assumptions concerning investment cost 142
7.3.3 Conditions and assumptions for operational cost 144
7.4 Calculation of desulfurization costs 145
7.4.1 Investment cost 145
7.4.2 Operational costs 149
7.5 Results of economic assessment 151
7.5.1 Comparison of methods and sorbents for in-situ desulfurization 151
7.5.2 Sensitivity analysis for the implementation of CaBa – sorbent 155
8 Conclusions and outlook 161
9 References 167

Directory of Figures

Figure 1-1: Process scheme of a hot gas cleaning setup integrated in a setup for the production of SNG 2
Figure 2-1: Gravimetric annual potential and use of alternative biomass stocks in Germany[11] 4
Figure 2-2: Energy-based annual potential of unexploited alternative biomass stocks in Germany[11] ... 4
Figure 2-3 Flow sheet and basic data of the heat pipe reformer technology[42] 12
Figure 2-4: Setup of "Güssing" FICFB-process and gas cleaning route with the aim of syngas use in a gas engine[47] 14
Figure 2-5: Setup of "GoBiGas" FICFB-process and gas cleaning route with the aim of producing Bio-SNG as vehicle fuel[5] 15
Figure 2-6: Applicable ranges of power output for different conversion technologies and their corresponding range of efficiency[37] 18
Figure 2-7: Limitations of suitability due to the applicable temperature ranges of different potential sorbent materials for hot gas desulfurization compared to the relevant temperature range of fluidized bed biomass gasification (red square)[48,91] 26
Figure 3-1: Concept for optional subsequent steps in a combined hot gas cleaning process[107] 32
Figure 4-1: Thermodynamic equilibrium curves of manganese-based desulfurization for different steam contents 38
Figure 4-2: Thermodynamic equilibrium curves of copper-based desulfurization for different steam contents 39
Figure 4-3: Different experimental and simulated results of the decomposition pressure of CO_2 over $CaCO_3$[109] 40
Figure 4-4: Thermodynamic equilibrium curves of calcium-based desulfurization for different steam contents 42
Figure 4-5: Thermodynamic equilibrium curves of barium-based desulfurization for different steam contents 43
Figure 4-6: Influence of pressure on the calcium-based desulfurization equilibrium with respect to the increased partial pressure of CO_2 45
Figure 4-7: Property diagram of manganese in dependence of the partial pressure of oxygen 47
Figure 5-1: Flow chart of the experimental setup[111] 52
Figure 5-2: Fixed orifice for leveling the amount of injected steam[26] 53
Figure 5-3: Setup of the experimental test rig in final configuration 55
Figure 5-4: (A) Differential (4-B) and absolute (4-A) pressure sensors with additional sampling point for gas analysis (4-F), (B) R&I scheme at initial setup, (C) R&I scheme at final setup 56
Figure 5-5: Gas warning system with sensors, fuel hopper and ventilation 57
Figure 5-6: Setup principle of nozzle and fixation at the bottom of the reactor (A), Nozzle for steam injection with protective hood (6B-A) and wire mesh (6B-B) covering the outlet jets for steam (B) ... 58
Figure 5-7: Installation of reactor heating tube without support (A) and with support and fixed thermocouple in final configuration (B) 59
Figure 5-8: Control interface with initial setup (A) and additional control and feedback values (Steam inlet, temperature gas-outlet, different heating zones) in final configuration (B) 60
Figure 5-9: Flow chart of the test gas manifold used for elevation of the sulfur content in the gas (Temperature controlled parts indicated with red lines) 63

Figure 5-10: Impinger bottles for gas cleaning – 2 x water, 1 x RME, 2 x isopropanol, 2 x glass wool (only first one shown) 64
Figure 5-11: Detailed flow sheet of the experimental setup for gas cleaning and measurement[37] (adapted) 65
Figure 5-12: Working principle of the gas analyzer module Uras-14, applied for the detection of CO, CO_2, CH_4 and O_2 (different measuring technique)[37] 67
Figure 5-13: Working principle of a flame ionization detector[117] 69
Figure 5-14: Flow chart of the sampling system of the GC (Varian, CP 3800, SN: 103953) employed for sulfur analysis[116] 71
Figure 5-15: Working principle of a pulsed flame photometric detector[118] 72
Figure 5-16: Time related peaks of light emission for specific detection of sulfur content[118] 73
Figure 6-1: Trend of temperatures inside the reactor (t_FB-1, t_FB-2, t_freeboard) and in the product gas line (t_syngas) at the beginning of an experiment 78
Figure 6-2: Composition of the syngas produced by gasification of wood pellets in the allothermal fluidized bed gasification test rig 78
Figure 6-3: Sulfur content in the produced gas depending on the sample point and duration of measurement (Table 6-3: Experiments NS_FI#1, CaO_FI#2) 80
Figure 6-4: Deviation of particle size fractions in the size range of 80 to 500 µm for the different CaO-based sorbent materials 82
Figure 6-5: Sorbent charges wrapped in small amounts of paper to prevent agglomeration 84
Figure 6-6: Trend of residual sulfur content upon addition of lime as desulfurization sorbent with respect to different sulfurous components, (775 °C reactor temperature, 825 °C freeboard temperature, steam-excess-ratio 4, Table 6-3: Experiment CaO_EQ#1) 87
Figure 6-7: Comparison of effect of the addition of lime onto the composition and content of tar components in the gas (Without lime: mean value of 14 samples, after addition of lime: mean value of 20 samples) 88
Figure 6-8: Content and composition of sulfurous tar components in the gas with respect to the effect of the addition of lime (Mean value of 6 measurements, from 2 samples each) 89
Figure 6-9: Residual H_2S content of produced gas under application of different sorbents at standard conditions (775 °C reactor temperature, 825 °C freeboard temperature, steam-excess-ratio 4, Table 6-3: Experiments CaO_EQ#1, CaCO3_TI#1, CaMg(CO3)2_EQ#1, CaOMgO_SI#2) 91
Figure 6-10: Influence of the particle size on the desulfurization equilibrium, comparing lime and fully calcined dolomite (dolomite f.c.) (Table 6-3: Experiments CaOMgO_PS#2, CaOMgO_PS#1, CaO_PS#1, CaO_PS#2) 92
Figure 6-11: Influence of sorbent amount on the achieved steady state desulfurization for addition of lime in the range of stoichiometry (Table 6-3: Experiments CaO_SI#1 - CaO_SI#4) 94
Figure 6-12: Comparison of different values of steady state desulfurization in relation to the Ca/S for addition of lime in the range of stoichiometry 95
Figure 6-13: Comparison of desulfurization behavior for addition of varied amounts of fully calcined (f.c.) dolomite in the over stoichiometric range (Table 6-3: Experiments CaOMgO_SI#1, CaOMgO_SI#2) 96
Figure 6-14: Variation of gasification temperature with a stepwise increase of the reactor temperature from 700 to 775 °C at a constant freeboard temperature of 775 °C. Temperatures are shown for the experimental run with dolomite. Thermodynamic equilibrium shown is based on equilibrium calculations (compare Figure 4-4) (Table 6-3: Experiments CaCO3_TI#1, CaMg(CO3)2_TI#1) 97

Figure 6-15: Comparison of residual H_2S content under steady state conditions for lime and dolomite upon variation of steam-excess-ratio (σ); average values of several hours of measurement for each setting (Table 6-3: Experiments CaO_SC#1, CaCO3_SC#1, CaMg(CO3)2_SC#1)..... 99
Figure 6-16: Change of gas composition upon increase of steam-excess-ratio from 4 to 5 with Figure 6-16 (A) showing CO and Figure 6-16 (B) showing H_2 gas analysis data 99
Figure 6-17: Estimate of the total amount of adsorbed sulfur by numerical integration of the desulfurization effect shown by the example of fully calcined (f.c.) dolomite (Table 6-3: Experiment CaOMgO_SI#1) 101
Figure 6-18: Comparison of conversion of CaO in different sorbents according to the molar ratio *γ* and sorbent properties..... 102
Figure 6-19: Preparation procedure of the pelletized CaBa sorbent – (A: Pressed tablets from fines of original CaBa, B: Tablets after calcining in muffle furnace, C: Grinding of the tablets in a mortar, D: prepared sorbent "CaBa-pelletized with a particle size fraction of 250 -1000 µm) 105
Figure 6-20: SEM (A and B) pictures of original CaBa sorbent with element sensitive EDX pictures of the magnified area (C: Oxygen, D: Magnesium, E: Silicon, F: Calcium, G: Iron, H: Sulfur, I: Barium) . 108
Figure 6-21: SEM (A and B) pictures of the pelletized CaBa sorbent with element sensitive EDX pictures of the magnified area (C: Oxygen, D: Magnesium, E: Silicon, F: Sulfur, G: Calcium, H: Iron, I: Barium)..... 109
Figure 6-22: SEM (A and B) pictures of the pelletized CaBa sorbent after 56 hours of in-situ desulfurization (85 ppm_v H_2S feed); with element sensitive EDX pictures of the magnified area (C: Oxygen, D: Magnesium, E: Silicon, F: Sulfur, G: Calcium, H: Iron, I: Barium)..... 110
Figure 6-23: SEM (A) picture of the bed material olivine with element sensitive EDX pictures of the magnified area (B: Oxygen, C: Magnesium, D: Silicon, E: Potassium, F: Calcium, G: Iron, H: Sulfur I: Barium) after use in the fluidized bed for 56 hours of in-situ desulfurization (85 ppm_v H_2S feed) 111
Figure 6-24: XRD results of the tested CaBa sorbent. A original, B pelletized, C sulfided (Table 6-7: CaBa_2, 56 hours in BFBG, 85 ppm_v H_2S feed)..... 112
Figure 6-25: Trend of temperatures in the reactor, freeboard and product gas line upon addition of CaBa sorbent. (Ba/S ratio 7.71, Table 6-7: Experiment CaBa_1) 116
Figure 6-26: Agglomerated sorbent and bed material after an experiment with original CaBa 117
Figure 6-27: Comparison of different CaBa sorbents with an addition of 15 g CaBa each (760 °C reactor temperature, Table 6-7: Experiments CaBa_3, CaBa_4, CaBa_5) 118
Figure 6-28: Desulfurization results upon variation of the added amount of CaBa sorbent with according Ba/S ratios (Table 6-7: Experiments CaBa_5, CaBa_1) 119
Figure 6-29: Desulfurization results upon varied partial pressure of H_2S in the gasifier by increasing the initial feed content from 85 to 140 ppm_v H_2S (Table 6-7: Experiments CaBa_5 and CaBa_6) 120
Figure 6-30: Correlation between overall speed of reaction and the partial pressure of reactant A[135] 121
Figure 6-31: Desulfurization results upon varied gasification temperatures with according Ba/S ratios (Table 6-7: Experiments CaBa_5 and CaBa_7) 122
Figure 6-32: Effect of an increased reactor temperature on the observed rate of reaction[134] 123
Figure 6-33: Influence of increased amounts of added sorbents with a constant molar Ba/S-ratio of about 2, at reactor temperatures of 810 °C (Table 6-7: Experiments CaBa_7 and CaBa_9)) 124
Figure 6-34: Interpolation of desulfurization results obtained by experimental investigation (Table 6-7: CaBa_1, CaBa_5, CaBa_7, CaBa_9) 125
Figure 6-35: Mixed desulfurization with CaBa and lime added in a weight ratio of 1:1 (760 °C reactor temperature, 840 °C freeboard, steam-excess-ratio 4) 127

Figure 6-36: Comparison of the effect of CaBa addition starting from a CaS-H_2S equilibrium (Table 6-7: CaBa_8) and H_2S concentrations below the onset of CaS formation (Table 6-7: CaBa_9) (Both experiments: 810 °C reactor temperature, 840 °C freeboard, steam-excess-ratio 4) 128
Figure 6-37: Investigation of the release of H_2S by CaS by desulfurization with lime and subsequent interruption of the CS_2 supply (760 °C reactor temperature, 840 °C freeboard, steam-excess-ratio 4) 129
Figure 6-38: (A) Working principle of a countercurrent FICFB – reactor, developed at Vienna University of Technology[137] (B) Flow pattern inside the gasification reactor with an example of consecutive desulfurization steps 131
Figure 6-39: Suggested process concept with adapted setup and conditions based on the results and conclusions obtained from the presented work 133
Figure 7-1: Estimate of costs for SNG-production based on the application of the heat pipe reformer technology or a comparative scale of gasification[142] 138
Figure 7-2: Additional equipment included in the estimate of investment costs (marked in red) for ZnO-fixed bed desulfurization 142
Figure 7-3: Additional equipment included in the estimate of investment costs (marked in red) for in-situ desulfurization 143
Figure 7-4: Sensitivity analysis of relevant parameters in the calculation of specific investment cost 148
Figure 7-5: Comparison of the specific costs of desulfurization for different in-situ sorbents with the sole ZnO-based desulfurization in a downstream fixed bed. Colors mark the type of desulfurization ranges for the different experiments (marked by numbers) 152
Figure 7-6: Specific costs of combined desulfurization with limestone and a downstream ZnO-fixed bed with a varied amount of steam (Background colors indicating the regimes of the specific sorbent material acting as desulfurization agent) 155
Figure 7-7: Specific costs of combined desulfurization with CaBa and a downstream ZnO-fixed bed under variation of the estimated cost for the production of CaBa sorbent (Background colors indicating the regimes of the specific sorbent material acting as desulfurization agent depending on the combination of sorbents as indicated by the numbers) 156
Figure 7-8: Specific cost of combined a downstream ZnO-fixed bed with in-situ desulfurization under application of CaBa, limestone and a combination of all three under an estimated cost for the production of CaBa sorbent of 1 €/kg 158

Directory of Tables

Table 2-1: Cost estimates for different alternative fuel types before and after required types of treatment for preparation as gasification fuel (ODW-organic dry waste)(a: mix, b: crush/chip, c: sieve/shift, d: compost, e: dry (thermal), f: pelletize)[7] 5
Table 2-2: Ultimate and proximate analysis for different alternative fuels for gasification (daf = dry, ash free)[7] 8
Table 2-3: Different categories of gasification technologies[13] 10
Table 2-4: Specifications of different gasifiers[35,13] 10
Table 2-5: Composition of the produced syngas from the HPR gasifier under application of pellets as fuel[44] 13
Table 2-6: Composition of the produced syngas at Güssing gasifier under application of pellets as fuel[48] 14
Table 2-7: Allowable tolerances concerning the different types of destined end application for energy conversion (n.a means no data available) 17
Table 2-8: Results for the application of different sorbents for hot gas desulfurization under according to literature, conditions: BG - bottle mixed gas, GG - gasifier gas 30
Table 4-1: Ultimate and proximate analysis of the wood pellets applied as fuel 34
Table 4-2: Comparison of simulated and experimental gas composition 36
Table 5-1: Different parts of the gasifier shown in Figure 5-3 54
Table 5-2: Antoine parameters for carbon disulfide with pressure in bar and temperatures in Kelvin[113] 62
Table 5-3: Overview of analytical tools and methods 65
Table 6-1: Comparison of different mean gas compositions for varied methods of sulfur elevation .. 79
Table 6-2: Particle properties of tested CaO-based materials, the differences to 100% in the elemental composition being oxygen and trace elements (SA –Surface area) 83
Table 6-3: Experiments with CaO-based sorbents (CaO-SS – steady state of CaO-based desulfurization, OS – over stoichiometric, excess addition of sorbent in nonspecific ratio) 85
Table 6-4: Comparison of syngas composition and properties before and after the addition of lime. 89
Table 6-5: Comparison of conversion of different sorbents 101
Table 6-6: Particle properties of tested BaO-based materials, the differences to 100% in the elemental composition being oxygen and trace elements 106
Table 6-7: Experiments performed with BaO-based sorbents 114
Table 7-1: Estimated cost ranges for different process steps in SNG synthesis[142] 139
Table 7-2: Gas composition used for estimation of desulfurization cost (experimental) compared to the gas produced from an HPR-gasifier 141
Table 7-3: Amortization data for calculation of the specific investment cost (WACC –weighted average cost of capital) 143
Table 7-4: Estimated investment costs for downstream fixed bed desulfurization with ZnO 146
Table 7-5: Estimated investment costs for in-situ desulfurization 147
Table 7-6: Calculation of specific costs of investment for ZnO-fixed bed and in-situ desulfurization based on the cost estimates shown in Tables 7-4 and 7-5 147
Table 7-7: Input values of sensitivity analysis for calculation of the specific costs of investment (WACC –weighted average cost of capital) 148

Table 7-8: Calculation of cost for sorbent supply and disposal..... 149
Table 7-9: Experimentally determined residual H_2S content as the lower limit of desulfurization.... 150
Table 7-10: Calculated composition of costs for desulfurization of a syngas with 1400 ppm_v H_2S feed using different sorbent combinations according to Eqs (60) and (61)..... 153
Table 7-11: Minima of H_2S equilibrium curves for different steam contents as determined by thermodynamic equilibrium calculations..... 154

Nomenclature

Chemical symbols

Chemical symbol	Species
BaO	Barium oxide
BaS	Barium sulfide
C	Carbon
Ca	Calcium
CaO	Calcium oxide (Lime)
$CaCO_3$	Calcium carbonate (Limestone)
CaS	Calcium sulfide
CH^*	Hydrocarbon radical
$C_{\nu_1}H_{\nu_2}$	Hydrocarbon in undefined composition
$CH_xO_yS_z$	Biomass in undefined composition
Cl	Chlorine
CO	Carbon monoxide
CO_2	Carbon dioxide
COS	Carbonyl sulfide
CH_4	Methane
CS_2	Carbon disulfide
Cu	Copper
CuO	Copper oxide
CuS	Copper sulfide
e^-	Electron
H_2	Hydrogen
H_2O	Water
H_2S	Hydrogen sulfide
HCO^+	Cation
K	Potassium
$Me_{\nu_1}O_{\nu_2}$	Metal oxide in undefined composition
MeS	Metal sulfide
Mg	Magnesia
$MgCO_3$	Magnesium carbonate
MgO	Magnesium oxide
MnO	Manganese oxide
MnS	Manganese sulfide
Na	Sodium
O^*	Oxygen radical

O_2	Oxygen
P	Phosphor
S	Sulfur
Si	Silicon
ZnO	Zinc oxide

Formula symbols

Formula symbol	Unit	**Description**
a_I	-	Yearly capital recovery factor
Ar	-	Archimedes number
c	$\frac{mol}{l}$	Concentration
c_i	$\frac{ct}{kWh}$	Specific investment costs
c_{op}	$\frac{ct}{kWh}$	Specific operational costs
$c_{op\_syngas,i}$	$\frac{ct}{kWh}$	Specific operational costs for component i
c_p	$\frac{kJ}{mol \cdot K}$	Molar heat capacity
$c_{S,i}$	$\frac{ct}{mol_{H2S}}$	Specific cost of sorbent consumption and disposal
C_{total}	€	Total costs
d_{max}	*m*	Maximum allowed particle diameter
d_{min}	*m*	Minimum allowed particle diameter
d_p	*m*	Particle diameter
dT	*K*	Temperature difference
EAC	€	Equivalent annual costs
G	kJ	Gibbs Enthalpy
G_m^{ϕ}	$\frac{kJ}{mol}$	Molar integral Gibbs Energy of phase Φ
H	$\frac{kJ}{mol}$	Enthalpy at actual conditions

H_{298}	$\frac{kJ}{mol}$	Enthalpy of formation at reference conditions (298.15 K, 1 bar)
$\mathrm{H_2S}_{adsorbed}$	*mol*	Adsorbed H_2S
$\Delta H_2S_{initial-actual}$	ppm_v	Depletion of H_2S in the gas
$H_2S_{(ll,i)}$	ppm_v	Lower limit of desulfurization for component i
h_a	*h*	Full load hours per year
H_l	$\frac{kJ}{kg}$	Mass based lower heating value
$H_{l(n)}$	$\frac{kJ}{m^3_{std}}$	Lower heating value of the gas at standard conditions (273.15 K, 1.01325 bar)
$H_{l(n),i}$	$\frac{kJ}{m^3_{std}}$	Lower heating value of component i at standard conditions (273.15 K, 1.01325 bar)
ΔH_R	$\frac{kJ}{mol}$	Enthalpy of reaction
i	%	Interest rate
I_0	$\frac{W}{m^2}$	Intensity of electromagnetic wave at emitter
I_1	$\frac{W}{m^2}$	Intensity of electromagnetic wave at receiver
I_a, I_b	-	Indicators for fuel quality
l	*m*	Path length of light beam through sample
$M_{CH_{v_1}O_{v_2}}$	$\frac{g}{mol}$	Molar mass of fuel
$\dot{m}_{fuel}$	$\frac{kg}{h}$	Mass flow of fuel
M_{H_2O}	$\frac{g}{mol}$	Molar mass of water
n_{CaO}	*mol*	Mol of CaO in the gasifier
n_{CaS}	*mol*	Mol of CaS formed
$\dot{n}_{gas,dry}$	$\frac{mol}{min}$	Molar flow of dry gas
n_i^{ϕ}	*mol*	Molenumbers of the phase constituents i
p_{abs}	*bar*	Absolute pressure
p_{CS_2}	*bar*	Partial pressure of CS_2
PVA	-	Present value of annuity factor

$\dot{Q}_{fuel}$	*kW*	Heat flow of fuel
$\dot{Q}_{syngas}$	*kW*	Heat flow of gas
$\dot{Q}_{SNG}$	*kW*	Heat flow of synthetic natural gas
Re_{fl}	-	Reynoldsnumbers for the incipient point of fluidization
Re_{pd}	-	Reynoldsnumbers for the onset of pneumatic discharge
S	$\frac{kJ}{mol}$	Entropy at actual conditions
S_{298}	$\frac{kJ}{mol}$	Entropy at reference conditions (298.15 K, 1 bar)
t	*a*	Allowance for depreciation
T	*K*	Actual Temperature
T_{298}	*K*	Reference temperature (298.15 K)
$\Delta t_{measurement}$	*min*	Time between measurements
u_{pd}	$\frac{m}{s}$	Superficial velocity at onset of pneumatic discharge
u_{fl}	$\frac{m}{s}$	Superficial velocity at the incipient point of fluidization
u_s	$\frac{m}{s}$	Superficial velocity
$\dot{V}_{gas}$	$\frac{m^3_{std}}{h}$	Volume flow of gas at standard conditions (273.15 K, 1.01325 bar)
$v_{m,gas}$	$\frac{l}{mol}$	Specific molar volume of a gas at standard conditions (273.15 K, 1.01325 bar)
$w_{H_2O,Fuel}$	-	Mass fraction of water in the fuel
X_{CaO}	-	Conversion of CaO
x_i	-	Molar fraction of component i
γ	-	Molar ratio of calciumoxide to sulfur
δ	-	Molar ratio of bariumoxide to sulfur
$\varepsilon(\lambda)$	$\frac{m^2}{mol}$	Molar attenuation coefficient in dependence of wavelength
ζ_{H_2O}	-	Mass ratio of steam entering the reactor
$\zeta_{H_2O,min}$	-	Minimum amount of steam for stoichiometric gasification

$\eta_{cold\ gas}$	-	Cold gas efficiency
ν_i	-	Stoichiometric factor
ν_s	$\frac{m^2}{s}$	Kinematic viscosity of steam
ρ_p	$\frac{kg}{m^3}$	Density of particle
ρ_s	$\frac{kg}{m^3}$	Density of steam
σ	-	Steam excess ratio

1 Introduction

With respect to the aim of increasingly replacing fossil energy conversion with renewable and sustainable alternatives, the use of biomass as an energy carrier takes an outstanding role. As biomass is stored chemical energy its' conversion can be adjusted to the demand, as well as provide a base-load for heat and electricity in a renewable based power supply. The use of biomass can be considered as CO_2 neutral as the release of greenhouse gases during combustion is equivalent to the intake from the atmosphere on a midterm timescale regarding a cycle of matter. A limit for the potential of biomass in a renewable energy supply is clearly given by the availability of suitable sources under consideration of several restraints concerning sustainability and land use. On a worldwide basis the technical potential of biomass is estimated to be about 10 - 25 % of primary energy supply for the year 2050, depending on the scenario of development in demand and different restrictions concerning sustainability.[1]

Besides the direct contribution of biomass as a source of reliable sustainable energy, the use of biomass offers the possibility of a stabilizing effect on the fluctuating energy supply from other renewable sources like wind and photovoltaics. This possibility is given by the technological option of hydrogen production with excess electrical energy, and subsequent conversion of H_2 to Methane (CH_4) with the carbon contained in biomass.[2] The grid injection and cavern storage of such methane is a suitable part to a solution concerning the required energy storage in a renewable based energy supply. This process route is especially suited for inclusion in the thermal conversion of biomass to a syngas with subsequent catalytic methanation to SNG suitable for injection into the public grid. Thermal gasification in a fluidized bed is a process that yields highest conversion efficiency with hot gas efficiencies of up to 95 %[3] and offers broad flexibility toward the input of different fuels. The gasification of wood chips and wood pellets is an established process and is state of the art. The conversion of the produced gas into SNG is at a stage of proof of concept with examples in the range of 8 to 32 MW_{th} fuel input.[4] Besides the technological feasibility, the process lacks economic profitability even for modern installations in a commercial power range.[5] This originates partly from an irresponsibly low price for fossil fuels in various countries, with natural gas energy prices ranging from 0.06 to 0.5 ct/kWh in Qatar and the US and about 2 ct/kWh in most western European countries.[4] This impedes motivation for investment in sustainable alternatives without subsidiaries. On the other hand, even for large scale gasification installations a final price of about 4.1 to 4.6 ct/kWh of produced gas is estimated as midterm perspective for the use of woody fuels.[4,6]

An option for further increasing the economic margin of thermal gasification of biomass is the application of lower grade fuels as compared to wood, which might negate or even inverse the cost for fuel input in the case of discharge materials. The benefits of a better use of the technological potential in existing biomass sources and lower cost for fuel input are counteracted by the lower degree of homogeneity and relevantly higher amount of trace elements commonly contained in such alternative fuels.[7] These trace elements lead to a series of technical challenges, starting from an increased tendency to form ash-agglomeration due to the formation of sticky ash melts, continued by an increased release of corrosive and toxic gaseous components such as HCl, H_2S and COS. In the case of a pursued catalytic conversion of the produced gas, sulfurous components in particular act as a poison by blocking the active catalytic sites due to the increased reactivity of sulfur with metallic

surfaces. This leads to the requirement of appropriate technical solutions for the stabilization of the gasification process, and an increased effort in gas cleaning prior to any catalytic conversion.

In order to evaluate different process options for the cleaning and upgrade of biomass derived syngas from thermal gasification of biomass, the Austrian Research Promotion Agency (FFG) has funded the research project “InnoGasClean” as framework of the presented study. As an example thereof, Figure 1-1 shows the process scheme of a hot gas cleaning process with included catalytic conversion of the syngas to SNG.

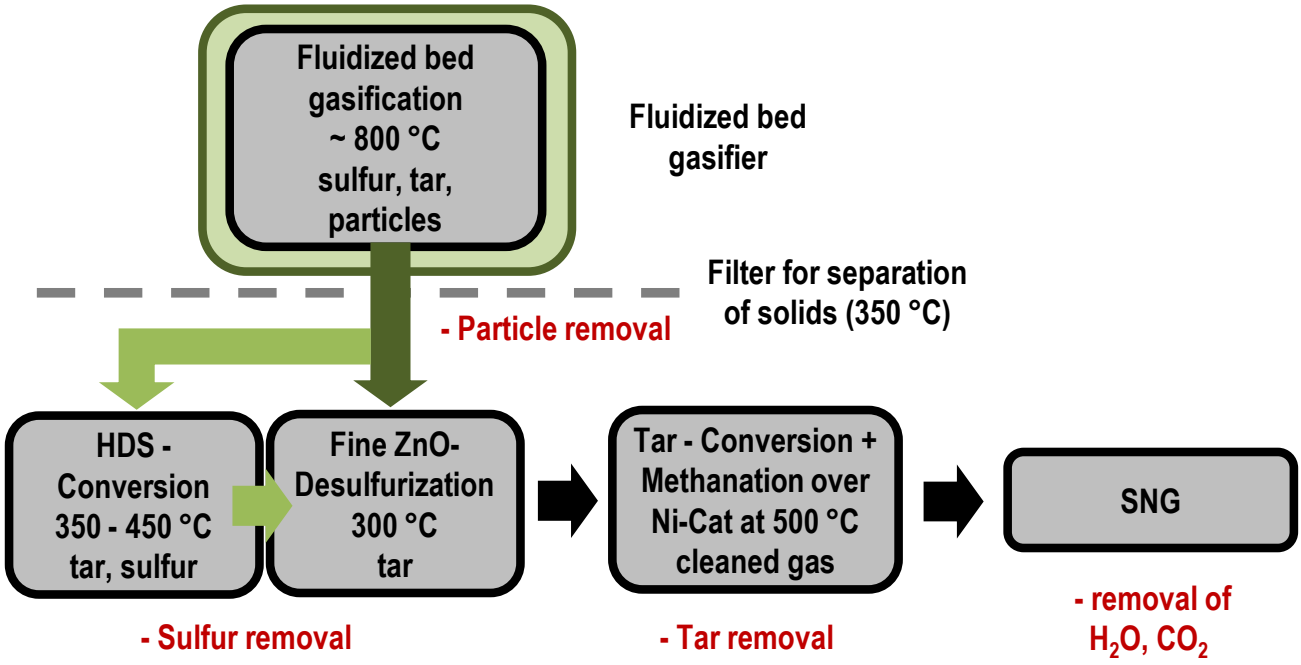

Figure 1-1: Process scheme of a hot gas cleaning setup integrated in a setup for the production of SNG

Besides the economic comparison of cold- and hot gas cleaning processes, the concept of in-situ desulfurization was investigated within the above mentioned FFG-project “InnoGasClean” as the main focus of the presented work. Intended as a process step for coarse desulfurization, this process option aims at retaining the sulfur within the fluidized bed of the gasifier by means of addition of suitable sorbent materials. Such a coarse desulfurization is especially suited for the application with alternative fuels that contain increased amounts of sulfur. The implementation of an in-situ desulfurization can therefore contribute to achieve economic feasibility as one of the main exigencies in establishing SNG-production by gasification of alternative biomass fuels.

Subsequently the potential and limitations given by the use of alternative fuels, as well as the state of the art in gasification and gas cleaning technologies are outlined. This shall explain the motivation for the work and result in the objective and approach of the presented experimental study conducted at the Graz University of Technology.

2 Fundamentals and state of the art

The following section shall provide an overview of the fundamentals in biomass gasification and gas cleaning technologies such as to describe the state of the art in the relevant fields of technology connected to the performed research.

2.1 Biomass potential

The use of biomass and its share in a non-fossil based energy supply system is limited by the requirement to not impede supply chains in food production or cause competition for available agricultural space. Further the intensification of land use connected with exploitation of the technical biomass potential must not leach the soils or increase the greenhouse gas emissions itself.[8] Due to the different interpretation of these requirements and complex assessment of connected cycles of matter, the estimated potential for the sustainable use of biomass for energy supply is not congruous between the various studies on the topic. In the example of Europe 27, the technical potential of biomass as a share in a renewable energy system is estimated to be in the range of 4 to 36 % of total primary energy use for the year 2020.[9] The IPCC report on renewable energy summarizes worldwide statistics and projections for the primary energy supply. For the year 2050 it estimates a technical biomass potential between 50 to 500 EJ/y on a worldwide basis, which equals roughly 10 to almost 100 % of the global primary energy supply of today.[1] The main reasons that lead to these discrepancies are ambiguous and inconsistent definitions of potentials, a lack of consistent and detailed data on current biomass production and land productivity, varying methods of estimating future biomass production and availability as well as ambiguous and varying assumptions on system-external factors that influence biomass potentials.[9] A technical potential between 10 to 25 % of the primary energy supply can be stated as an estimated future range depending on developments of the energy demand and land use.[1, 9]

Despite the different estimates of the various studies concerning the absolute potential of biomass for a contribution to a sustainable energy supply, the studies agree in the importance of residues from agriculture and forestry.[10] Using Germany as an example, the unused technical potential of biogenic residues is estimated to be in the range of 448 PJ/a.[11] With an annual consumption of 13.132 PJ in 2015, this equals a theoretical contribution of 3.4 % to the primary energy demand or an increase of 50 % to the currently provided amount of 6.7 % of primary energy by biomass in Germany.[12] The distribution of available mass flows of residual biomass and their current use is shown in Figure 2-1. A translation of the unused technical potential of these residues into related energy content based on biochemical conversion of excrements and thermochemical use of others, is shown in Figure 2-2.[11]

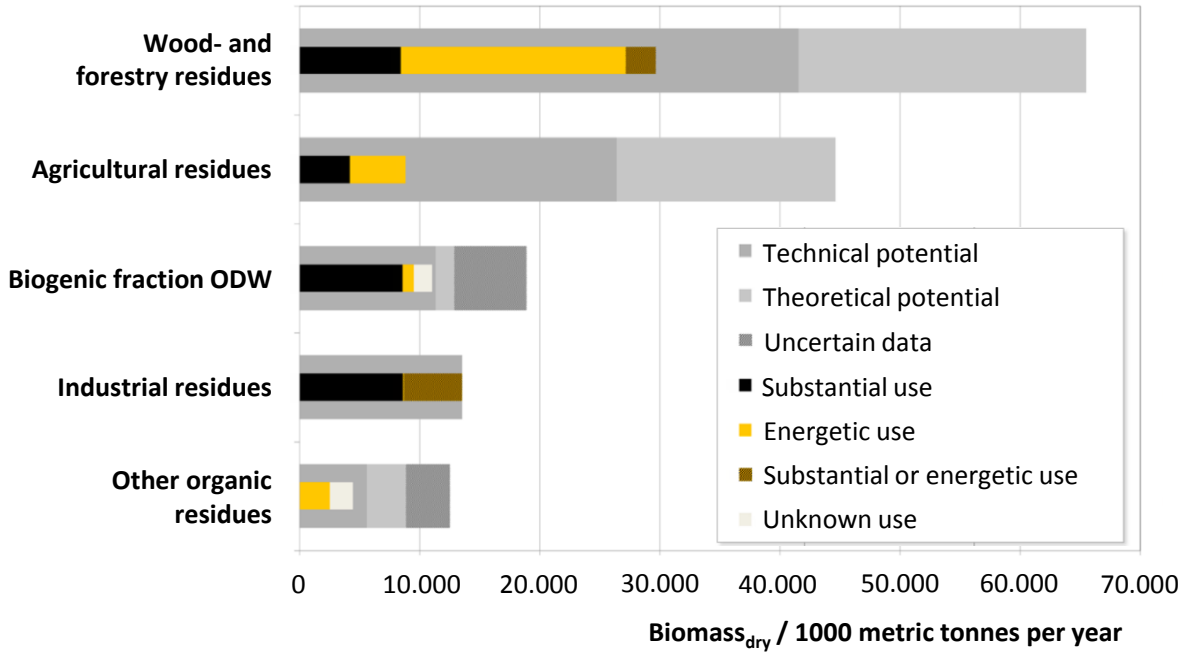

Figure 2-1: Gravimetric annual potential and use of alternative biomass stocks in Germany[11]

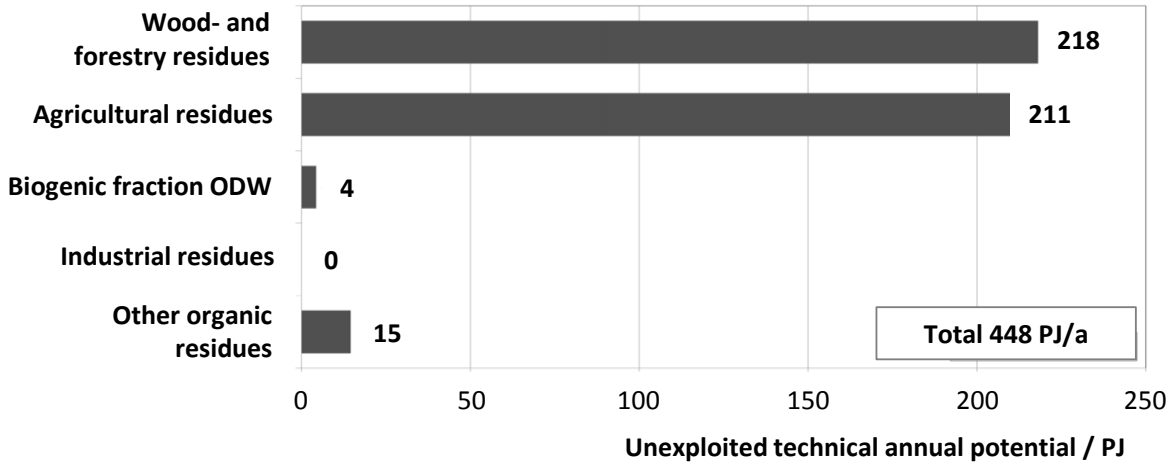

Figure 2-2: Energy-based annual potential of unexploited alternative biomass stocks in Germany[11]

The unexploited technical potential shown in Figure 2-2 needs to result in an economic potential for the conversion of the different available sources of biomass into energy carriers or electricity. Such a potential, especially for waste materials, might be given due to the low and even negative price for fuel input. Examples of such waste materials, the process steps required as pre-treatment in order to transform the raw materials into an alternative fuel and the related costs are listed in Table 2-1.

Table 2-1: Cost estimates for different alternative fuel types before and after required types of treatment for preparation as gasification fuel (ODW-organic dry waste)(a: mix, b: crush/chip, c: sieve/shift, d: compost, e: dry (thermal), f: pelletize)[7]

Fuel type	Raw price fuel	Pre-treatment					Costs	Physical shape of product
	€/GJ	a	b	c	d	e	€/GJ	
Park and public garden wood	-2 to -4		x	x	x		4	Chips <25 mm
Cacao shells	0	x					0.4	Shells < 30
Verge grass	0 to -5		x	x	x	x	6	Pellets
Paper residue sludge	-8 to -16	x			x		2	Granulates
Sewage sludge	-8 to -16	x			x		1	Granulates

Most waste raw materials require several process steps of pre-treatment before they are suited as alternative fuels in biomass gasification. These include mixing, crushing, sieving, composting, drying and pelletizing. As a result, the negative prices of the raw materials cannot be maintained after pre-treatment. But once the necessary steps required for upgrading of the raw materials are limited, the specific costs of alternative fuels are still low with 0.4 – 1 €/GJ as compared to 11.4 €/GJ in the case of wood pellets.

Under consideration of the technical potential shown in Figure 2-2 and the availability of biomasses with low to negligible cost, an economic potential is mostly determined by the process of conversion for which the thermal gasification is the most efficient option.[3]

2.2 Biomass gasification

Thermal gasification of biomass describes the process of transforming a solid biogenic fuel into gaseous state by means of a gasification agent at elevated temperature. The gasification of solid or liquid biomass can be divided according to the prevailing temperature level and the reaction with a gasification agent into the four main steps listed below.

Drying and heating occurs in the low temperature range of up to 200 °C.[13] Humidity that is contained in the fuel in ranges of 6 to >50 wt% is evaporated. This process can consume a relevant share of the energy contained in the fuel and limits the use of high moisture fuels for certain gasification applications. (Table 2-4)

Pyrolysis follows after the drying step at temperatures above 150 °C. It describes the process of carbonization of the biomass under the release of permanent gases and volatile hydrocarbons. These volatile hydrocarbons range from primary hydrocarbons derived from the decomposition of large molecules in organic matter to tertiary tars which are formed by polymerization and recombination of aromatic hydrocarbons at higher temperatures.[14] According to the definition stated in the "tar-protocol", condensable hydrocarbons with a molar weight greater than that of benzene are summarized under the term "tars".[15]

Oxidation and *Reduction* are conversion steps that rely on the addition of a gasification agent, as the conversion of carbon into gaseous components does not fully occur by temperature increase alone due to the stoichiometric composition of biomass with excess carbon contained. The oxidation of carbon is a strongly exothermic process and occurs according to the reaction (Eqs (1),(2)) in the presence of oxygen at temperatures above 500 °C.

$$C + O_2 \leftrightarrow CO + O^* \qquad \Delta H_R = -110.5 \frac{kJ}{mol} \qquad (1)$$

$$C + O_2 \leftrightarrow CO + O^* \leftrightarrow CO_2 \qquad \Delta H_R = -393.5 \frac{kJ}{mol} \qquad (2)$$

The exothermic formation of CO_2 is connected to a decline of the chemical energy content in the produced syngas and a release of heat. Depending on the process variation, this heat might be inevitable for maintaining the temperature level required for the endothermic gasification steps of drying, pyrolysis and reduction. This is the case for autothermal gasification, commonly with air or oxygen as gasification agents, where the required heat is released during the gasification itself. The result is a lowered energy content in the produced gas, especially in the case of gasification with air due to the dilution of the syngas with inert nitrogen. In case of gasification with oxygen such a diluting effect can be prevented, but the required separation of air prior to gasification leads to increased process cost and thus reduced profitability especially in smaller biomass applications.[13]

In autothermal applications the reduction of carbon follows the oxidation at a temperature level above 800 °C under the presence of different permanent gases according to Eqs (3),(4),(5).[16]

$$C + CO_2 \leftrightarrow 2\,CO \qquad \Delta H_R = +159.9 \frac{kJ}{mol} \qquad (3)$$

$$C + H_2O \leftrightarrow CO + H_2 \qquad \Delta H_R = +118.5 \frac{kJ}{mol} \qquad (4)$$

$$C + 2H_2 \leftrightarrow CH_4 \qquad \Delta H_R = -87.5 \frac{kJ}{mol} \qquad (5)$$

The chemical reactions that take place in the reduction phase of carbonization are, with the exception of Eq (5), endothermic and require external heat in order to proceed. Whereas, in autothermal processes the heat is provided by the oxidation of carbon, it can also be supplied by heat transfer into the system. Gasification systems with an external heat supply are classified under the term “allothermal” gasification.[13] Different process setups have been proposed to establish such a continuous heat supply to the gasification reactor of which the most relevant are presented in section 2.3. Such allothermal gasifiers produce a gas of higher caloric value as compared to autothermal gasifiers due to the absence of excess carbon oxidation (Eq (1)). Furthermore a dilution of the gas with nitrogen is prevented. Allothermal gasifiers still require a gasification agent for the conversion of carbon according to the reactions (3),(4) and (5). Most commonly steam is applied due to availability and the advantage of an increased H_2 content and thus a higher caloric value in the produced gas. Further the H_2/CO ratio in the gas is beneficial with steam gasification and adjustable to the value of 3 which is the optimum for further synthesis of substitute natural gas (SNG) as a biogenic alternative to natural gas.[17,18] Examples of other synthesis processes are the production of

Fischer Tropsch fuels (FT-Fuels) or the synthesis of methanol from syngas with required H_2/CO ratios from 0.6 to 2, depending on the applied catalyst.[19]

In addition to the oxidation and reduction of excess carbon under addition of a gasification agent, the remaining char also reacts with components of the gaseous phase, whereby especially the Boudouard reaction (Eq (3)) plays an important role in converting the solid carbon.[13] The composition of the gas phase is mainly determined by a set of homogeneous reactions. The main reactions are the water gas shift (Eq (6)), the methanation reaction (Eq (7)) and the Sabatier-reaction (Eq (8)), whereby the later consist of a linear combination of the first two.[18]

$$CO + H_2O \leftrightarrow CO_2 + H_2 \qquad \Delta H_R = -42\ \frac{kJ}{mol} \qquad (6)$$

$$CO + 3 \cdot H_2 \leftrightarrow CH_4 + H_2O \qquad \Delta H_R = -206\ \frac{kJ}{mol} \qquad (7)$$

$$CO_2 + 4 \cdot H_2 \leftrightarrow CH_4 + 2 \cdot H_2O \qquad \Delta H_R = -165\ \frac{kJ}{mol} \qquad (8)$$

A conversion of higher hydrocarbons and tars, released during pyrolysis, occurs at the later stages of gasification according to different mechanism. These include thermal cracking (Eq (9)) and partial oxidation (Eq (10)) as well as steam reforming (Eq (11)) as part of a series of secondary gasification reactions.[13]

$$C_{\nu_1}H_{\nu_2} \rightarrow C_{\nu_3}H_{\nu_4} + C_{\nu_5}H_{\nu_6} \qquad (9)$$

$$C_{\nu_1}H_{\nu_2} + \nu_1 \cdot O_2 \rightarrow \frac{\nu_2}{2} \cdot H_2O + \nu_1 \cdot CO + \nu_3 \cdot CO_2 + \nu_4 \cdot H_2 \qquad (10)$$

$$C_{\nu_1}H_{\nu_2} + \nu_1 \cdot H_2O \rightarrow \left(\frac{\nu_2}{2} + \nu_1\right) \cdot H_2 + \nu_1 \cdot CO \qquad (11)$$

The content of tars in the final product gas has to be kept as low as possible, as their presence increases the dew point of the gas which easily leads to condensation at cold spots in the periphery of the gasifier. This process of fouling can lead to increased pressure drops or even blocking of pipelines. Besides, the removal of tars is a precondition for most end applications of the produced gas as shown in Table 2-7. Inferentially the production of a tar lean gas is one of the primary exigencies in the development of technical gasifiers.

Besides the various options for gasifier setups and process variations, the choice of fuel is crucial for stable gasification conditions and has to comply with the requirements of the gasification process mainly concerning humidity, ash content and ash composition. The use of woody fuel, conditioned to pellets or chips, is state of the art for many gasification processes.[20] The benefits are a low ash content and high ash melting point, as well as a comparatively high degree of homogeneity which allows for reproducible conditions in the reactor. Furthermore woody fuels are characterized by a low content of corrosive components which is beneficial for longevity of the periphery. As shown in section 2.1 an additional technical potential is given by alternatives to woody fuels with the major

advantage of lower specific cost, and therefore increased economic compatibility.[21] A major drawback is the increased content of impurities such as sulfur and chlorine that lead to corrosive gaseous components during gasification and the significantly higher content of ash, that requires effective process approaches to prevent accumulation of ash and ash derived agglomerates in the reactor.[22,23] An overview of the composition of different fuels is shown in Table 2-2

Table 2-2: Ultimate and proximate analysis for different alternative fuels for gasification (daf = dry, ash free)[7]

Fuel		Willow	Woody excess fraction of ODW	Park wood (bio dried)	Cacao shells	Verge grass	Paper residue sludge	Sewage sludge
Water	$wt\%_{ar}$	17	12.8	14.8	13.4	7.3	10.7	10.6
Ash	$wt\%_{dry}$	2.13	42.8	18.3	10.5	17.6	47.3	36
Vola-tiles	$wt\%_{daf}$	83.5	75.2	74.5	75.8	79	82.2	86.2
LHV	MJ/kg	18.8	18.2	18.6	19.3	18.7	13.9	21.5
C		48.7	50.7	51.5	53	49.9	43.5	52.2
H	$wt\%_{daf}$	5.91	5.7	5.7	5.85	5.68	5.58	7.27
O	$wt\%_{daf}$	44.5	41.7	41.3	37.6	40.9	48.9	30.7
N	$wt\%_{daf}$	0.88	1.56	1.16	3.39	2.47	1.37	7.06
S	$wt\%_{daf}$	0.045	0.26	0.25	0.22	0.18	0.65	2.61
Cl		0.016	0.068	0.027	0.016	0.86	0.046	0.15
Al		0.062	14.9	6.88	n.a.	n.a.	125.7	31.6
Ca		5.83	40.0	18.4	2.51	15.71	182.1	60.2
Fe		0.070	9.10	4.46	n.a.	n.a.	5.56	79.6
K		2.63	17.8	7.44	30.9	26.2	6.95	3.44
Mg	$wt‰_{daf}$	0.526	4.37	2.42	5.40	2.24	4.73	5.81
Na		0.188	6.92	4.46	0.033	1.81	0.723	2.58
Ni		0.026	2.62	0.651	0.012	0.002	0.014	0.258
P		0.733	3.82	0.856	3.67	2.99	2.92	34.4
Si		0.639	61.9	24.2	8.49	46.8	120.9	51.6

The compositions of alternative fuels shown in Table 2-2 have to be considered as examples. The growth rate and location of origin significantly influences the content of trace components even within the same type of agricultural fuel.[24] By comparison of the content of ash constituents, sulfur and chlorine contained in willow as a woody fuel with waste materials summarized in Table 2-2, the increased amount of such problematic components in alternative fuels is demonstrated. While wood pellets contain sulfur in the range of 0.016 wt% and chlorine in the range of 0.003 wt% (Table 4-1), willow wood chips with a bark fraction contain already increased amounts of sulfur and chlorine of 0.045 and 0.016 wt%, respectively. Upon gasification, such sulfur contents in the fuel translates to an H_2S content of the syngas in the range of 20 to 100 ppm_v respectively.[25,26] In contrast to these woody fuels, waste materials such as paper residue sludge or sewage sludge contain sulfur in the range of 0.65 to 2.61 wt% which causes H_2S content far above 1000 ppm_v up to 0.5 percent H_2S in the gas.[27] The increased content of sulfur and chlorine components contained in most alternatives to woody fuels lead to high temperature corrosion in the plant periphery. As these trace elements are released

from the fuel during gasification, the application of alternative fuels increases the requirement of corrosion resistant material grades in the construction of the gasification plant. Besides increased corrosion, sulfur and chlorine act as poison in most downstream catalytic conversion steps or have to be removed due to the specifications of the destined end use of the produced gas. Inferentially these components increase the demand on process steps for gas treatment as elucidated in sections 2.4, and 2.5.

Besides the content of sulfur and chlorine, the amount and composition of ash forming elements is a relevant criterion for the suitability of a fuel for gasification. Depending on the composition of ash forming elements, the melting point of the ash is different for each fuel. Except in the case of slagging entrained flow gasification (Table 2-3), a stable gasification above the fuel-specific incipient temperature of ash melting is not feasible due to the formation of agglomerates in the reactor with the risk of defluidization or blockages. Different indicators (Eqs (12)(13)) are available, especially in the field of combustion, to assess the tendency of sintering based on the ratio of ash forming elements in the fuel.[28]

$$I_1 = \frac{Na + K}{2S + Cl} \quad \textbf{(12)}$$

For a ratio $I_1 > 1$ a fuel is considered problematic as sodium and potassium majorly influence the formation of agglomerates due to incorporation into the silicate-lattice of the bed material and formation of sticky layers. The presence of sulfur and chlorine in a fuel might circumvent agglomeration related problems due to the formation of volatile components such as KCl, which leave the gasifier with the gas phase but on the other hand increase the corrosivity of the gas. Another indicating ratio of trace elements in the fuel is applied to describe the probability of the formation of a non-sticky outer coating on a bed material particle.[28]

$$I_2 = \frac{Na + K + Si}{Ca + P + Mg} \quad \textbf{(13)}$$

For a ratio I_2 smaller than 1, a refractory outer coating is likely to form and prevent the sintering of particles. A technical option for influencing and thus increasing the incipient temperature of ash-melt formation and agglomeration of the bed material is the addition of additives such as Kaolin ($Al_2Si_2O_5(OH)_4$) or Ca-containing materials to the gasifier.[29] Whereas the addition of Ca positively influences the above stated indicator (Eq (13)), the addition of Alumina has a major positive influence on reversing the depolymerization of the silicate lattice in the bed material, which is caused by the incorporation of alkalines.[29] Such process options to increase the feasibility of gasification of alternative and waste fuels are being intensively investigated.[30-34] Until now a long term stable gasification of waste fuels is not yet established.[29]

2.3 Gasifier types and process variations

A variety of technologies and gasifier types is available for the gasification of biomass, suited for different output ranges and applications of the produced gas. These can be differentiated by:[13]

- The type of gasifier (fixed bed, fluidized bed, entrained flow)
- The method of heat provision (allothermal vs autothermal)
- The type of gasification medium (air, oxygen, steam)
- The pressure level inside the gasifier (pressurized vs atmospheric gasification)

An overview of the different types of gasifiers commonly found in literature is shown in Table 2-3.

Table 2-3: Different categories of gasification technologies[13]

Fixed bed gasification	Fluidized bed gasification	Entrained flow gasification
Downdraft gasifier	Stationary fluidized bed	Slagging
Updraft gasifier	Circulating fluidized bed	Non slagging
Other fixed bed processes	Twin fluidized bed	

Depending on the technological design of the gasifier, the conversion process and the produced gas exhibit specific properties, concerning the applicable size range, the gas purity and the efficiency. An overview of these specifications is listed in Table 2-4 for different gasifier categories. The different gasifier setups are subsequently presented in more detail with respect to either allothermal or autothermal operation.

Table 2-4: Specifications of different gasifiers[35,13]

Gasifier	Downdraft	Updraft	Bubbling fluidized bed	Circulating fluidized bed	Twin fluidized bed	Entrained flow
Technology, Design	Simple and proven, simple reactor with relatively low investment cost		Plants with higher investment cost, proven technology with coal		Complex construction	Complex construction
Max. Fuel Moisture [%]	25	60	<55	<55	11-25	<15
Tar [g/m^3_{std}]	0.1 - 6.0	10 - 150	1 – 23	1 - 30	0.5 – 10	< 0.1
Admissible power output [MW_{el}]	up to 1	up to 10	1 - 20	2 - 100	2 – 50	5 - 100
Process flexibility	Very limited. Any change in process variables needs a new design		Flexible to loads less than design		Flexible to loads less than design	Very limited. Size and energy content of the fuel must be in a narrow range
Hot gas efficiency [%]	85 – 90	90 – 95	~ 90	~ 90	90 – 95	~ 80

2.3.1 Autothermal gasifiers

As shown in Table 2-4 fixed bed gasifiers are advantageous in the small scale of product gas output in the range of few kW up to 10 MW in the case of updraft gasifiers. While downdraft gasifiers are characterized by the same flow direction of gasification medium and fuel, updraft gasifiers are operated under counter current conditions with a downward fixed bed of fuel and an upward flow of the gasification medium. Therefore the hot product gas crosses the pyrolysis and drying zone of the fuel before it leaves the reactor from the top. This is beneficial for drying of the fuel but disadvantageous concerning the tar content in the gas as shown in Table 2-4. As the power input of heat to a fixed bed is limited, such systems are only suited for autothermal operation where the required heat is produced via exothermic reactions inside the reactor. Due to the simplicity of their design fixed bed gasifiers allow for the application in micro-scale combined heat and power supply in the range of 100 kW and below. Such systems have also been established without the necessity of elaborate gas cleaning systems.[36] With respect to the investigation of in-situ desulfurization, as part of a gas cleaning process, the application in fixed bed gasifiers is of minor importance for the conducted work.

Another category of gasifiers listed in Table 2-3 is the entrained flow gasifier, which is suited only for autothermal operation. A powdered fuel is burned in a dust flame under addition of oxygen and steam at temperatures in the range of 1300 to 1500°C.[13] Such gasifiers are predominantly deployed in the field of coal gasification but allow for the admixture of biogenic fuels. An advantage of these systems is the thermal cracking of higher hydrocarbons due to the elevated temperatures prevailing in the oxidizing zone of the reactor. This leads to low tar contents below 0.1 g/m^3_{std} as shown in Table 2-4. A disadvantage in the context of biomass gasification is the required large power range of such gasifiers due to the necessity of air separation and complexity of the process structures (Table 2-4). Due to the decentralized occurrence of biomass and significantly lower energy content as compared to coal, long transport routes for biomass have to be avoided.[37] A further disadvantage is the requirement of a finely dispersed fuel with high surface area and thus small particle size, due to the requirement of an instantaneous reaction in the high temperature zone of the dust flame. This can consume up to 0.08 kW_{el}/kW_{th} of electric energy relative to the heating value.[38] Due to different process conditions as compared to the moving bed technologies, this type of gasifier is not further considered for the implementation of in-situ desulfurization in the course of the presented work.

The use of oxygen and steam mixtures as gasification agent is also established in bubbling and circulating fluidized bed applications (Table 2-3). The drawback of increased cost of the gasifying agent as compared to pure steam is compensated with plant size and the simplicity of the gasifier design, as no external heating is required. Such gasifiers are proven technology in the field of coal gasification (Table 2-4). An example of biomass based process application is the fluidized bed gasifier in Värnamo, Sweden with pressurized oxygen-based gasification and a fuel input of 18 MW_{th}.39 An upscale of this process approach is scheduled within the Bio2G project with the aim of a production capacity of 200 MW biogenic SNG in Malmö/Landskrona, Sweden.[4,40]

2.3.2 Allothermal gasifiers

Besides the above mentioned autothermal process options for gasification, the moving bed technologies based on a fluidized bed allow for a sufficient external heat input due to the high fluctuations inside the bed which enable effective heat transfer by convection and radiation. Such

allothermal processes are well suited for the production of a syngas with the aim of further catalytic upgrading, as the gas is not diluted by nitrogen once steam is deployed as gasification agent. The provision of heat is possible either via electric heating or more commonly, by coupling a fluidized bed for gasification with a fluidized bed for combustion in a twin fluidized bed setup (Table 2-3). The bed material of such fluidized bed processes can consist of common quartz sand (SiO_2) in a fluidizable particle size range without catalytic effect on the reformation of the produced gas. The application of catalytically active components such as olivine ($(Fe,Mg,Cu)SiO_4$) or dolomite ($CaMg(CO_3)_2$) compensates for the absence of explicit reaction zones, in a homogenously mixed fluidized bed, by the improved conversion of hydrocarbons.[19,41] Concerning the technological solutions for heat transfer into the fluidized bed, different systems have been developed that can be divided into different combinations of stationary bubbling fluidized beds and circulating fluidized beds. An overview of some relevant technological approaches is shown subsequently.

HPR - Technology

An example for the application of the bubbling fluidized bed technology is the Heat-Pipe reforming reactor distributed by agnion technologies.[42] It is based on the combination of two stacked bubbling fluidized beds. The lower fluidized bed is operated under autothermal conditions and acts as a combustor for the provision of heat for the allothermal gasification in the reformer. A flow chart of the process setup is shown in Figure 2-3.

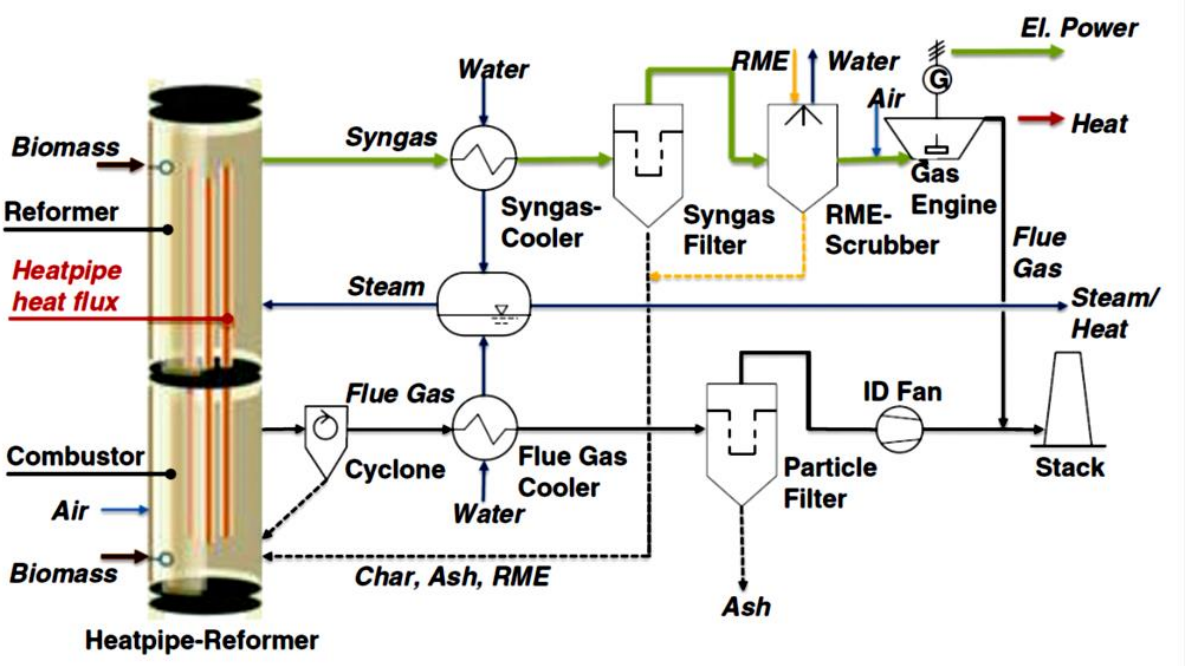

Figure 2-3 Flow sheet and basic data of the heat pipe reformer technology[42]

The heat transfer from the combustor to the reformer is established via heat pipes allowing a strict separation of the different reactor zones. The temperature of 900 °C in the combustor is sufficient to evaporate a working fluid inside the heat pipes which then rises as vapor and condensates in the reformer part of the heat pipes. The phase transition allows for heat transmission numbers magnitudes above a mere convection-based heat transfer. Due to the almost ideal mixing inside the fluidized beds, the transfer of heat into the heat pipes in the combustor section and into the fluidized

bed of the reformer section can be established with a temperature difference of only 100 K. This leads to temperatures of about 800 °C in the reformer.[43] The gasifier is run using either wood chips or pellets as fuel and is operated under pressurized conditions at a pressure of 4 bar_{abs}.[44] The strict separation of reactors with adjustable steam excess rates for gasification and fluidization of the bed material in the reformer, allows for the production of a hydrogen rich and nitrogen lean syngas with a composition as shown in Table 2-5.

Table 2-5: Composition of the produced syngas from the HPR gasifier under application of pellets as fuel[44]

H_2	CO	H_2O	CO_2	CH_4	N_2	Tar
Vol %						g/m^3_{std}
24.3	10.6	43.4	12.4	5	4.2	4 - 8

Such a gas is well suited for further catalytic conversion processes. The elevated operational pressure of 4 bar_{abs} in combination with a catalytic hot gas cleaning significantly increases the overall efficiency of a polygeneration for production of heat, SNG or other chemical products derived from syngas.[37] Process examples of the heat pipe reformer technology are gasifiers in Pfaffenhofen (Germany) with a thermal fuel input of 0.5 MW[44] and Achental (Germany) with a thermal fuel input of 1.3 MW.[45] The comparatively small scale of this gasifier allows for a local infrastructure for the production of fuel and the consumption of produced heat.[43]

FICFB - Technology

Besides the possibility of heat input to the reforming reactor via heat pipes, the bed material itself can be deployed as a heat carrier. This is the case for the fast internally circulating fluidized bed gasifier (FICFB) technology developed at University of Technology Vienna.[46] Once again two fluidized beds are combined whereby in the case of FICFB technology, a circulation of the bed material from the combustor unit to the reformer warrants the supply of heat for the endothermic reforming reactions in steam gasification (Eq (4)). A flow sheet of the process setup in an 8 MW_{th} demonstration plant for the FICFB process is shown in Figure 2-4.

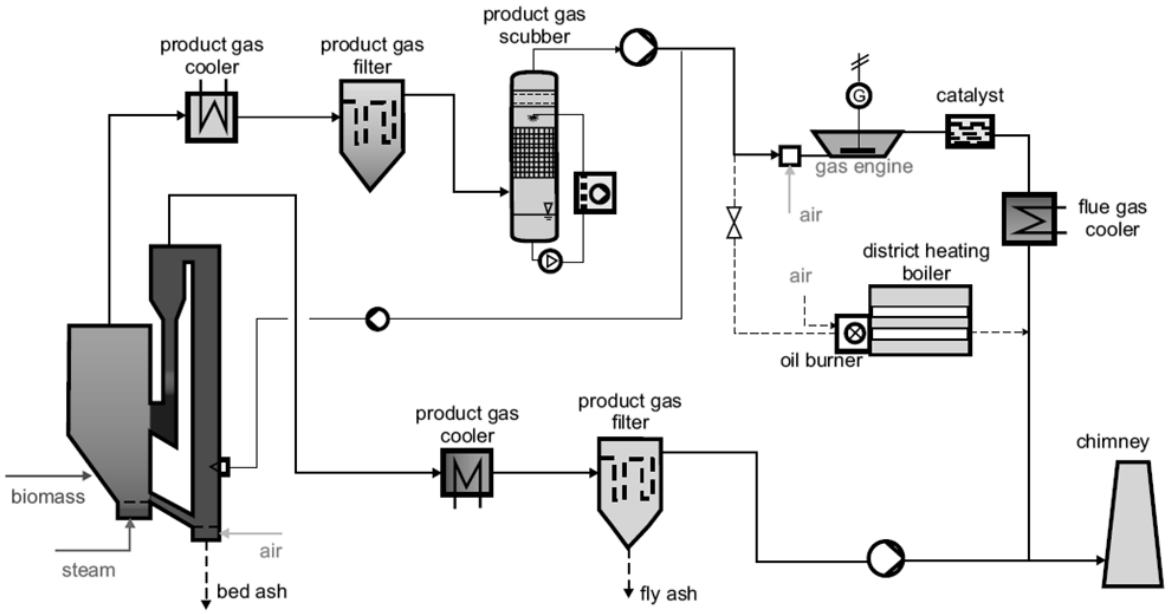

Figure 2-4: Setup of "Güssing" FICFB-process and gas cleaning route with the aim of syngas use in a gas engine[47]

The combustor is implemented as an air blown circulating fluidized bed and operated under slightly over stoichiometric air ratio (λ = 1.05)[46] at a temperature of about 1000 °C.[19] The flue gas from the combustor is led through a heat exchanger to avail of process heat. The hot bed material is separated from the flue gas in a cyclone and fed to the bubbling fluidized bed of the reformer unit. The bed is fluidized with steam at a temperature of about 850 °C[46] and facilitates the production of an H_2-rich and N_2 lean syngas with an approximate composition shown in Table 2-6 for the gasification of wood pellets.

Table 2-6: Composition of the produced syngas at Güssing gasifier under application of pellets as fuel[48]

H_2	CO	H_2O	CO_2	CH_4	N_2	Tar
Vol %						g/m^3_{std}
36	25	17	11	7	4	1.5-4.5

Together with a constant flow of bed material, the unconverted char is directly conveyed from the reformer to the combustor by a chute. In the combustor, the unconverted char from the reformer acts as fuel for the oxidation reactions that are necessary for heating the bed material. As a full conversion of char in the reformer is not intended, the gasifier can be operated with relatively low weight based steam to biomass ratios of 0.6 to 0.7. This is in contrast to the setup of the heatpipe reformer, where a rather full conversion of char is pursued and a steam to biomass ratio of 1.15 $kg_{steam}/kg_{biomass,dry}$ is applied. The low steam to biomass ratio in FICFB technology in return leads to a low steam content in the produced syngas of only about 17 vol%. In the process setup of the Güssing gasifier the product gas is then cooled and cleaned in a scrubber before it is combusted in a gas engine. With the setup depicted in Figure 2-4 an output of about 2 MW electricity can be generated with an efficiency of about 25 %.[46]

Different options for process routes are pursued in other FICFB-based gasifier applications like the GoBiGas project in Gothenburg, Sweden.[5] A first technological stage of the GoBiGas plant produces SNG from wood pellets made of forest residues with a thermal input of 32 MW_{th}. A second stage of development with about 150 MW_{th} fuel input and the aim of producing 100 MW biogenic SNG is planned for the year 2017.[4] Even though the gasifier technology is the same as in Güssing, the required process steps for gas treatment are far more complex once the production of biogenic SNG is pursued. A simplified flow chart of the process setup in Gothenburg is shown in Figure 2-5.

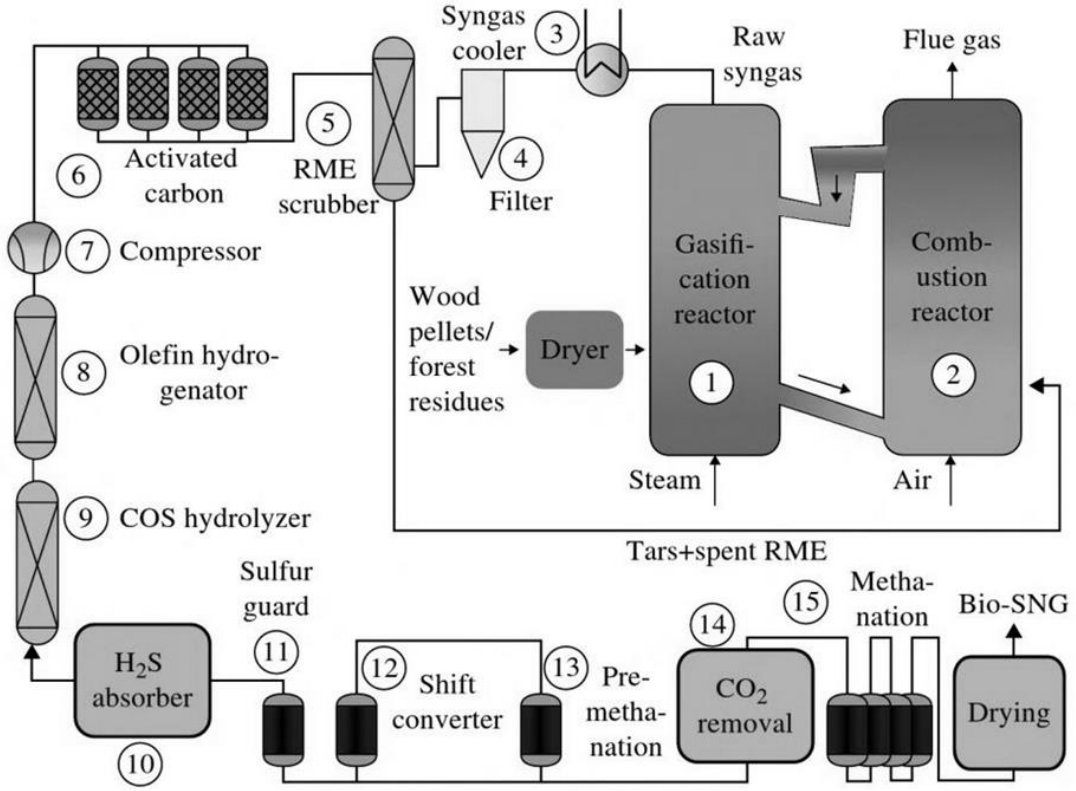

Figure 2-5: Setup of "GoBiGas" FICFB-process and gas cleaning route with the aim of producing Bio-SNG as vehicle fuel[5]

As further discussed in section 2.4, the tar removal in the GoBiGas plant (Figure 2-5) is done via a cold gas scrubbing process (5). A series of catalytic (8,9,12,13 and 15), adsorptive (6 and 11) and absorptive (10 and 14) steps are installed to warrant a sufficient quality of the produced SNG for the grid injection and a later use as a vehicle fuel.[5]

Another established option for the implementation of allothermal gasification is the Milena gasifier developed by ECN, which reverses the current of bed material with a circulating fluidized bed in the gasifier and a bubbling fluidized bed in the combustor.[49] Compared to the FICFB process, a lower share of H_2 with 18-20 vol% and higher amount of CO and tar with 40 vol% and about 40 g/m^3_{std} respectively, are contained in the gas.[49,50]

As shown in Table 2-4 and discussed above, the various types of gasifiers and process conditions exhibit specific advantages and disadvantages depending on the application scenario. A relevant criterion for the choice of gasification technology is the applied type of fuel and the destined end use of the produced syngas and thus the necessity for gas treatment according to the specific tolerance margins for trace substances. Concerning the flexibility towards different fuels, fluidized bed

gasification is considered to be the most suited process option.[38] Allothermal gasification with steam further exhibits the benefit of producing a nitrogen lean gas with high hydrogen content, suitable for further catalytic conversion processes. While the high steam content of the gas produced from the HPR – gasifier is beneficial to prevent carbon depositions on downstream catalysts, it is detrimental towards the thermodynamics of desulfurization as further discussed in section 2.5.1. On the other hand, the gas composition shown in Table 2-5 most closely represents the conditions of the experiments conducted in the course of the presented work. A disadvantage of fluidized bed gasification is the inevitable content of tars in the produced gas due to the absence of distinct reaction zones inside the gasifier. The tar content can be reduces by application of catalytically active bed materials and ensuring sufficient residence times for interactions between the bad material and the produced gas. Up to now the technical application of a syngas derived from fluidized bed gasification cannot be established without an intermediate chain of process steps for gas cleaning as described subsequently.

2.4 Gas cleaning[1]

The major contaminants in the syngas, produced by gasification of biomass, are particles, tars and alkalines, as well as sulfurous compounds and halogens.[13] While the release of sulfurous components and halogens is directly related to the composition of the applied type of fuel, with examples given in Table 2-2, the amount of particles, alkalines and especially tars is influenced predominantly by the gasification conditions and the type of gasifier used.[13] According to equilibrium calculations, higher hydrocarbons would basically be absent in a product gas obtained from gasification at about 800 °C.[51] This means that the chemical equilibrium is on the product side of tar reducing reactions such as thermal cracking, partial oxidation or steam reforming (Eqs(9), (10), (11)).[18]

In practical application a certain amount of unconverted tars in the raw gas is effectively inevitable with major differences between the different types of gasifiers (Table 2-4). Steam blown allothermal fluidized bed gasifiers are in the medium range concerning the achievable tar loads with ranges from approximately 0.5-30 g/m^3_{std}.[13] Particle loads, on the other hand, are quite high for fluidized bed gasifiers with values of up to 100 g/m^3_{std}.[13]

The necessity for post treatment and cleaning of the produced syngas depends on the initial content of the contaminants mentioned above, as well as the intended process route of the produced gas. The required degree of purity is much higher for catalytic conversion processes as compared to the direct combustion in a gas engine. Besides the requirements and tolerances of the commodities for gas utilization, the necessity for gas cleaning might also be founded in legal restrictions limiting the exhaust of pollutants into the environment. In the example of Germany, such legal restrictions are given in detail by the BImSchG[52]

A comparison for the allowable tolerances concerning different types of impurities in the produced syngas is listed in Table 2-7 with regard to the different types of destined end application for energy conversion.

[1] Segments of this section have already been published by Husmann *et al.*[27]

Table 2-7: Allowable tolerances concerning the different types of destined end application for energy conversion (n.a means no data available)

Contaminant	Gas engine[13]	Gasturbine[13]	Fuel Cell[53],[54]	FT-synthesis[55]	SNG - synthesis[3]
Particles [mg/m^3_{std}]	< 50	< 30	< 1	Essentially removed	< 0.1
Tars	≤ 100 mg/m^3_{std}	n.a	≤ 10.000 mg/m^3_{std}	< 2 ppm_v	< 0.1 mg/m^3_{std}
Alkalines	< 50 mg/m^3_{std}	0.25 mg/m^3_{std}		< 0.01 ppm_v	< 0.01 ppm_v
NH_3	< 55 mg/m^3_{std}	< 55 mg/m^3_{std}	< 5000 ppm_v	< 1 ppm_v	n.a
H_2S,COS	< 1150 mg/m^3_{std}	n.a	< 0.1-1 ppm_v	< 1 ppm_v	< 0.1 ppm_v
Halogen	< 500 mg/m^3_{std}	n.a	< 1 ppm_v	< 0,01 ppm_v	< 0.1 ppm_v

As shown in Table 2-7 the purification of the raw gas into a suitable feed for FT-synthesis or the conversion to SNG for grid injection, requires a significantly higher degree of purity as compared to the combustion in a gas engine. While a gas engine is mostly sensitive to particles and tars as such components can cause fouling and blockages of valves and pistons, synthesis processes require the removal of basically all contaminants to ensure longevity of the applied catalysts. An exception towards the tolerance for tar loads in the gas is the use in a solid oxide fuel cell (SOFC) as tars are electrochemically converted into CO_2 and H_2O.[54]

Besides the required degree of gas purities the different conversion technologies differ by the achievable efficiency and the applicable range of power output from the facility. The application of the different technologies for biomass and biomass derived syngas is limited by the lower energy content of biomass as compared to coal and therefore significantly increased logistic effort for fuel acquisition in the range above 100 MW_{th}.[37] A comparison of different technologies for energy conversion is shown in Figure 2-6.

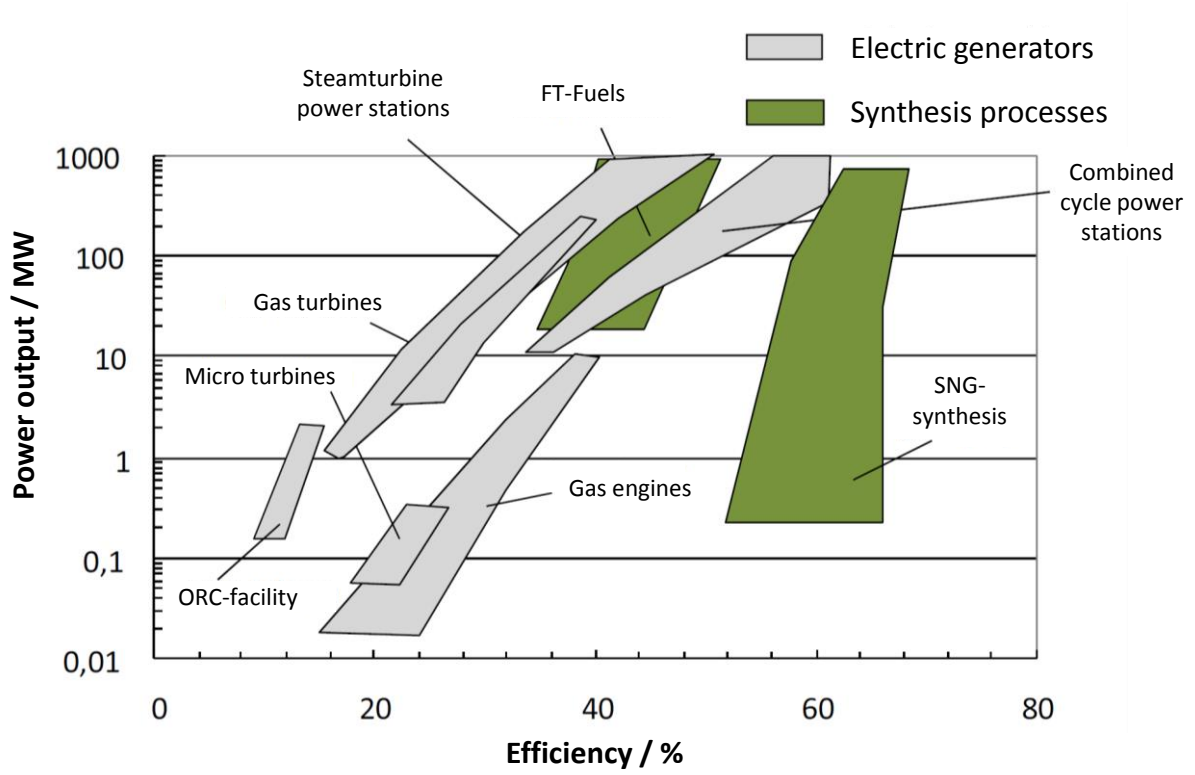

Figure 2-6: Applicable ranges of power output for different conversion technologies and their corresponding range of efficiency[37]

Considering a rather decentralized conversion of biomass in the range of power output of 1-10 MW the catalytic conversion especially into SNG with energetic valorization in large combined cycle plants would be the most efficient option.[37] As discussed in section 2.3, the production of a syngas by means of steam-blown allothermal fluidized bed gasification seems the most viable option for such a scenario. Considering an economic valorization, the large scale production of SNG in autothermal oxygen-blown or allothermal steam-blown fluidized beds, with subsequent use for example as vehicle fuel, is a promising process route for the near future. It is especially pursued in northern Europe.[4,40] The increased effort necessary for gas cleaning is therefore justified individually depending on the prospects of product valorization. Two fundamentally different technological options as process routes for gas cleaning are presented subsequently, whereby cold gas cleaning is based on physical separation and absorption and hot gas cleaning is based on thermal or catalytic cracking and adsorption.[5] The different options for particle removal such as cyclone separation, hot gas filtration and electrical filters are not discussed further with details given elsewhere.[13,51] The most challenging components in gas cleaning are sulfur and tars that have to be treated separately for both, hot gas and cold gas cleaning.[6]

2.4.1 Cold gas cleaning

Cold gas cleaning of biomass derived syngas can be described as state of the art technology and is applied in most gasifier setups which require gas cleaning.[5,13] As an example of an existing process setup based on cold gas cleaning the “GoBiGas”-plant (Figure 2-5) is taken as a reference for explanation of the chain of process steps. Cold gas cleaning is based on the physical absorption or separation of tars and mostly chemisorbtive processes for sulfur removal. In contrast to the hot gas

cleaning described in section 2.4.2, cold gas cleaning is based on processes operated at temperatures below the tar dew point of the gas. As condensation of tars leads to fouling and blockages in the plant periphery, cold gas cleaning therefore requires a tar removal instantly after cooling the syngas. This leads to a process setup where tar removal has to occur upstream of sulfur removal if cold cleaning processes are applied.

2.4.1.1 Tar removal

By definition,[15] tars condensate upon cooling of the gas which can either be done in water as a lipophobic solvent or in organic solvents such as rapeseed methyl ester (RME). As the use of water yields higher residual tar levels of 20-40 mg/m^3_{std} and produces a toxic waste, commonly organic solvents are applied as solvent.[13] Besides the physical separation due to cooling of the gas to temperatures below its' tar dew point, the solubility of organic hydrocarbons in the lipophilic solvent leads to lowered residual tar concentrations of 10 mg/m^3_{std}.as compared to water-based systems.[13,47] The saturated solvent is later used as a fuel supplement in the combustor as for example of the Güssing and GoBiGas gasifiers as well as the HPR-gasifier.[5,6] In the setup of GoBiGas the lean gas is post treated in an adsorber over activated carbon and then pressurized for hydrogenation of olefins and sulfur removal steps.[5]

2.4.1.2 Sulfur removal

The sulfur contained in the gas is present mostly as H_2S but COS and mercapthanes as well as thiophenes also appear in smaller quantities.[6] Some gas treatment systems, like Rectisol,[6] are able to remove COS together with H_2S and CO_2. But as this process requires high technical effort including cooling of the gas to about -40 °C and compression to 30-60 bar_{abs} with commonly methanol as a washing fluid, it is suitable only for large scale processes (> 10000 m^3_{std}/h) as common in coal gasification.[13] Other chemisorption based processes, in particular amine washes, require that COS is converted to H_2S for sufficient sulfur removal.[6] Depending on the applied scrubbing process, a conversion via hydrodesulfurization (HDS) of organic sulfur-components and COS might thus be required prior to sulfur removal as shown in the setup of the GoBiGas plant (Figure 2-5). As heat is required for the conversion of organic sulfurs to H_2S via the reaction shown in Eq (14) and methanation steps shown in Figure 2-5, several heat exchanging steps are required in cold gas cleaning.[5]

$$COS + H_2O \leftrightarrow H_2S + CO_2 \quad \textbf{(14)}$$

In the case of the GoBiGas setup, the HDS-step is supplemented with a chlorine adsorption catalyst based on potassium carbonate. The removal of H_2S is established by an Amine scrubbing process which also removes 50% of the CO_2.[5] The application of different solvents (Rectisol, Purisol, DEA, DMEA) for sulfur removal is technologically proven in the field of coal gasification and yields residual sulfur loads below 1 ppm_v.[6] Due to the complexity of their design, scrubbing processes are economically suitable only for large scale gasifiers.[13] As sulfur loads are commonly low for the application of wood as biomass fuel, the recapture of elemental sulfur via Claus-Process, as performed in coal technology, is not a viable option for small scale biomass applications.[6]

The advanced stage of process development and versatility of the established scrubbing technology clearly is an advantage for the application for tar and sulfur removal from biomass derived syngas. A

drawback is the loss of thermal efficiency due to the necessity of several heating and cooling steps involved in the process. In addition to the loss of efficiency, the removal of heat from tar loaded gas can easily lead to undesired tar condensation and clogging of the heat exchanger surfaces.[5,46]

2.4.2 Hot gas cleaning

In order to improve thermal efficiency, the process route of hot gas cleaning aims at a minimization of the necessary heating and cooling steps during the purification of the produced syngas. This means that the process steps for tar- and sulfur removal are ideally established at the temperature levels available through the gasification process without additional heating steps. The concept of hot gas cleaning further includes the removal of tars above the incipient temperature of tar condensation. This allows flexibility in the alignment of process steps for tar- and sulfur removal concerning the fouling based on tar condensation. On the other hand most processes for catalytic tar removal require a sulfur free gas and therefore an upstream removal of sulfur, which is in contrast to the setup of cold gas cleaning.

2.4.2.1 Tar removal

For the removal of tars, different primary or secondary methods are available which are based on either thermal or catalytic cracking of higher hydrocarbons into permanent gases. The concept of thermal cracking implies the elevation of temperature in the raw gas to above 1000 °C.[13] As a primary measure in biomass gasification this approach is suited only for slagging entrained flow gasification due to the formation of ash melts at such gasification temperatures.[38] As a secondary method the required energy for heating of the gas can be released by partial oxidation of tars and combustible components or externally supplied, for example via a plasma arc.[13] The loss of chemical energy in the first and high cost and electricity input for the latter makes thermal cracking unattractive for biomass applications.

Catalytic cracking of tars is commonly executed at temperatures of around 800 °C with either catalytically active minerals such as lime, olivine or dolomite or metals like iron (Fe) and nickel (Ni). An extensive study on the application of lime and dolomite for in-bed tar reforming was performed by Corella and colleagues.[56-60] The in-bed application of catalytically active materials in fluidized bed gasification can be considered as state of the art[61] and can be combined with any of the downstream options for purification. Requirements for suitable supplements or bed materials are a high attrition residence and catalytic activity, in combination with a low price.[19] The addition of calcined dolomite to the fluidized bed of the gasifier allows to reduce the tar content in the dry product gas from two digit numbers down to 1-2 g/m^3_{std}, while with olivine the corresponding average value is 5-7 g/m^3_{std}.[61] A major drawback for the application of lime and dolomite as bed materials is the poor mechanical strength, especially after calcination.[62] The use of olivine is therefore established as the best compromise between the above mentioned exigencies.[61] Besides catalytically active minerals, the addition of nickel is an option that exhibits superior performance in the conversion of tars by catalysis of the steam reforming reaction (Eq (11)). The application of Ni at elevated temperatures of about 800 °C is beneficial in terms of sulfur intoxication as the formation of sulfide (NiS) is less pronounced. On the other hand the use of Ni-doped materials in fluidized beds is critical due to the formation of toxic Ni-dust in the gasifier. The option of installing Ni-doped catalytically active filter candles in the freeboard of the gasifier for inclusion of both, particle separation and tar reforming, is pursued in the “unique” concept.[61] In combination with catalytically active bed material and

supplements, the concept aims at the gasification and conditioning of biomass derived syngas in a single vessel, as further discussed in section 2.5. With the benefit of no need for external heating the application of catalytically active filter candles inside the gasifier, contrariwise suffers from the formation of a deactivating dust layer on the candles and inside the pores.

A downstream application of nickel at elevated temperatures of 800 °C is feasible, but requires external heat or partial oxidation of the gas which again, lowers the heating value of the produced gas and requires air separation if dilution with nitrogen is to be averted. As investigated by Kienberger et al.[18] the application of nickel for catalysis of steam reformation is also possible at significantly lower temperatures of about 500 °C. Some of the heat required for tar cracking is released by the parallel occurring highly exothermic methanation reaction (Eq (7)) as presented in a novel concept for mid-temperature gas cleaning with the prospect of SNG synthesis.[18]

Under syngas conditions with H_2/CO-ratios other than 3 the methanation reaction is part of a shift of permanent gas components in the syngas towards a CH_4 rich raw SNG (Eq (15)).[18]

$$\nu_1 \cdot CO + \nu_2 \cdot H_2 + \nu_3 \cdot CO_2 + \nu_4 \cdot H_2O + \nu_5 \cdot CH_4 \leftrightarrow \nu_6 \cdot CH_4 + \nu_7 \cdot CO_2 + \nu_8 \cdot H_2O \quad \textbf{(15)}$$

Especially in process approaches for the production of SNG, which are based on cold gas cleaning (Figure 2-5) the conversion of syngas to methane (Eqs (7) and (15)) is commonly established in a separated reactor vessel downstream of the process step of tar removal. This is not the case for a hot gas cleaning based on the parallel conversion of tars and catalysis of methanation over a Ni-catalyst at temperatures of about 500 °C. The inclusive concept of a combined tar removal and methanation step is thus beneficial concerning the simplicity of design and the reduced number of required reactor vessels and process steps.[37] A tar conversion of over 90 % can be achieved with this integrated upgrading process with the aim of SNG-grid injection.[18] A separation of excess H_2O and CO_2 has to be installed downstream of the combined methanation and tar removal reactor if the production of SNG is pursued.

In general, the catalytic tar removal offers the possibility of increased thermal efficiency of the overall process as excessive temperature changes in the gas are avoided. Further the heating value contained in the tars is transformed into the product gas and not separated for injection in the combustor unit, as commonly done in cold gas cleaning. On the other hand, a deactivation of the Ni-catalyst occurs due to carbon deposition caused by the lower H/C ratio in unsaturated hydrocarbons, as compared to the CH_4 produced during methanation. Besides that, a sulfur removal upstream to the catalytic conversion is inevitable, whereby even low concentrations of residual organic sulfurous compounds degrade the Ni-catalyst over time.[18] The intoxication of the Ni-catalyst by sulfur can be prevented by adsorptive process steps for sulfur removal as described subsequently.

2.4.2.2 Sulfur removal

The adsorptive desulfurization of syngas from gasification aims primarily at removing H_2S which is by magnitudes, the main sulfurous compound formed in a reducing atmosphere followed by minor components such as COS, methylmercaptane and sulfurous tars. Adsorptive desulfurization as a secondary method for sulfur removal can be applied in a wide temperature range, commonly between 300-600°C[63]. It is based on the formation of a chemisorbtive bond by reaction of H_2S and a metal oxide (Me_xO_y)(Eq (16))

$$Me_{\nu_1}O_{\nu_2} + \nu_1 * H_2S + (\nu_2 - \nu_1) * H_2 \leftrightarrow \nu_1 * MeS + \nu_2 * H_2O \quad \textbf{(16)}$$

Criteria for desulfurization sorbents concerning economical and operational suitability can be summarized as:[63]

- High adsorption capacity for H_2S. This reduces both sorbent quantity and process equipment size.
- Fast adsorption kinetics
- Mechanical properties: low attrition rate and able to tolerate high temperature.
- Chemical properties: stable in reducing environment containing steam and hydrocarbon
- Regenerable through a suitable pathway while maintaining efficient sulfur sorption capacity during repeated sulfidation-regeneration cycles.
- Multicomponent removal of other impurities like NH_3 and HCl

Extensive studies have been performed based on the oxides of Zn, Fe, Cu, Mn and Ce as sorbent materials. The combination of different metal oxides allows a design to enhance specific characteristics such as thermal tolerances, sulfur capacity, regeneration properties or the combined removal of multiple pollutants. Such costly sorbents also increase the necessity of applications with multiple regeneration-desulfurization cycles.

Concerning single metal oxides, the application of ZnO is the most economically viable option and commercially applied for medium scale applications in biomass gasification.[51] A desulfurization down to 1-2 ppm_v H_2S is feasible under application of a commercially available ZnO-based sorbent for desulfurization in real gasifier derived syngas with a steam content of 43 % at 300 °C.[64] While several studies claim the feasibility of regeneration of ZnS to ZnO[65-67], others pointed out the limits of such multi-cycle applications.[64,68] The described positive regeneration properties commonly obtained under conditions of bottle mixed syngas, did not prove to be reproducible by application of real gasification derived syngas in long term experiments.[64]

Especially for the use of alternative fuels the increased sulfur content (Table 2-2) can easily translate to H_2S contents of several hundred ppm_v in the produced gas. Considering a limited technical feasibility of regeneration, the increased consumption of costly metal oxide sorbents for adsorption-based desulfurization in a fixed bed reactor vessel, might lead to an over-proportional increase in operational cost. An option is the application of sorbent materials that are either cheaper as compared to ZnO, as the standard sorbent material, or facilitate multiple regeneration cycles. Another option is a staged system based on cheap sorbent materials for coarse desulfurization in combination with a downstream guard bed of ZnO for deep desulfurization. With regard to the simplicity of the process, such a coarse desulfurization ideally has to be established inside the gasifier as in-situ process.

2.5 In-situ desulfurization[1]

The concept of in-situ desulfurization aims to reduce the overall effort involved in gas cleaning by introducing a coarse desulfurization, which does not need an additional downstream apparatus. The implementation of in-situ desulfurization is beneficial for apparatus cost and process simplicity but places high demands on the thermal and mechanical stability and thermodynamic properties of the applied sorbent. Current applications can be found mostly with limestone in the field of coal combustion, where the oxidizing atmosphere leads to the formation of calcium sulfate ($CaSO_4$) instead of the sulfide formed under reducing conditions in gasification (Eq (16)). With the advance of internal gasification combined cycle (IGCC) technology for generation of power and chemicals from coal[70] the application of in-situ desulfurization is extended to gasification processes[71] Examples thereof are listed in literature.[71-74] With applications in the demonstration range of up to 100 MW_{el}, the use of in-situ desulfurization sorbents is a promising concept for the in-bed capture of sulfur in an allothermal bubbling fluidized bed gasifier (BFBG). It is even more suited for the application in a circulating fluidized bed (CFB) or twin Fluidized bed gasifier, as the agglomeration of loaded sorbent can be easily circumvented by separation of fines from the circulating bed material.[72]

Even though the addition of limestone for gas conditioning is applied in industrial scale of 100 MW_{el} in coal gasification, results of experimental investigations on in-situ desulfurization in literature are scarce. Even if the final application is supposed to be an in-situ desulfurization process, the published results are commonly based on fixed bed experiments in a plug flow reactor under application of bottle mixed gases. This holds true for investigations concerning coal gasification but especially for the application in biomass gasifiers with commonly lower gasification temperatures and higher steam contents during the gasification process. In the prospect of the conducted work with a focus on allothermal steam gasification of biomass in a fluidized bed, some relevant restrictions have to be considered in the selection of potential sorbent materials for in-situ desulfurization. This is due to the high temperatures and friction in the fluidized bed and the detrimental conditions for the thermodynamics of desulfurization reaction (Eq (16)) in a high steam atmosphere of biomass gasification at elevated temperatures.[71]

The conditions of biomass gasification vary from those in coal desulfurization, what has to be taken into account for comparison of previous results of other researchers. In the course of a survey of previous results, the investigations on high temperature desulfurization of 800 °C and above are considered, even those in the context of coal gasification with experimental procedures based on bottle mixed gases. The results are then compared under the aspect of different thermodynamic conditions of the desulfurization process (Table 2-8). The influences which have to be taken into account for a valid comparison of the obtained results from other researchers are explained subsequently.

2.5.1 Thermodynamic considerations

As a primary method for the reduction of the sulfur content in the produced syngas, in-situ desulfurization is a special case for the application of high temperature desulfurization. Same as the secondary measure of fixed bed desulfurization in a downstream plug flow reactor, it takes place by

[1] Segments of this section have already been published by Husmann *et al.*[27,69]

sulfidation of metal oxides according to Eq (16). Most of the previous work concerning high temperature desulfurization in the range of 800 °C is focused on the application in a syngas obtained from coal gasification. This leads to different conditions concerning thermodynamic considerations compared to biomass gasification. Gasification of coal commonly uses process setups with pure oxygen or mixtures of oxygen and steam with higher gasification temperatures at a range of 900 to 1100 °C resulting in a syngas with low steam contents of 2 – 20 vol%.[75,76] In the field of coal technology extensive studies have been published on the application of lime and dolomite as desulfurization sorbents. Many of these investigations are based on thermogravimetric analysis[77-82] and /or bottle mixed gas in conventional plug-flow fixed bed reactors.[83,84] Some are based on real gasification applications.[72,73] Compared to the predominantly published results on in-situ desulfurization of coal derived gases[72,73,85] the partial-pressure of steam is elevated in biomass gasification. Especially for allothermal steam gasification, the steam content of the syngas is in the range of 15 – 60 vol%.[86,87] Due to the formation of H_2O as a product of the desulfurization reaction (Eq (16)), the high steam content of the syngas is a major challenge for the implementation of in-situ desulfurization in biomass gasification.[87] The equilibrium of Eq (16) depends on the steam content and the temperature, whereby high steam contents and temperatures shift the reaction to the reactant side. Assuming a surplus of sorbent, the sorbent specific equilibrium constant of desulfurization K_{eq}^{b} can be expressed as a ratio between the gas phase reactions (Eq (17)).[88]

$$K_{eq}^{b} = \left\{\frac{[H_2O]}{[H_2S]}\right\}_{eq} \quad \textbf{(17)}$$

The formation of a sulfide phase in the sorbent takes place until the ratio of partial pressures between H_2O and H_2S equals the temperature dependent equilibrium constant K_{eq}^{b}. Under high steam conditions in allothermal biomass gasification, the requirements for suitable sorbents for in-situ sulfur capture demand both thermal stability and an equilibrium constant that is high enough to achieve low residual sulfur contents even at elevated temperature.[87] The sorbent-specific influence of the steam content is complex due to parallel occurring phase transitions and side reactions. Due to the numerous influencing factors on the equilibrium of desulfurization under application of different metal oxides, a prediction of the residual H_2S content under equilibrium conditions is ideally obtained by numerical thermodynamic equilibrium calculation.

The calculation of the equilibrium composition in numerical solvers, such as for example FactSage, is not based on the progress of specific reaction pathways, as the calculation of complex multiphase systems based on single reactions can easily lead to faulty results if interactions of components or phase transformations are ignored.[89] A complex equilibrium calculation is therefore based on the minimization of the total Gibbs energy of the system by the numerical solution of multivariable transcendental equation systems under the condition of a multiphase minimum of G.[90]

$$G = \sum \left(\sum n_i^{\phi}\right) G_m^{\phi} = min \quad \textbf{(18)}$$

In equation (18) G_m^{ϕ} is the molar integral Gibbs Energy of phase Φ and n_i^{ϕ} are the molenumbers of the phase constituents i of this phase. The inner sum refers to the respective phase composition; the outer sum runs over all phases. The integral molar Gibbs Energy of each stable product phase is required for the correct solution of the above equation. With a given set of input components the numerical solver produces all possible combinations of output components that are stable at the

given conditions concerning pressure and temperature. With a known molar Gibbs Energy of all the possible stable product phases the program calculates the respective molenumbers n_i^{ϕ} of each product component in order to yield an overall minimum of Gibbs energy of the system at a specific temperature and pressure.[89]

The data needed for the solution of these matrix systems has to be available from extensive databases of property data for stoichiometric substances in the form of enthalpy of formation and entropy at standard conditions (Eqs (19) and (20)).[89]

$$H = H_{298} + \int_{T_{298}}^{T} c_p * dT \quad \textbf{(19)}$$

$$S = S_{298} + \int_{T_{298}}^{T} \frac{c_p}{T} * dT \quad \textbf{(20)}$$

The corresponding Gibbs enthalpy can be calculated from the Gibbs-Helmholtz relation (21).

$$G = H - T * S \quad \textbf{(21)}$$

Under application of such thermodynamic equilibrium calculations the prediction of various influencing factors such as steam content, temperature, gas composition and pressure is possible. Numerical investigations by Yrias et al.[81] show the influence of pressure in the context of calcium-based desulfurization. The influence of pressure is based on the partial pressure of CO_2 and the superimposed transition of calcium-carbonate to lime and therefore significates an exception with regard to other sorbent materials in the field of in-situ desulfurization.

Besides the steam content, the temperature is an important influencing factor on the achievable thermodynamic equilibrium due to the temperature dependency of the equilibrium constant K_{eq}^{b} (Eq (17)). Furthermore the temperatures inside the gasifier of 800 °C and above, limit the choice of suitable sorbents for in-situ desulfurization. Based on the composition of coal gas, a simulated thermodynamic equilibrium calculation was performed by Westmoreland et al. resulting in the applicable ranges of temperature for different sorbent materials.[91] This study lays a foundation for a comprehensive evaluation of suitable in-situ sorbent materials with an overview of the obtained results shown in Figure 2-7.

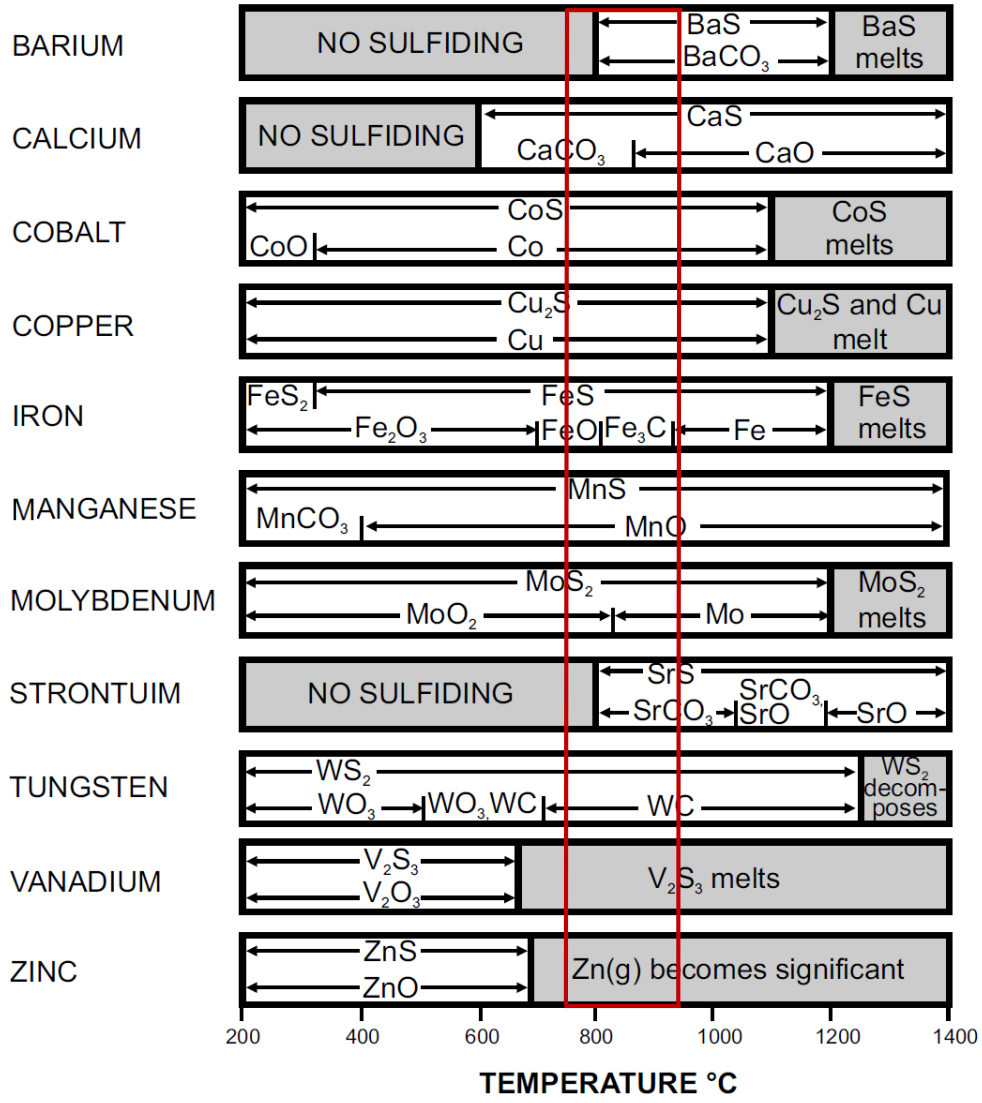

Figure 2-7: Limitations of suitability due to the applicable temperature ranges of different potential sorbent materials for hot gas desulfurization compared to the relevant temperature range of fluidized bed biomass gasification (red square)[48,91]

The evaluation of applicable temperature ranges for different sorbent materials shown in Figure 2-7 is compared to the temperatures of gasification in the range of 750 – 950 °C, commonly established in fluidized bed gasification (indicated by red square). At the applicable temperatures of 800 °C and above, a selection of sorbents suitable for in-situ desulfurization consists of barium, calcium, cobalt, copper, iron, manganese, molybdenum, strontium and tungsten. This selection considers only thermal stability based on the melting point of the metal and does not take into account thermodynamic properties like the affinity towards the formation of sulfides (Eq (17)) at elevated temperatures. Further restrictions are given due to availability and costs as for the example of tungsten. On the other hand thermal stability of single metals can be increased by the addition of certain additives as for the example of zinc titanate (Zn_2TiO_4). The addition of additives can as well be implemented in order to preserve a thermodynamically active oxidation state such as to prevent reduction of metal oxides in the reducing H_2-rich atmosphere within the gasifier. A representative survey of potential sorbents and results obtained by other research groups is presented subsequently.

2.5.2 Results in literature

The results presented below are given as references for desulfurization results with the respective sorbent materials under high temperature conditions comparable to those of an in-bed application. The results are commonly obtained by fixed bed experiments under application of bottle mixed gas referring to coal gas composition, with relevantly lower steam contents compared to biomass derived syngas. Exceptions from the common fixed bed experiments with simulated gas are explicitly mentioned in the sections below.

Zinc: Sorbents based on ZnO are supposed to be the most appropriate materials for sulfur removal at the lower to medium temperature range[92,93], but without stabilization they are not suitable for in-situ application at temperatures of 800°C and above. Part of the ZnO would constantly be reduced to elemental Zn which would evaporate due to a substantial vapor pressure at temperatures above 600°C. (Figure 2-7) Zinc titanates have the advantage of increasing the feasible temperature range, but loss of ZnO and thus decreased sorption capacity over multi-cycle use is still observed.[65]

Bu et al.[65] developed two ZnO-based sorbents consisting mainly of Zn_2TiO_4 with some 2 wt% addition of Cu/Mn oxides for one of the samples. They examined the sorbents in different tests for physical properties, attrition resistance and desulfurization capabilities under different conditions. Fixed bed testing within the temperature range from 450 to 800 °C with a gas composition of 20 vol% H_2, 15 vol% H_2O and N_2 as balance showed an optimum temperature around 700 and 800 °C, respectively, depending on the sorbent tested. In 17 repetitive cycles the sorbent capacity declined by 14 wt% concerning sulfur loading. In a real hot coal gas environment (15-17 vol% H_2, 12–15 vol% CO, 0.7–1.6 vol% CH_4, 11.7–13.1 vol% CO_2, 53–56.5 vol% N_2) at a temperature of about 500 °C sorption tests in a circulating fluidized bed yielded a desulfurization of about 7000 ppm to 13 ppm_v.[65]

Manganese: Being a cheap sorbent with good regeneration and thermal stability properties, manganese oxide exhibits some benefits as sorbent material.[51] It is proposed that manganese sorbents are especially suitable for the use in high steam and high carbon syngas environment as occurring in biomass gasification.[87] Intense analyses of MnO as sulfur sorbent for coal derived syngas have been carried out by Slimane et al.[75,94,95] pointing out the stability of Manganese sorbents against reduction or volatilization even under changing process conditions as a major favorable feature of this sorption material. The high melting point of all formed manganese species enables the long term use at temperatures in excess of 800°C without significant volatilization of the sorbent.[75]

Fixed bed testing of a manganese-based sorbent material developed by Slimane et al.[75] revealed a residual sulfur concentration of about 222.5 ppm_v after fixed bed testing with a simulated coal gas (13 vol% H_2, 24 vol% CO, 5 vol% CO_2, 5% H_2O, 3% H_2S, 50 vol% N_2) at 900 °C. This is close to the calculated equilibrium concentration of 256 ppm_v under these conditions. Another discovery was the improvement of sorbent kinetics after consecutive loading and recycling tests, after recovery of the sorbent at temperatures above 900°C in air. In order to lower the achievable equilibrium H_2S level Alonso and Palacios[96] investigated the combination of manganese based sorbents with either 10 mol% CuO or ZnO in a quartz tube reactor at 700 °C with gas composed of 1 vol% H_2S, 10 vol% H_2, 5 vol CO_2, 15 vol% CO, 15 vol% H_2O and N_2. With no measureable positive effect of CuO addition, the addition of ZnO revealed its effect by x-ray diffraction (XRD) analysis, showing - with 77% compared to 22 % - a significantly higher share of tetragonal Mn_3O_4 crystallite phase in the sorbent structure. This change in crystallite structure results in a higher sorbent performance with Mn_3O_4 having the

highest equilibrium constant among Manganese oxides. Even after 70 cycles of sulfidation and regeneration, the concentration of H_2S in the outlet gas is about 5 ppm, showing that ZnO is still present in the crystallite lattice.

Copper: The use of CuO-based sorbents under the above mentioned conditions of high temperature and reducing syngas atmosphere is also questionable due to the reduction to elemental Cu resulting in a relevantly higher equilibrium concentration of H_2S. Furthermore, the use of elemental copper in high temperature environments is potentially critical due to sintering effects.[97] Besides the sintering of different particles, a layer formation of sintered CuS has been documented to form on the particle surface and thus reduce the sorbent utilization by increasing the diffusion barrier for a desulfurization reaction.[98,99]

In order to stabilize copper in an oxidized state different sorbent supports like Al_2O_3[100], Cr_2O_3[97,101], SiO_2 and TiO_2 or mixed metal combinations like Cu-V[102], Cu-Mo, Cu-Mn[103], and Cu-Ce[87] were tested for their suitability. Stemmler et al.[86] investigated an in-bed desulfurization concept for the Güssing gasifier (Figure 2-4). They achieved a desulfurization of 350 to 250 ppm_v with simulated Güssing-gas-composition (Table 2-6) using CuO-Olivine as sorbent at 800-900°C under fixed bed conditions. These results are close to the equilibrium H_2S levels for metallic copper, indicating no stabilization effect from Olivine. Abbasian and Slimane[97] as well as Li and Flytzani-Stephanopoulus[101] investigated the use of Cu with Cr_2O_3 and Cu with CeO_2 as sorbent combinations. Such stabilized Cu sorbents were tested in the temperature range from 650-850 °C in a fixed bed reactor with gas consisting of 20 vol% H_2 and 10 vol% H_2O in N_2. Desulfurization levels of 5-10 ppm H_2S were reached, being far below the equilibrium level for elemental Cu thus demonstrating the occurrence of synergetic effects of mixed metal sorbents. For Cu/Cr_2O_3 sorbent the formation of a stable $CuCr_2O_4$ phase was confirmed, whereby for CuO/CeO_2 the reduction of Cerium and thus its participation in sulfidation is attributed to the good sorbent performance. Further investigations on the interaction between ceria and copper have been undertaken, proving this effect.[104] Considering economic aspects, CuO-sorbents are more expensive than ZnO-based sorbents. CuO supported on Cr_2O_3 and doped with other metals is commercially available as the so-called Adkins-catalyst, used in the conversion of fatty acids or other oleochemical applications. The use of such Cu-based material might be beneficial compared to ZnO due to superior behavior concerning multi-cycle use. Abbasian et al.[97] investigated the reforming properties of CuO/Cr_2O_3 sorbents in a simulated coal derived syngas (10 vol% H_2, 20 vol% CO, 10 vol% CO_2, 10 vol% H_2O, 2 vol% H_2S in N_2). After cyclic sulfidation and regeneration at a temperature of 600 °C and 750°C respectively, they stated an increase in desulfurization capacity over the first 14 cycles. After 20 loading cycles no significant deterioration of the sorbent capacity was observed.

Calcium: Concerning sorbent cost, availability and toxicity, calcium-based sorbents show superior properties as compared to the above-mentioned materials. Calcium based sorbents are naturally occurring as limestone or dolomite, where the latter consists of a mixture of $CaCO_3$ and $MgCO_3$ with a $MgCO_3$ content of commonly 20 – 45 wt%.[81] The composition of different minerals and content of trace elements varies according to the natural origin of the sorbent material. Yrias et al.[81] have compared different dolomite and limestone compounds according to composition and desulfurization performance. In this context, Zevenhoven et al.[105] concluded that a general statement about the performance of different calcium-based sorbents is not advisable, as the observed initial reaction rates and product layer diffusion could not be attributed to porosity but rather to influences of other catalytic metals contained. Therefore, the contents of trace elements in these sorbents and interactions thereof have a scope of impact that is beyond single metal oxide assessment. As in-bed

sorbents, calcium based materials show a favorable temperature dependence of reactivity for the use above 800 °C as occurring in fluidized bed gasification. Superimposed to the equilibrium of sulfidation (Eq (16)) the carbonate equilibrium determines the present form of Ca-sorbent according to Eq (31). The calcined form, occurring at increased temperature (Figure 2-7), shows a significantly higher reactivity towards CaS formation, resulting in lower limits of the desulfurization equilibrium for calcined lime.[106]

According to literature, H_2S equilibrium values based on calcined CaO as sorbents range between 100-500 ppm_v depending on the gas composition and steam content at around 800-900 °C.[81,106] Still Stemmler et al.[86] tested different Ca-based sorbents with simulated Güssing Gas composition (Table 2-6) and achieved a desulfurization down to 190 ppm for dolomite and 50 ppm for slag lime which is far below the calculated CaO-based equilibrium.

Barium: Barium is present as a stable carbonate even at temperatures far above 800 °C (Figure 2-7). As $BaCO_3$ is not favorable for desulfurization purposes and less affine towards formation of sulfide as compared to calcium, the application of barium as desulfurization sorbent is commonly not considered in the context of syngas desulfurization.[63,91] In a recent work conducted by "Forschungszentrum Jülich", a novel BaO-based sorbent has been synthesized with the aim of stabilizing barium as BaO.[86] The sorbent consists of a mixed solution phase of BaO in CaO. In order to achieve a solubility of BaO in CaO, the sorbent is tempered at a temperature of 1600 °C. The preparation procedure of this sorbent (CaBa) is supposed to stabilize BaO in its oxidized form and prevent the formation of $BaCO_3$, which would normally occur under the influence of a carbon rich atmosphere present in syngas.[86]

The recently developed CaBa sorbent validated the potential of stabilized BaO, and was successfully tested in fixed bed application in a plug flow reactor.[86] A desulfurization from 400 ppm_v down to below 0.5 ppm_v H_2S was demonstrated with bottle mixed syngas containing 17 % H_2O. The stabilized BaO has an equilibrium-constant high enough to desulfurize the syngas to such low levels if the temperature level is kept above the calcination temperature of the embedding CaO-phase. According to experimental results, even a dechlorination down to below 0.5 ppm HCl is possible at a temperature level of 800-900 °C. The regeneration of this sorbent has to be experimentally confirmed, but according to Stemmler et al. a regeneration could be possible by cooling down the sorbent under non oxidizing atmosphere, thus preventing the formation of barium sulfate.[86] Still attrition of the sorbent might prevent ongoing multicycle use.

Iron, cobalt and tungsten-based sorbents are not further considered, as thermodynamics predict a significantly lower potential under high steam conditions and thus a low capture efficiency at the intended process conditions.[91,106] An overview of some relevant results in literature that sufficiently represent the conditions of in-situ desulfurization is given in Table 2-8.

Table 2-8: Results for the application of different sorbents for hot gas desulfurization under according to literature, conditions: BG - bottle mixed gas, GG - gasifier gas

Sorbent material -	Conditions	Temperature / Pressure$_{abs}$ °C/bar	Gas-composition Vol %	Initial H_2S Vol%	Residual H_2S ppm_v	References -
Zn_2TiO_4 + 2 wt% Cu/Mn	GG	450-800/1	H_2:15-17, CO: 12–15, CH_4: 0.7–1.6, CO_2: 11.7–13.1, N_2: 53–56.5	0.7	13	Bu et al.[65]
CuO	BG	800-900/1	36 H_2, 11 CO_2, 25 CO, 17 H_2O, 4 N_2, 7 CH_4	0.04	250	Stemmler et al.[86].
Cu-Mo-Mn-zeolite	BG	871/2	13.8 H_2, 11 CO_2, 12.5 CO, 1 CH_4, balance N_2	0.2	100	Gasper- Galvin et al[103]
Cu-Cr-O	BG	650-850/1	20 H_2, 10 H_2O, balance N_2	2	5-10	Li et al.[101]
MnO	BG	800-1000/1	13 H_2, 24 CO, 5 CO_2, 5 H_2O, balance N_2	3	200	Silmane et al
Mn-Al-O	BG	400-1000/1	17 H_2, 2.1 H_2O, 35 CO, balance Ar	0.6	5	Bakker et al.[88]
90 mol% MnO+ 10 mol% ZnO	BG	700/1	10 H_2, 5 CO_2, 15 CO, 15 H_2O balanceN_2	1	5	Alonso et al.[96]
CaO	BG	800-900/1	36 H_2, 11 CO_2, 25 CO, 17 H_2O, 4 N_2, 7 CH_4	0.04	190	Stemmler et al.[86].
BaO in CaO	BG	800-900/1	36 H_2, 11 CO_2, 25 CO, 17 H_2O, 4 N_2, 7 CH_4	0.04	< 1	Stemmler et al.[86].

Reviewing experimental results shows that through the use of stabilized sorbents in a fixed-bed set up, residual H_2S contents of about 10 ppm_v have been achieved for various sorbent combinations under high temperature conditions. This accounts for $ZnTiO_4$ mixed with traces of Mn and Cu[65], CuO-sorbent on Cr_2O_3,[101] Mn_3O_4 sorbent with addition of ZnO[96] and BaO sorbent stabilized in a CaO solid solution[86]. Still the steam content being essential for sulfidation equilibrium is usually lower as most of the former research is dedicated to coal gas desulfurization. High steam conditions have been investigated by Cheah et al. resulting in insufficient desulfurization results for the tested CeCuO and Mn-sorbents.[87] On the other hand, the results by "Forschungszentrum Jülich"[86] demonstrate that achieving a residual H_2S content of less than 1 ppm_v is possible under high temperature and high steam conditions.

According to thermal limitations and after consideration of kinetic properties and data from literature, a limited group of sorbents remain as potentially suitable candidates for in-situ desulfurization. This includes manganese, copper, calcium and stabilized barium which are considered for further evaluation within the presented work.

3 Motivation and Approach

In gasification technology, cold gas cleaning processes are state of the art, with an example shown in Figure 2-5. A major improvement in the overall efficiency of synthesis processes can be achieved if excessive temperature changes due to cooling of the gas to temperatures below 30 °C, needed for tar removal, are avoided. Additionally the reduction of temperature in a tar loaded gas is likely to cause operational problems due to tar condensation related fouling on heat exchanger surfaces.[5,46] A promising alternative approach is the conversion of tars over a Ni-catalyst during methanation at a medium temperature of 500 °C. This process setup comes along with the benefit of transforming a major part of the heating value contained in the biomass tars into the produced SNG. A necessary requirement for such a Ni-based catalytic conversion is the upstream removal of sulfurous compounds as these would act as a poison on downstream catalysts. With the intended conversion of tars, the removal of sulfur necessarily has to be established above the incipient condensation temperature of tars. Intensive research has been conducted for removal of sulfur in the mid or high temperature range, especially in the field of coal gasification. Due to the high cost of most adsorbent materials investigated under research conditions, a multi-cycle use without degradation would be indispensable to warrant their deployment in process applications. ZnO is a standard adsorbent material, used for desulfurization in the small to midscale power range at medium temperature. Adsorbent materials based on ZnO offer a suitable combination of a comparatively low price and a low desulfurization equilibrium in the range of 1 ppm_v H_2S at moderate temperatures in the range of 300-450 °C.[51] With the comparatively low sulfur content of a gas derived from wood pellet or wood chip gasification in the range of 20 to 100 ppm_v, the application of ZnO based materials might be a reasonable option.

With the aim of increasing the margin of profitability in the production of SNG and other synthesis products from fluidized bed gasification of biomass, the use of cheaper alternatives to wood seems a viable solution. The drawback of such alternative fuels is their higher content of trace elements and sulfur, leading to an increased release of H_2S during gasification (Table 2-2). Once the sulfur content in the gas increases, a desulfurization based on the fixed bed application of ZnO will easily negate the benefit of a cheaper fuel by increased consumption of sorbent. The regeneration of ZnO-based sorbents did not prove successful to compensate for the increased consumption in long term studies based on real gasifier derived syngas.[64] Besides the options for sulfur removal downstream of the gasifier, an in-situ removal of sulfur directly within the fluidized bed of the gasification reactor opens up the opportunity of application of cheap or multi-cycle materials in a simplified process design as shown in Figure 3-1.

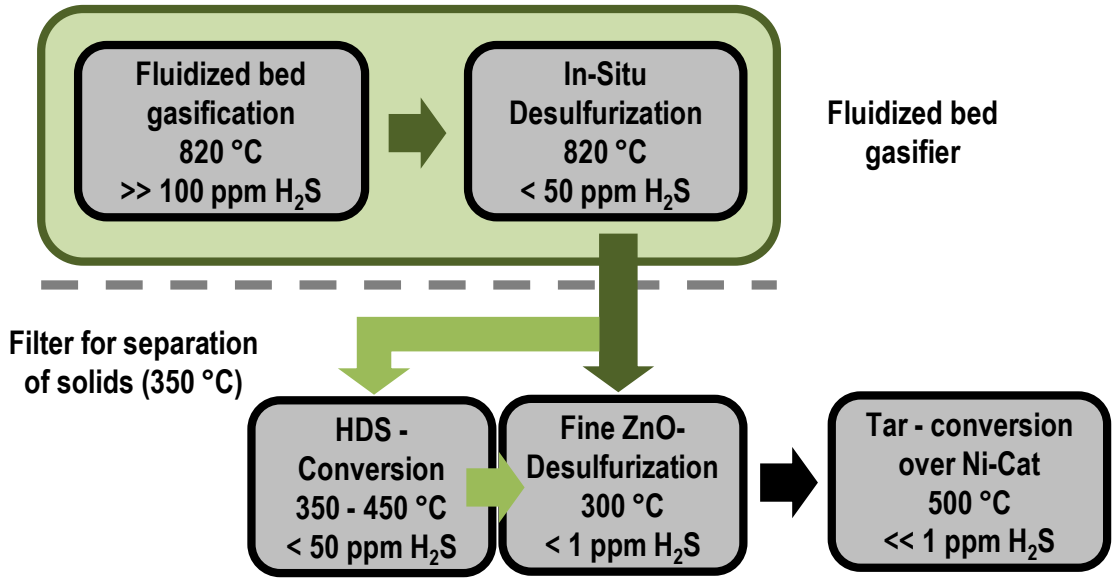

Figure 3-1: Concept for optional subsequent steps in a combined hot gas cleaning process[107]

Depending on the achievable level of H_2S by in-situ desulfurization, different optional process routes might be applicable as depicted in Figure 3-1. This includes an HDS - conversion step to convert organic sulfurous compounds to H_2S once organic sulfurs rise to a crucial level with an increased sulfur content of the fuel. The H_2S is then captured as ZnS in the downstream deep cleaning unit based on ZnO fixed bed adsorption. The number of necessary cleaning steps in this concept depends on the effectiveness of in-situ desulfurization. With the aim of simplifying the process of hot gas cleaning, the implementation of in-situ desulfurization would ideally allow for a direct ZnO-based fixed bed desulfurization with consecutive conversion of tars over a Ni-catalyst. As the conditions inside the fluidized bed reactor are detrimental concerning the thermodynamics of sulfur sorption and require attrition and heat resistant sorbent materials, the implementation of in-situ desulfurization as an effective and competitive process step is challenging.

Inferentially the objective of this presented work was to investigate suitable materials for the application as in-situ desulfurization sorbents. Besides requirements concerning the thermodynamic and mechanical suitability, the sorbent material has to be the better economic option as compared to mere ZnO-based fixed bed desulfurization. The assessment of suitable sorbent materials was first investigated by means of thermodynamic equilibrium calculations in order to analyze the theoretical minimum value of achievable desulfurization. The most suitable materials were then tested in real gasification experiments based on a fluidized bed gasification test rig in the range of 2.5 kW fuel input. This gasifier was applied for the production of a sulfur-enriched syngas produced by means of allothermal gasification of wood pellets at atmospheric pressure. An elevation of sulfur content in the gas was established by the addition of CS_2 together with steam as the gasification agent. The evaluation of in-situ desulfurization was based on the decline of residual sulfur content upon the addition of sorbent materials to the fluidized bed of the gasifier. With respect to the accordance between thermodynamic simulations and the obtained experimental results, a parameter study of the gasification conditions was conducted. The experimental results are concluded with an economic evaluation in order to assess the options for process improvement by implementation of in-situ desulfurization as compared to mere ZnO-based fixed bed desulfurization from an economic point of view.

4 Thermodynamic assessment of sorbent materials

The thermodynamic processes in a real gasification reactor are of utmost complexity and consist of various parallel steps including heat transfer, mass transfer and numerous chemical reactions. Inferentially, calculating the equilibrium of a set of single chemical reactions is not a useful tool for describing the behavior of the overall system. In order to predict the achievable residual H_2S content of the gas phase under application of different metal oxides for in-situ desulfurization, a numerical assessment of the thermodynamic equilibrium is more appropriate. With the aim of evaluating the thermodynamic limitations of different sorbents for in-situ desulfurization, such a numerical thermodynamic simulation was performed. The conditions, assumptions and the obtained results are elucidated subsequently.

4.1 Simulative conditions & assumptions[1]

Most of the published experimental results for H_2S sorption equilibria are destined for coal derived syngas composition (Table 2-8). Such syngas contains less steam, as coal is usually gasified in oxygen with little or no steam added.[76] Thus the results are not directly transferable to the syngas obtained from gasification of biomass in allothermal steam gasification with relevantly higher steam content as elucidated in section 2.5.1. In order to generate a better prediction of achievable H_2S concentrations in the syngas after in-situ desulfurization, gasification conditions of the gasification test rig at TU Graz (Figure 5-1) were simulated under application of the program FactSage 6.4.[90] For the theoretical calculation of the equilibrium composition of the gas phase, with special respect to the content of residual sulfur, the FactSage 6.4 Gibbs energy minimization tool was applied.[90]

The applied system allows for the calculation of complex multicomponent systems by the standardized collection of heat capacity data. Several additional databases are available to include the influence of for example magnetism or other complex interactions that might affect the phase equilibrium.[90] For the assessment of results in the presented work, Fact Pure Substances database and Factmisc database were included in the calculation, as the contained thermodynamic data for the System S-Fe-Mn-Cu is more specific within this extended set.[90] The calculation of ash composition is contained according to the content and composition of ash forming elements that are set as input value for the calculation.

The simulated results are destined as a preparative study for successive experimental investigation with a fluidized bed gasification test rig at TU Graz (Figure 5-1). Wood pellets are the standard fuel for gasification experiments performed in the BFBG at TU Graz. In opposite to many high sulfur fuels, wood pellets have a low content of ash forming elements and can therefore be gasified under long-term stable conditions without detrimental effects like defluidization of the fluidized bed inside the gasifier With the objective of reproducing the permanent gas composition of experimentally

[1] Segments of this section have already been published by Husmann *et al.*[27]

obtained syngas, the input of elements for simulation, was chosen according to an elemental analysis of the wood pellets applied as standardized fuel. The elemental composition is shown in Table 4-1.

Table 4-1: Ultimate and proximate analysis of the wood pellets applied as fuel

Component	Unit	Content
C	wt%,dry	51.2
H		6.1
O		42.8
N		0.36
Ash	wt%,dry	0.4
Fixed C		16.2
Humidity	wt%	8.4
Cl	wt‰,dry	0.03
S		0.16
Ca		0.91
K		0.32
Mg		0.13
Na		0.01
P		0.47
Si		0.15

The analyzed sulfur content of the applied wood pellets is 0.016 wt% (+/- 10 $\%_{rel}$), which results in a syngas with a H_2S fraction of about 20 ppm_v under the given conditions of gasification explained in section 5.1. This is below the level of thermodynamic equilibrium for most sorbents at 820 °C, therefore no formation of sulfide (Eq (16)) would occur. In order to determine the equilibrium content of H_2S in the presence of different in-situ sorbents, the input value for the sulfur content of the fuel has been raised for simulation. The standard sulfur content was elevated from 0.016 wt% dry biomass to 0.48 wt% dry biomass resulting in a gaseous volumetric H_2S content of about 1400 $ppm_{v,dry}$ according to simulation. This sulfur content represents, for example, a mixed gasification of sewage sludge and wood chips (Table 2-2). Other input parameters like the content of ash forming elements were left unchanged compared to wood pellet composition. The applied method allows for the selective investigation of desulfurization properties without the complex influence of ash related issues in gasification of biomass. This accounts for a simulative approach as well as for an experimental confirmation of theoretical results as elucidated in subsequent sections of this work.

Under simulated equilibrium conditions the methane content of the gas is negligible at 800 °C. This is not in accordance to the actual composition obtained by measured data (Table 4-2). Therefore, the detected fraction of about 5-10 $vol\%_{dry}$ methane in the syngas under experimental conditions, was transformed into N_2 and added to the inert N_2-fraction of the simulated gas. In order to maintain the elemental balance, the contents of carbon and hydrogen destined to form methane were subtracted from the original fuel composition according to Stemmler et al.[86] Deviations due to formation of higher hydrocarbons, nitrogen compounds and tars are of minor impact[48] and therefore not

considered in this simulative approach. Variations of sorption equilibria have been numerically examined in the temperature range between 600 – 1000 °C as this covers most of the data from literature considered as hot gas cleaning.[51]

The influencing factors studied within this work via thermodynamic assessment are:

- the steam content in the syngas
- the operational pressure of the gasifier
- the sulfur content
- the sorbent content

The variation of the steam content was performed according to different distinct values of the steam-excess-ratio. The steam-excess-ratio σ is defined as shown in Eq. (22) and calculated as demonstrated below. It refers to the mass ratio of steam, used as gasification agent in fluidized bed gasification and was adjusted as an input value for simulation.

$$\sigma = \frac{\zeta_{H_2O}}{\zeta_{H_2O,min}} \quad \textbf{(22)}$$

The mass ratio of steam entering the reactor is indicated by ζ_{H_2O}. The value $\zeta_{H_2O,min}$ indicates the minimum amount of steam for stoichiometric gasification. As follows from the gasification reaction (Eq. (23)), $\zeta_{H_2O,min}$ can be determined as shown in Eq. (24). With a known elementary composition of the fuel, the molar ratios of oxygen and hydrogen, ν_2 and ν_1, as well as the molar weight of the fuel $M_{CH_{\nu_1}O_{\nu_2}}$ can be calculated. $w_{H_2O,Fuel}$ indicates the mass fraction of water in the fuel.

$$CH_{\nu_1}O_{\nu_2} + (1-\nu_2)\cdot\ H_2O \leftrightarrow CO + \left(\frac{\nu_1}{2} + 1 - \nu_2\right)\cdot H_2 \quad \textbf{(23)}$$

$$\zeta_{H_2O,min} = \frac{M_{H_2O}}{M_{CH_{\nu_1}O_{\nu_2}}}\cdot\ (1-\nu_2)\cdot(1-w_{H_2O,Fuel}) \quad \textbf{(24)}$$

Under real experimental conditions, a steam-excess-ratio of 4 proved to yield the most stable operational conditions of gasification.[37] Under simulated conditions, the steam excess ratio was varied in the range from 4 to 8 such as to evaluate the influence of the resulting steam content under thermodynamic equilibrium conditions. As standardized input for thermodynamic calculation, the amount of sorbent for desulfurization was set as 1 mol% of the overall elemental input values of components. With these elemental input values, obtained by fuel analysis, steam-excess ratio and additional considerations like an increased sulfur content and suppressed formation of methane, the equilib tool of FactSage 6.4 then calculates the overall thermodynamic equilibrium of formed products according to Eq (18). The input setting of 1 mol% of sorbent for desulfurization is a clear excess to the necessary amount for stoichiometric conversion according to Eq (16) with a ratio of sorbent to sulfur of around 15. For CaO sorbent this equals a content of 10.8 wt% of the fuel input.

Except for the formation of methane, no product component was suppressed in its formation as standard settings of thermodynamic assessment. On the other hand only the permanent gas components H_2, N_2, CO, CO_2 plus steam and H_2S are present in the gas in contents above 10 ppm_v according to thermodynamic equilibrium calculation. In order to simulate the equilibrium of the

reaction between BaO and H_2S under formation of BaS, the carbonization of BaO to $BaCO_3$ had to be suppressed by excluding the formation of $BaCO_3$ in the equilibrium calculations. Under the investigated process conditions, BaO would be readily converted to $BaCO_3$ at thermodynamic equilibrium. However Stemmler et al. experimentally confirmed the stabilization of BaO by formation of a solid solution with CaO resulting in a mixture of about 10 mol% BaO in CaO.[86]

4.2 Results of thermodynamic assessment[1]

As a first preparative step for later experimental evaluation of suitable sorbent materials for in-situ desulfurization, a fact-sage based thermodynamic calculation was performed according to the boundary conditions described in section 4.1. Regarding the predicted composition of the syngas, equilibrium calculations do not produce the same results for the corresponding input of fuel and steam in experimental investigations. Simulation of the gas composition with data obtained from fuel analysis (Table 4-1) and a steam-excess-ratio of 4 resulted in higher hydrogen and lower steam content as compared to experimentally obtained data from gas analysis at the same input ratio. A comparison of simulated and experimentally determined gas composition from experiments at Graz University of Technology (Figure 5-1) is shown in Table 4-2 for different set values of steam-excess-ratios for the simulated gas compositions at a temperature of 820 °C.

Table 4-2: Comparison of simulated and experimental gas composition

Data		Simulated					Experimental
Steam-excess-ratio	-	4	5	6	7	8	4
Steam content	mol%	29.0	34.7	39.6	43.9	47.6	40.2
H_2	mol%	35.4	33.1	31.1	29.2	27.5	23.7
CO_2	mol%	11.7	11.9	11.8	11.6	11.3	11.4
CO	mol%	14.0	11.1	9.0	7.7	6.4	15.0
$N_2 + CH_4$	mol%	9.8	9.0	8.2	7.7	7.1	9.8

The steam content of about 40 vol% present in the syngas under experimental conditions (Table 4-2) originates partly from the fuel with a water content of about 8 %. Mostly it originates from the steam that is used to fluidize the bed material and acts as a gasification agent in the BFBG. According to studies on coke formation on downstream catalytic gas cleaning units and validation of stable process conditions conducted by Kienberger[37], a steam-excess-ratio of 4 has been established as standard process condition for the evaluated gasification process. The steam content in the syngas is also influenced by gas phase reactions like the water-gas shift reaction (Eq (6)) and methanation reaction (Eq (7)) whereby the formation of methane is suppressed in the simulative approach as explained in section 4.1.

[1] Segments of this section have already been published by Husmann *et al.*[27]

For the same input values with a steam-excess-ratio of 4 the simulated gas consists of only 29 vol% steam as compared to 40 vol% in the experimentally obtained syngas. This difference is explained by a non-equilibrium state in real process conditions, which becomes obvious by the presence of methane that is predicted to substantially not exist at temperatures above 600 °C according to equilibrium calculations. Within the temperature range from 500 to 1000 °C, the simulated steam content in the gas changes about 16 % according to the temperature dependent shifts in the equilibrium of gas phase reactions mainly Eq (6). As the water-gas shift reaction is slightly exothermic its equilibrium is shifted to the reactant side with rise in temperature, therefore the water content of the gas rises with increased temperature. Comparing the total steam content in the gas with respect to its dependence on the steam-excess-ratio listed in Table 4-2, a steam-excess-ratio of 6 most closely describes the composition of experimental syngas obtained with a steam-excess-ratio of 4. The obtained gas compositions provide the background for further simulative assessment of possible materials for sulfur sorption. Under application of FactSage 6.4, specific desulfurization equilibria can be determined for different sorbent materials based on the overall minimization of Gibbs enthalpy for a variation of different influencing parameters.

4.2.1 Influencing parameters

According to the desulfurization reaction (Eq (16)), the achievable desulfurization equilibrium is a function of the steam content and the temperature dependent sorbent specific equilibrium constant (Eq (17)). The Equilib-Tool of FactSage provides the possibility to verify this correlation for different sorbent materials thus taking into account transitions of oxidation state of the sorbent materials and gas phase interactions depending on different gasification conditions.[90] For a better understanding of these influences, a simulative assessment for different sorbent materials has been performed under variation of various parameters. Besides steam content and temperature, these include pressure and the C/H-ratio of the fuel, as well as the amount of sorbent and composition of sulfur species.

4.2.1.1 Steam content

Being on the product side of the desulfurization reaction (Eq (16)) the steam content of the gas has a major impact on the equilibrium between H_2S and sulfide formation. Higher steam contents hinder the formation of metal sulfide and therefore the removal of H_2S from the gas. Inferentially sorbent specific behavior with varying steam content is an essential criterion for the evaluation of suitable sorbents for in-situ application. According to the simulated results, the dependence between the content of steam in the syngas and the residual level of H_2S varies for different sorbents. Therefore, the influencing effects on the changes in the H_2S equilibrium values with varying steam-excess-ratios have to be considered separately for each sorbent.

Manganese is a cheaply available sulfur sorbent that is present at the conditions within the gasifier as MnO. For MnO the desulfurization follows Eq (25) with the corresponding change of equilibrium upon varied steam content shown in Figure 4-1.

$$MnO + H_2S \leftrightarrow MnS + H_2O \quad \textbf{(25)}$$

The effect of steam content and temperature is consistent with Eq (25), as for rising temperature and rising steam content the equilibrium values for H_2S content increase. This is a consequence of the exothermic sulfidation reaction under formation of H_2O.

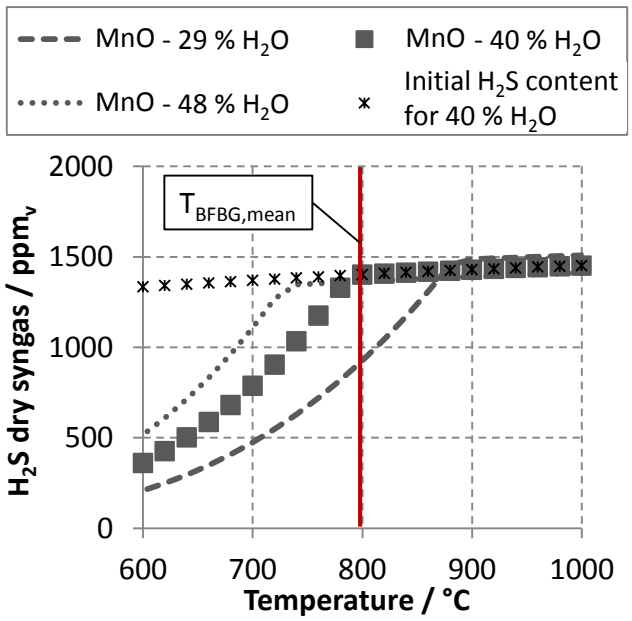

Figure 4-1: Thermodynamic equilibrium curves of manganese-based desulfurization for different steam contents

As shown in Figure 4-1, the calculated equilibrium curves for Eq (25) result in high values of residual H_2S in the gas. At the intended process conditions for in-situ application of about 800 °C and a steam content of about 40 vol%, no sorption of H_2S is predicted by thermodynamics. Even for a lower steam content of 29 vol% the application of manganese for desulfurization does not seem to be a suitable option, as the thermodynamic equilibrium values are still in the range of 1000 ppm_v residual H_2S. Inferentially it can be stated that the use of single metal sorbents based on manganese are not recommendable according to equilibrium calculations, as the values for residual H_2S at 800 °C are generally above applicability.

Copper and copper-based sorbents are known for their high affinity towards sulfur sorption due to the high equilibrium constant of the copper-based desulfurization reaction (Eq (26)) with CuO as the stable oxide.

$$CuO + H_2S \leftrightarrow CuS + H_2O \quad \textbf{(26)}$$

Figure 4-2 shows the simulated sorption equilibrium values for CuO sorbent, whereby copper oxide is readily reduced to elemental copper at the considered process condition over the entire temperature range. This would exclude unstabilized CuO-sorbent in an experimental application, as elemental copper would melt in the fluidized bed and cause defluidization or even evaporate and then condense downstream with the risk of pipe blocking and process failure.

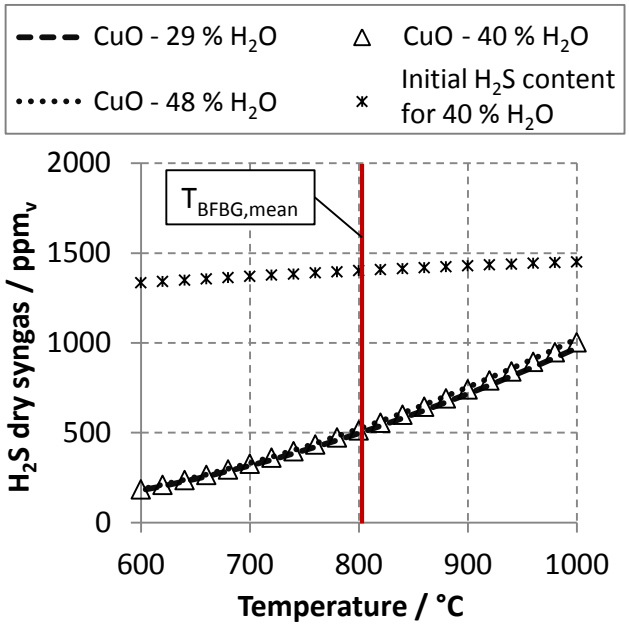

Figure 4-2: Thermodynamic equilibrium curves of copper-based desulfurization for different steam contents

As shown in Figure 4-2 the variation of the steam content of the syngas in the range between 29 and 48 vol% barely shows any influence on the predicted equilibria for H_2S sorption. This is in clear contrast to the simulated results for other sorbent substances. The most pronounced deviation at 1000 °C is only at 5 % between the value for highest and lowest steam content. The observed effect is explained by the application of the law of mass action on Eqs (27), (28) and (29) which are shifted to the reactant side by a higher steam content in the gas and therefore stabilize copper in its oxidized form.[108]

$$CuO + H_2 \leftrightarrow Cu + H_2O \quad \textbf{(27)}$$

$$2CuO + H_2 \leftrightarrow Cu_2O + H_2O \quad \textbf{(28)}$$

$$Cu_2O + H_2 \leftrightarrow 2Cu + H_2O \quad \textbf{(29)}$$

As CuO and Cu_2O show a significantly higher affinity towards the formation of CuS and Cu_2S as compared to elemental copper, the negative effect of steam on the desulfurization reaction (Eq (26)) is negated by its' stabilizing effect on the active form of the sorbent itself. The unconventional behavior of CuO sorbent with varied steam content can be explained further by the rising O_2-partial pressure and lower partial pressures of H_2 and CO (Table 4-2) with rising steam content of the syngas. H_2 as well as CO are strong reducing agents under formation of H_2O (Eqs (27)-(29)) and CO_2. At the intended process conditions and a temperature of 800 °C, the O_2-partial pressure is in the range of 10^{-17} bar under equilibrium conditions. It rises with temperature as exothermic oxygen consuming reactions are shifted towards the reactant side and with a lower ratio of C/O in the gas as is valid for a higher steam-excess-ratio. Therefore, the atmosphere for sulfidation reaction is less reducing at higher steam content, and the influence of CuO on sorption equilibrium is more pronounced.

Calcium as an earth alkaline metal is available abundantly in naturally occurring calcium based sorbent materials such as limestone ($CaCO_3$) and dolomite ($CaCO_3$ + $MgCO_3$). Exposed to the high temperatures of gasification conditions, these minerals undergo the calcination reaction, as shown for dolomite (Eq (30)) and for limestone (Eq (31)). Dolomite is calcined in two steps when temperature is increased, with half-calcined dolomite being the intermediate product.

$$CaCO_3 + MgCO_3 \leftrightarrow CaCO_3 + MgO + CO_2 \leftrightarrow CaO + MgO + 2CO_2 \quad \textbf{(30)}$$

$$CaCO_3 \leftrightarrow CaO + CO_2 \quad \textbf{(31)}$$

The calcination reaction is a heterogeneous equilibrium reaction. This means that the equilibrium constant is a function of the CO_2 partial pressure only as the activity of solids remains constant within the system (Eq (32))

$$K_p = p(CO_2) \quad \textbf{(32)}$$

The partial pressure of CO_2 that is established in a closed system during the decomposition of $CaCO_3$ to CaO is called the decomposition pressure and can be depicted as a function of temperature as shown in Figure 4-3 for a comparison of experimental and theoretical investigations.[109]

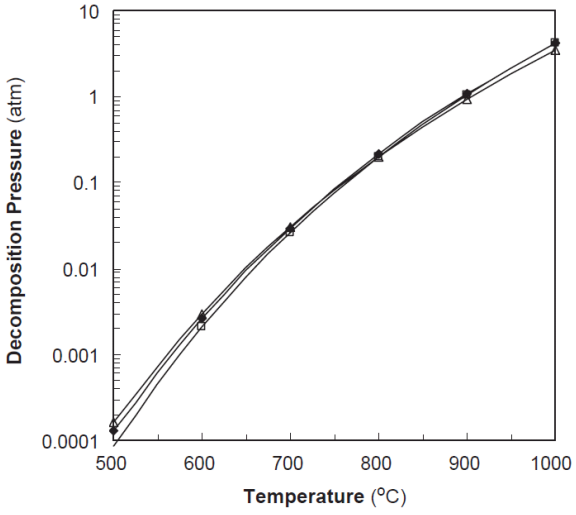

Figure 4-3: Different experimental and simulated results of the decomposition pressure of CO_2 over $CaCO_3$[109]

According to the conducted equilibrium calculations which are presented herein (Figure 4-4), there is only one stable form, so either CaO or $CaCO_3$, present in the system. As the the simulation is conducted under constant pressure conditions and the fraction of sorbent considered in the simulation is at 1 mol % of total reactants, the increase of partial pressure of CO_2 due to calcination is minor. The behavior of partial pressure of CO_2 upon calcination at different constant values of absolute pressure is shown in Figure 4-6. In the considered simulated case with stepwise increments of temperature by 20 K the calcination reaction is therefore not present under equilibrium conditions. The same is the case for industrial calcination applications conducted at a temperature of about 950 °C under non pressurized conditions in an open system. The conversion of $CaCO_3$ to CaO is

therefore only limited by the speed of reaction and not by the equilbrium of the calcination reaction as the CO_2 partial pressure is well below the decomposition pressure at 950 °C (Figure 4-3).[109] An industrial application of the carbonate equilibrium is found in chemical looping processes where CaO is added in excess such as to capture CO_2 from the gas by formation of $CaCO_3$.[13] The extent to which CO_2 can be removed from the system is limited by the decomposition pressure, which marks the equilibrium state of the calcination reaction. As the decomposition pressure decreases with temperature, chemical looping is effectuated at the lowermost allowable temperatures under consideration of the decreasing speed of reaction at low temperatures.[13]

Under real process conditions the calcination reaction does not occur instantly and due to diffusion effects inside the particle a certain delay in the onset of calcination will appear between the outer shell and the inner core of the carbonated particle.[109]

Parallel to the calcination, the desulfurization occurs for both dolomite and limestone in carbonated as well as calcined form. With CaO being the active component and MgO passing through the reaction as an inert,[72] the desulfurization follows according to Eq (33).

$$CaO + H_2S \leftrightarrow CaS + H_2O \quad \textbf{(33)}$$

It has also been shown that a direct desulfurization with uncalcined limestone and half calcined dolomite ($CaCO_3$ + MgO) is possible directly without prior formation of calcined intermediates (Eq (34)).[77]

$$CaCO_3 + H_2S \leftrightarrow CaS + H_2O + CO_2 \quad \textbf{(34)}$$

As MgO is not active towards desulfurization under the investigated conditions of desulfurization, the evaluation of thermodynamic equilibrium is based on calcium alone. The simulated equilibrium curves for calcium as a sorbent material, displayed in Figure 4-4, show a minimum due to the transformation of $CaCO_3$ to CaO (Eq (31)) once the partial pressure of about 0.1 bar CO_2 in the gas phase falls below the decomposition pressure of the carbonate at a temperature of about 760 °C (Figure 4-3).

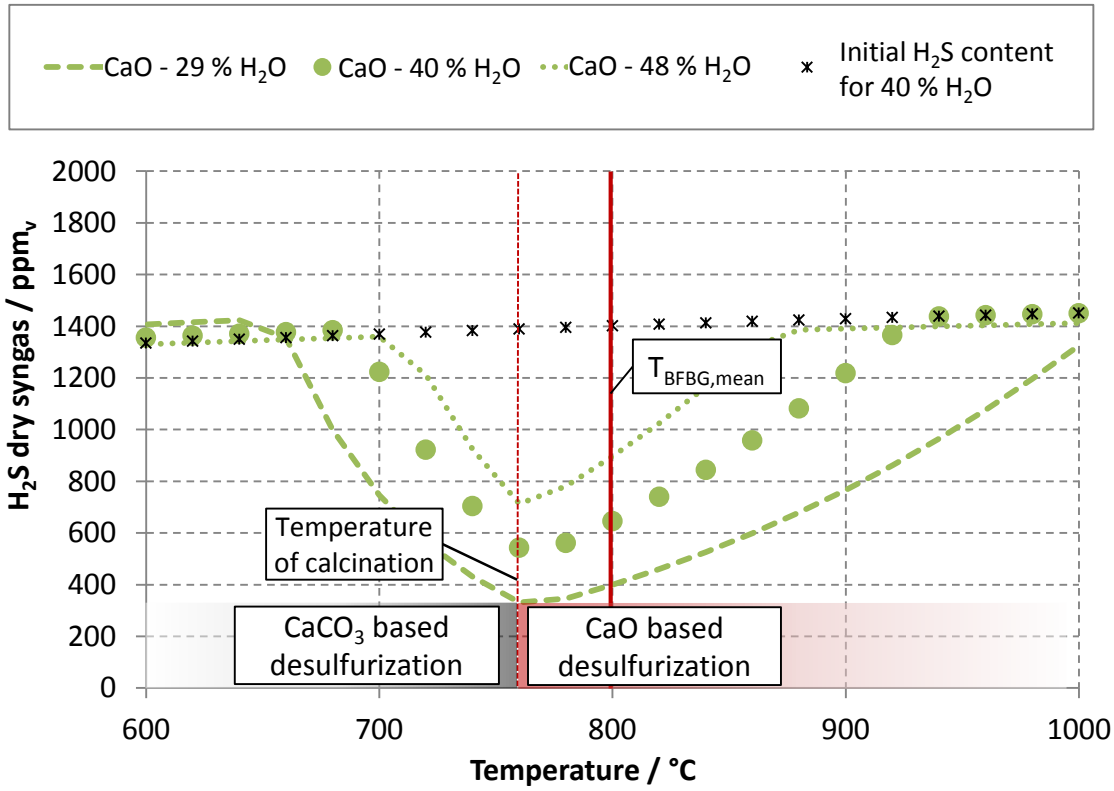

Figure 4-4: Thermodynamic equilibrium curves of calcium-based desulfurization for different steam contents

Until a temperature level of 760 °C, calcium is present as carbonate for the conditions prevailing in the gasification reactor. The minimum temperature allowing the onset of the endergonic calcination reaction depends on the partial pressure of CO_2. Below the temperature of calcination the desulfurization occurs directly by sulfidation of carbonate according to Eq (34).

The onset of carbonate–based desulfurization depends on the steam content in the gas and occurs at higher temperatures for higher steam contents. As shown in Figure 4-4 the equilibrium calculations predict the formation of CaS starting from 720 °C for a steam content 48 vol%, whereas for a lower steam content of 29 vol% the onset of CaS formation starts at about 680 °C. The temperature of initial H_2S-sorption lowers as the difference in chemical potential of the desulfurization reaction (Eq (34)) increases with lower steam content. Therefore the formation of CaS is more favorable for lower steam contents as the equilibrium of Eq (34) is shifted further to the product side. As a consequence, the overall minimization of Gibbs enthalpy yields in the formation of CaS even though the equilibrium of the competitive calcination reaction (Eq (31)) is still on the carbonate side, with no CaO present at temperatures below 760 °C for the simulated gas composition. The minimum of equilibrium curves is equal for the different steam contents and are identical with the temperature of calcination where all the $CaCO_3$ is transformed to CaO. With further rise in temperature, the desulfurization follows Eq (33).

The behavior of CaO-based desulfurization is comparable to that of MnO except for the higher equilibrium constant of CaO, which leads to lower residual H_2S contents even at elevated temperature.

Barium is not commonly considered as active component in the context of syngas desulfurization. This is due to the formation of a stable carbonate ($BaCO_3$) under the carbon-rich syngas atmosphere. $BaCO_3$ does not decompose until temperatures of about 1200 °C and is not an active desulfurization agent, with especially a lower equilibrium constant as compared to $CaCO_3$, which makes it unattractive for gas cleaning purposes. This is in contrast to the application of stabilized BaO in a CaO matrix with very promising results according to previous research.[86] In this mixed sorbent, BaO is the active phase responsible for the equilibrium content of H_2S in the gas phase with desulfurization according to Eq (35).

$$BaO + H_2S \leftrightarrow BaS + H_2O \tag{35}$$

The CaO matrix only stabilizes the BaO against formation of $BaCO_3$. Therefore a prediction of the achievable values for residual H_2S level is valid under consideration of BaO only with simulated exclusion of $BaCO_3$ formation as described in section 4.1. In accordance with research conducted by Stemmler et al.[86] the FactSage 6.4 simulation predicts the achievement of equilibrium values below 5 ppm_v for residual H_2S content in the syngas when using a stabilized BaO-sorbent as shown in Figure 4-5.

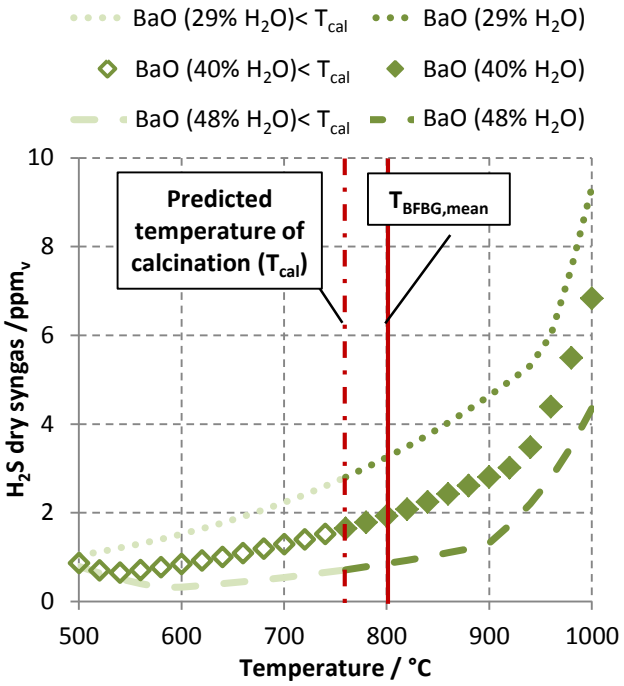

Figure 4-5: Thermodynamic equilibrium curves of barium-based desulfurization for different steam contents

As shown in Figure 4-5, a variation of the steam content from 29 to 48 vol% leads to an increase of the equilibrium values from 0.9 to 3.3 ppm_v H_2S for the mean operation temperature of the gasifier. This is more than two magnitudes below the thermodynamic equilibrium of the other sorbent materials (Ca, Cu and Mn) considered in this thermodynamic assessment. Simulated values for temperatures below the predicted temperature of calcination to CaO (31) have to be considered as theoretical only, as the transformation of the CaO matrix to $CaCO_3$ prevents the sulfidation of BaO to BaS. This has been determined experimentally by an increased residual H_2S content at reduced

temperatures.[86] Therefore an application of this sorbent below calcination temperature cannot be possible under real process conditions. The low simulated values of thermodynamic equilibrium of the desulfurization reaction at temperatures below 760 °C therefore have to be considered as theoretical only. The buckle in the equilibrium curves at elevated temperatures of 900 to 940 °C depending on the steam content, is caused by transformation to $BaOH_2$ and also a theoretical event caused by the suppression of $BaCO_3$ formation in the thermodynamic calculation.

Zinc was also evaluated as applications of ZnO-based stabilized desulfurization sorbents are published in literature.[65] The simulated results for ZnO-sorbent show no unexpected behavior with variation of the steam content. The H_2S equilibrium values for 800 °C range from 123 ppm_v at a steam content of 29 vol% to 274 ppm_v at a steam content of 47 vol%. As an expected continuous volatilization of the ZnO due to significant vapor pressure of elementary zinc at temperatures above 450 °C is not considered in the simulation, simulated data for ZnO desulfurization at 800 °C is not regarded as a realistic preview for experimental results.

4.2.1.2 Pressure

As described above, in the simulative approach the formation of methane is suppressed in order to represent the non-ideal conditions in real gasification experiments. The water-gas shift reaction (Eq (6)) as the main remaining gas phase reaction is equimolar. A pressure-dependence is therefore not expected concerning the composition of the gas phase. The same accounts for the desulfurization reaction itself (Eq (16)) as the conversion of metal oxides into metal sulfides is also equimolar. The influence of pressure on the conversion of oxidation state of sorbents also proved to be negligible. This excludes the conversion of $CaCO_3$ to CaO with the calcination reaction being strongly dependent on the CO_2 partial pressure. Therefore, the pressure influence on CaO sorbent performance is relevant for possible process applications with elevated pressure. This is displayed in Figure 4-6 with the corresponding CO_2 partial pressures. The values are simulated for a gas containing 40 vol% steam thus equaling a steam-excess-ratio of 6. The CO_2 content is approximately 12 vol% (Table 4-2).

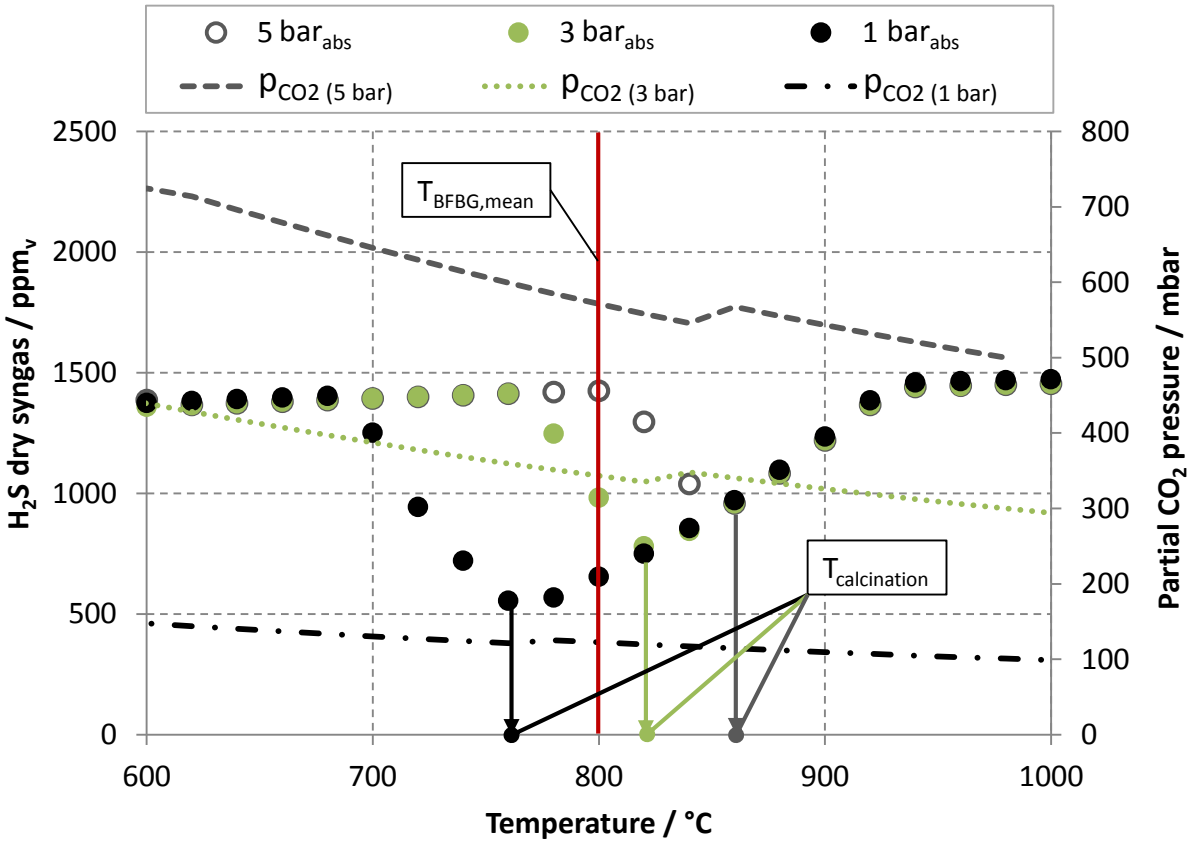

Figure 4-6: Influence of pressure on the calcium-based desulfurization equilibrium with respect to the increased partial pressure of CO_2

As shown in Figure 4-6, the temperature of calcination, which is equivalent to the minimum of desulfurization equilibria, rises with increased partial pressure of CO_2 in accordance with Figure 4-3. This inferentially leads to a rise of the minimum values of residual H_2S in the gas phase. For atmospheric pressure the onset of carbonate based desulfurization (Eq (34)) starts at 700 °C with a minimum of about 543 ppm$_v$ H_2S at 760 °C. At a pressure of 3 bar$_{abs}$ the onset of desulfurization is increased to a temperature of 780 °C with a minimum of the desulfurization equilibrium of 780 ppm$_v$ H_2S at 820 °C which is already above the mean gasification temperature in the investigated gasification process. With a further increase of pressure to 5 bar$_{abs}$ no desulfurization effect is to be expected at a mean gasification temperature of 800 °C and the minimum of desulfurization equilibrium curves is increased to 1000 ppm$_v$ H_2S at 860 °C. It can therefore be stated that in case of the application of a CaO-based sorbent a low gasification pressure is clearly advantageous concerning the achievable residual H_2S content. Even at slightly increased pressures of 4 bar$_{abs,}$ as for example present in the HPR-process (Figure 2-3), the theoretical minimum of desulfurization, given by the thermodynamic equilibrium, is relevantly increased due to the increased partial pressure of CO_2 and therefore inhibited calcination (Eq (31)). Concerning the process operation, a gasification at atmospheric pressure and a temperature in the range of 760 °C would be optimal for CaO-based desulfurization, according to the results presented in Figure 4-6.

4.2.1.3 Sulfur species, sulfur and sorbent content

As the Equilib-Tool within FactSage calculates the overall equilibrium of all the contained substances and the possible formation products, it is only the elemental ratio of the initial compounds determining the product composition. Therefore, the differentiated simulative investigation of sorption equilibria of diverse sulfurous compounds with the investigated sorbents is not possible, as products will always be formed according to the overall minimization of Gibbs enthalpy. Thus the variation of sulfurous input compound does not change the result of minimum Gibbs enthalpy calculations when the elemental ratio of overall input remains unchanged.

The same is true for different sulfur contents in the reaction mixture where variations show little effect on the result of Gibbs enthalpy calculation as long as the sorbent is added in abundance and the sulfur content is small compared to the permanent gas fractions in the syngas. This accounts especially for the amount of steam as product of the desulfurization reaction. In this case the formation of H_2O during sulfidation of the sorbent has a negligible influence on the gas composition and the corresponding thermodynamic equilibria. Variations of the sulfur content of a simulated gasification fuel in the range of below 1 percent therefore do not relevantly shift the corresponding equilibrium of desulfurization as long as the sorbent is present in excess.

The precondition of sorbent excess was true for all the sorbent specific simulations of desulfurization equilibria with a molar stoichiometric ratio of 10 concerning sorbent to sulfur. Some of the sorbents simulated, especially CaO, contribute in the ash forming process and therefore influence the formation of volatile ash components such as KCl or NaOH. But as the content of other ash forming elements is low for simulation of wood gasification, exceeding the stoichiometry for desulfurization leads to deposition of sorbent in the solid fraction. Therefore a variation of sorbent content only varies the solid to gas ratio in the product but the equilibria remain unchanged.

4.2.2 Suitable sorbent materials

The performed parameter variation with respect to the influence on the corresponding equilibrium curves of desulfurization allows conclusions about the suitability of different materials as sorbents for in-situ desulfurization.

4.2.2.1 Evaluation of simulated results

Manganese: For MnO sorbents the calculated equilibrium values confirm a strong influence of the steam content and result in values that do not justify the use of simple manganese sorbents for in-situ application. This does not take into account the possibility of a stabilization of manganese as Mn_3O_4 its most affine oxidation state towards the formation of MnS. A comparison of equilibrium constants for the desulfurization reaction with the different manganese species is given in studies conducted by Bakker et al.[88]. As reported by Alonso and Palacios[96], the addition of 10 mol% ZnO to a manganese-based sorbent can evoke such a stabilization. Equilibrium calculation for Mn_3O_4 under the exclusion of MnO formation predicts a desulfurization down to 48 ppm_v H_2S at 800 °C and a steam content of 40 vol%. To evaluate the possibility of stabilizing manganese as Mn_3O_4 under the intended process conditions the simulated oxygen partial pressure in the equilibrium gas composition with 40 vol% steam content is shown in Figure 4-7 superimposed to a property diagram of Mn-species. The application of equilibrium calculations at low temperatures in the range below

600 °C has to be considered as theoretical only, given that Mn_3O_4 as well as MnO are stable species in air at room temperature.

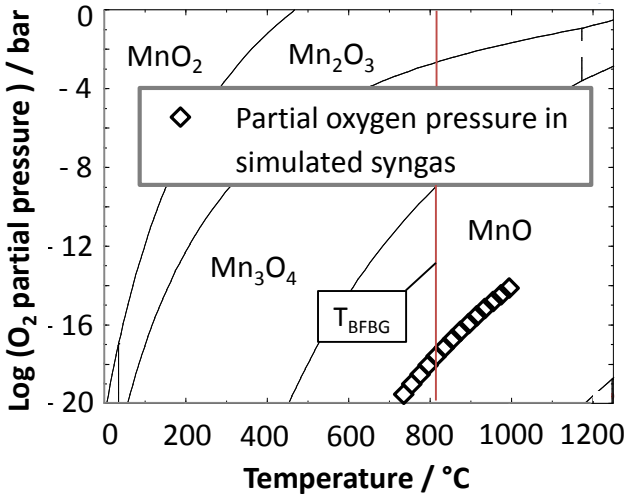

Figure 4-7: Property diagram of manganese in dependence of the partial pressure of oxygen

Rising temperatures and decreasing oxygen partial pressures promote the reduction of MnO_2 to MnO as seen in Figure 4-7. At a temperature of 800 °C a pO_2 of 10^{-4} to 10^{-9} bar would be required to sustain manganese in Mn_3O_4 oxidation state. Clearly the equilibrium state of manganese is the reduced MnO-phase in non-stabilized sorbents for the intended process conditions. The effect of ZnO addition on lattice stabilization against the prediction for single-phase behavior needs experimental assessment. Unless the stabilization in Mn_3O_4 oxidation state can be warranted or further promising results on the combination of manganese and rare earth sorbents under high steam conditions are published, manganese-based sorbents do not seem to be a suitable option for in-situ desulfurization at the investigated process conditions.

Copper: Evaluating the simulated results for MnO sorbents, the influence of the steam content shows a behavior according to the law of mass action with H_2O as the equilibrium-determining component. Due to a superimposed transition of oxidation state, which is delayed by a higher steam content, the variation of the H_2O fraction between 29 and 48 vol% does not significantly influence the H_2S equilibrium value for CuO sorbent. This qualifies stabilized CuO sorbents for potential use under high steam content conditions. On the other hand, even for stabilized Cu-based sorbents a continuous evaporation of elemental copper seems likely for in-bed application at temperatures above 800 °C. Additionally it has to be considered that Cu-based sorbents would only be appropriate for bulk sulfur removal if they were usable in multiple sulfidation-/regeneration-cycles without significant deterioration of the sorbent properties. This is especially valid with respect to the motivation of reducing the overall cost for desulfurization by introducing in-situ desulfurization as a process step for coarse desulfurization (Figure 3-1). In-situ desulfurization is an option of reducing the consumption of ZnO as standard sorbent in fixed bed desulfurization at mid-temperature, whereby ZnO is the cheaper sorbent as compared to Cu-based materials. Inferentially it can be stated that the use of copper-based sorbents, even in a thermally stabilized form, does not seem advisable given the fact that the simulated equilibrium for CuO is in the same range as CaO-based desulfurization under the investigated high temperature conditions of about 800 °C.

Calcium: For the application of CaO-based in-situ desulfurization a minimum residual H_2S content of about 500 ppm_v is predicted (Figure 4-4) for a syngas with a steam content of about 40 vol%. This value is still high and above the upper limit of 100 ppm_v H_2S, depicted in Figure 3-1 as a benchmark criterion for the implementation of in-situ desulfurization. Inferentially the application of a CaO-based sorbent for in-situ desulfurization can only be justified for a syngas with an initial H_2S concentration significantly above the thermodynamic minimum of 500 ppm_v given by the investigated process conditions. Moreover it can be stated that CaO-based in-situ desulfurization would only be suited as a preliminary coarse desulfurization, ideally in combination with other more sophisticated sorbent materials, which allow further in-bed depletion of sulfur from the gas.

Barium: The latter might hold true for the application of a mixed solution phase of BaO in CaO as previously tested by Stemmler et al.[86] The simulated results for this BaO-based sorbent (Figure 4-5) confirm low equilibrium values below 5 ppm_v H_2S for the investigated process conditions. This is more than two magnitudes below the thermodynamic equilibrium of Mn, Cu and Ca, as the other potential sorbent materials considered in the thermodynamic assessment. The obtained simulated results therefore qualify a combined CaO-BaO sorbent as highly promising material for in-situ desulfurization.

Zinc: Simulation for ZnO-H_2S-equilibrium resulted in values of about 200 ppm_v as the equilibrium value at the intended process conditions. As the continuous volatilization of elemental zinc into the gas phase and clogging of the fluidized bed by formation of agglomerates due to sintering of ZnO is not regarded in a simulative approach, these results are not transferable to experimental application. Therefore, if at all, only stabilized ZnO sorbents, as presented by Bu et al.[65], bare some potential to be employed for in-situ desulfurization. Considering the higher cost of stabilized ZnO sorbent and increased equilibrium H_2S levels with increased temperatures, the benefit compared to the employment of untreated ZnO at lower temperatures is doubtable.

4.2.2.2 Comparison with results in literature

Considering the benchmark of mid- temperature ZnO desulfurization, no sorbent based on a single metal oxide seems to be suitable for in-situ application according to the simulated results. Comparing the results obtained by the thermodynamic assessment presented herein, with results from literature as listed in Table 2-8, the conducted thermodynamic simulation predicts relevantly higher residual values of H_2S content. This can be mostly attributed to differences in process conditions concerning the steam content and the reaction temperature as the results in literature are commonly obtained in the context of coal desulfurization. For the example of manganese the thermodynamic equilibrium at 800°C is about 1500 ppm_v H_2S considering a steam content of 40 vol% in the syngas. Slimane et al obtained a desulfurization from 3 % down to 200 ppm_v H_2S in a gas with 5 vol% H_2O at a temperature between 800 – 1000 °C. Alonso et al.[96] developed a manganese based sorbent which allows a desulfurization from 1 % H_2S down to 5 ppm_v at 700 °C and a gas containing 15 vol% H_2O. This is clearly below the thermodynamic equilibrium of single metal MnO-based desulfurization (Eq (25)) at these conditions, but can be attributed to the effect of the addition of 10 mol% Zn to MnO on crystal lattice structure, stabilizing the Manganese as Mn_3O_4.[96] Positive effects may therefore occur by stabilizing interactions between different metal components, which prevent the reduction of metal oxides in the case of stable mixed phases. Further examples thereof are the formation of Zn_2TiO_4 in Zinc-Titanate sorbents[65] or $CuCr_2O_4$ in a combined CuO/Cr_2O_3 sorbent[97,101] Such effects are not considered in the conducted assessment of thermodynamic equilibrium for

manganese, copper and zinc. Solely for BaO the stabilizing interaction with CaO is considered, as the experimental observation was reproducible by a minor manipulation such as suppressing the formation of $BaCO_3$ in the thermodynamic calculation.

Another effect not considered is the influence of traces of other elements such as those present in many Ca-based sorbents. The calculated equilibrium values shown in Figure 4-4 are based only on the CaO-CaS equilibrium at the specific conditions not considering further interactions of the mineral composition or the content of impurities. This includes the neglection of the negative effect of sintering of a CaS layer as documented in case of the application of a pure limestone[110] as well as unpredicted positive results for a slag lime as used by Stemmler et al.[86]

The adsorption of H_2S on the particle surface seems to be another reason for lower experimental H_2S values than predicted by simulated results. By measuring H_2S sorption on manganese and CeO + CuO particles, Cheah et al.[87] observed that by XRD measurements, in accordance with thermodynamic predictions for manganese sorbent, no crystalline phase of MnS was detectable. Yet a desulfurization effect could be measured which indicates surface sorption instead of sulfide formation. For the ceria sorbent the measured sulfur content after desulfurization was higher than the Cu-content of the sorbent, whereby thermodynamics would not predict any formation of Ce_2O_2S- phase under high steam conditions. Thus Cheah et al. concluded that for the prediction of the achievable desulfurization under surface determined conditions, thermodynamic modeling by minimization of Gibbs enthalpy in the bulk phase of the sorbent is not a sufficient tool anymore.[87]

Other influencing factors that need experimental assessment are sorbent specific properties such as catalytic activity towards the conversion of different sulfur compounds. These are not considered in Gibbs enthalpy minimization simulation. The latter can effectively determine the minimum achievable sulfur content in the cleaned gas. This accounts for the example of ZnO-sorbent at lower sorption temperatures where the residual sulfur content is relevantly determined by organic sulfur compounds like thiophenes and COS in the gas.[37] Experimental results also show a variation of kinetics with variation of the gas composition. Cheah et al.[87] observed a major influence of GHSV with increasing steam content whereby necessary residence times increased with elevated steam content of the gas. It is especially true for in-bed applications with statistic residence time distribution, due to sorbent attrition that such influence factors are important for dosage ratio and sorbent content, but are clearly beyond the scope of equilibrium calculation. Inferentially an experimental confirmation of the simulated results is necessary in order to obtain a validated statement about the suitability of in-situ desulfurization under the investigated conditions in biomass gasification.

5 Experimental setup and analytical methods

In the following sections the experimental and analytical setup deployed for the experimental investigations conducted within the presented work is described. Furthermore an overview of the applied measuring technique is given and the relevant analytical methods explained.

5.1 Design of experimental test rig[1]

The experimental investigations are based on gasification experiments in a laboratory scale biomass gasifier connected to a gas manifold, applied for the elevation of sulfur content in the produced syngas.[25,26,37] The setup of these experimental test rigs is subsequently described together with relevant adjustments made for the establishment of long-term stable experimental conditions necessary for the generation of reproducible results.

5.1.1 Gasifier

Experiments were carried out in a bubbling fluidized bed gasifier (BFBG) unit at TU Graz, adapted for high sulfur equilibrium investigations. Biomass is gasified in a bubbling fluidized bed at a temperature of approximately 800°C under allothermal conditions with steam used as fluidization medium.

[1] Segments of this section have already been published by Husmann *et al.*[69,111]

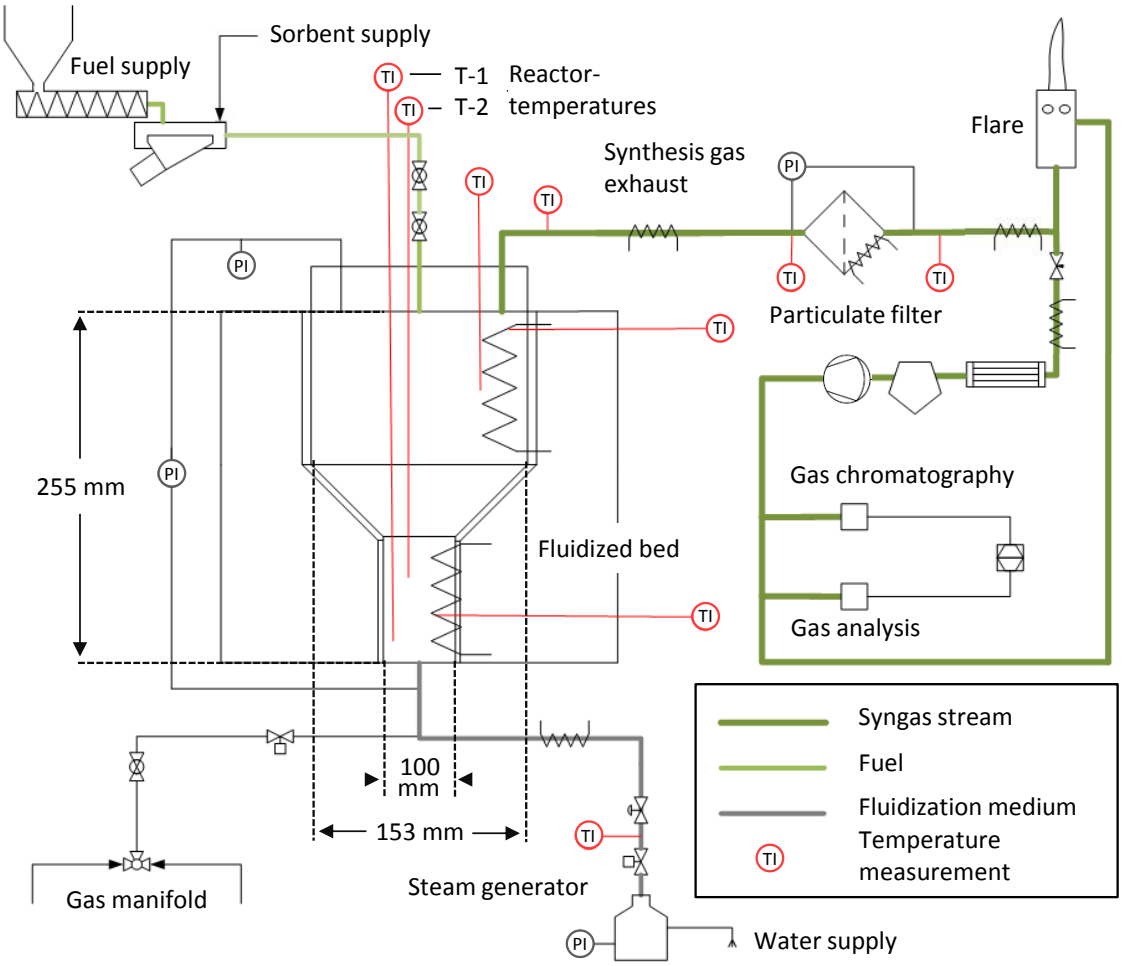

Figure 5-1: Flow chart of the experimental setup[111]

A schematic of the gasification system is shown in Figure 5-1. The fluidized bed as central gasification unit is connected to different parts of an operational periphery, indicated by different colors for the produced syngas stream, the fuel and for the fluidization medium, which is superheated steam. A steam generator injects superheated steam at 650 °C through a nozzle at the bottom of the reactor which diverts the steam to six downward oriented jets ensuring good back mixing and stable fluidization conditions (Figure 5-6). Fluidization is monitored by the spread of temperatures (T-1 and T-2) within the fluidized bed, which are supposed to be roughly equal under fluidized conditions. The temperature inside the steam generator, connected to the reactor by a fixed orifice (Figure 5-2), controls the mass flow of steam entering the gasifier. The mass flow of steam was determined by temperature dependent calibration of the steam generator.

Figure 5-2: Fixed orifice for leveling the amount of injected steam[26]

Steam and fuel supply were calibrated prior to each experiment to yield a rate of 500 g fuel/h and 540 g steam/h for standard operation conditions. This ratio equals a steam to biomass ratio of 1.15 $kg_{steam}/kg_{biomass,dry}$ or a steam-excess-ratio (σ) of 4 (Eq (22)). The experimentally applied steam-excess-ratio of 4 is sufficient for complete conversion of coke as observed in long-term experiments[37] and therefore differs from the settings of thermodynamic simulation as discussed in section 4.1.

The experiments on in-situ desulfurization aim to characterize a process for the application in a gas with high impurities and a sulfur content typical for waste fuels. Such fuels are not easily handled in a BFBG gasification process due to ash agglomeration and sintering of the fluidized bed. The purpose of the conducted study aimed explicitly at the investigation of in-situ desulfurization as process step in gas cleaning. The investigation of technological feasibility of gasification of high ash fuels was not in the focus of the experimental assessment. Therefore, wood pellets were chosen as fuel for gasification. In order to reach representative sulfur contents for the gasification of waste fuels, the sulfur concentration of the gasifier was increased as stated in section 5.1.3. The homogeneity and low ash content of wood pellets ensure long-term stable gasification conditions. This simplification was considered legitimate as the composition of permanent gases does not relevantly change for the use of different solid biomass gasification fuels with similar C,H,O-ratios.(Table 2-2) The ultimate and proximate data of analysis for the applied fuel are summarized in Table 4-1.

A charging screw in combination with a vibrating conveyor implements the dosage of fuel. Fuel is supplied from a hopper (Figure 5-3 (3-E)) to the inlet at the top of the reactor, and inserted by a system of two combined pneumatic ball valves, which act as an air lock (Figure 5-1). Due to the cyclical opening of the air lock, some air and thus nitrogen enters the reactor. This can be seen from the nitrogen fraction in the composition of the resulting gas. Every 90 s an average amount of 12.5 g of pellets is fed into the reactor, resulting in a total fuel mass flow of 500 g/h. With a heating value of 17.6 MJ/kg this equals an average fuel input of 2.45 kW. Temperatures in the reactor are controlled by means of two 3.5 kW electrical heating elements. The temperatures in the reactor are kept at an

average of 775 °C for the fluidized bed, and 825 °C in the freeboard of the reactor. Control of temperatures is enabled by a series of type-k thermocouples located as indicated in Figure 5-1. The reactor itself, shown in Figure 5-7, consists of austenitic steel (1.4841) with dimensions as shown in Figure 5-1. Olivine with a particle size of 200 to 300 µm and consisting of 50 wt% MnO, 42 wt% SiO_2, 8 wt% Fe_2O_3 and traces of NiO and CaO was used as the bed material. Depending on the addition of sorbent, either 1450 or 1500 g of olivine was added to the reactor prior to the experiment. The properties of sorbent added in the course of the conducted experiments are elucidated in sections 6.2.1 and 6.3.1. The particle size fraction used was within 80 to 1000 µm, with details shown in Table 6-2 and Table 6-6, as flow velocities are above the minimum fluidization velocity and below pneumatic transport for particles within this range.

Figure 5-3 shows a picture of the gasification test rig at its final state including the alterations made according to section 5.1.2. The details shown in Figure 5-3 are listed in table Table 5-1.

Table 5-1: Different parts of the gasifier shown in Figure 5-3

3-A	Gasifier
3-B	Steam generator
3-C	Control Unit
3-D	Fuel inlet
3-E	Fuel hopper
3-F	Filter housing for filter candle
3-G	Gas warning unit
3-H	Vent

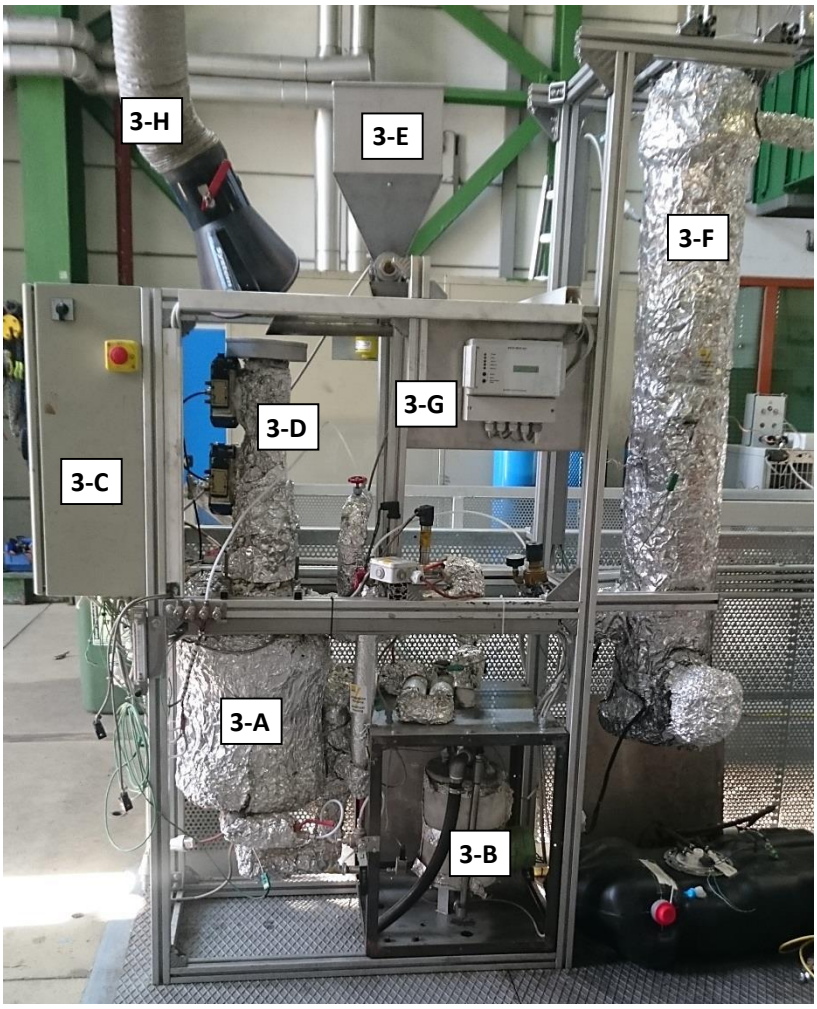

Figure 5-3: Setup of the experimental test rig in final configuration

5.1.2 Improvements in gasifier setup

The described gasifier is part of a test rig planned prior to the beginning of the experiments described in the presented work.[26,25,37] In a series of parameter studies, necessary for the description of the process, influences on the performance of in-situ desulfurization were investigated. For the execution of such experimental investigations, the test rig lacked some relevant features especially warranting the reproducibility of process conditions. The relevant changes in the hardware setup and software configuration are described subsequently.

5.1.2.1 Hardware setup

A feature concerning the reproducibility and monitoring of the process conditions was the replacement of sensors for total- (4-A) and differential (4-B) pressure in a horizontal position as shown in Figure 5-4. These sensors are connected to the high pressure side (4-C) of the gas outlet (4-F) and the low pressure side (4-D) of the steam inlet to the reactor, via heated lines (4-E) preventing the condensation of steam.

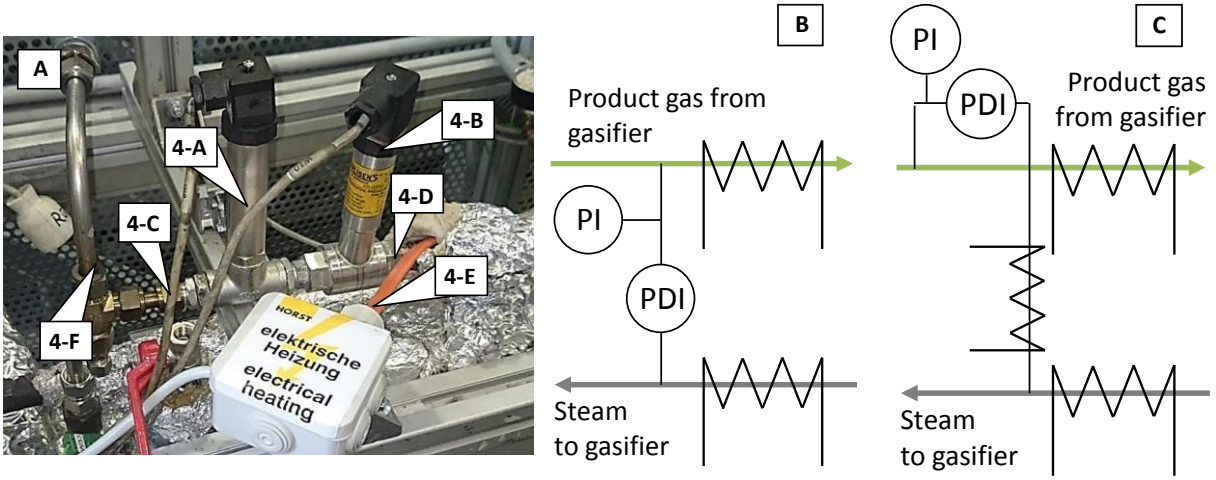

Figure 5-4: (A) Differential (4-B) and absolute (4-A) pressure sensors with additional sampling point for gas analysis (4-F), (B) R&I scheme at initial setup, (C) R&I scheme at final setup

As shown in Figure 5-4 B the sensors were connected to the steam generator and product gas lines in vertical position initially, without insulation or heating, leading to condensation and unreliable values especially regarding the differential pressure. As the differential pressure is now included in the alarm routine of the test rig, initiating an automated shut down if the values were above 90 mbar for 30 seconds, a reliable detection of the differential pressure is crucial. The inclusion of differential pressure into the safety routine is an important feature for increasing the safety during unattended operation as a blocking of the gas outlet of the reactor will be reliably detected and lead to a shutdown of the reactor. This was not the case with the initial configuration as the sensor for absolute pressure was connected to the product gas line and therefore did not detect a pressure increase in the reactor only. The conducted changes in the hardware setup, shown in Figure 5-4 A and C, lead to improved reproducibility of the process conditions. This was achieved by avoiding spontaneous backflow of condensate with erratically changed fluidization conditions by the horizontal positioning of the sensor for differential pressure (4-B) and connection by a heated line. Further an increased process safety was achieved by inclusion of the differential pressure into the safety routine as described above. Furthermore the installation of an additional gas sampling point (Figure 5-4 (4-F)) increased the flexibility and options for analysis of the produced syngas and for investigating the influence of the filter on the sulfur content and gas composition.

Another addition to the setup of the test rig was the integration of a gas warning system into the hardware of the gasifier (Figure 5-3 (3-G)). This was essential for operational security especially under non-attended operation. The gas warning system (5-A) is connected to two sensors (5-B) installed close to the fuel inlet (5-E) of the gasifier as apparent from Figure 5-5. These sensors are suitable for the detection of CO in the range of 0-300 ppm_v and H_2 in the range of 0-100% of the lower explosion limit of H_2 concentration. The gas warning system shown in Figure 5-5 was integrated into the software as well as into the hardware of the experimental test rig. A first alarm starting at 30 ppm_v CO causes an acoustic alarm signal and activates a software alarm including an e-mail warning. Two further alarm stages at 60 and 90 ppm_v CO deactivate the reactor heating and fuel supply, and then induce a complete hardware shutdown.

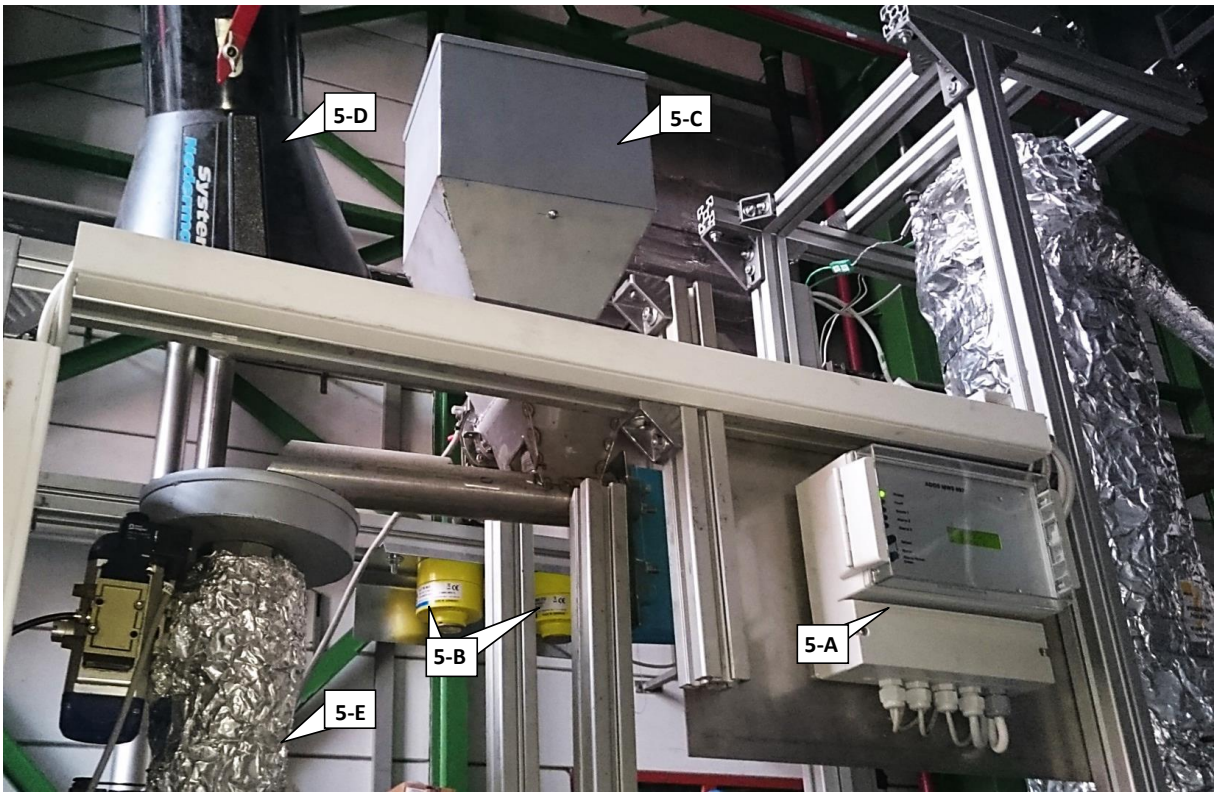

Figure 5-5: Gas warning system with sensors, fuel hopper and ventilation

In combination with the vent (5-D) shown in Figure 5-5, the installed gas warning system prevents the uncontrolled release of toxic or flammable gases into the working environment and therefore constitutes an indispensable security measure for long-term experimental runs including phases of unattended operation.

The initial internal configuration for fluidizing the bed material was a nozzle at the bottom of the gasifier diverting the steam to six downward oriented jets that were left open at their exhaust (Figure 5-6 A). These jets were formed by openings with 3 mm in diameter. As the openings were not covered, a backflow of the bed material with a particle size range of 200-300 µm was possible, especially once pressure peaks occurred inside the gasifier. The penetration of the jets openings by bed material and ash regularly led to the clogging of some of the jets. This led to limited reproducibility of the experimental result due to bad fluidization conditions as observed by increased differential pressure and changes in the spread of temperatures inside the fluidized bed. To prevent the partly blocking of the nozzle, the jet openings were covered with a metal mesh of a pore size of 80 µm (6B-B). In order to protect the fine metal mesh from friction within the fluidized bed and fixating its position without allowing a bypass of bed material or ash, the nozzle was additionally covered with a hood from stainless steel (6B-A) as shown in Figure 5-6 (B).

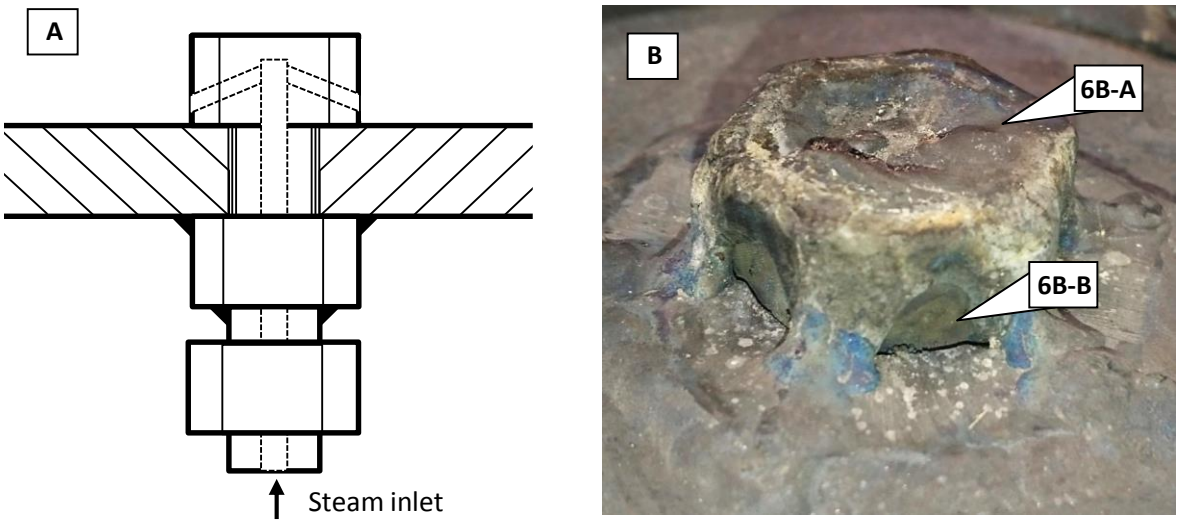

Figure 5-6: Setup principle of nozzle and fixation at the bottom of the reactor (A), Nozzle for steam injection with protective hood (6B-A) and wire mesh (6B-B) covering the outlet jets for steam (B)

The configuration shown in Figure 5-6 (B) reliably prevents blocking of single jets and continuously enables increased reproducibility of the experimental conditions within the gasifier. In order to prevent unnecessary wear of the metal mesh the operation mode was altered during startup of the gasifier. Once the temperatures in the gasifier were increased above 700 °C a nitrogen flow was enabled over the nozzle as to prevent the exposure of the mesh to oxygen at elevated temperatures. Once the steam flow for fluidization of the bed material was started the nitrogen supply was interrupted. With this mode of operation the reflux through the nozzle was prevented for a continued operation of over 1000 h without exchange of the equipment.

Another major improvement in the gasifier setup was the changed installation of the electrical tubes for heating the reactor. Initially the heating tubes were installed without support thus freely standing on bottom plate of the reactor (7A-A) at the inside of the reactor insulation. The electrical connectors (7A-C) are mounted on the outside of the reactor bottom plate (7A-A). The temperature of the heating tubes was controlled over a thermocouple, which was inserted from the side of the outer tubular casing of the gasifier. The tip of the thermocouple was fixed by a metal clip to the heating tube. During operation of the gasifier at temperatures between 750 and 800 °C, the electric tubes had to be heated to temperatures of about 950 °C. At these temperatures the metal mantle of the heating tubes becomes soft and no longer suspends its own weight. This led to a deformation of the tubes (7A-B) with the initial setup after use, as depicted in Figure 5-7 (A). It is clearly visible that the heating tube (7A-B) is no longer coiled regularly around the height of the inner fluidized bed reactor ((7B-D) shown in Figure 5-7 (B)), but is mainly limited to the downer part of the reactor height (removed in Figure 5-7 (A)). As the reactor is removed the nozzle for steam inlet (7A-D) can be seen in Figure 5-7 (A).

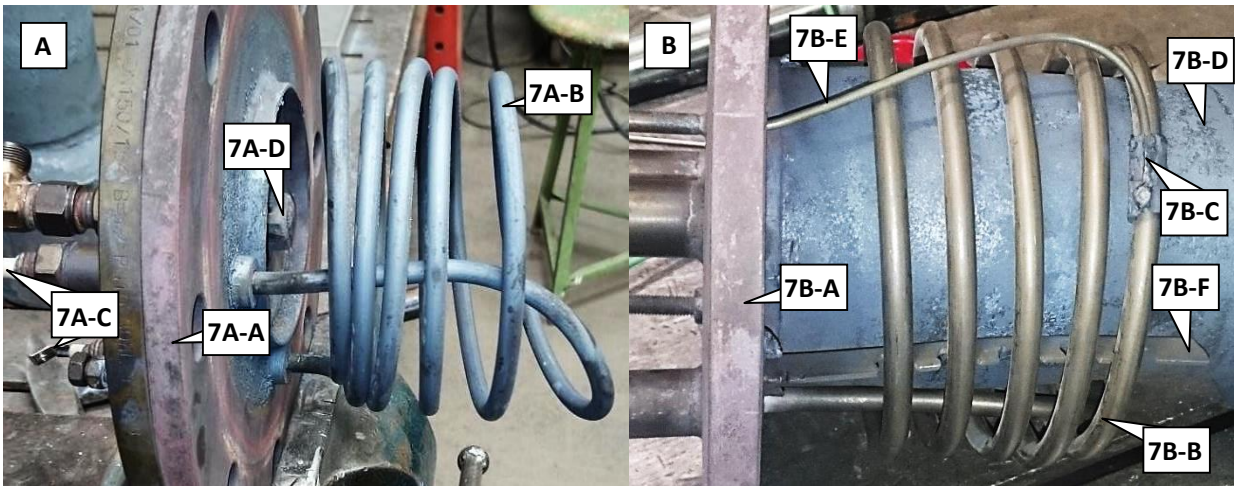

Figure 5-7: Installation of reactor heating tube without support (A) and with support and fixed thermocouple in final configuration (B)

Besides the uneven distribution of heat supply, the deformation of the heating tubes increased the risk of a separation between the thermocouple for regulation (7B-E) and the heating tube itself. Once this occurs the heating tube will easily overheat. As the tube is sensitive to electrical short-circuiting at temperatures above 950 °C, this led to a high breakdown-rate of the electrical heating tubes with the initial mode of installation (Figure 5-7 (A)).

Several changes were made (Figure 5-7 (B)) to increase the lifetime of the reactor heating and establish better reproducibility concerning the heat transfer into the reactor. In order to prevent the deformation of the heating tube at elevated temperatures, it was suspended by metal support (7B-F) keeping the reactor heating (7B-B) in its intended position. Additionally the positioning of the thermocouple (7B-E) was changed in order to warrant a more reliable fixation in direct contact with the mantle of the heating tube. As shown in Figure 5-7 (B) the thermocouple was later inserted from the bottom plate (7B-A) of the reactor casing and tied to the heating tube by a metal clasp (7B-C). The setup shown in Figure 5-7 (B) ensured a stable fixation even in case the position of the heating tube changed under high temperature conditions.

Another supplement to the hardware configuration of the test rig was the installation of an oval gear meter for detection of the inlet flow of water into the steam generator as further explained in section 5.1.2.2.

5.1.2.2 Software configuration

Along with the changes in hardware configuration, some relevant adjustments in the process software were necessary to increase the reproducibility of experimental conditions. Figure 5-8 shows a comparison between the user-interface at the initial configuration (A), as compared to the adjusted version after alterations in the process setup (B).

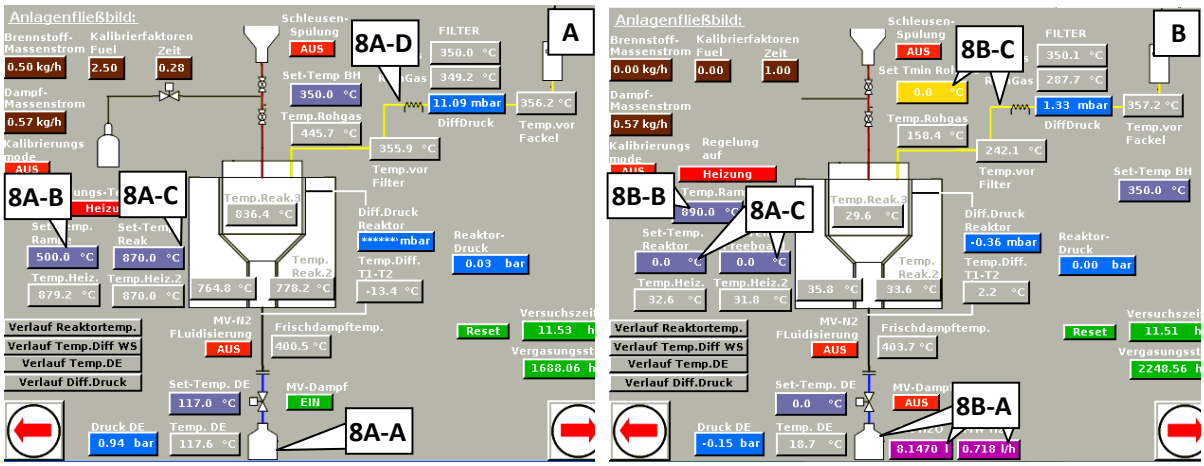

Figure 5-8: Control interface with initial setup (A) and additional control and feedback values (Steam inlet, temperature gas-outlet, different heating zones) in final configuration (B)

A major adjustment in the scope of process control was the implementation of a separate temperature regulation for the different reactor zones. Initially (Figure 5-8(A)) the input parameters for the temperatures in the gasifier consisted of a set point for a starting value during heat-up (8A-B) and only one temperature setting (8A-C) was available for the reactor as well as for the freeboard of the gasifier. The implementation of a separate temperature setting for the different zones (8B-C) facilitated a variation of the reactor temperature with a constant freeboard temperature such as to limit the influence of reduced coke conversion at reduced temperature. Additionally it prevented overheating of the electrical tubes as the set point can be easily adjusted to the specific demand at the different reactor zones depending on the conditions of operation. Together with the changes described in section 5.1.2.1, the lifetime of a single heating tube was increased significantly from a maximum of approximately 100 hours at the initial conditions, to more than 700 hours with the final hardware setup (Figure 5-7 (B)) and software configuration (Figure 5-8 (B)) for temperature control.

The amount of steam entering the reactor (8A-A) was not measured in the initial setup of the gasifier (Figure 5-8 (A)). Balancing the amount of injected steam by downstream condensation and consecutive gravimetric analysis proved to be prone to significant insecurities due to varying gas compositions and a fluctuating sampling stream compared to the main syngas flow as discussed in section 6.5. As a consequence an oval gear meter was integrated into the test rig to measure the flow of water into the steam generator (8B-A). In order to work as an indication for reproducibility of process conditions, the measured values had to be integrated into the user interface for direct feedback (8B-A). This was established by two additional counters, one showing the actual amount of water that was inserted into the steam generator during the past hour of experiment and another showing the total influx allowing the retrace of the average steam flow based on the duration of experiment.

An additional feature for process security integrated to the software setup of the test rig was an automated e-mail warning based on numerous different alarm modes to indicate critical process conditions. These include upper temperature and pressure limits for the reactor and piping system, as well as the inclusion of a gas warning system (Figure 5-5) integrated into the hardware of the test rig as described in section 5.1.2.1. Besides a warning function by e-mail, all the critical alarm values lead to a switch into a safe mode of the test rig as a security measure. An additional security feature for process control was integrated based on the outlet temperature of the product gas line (8A-D)

which was not linked to process safety in the initial setup (Figure 5-8 (A). The gas outlet is preheated to a temperature of 350 °C but raises to an actual temperature of about 500 °C under experimental conditions due to the exhaust of hot syngas from the gasifier. This temperature immediately drops once a blockage of fuel inlet occurs or the fluidization of the gasifier is interrupted due to the detection of an increased differential pressure. Therefore the manual setting of a control value for the minimum allowed temperature in the product gas line was introduced (8B-C) which significantly increases the safety in unattended operation. Once the allowed minimum value is undershot a safe shutdown of the gasifier is initiated.

5.1.3 Gas manifold

For the investigation of sorption equilibrium of most sulfur sorbents, the content of sulfur in the gas would be too low, as it is already below the thermodynamic equilibrium of most single metal oxide sorbents, as discussed in detail in section 4.2. For the example of CaO-based desulfurization, the thermodynamic equilibrium of the desulfurization reaction is at approximately 500 ppm_v H_2S for the conditions present in the gasifier. The decrease of sulfur content is to be expected only if the initial sulfur content of the produced gas is above this thermodynamic limitation of desulfurization. Inferentially the sulfur content of the gas had to be increased by several 100 ppm_v H_2S in order to demonstrate CaO-based desulfurization effects. Some preconditions for the increase of sulfur content were to be considered, such as:

- An instantaneous conversion to H_2S under gasification conditions is required
- A continuous automated supply has to be established in order to ensure stable and reproducible experimental conditions
- The increase of the H_2S content must not relevantly alter the composition of permanent gases in the produced syngas
- The enrichment of sulfur must adhere to the safety regulations of experimental work
- The least toxic alternative is to be preferred

From the given requirements many options for sulfur addition can be excluded, such as the addition of solid sulfurous components, which are difficult to handle in continuous automated dosage and might not ensure an instantaneous conversion to gaseous H_2S. The addition of gaseous sulfurous components from bottled gas is possible, but must adhere to the condition of not altering the composition of permanent gases. This excludes for example the application of diluted H_2S in N_2, if a final H_2S content above 1000 ppm_v is to be obtained in the produced syngas. Pure H_2S would suffice this requirement but is delicate to handle given a highly toxic component under pressurized conditions. For the increase of the H_2S content to values of about 1400 ppm_v the addition of CS_2, a component that is liquid at room temperature, was considered appropriate, as it suffices all of the criteria mentioned above. For the adjustment of the sulfur content to values of about 1400 ppm_v a N_2 stream is bubbled through a metal container filled with liquid CS_2 at a defined temperature under application of a gas manifold shown in Figure 5-9. The CS_2 rich stream is then diluted by mixture with additional N_2 to prevent condensation. The flow of CS_2 into the system can be controlled via the temperature of the container and the volume flow of the strip gas stream. The resulting overall inlet of sulfur is known through gravimetric measurement of the container filled with CS_2 and then concluded by the mass difference in relation to the operating time. A total resulting stream with a volume flow of 0.16 l/min at standard conditions (0 °C, 1 atm) is then directed to the reactor, mixed

with the fluidization steam and injected via the steam nozzle. Upon contact with the steam and permanent gas components of the produced syngas, the CS_2 is converted to H_2S according to the following reactions (Eqs. (36)-(38)).[112]

$$CS_2 + H_2O \leftrightarrow COS + H_2S \quad \textbf{(36)}$$

$$CS_2 + CO_2 \leftrightarrow 2COS \quad \textbf{(37)}$$

$$COS + H_2O \leftrightarrow H_2S + CO_2 \quad \textbf{(38)}$$

At a temperature of 750°C, the formation of H_2S from CS_2 is shifted to the product side according to equilibrium calculations. The required amount of additional sulfur in the form of gaseous CS_2 was estimated in order to ensure the H_2S content of the produced syngas of approximately 1400 ppm_v, such as to remain in accordance with the conditions of simulations described above.

Based on the simulation of the gasification process, an amount of 0.067 mol sulfur/h was necessary to represent a fuel equivalent to the simulated composition. This equals the addition of 12.55 ml/min gaseous CS_2 under standard conditions. With respect to the experimental setup shown in Figure 5-1 and a minimum adjustable flow of 41.6 ml/min (standard conditions) for the N_2 strip gas stream a required partial pressure of CS_2 in the gas phase of the container with liquid CS_2 can be calculated (Eq (39)).

$$p_{CS2} = p_{abs} \cdot c_{CS2} \quad \textbf{(39)}$$

Following the Antoine law with constants A, B and C as determined by Waddington et al.[113] (Table 5-2) the required temperature in the container is determined (Eq (40)).

Table 5-2: Antoine parameters for carbon disulfide with pressure in bar and temperatures in Kelvin[113]

A	[-]	4.067
B	[K]	1168.62
C	[K]	-31.616

$$Log_{10}(p_{CS2}) = A - \left(\frac{B}{T_{CS2-container} + C}\right) \quad \textbf{(40)}$$

With respect to a changing absolute pressure in the container due to fluctuations in the atmospheric pressure and varying differential pressures in the test rig, a mean value of 1050 mbar as absolute pressure was assumed, leading to an operational temperature of 8.2 °C in the container as standard setting. The applied method of sulfur elevation proved reproducible and sufficed the criteria of increasing the sulfur content without changing the composition of permanent gases (Table 6-1).

The applied gas manifold, depicted in Figure 5-9, is suitable for various applications such as catalyst deactivation and desulfurization experiments in a catalyst test rig. As shown in Figure 5-9, the gas manifold consists of several bottles of pressurized gas connected via mass flow controllers (MFC) to a humidifier with subsequent addition of CO_2. For the experiments performed, only a small part of the setup was relevant. These relevant parts are highlighted in Figure 5-9 whereas the sections that were not relevant for the experimental investigations are shaded gray.

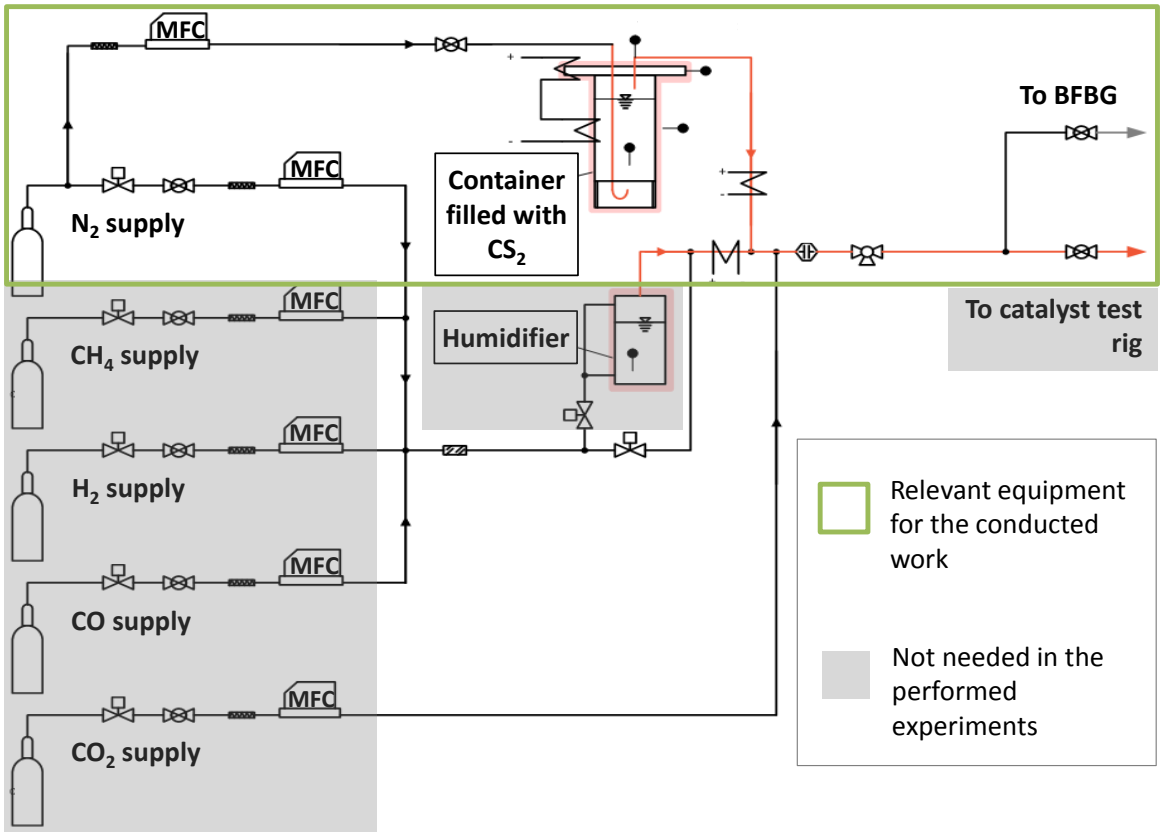

Figure 5-9: Flow chart of the test gas manifold used for elevation of the sulfur content in the gas (Temperature controlled parts indicated with red lines)

Besides the experiments with an initial H_2S content above 1000 ppm_v, experiments were performed with an initial H_2S content in the range of 100 ppm_v H_2S in the context of BaO-based desulfurization (section 6.3). For such experiments the method of sulfur supply was changed to the addition of a gas containing 3143 ppm_v H_2S in N_2. An amount of 0.25 l/min (standard conditions) of this gas suffices for the elevation of the sulfur content of 65 ppm_v in the produced syngas, considering a fuel-based sulfur content of 20-25 ppm_v H_2S in the syngas. The related increase in the N_2 fraction of the syngas is negligible as shown in Table 6-1. The criteria listed above as necessary requirements for methods for the elevation of sulfur content are therefore met by the addition of diluted H_2S if only a small increase of the sulfur content is required.

With the experimental setup described above, a series of experiments were performed in order to prove the functionality of the system and establish a systematic approach of sorbent characterization. An overview of the experiments that contributed to the results presented herein is listed in Table 6-3 for CaO-based desulfurization and Table 6-7 for BaO-based desulfurization.

5.2 Analytical setup and methods

For the purpose of analysis, a part of the product gas stream is separated from the main gas flow, which is continuously burned in a flare (Figure 5-1). By default, the separation of streams takes place downstream of the particulate filter consisting of a single metallic filter candle. The filter as well as all piping is heated to a temperature of 350 °C preventing the condensation of tars which could subsequently block the pipes. The gas for analysis is then cooled down using a series of impinger bottles as shown in Figure 5-10.

Figure 5-10: Impinger bottles for gas cleaning – 2 x water, 1 x RME, 2 x isopropanol, 2 x glass wool (only first one shown)

In the first two bottles, the steam contained in the gas is condensed at a temperature of about 20 °C. During the preparation of the impinger bottles for water condensation, an amount of 100 ml water and 3 ml 85% phosphoric acid was filled into the first bottle and 50 ml water with 2 ml of the acid in the second bottle. The acidification of the water has proven to shorten the time of saturation with H_2S from several hours to about half an hour in calibration experiments. After condensation of water, the bottles were weighted for gravimetric determination of the water content. The next steps of purification aim at the removal of hydrocarbons in organic methyl ester and two bottles filled with isopropanol. In order to lower the dew point of the tars contained in the gas below room temperature and to reduce stripping of isopropanol by the bubbled gas, a temperature of -10 °C was maintained by means of a cryostat. Subsequently the gas is adsorptively cleaned over glass wool and then dried in a redundant condenser at 3 °C before it enters the downstream analytical equipment as shown in Figure 5-11.

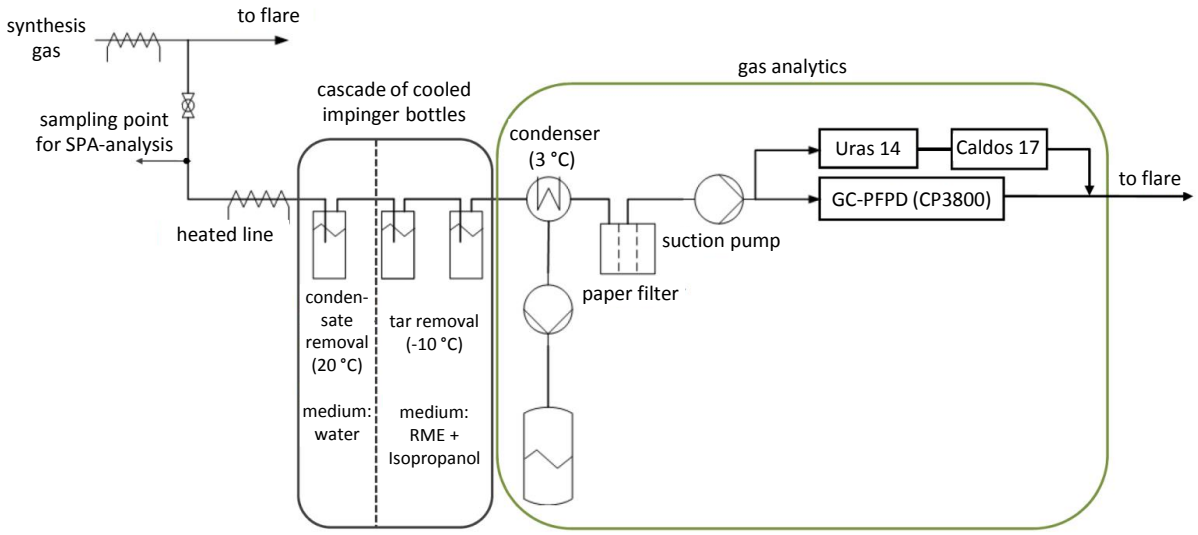

Figure 5-11: Detailed flow sheet of the experimental setup for gas cleaning and measurement[37] (adapted)

As the analytical tools for gas measurement are placed downstream of the impinger bottles for water condensation and the redundant condenser, all values referring to the gas composition and the data for sulfur analysis given in ppm_v, refer to the dry fraction of the gas. An overview of the different methods and analytical tools for gas analysis with respect to the detected components is listed in Table 5-3 including references to the corresponding sections, which contain a detailed description of the analytics.

Table 5-3: Overview of analytical tools and methods

Compound	Species	Analytical method	Analytical tool	Described in section
Permanent gases	CO, CO_2, CH_4	Non-dispersive infrared absorption	ABB, AO2000-Uras 14	5.2.1.1
	H_2	Thermal conductivity	ABB, AO2000-Caldos 17	5.2.1.2
	O_2	Electrochemical	ABB, AO2000-Uras 14	5.2.1.1
Sulfur	H_2S, COS, CS_2, CH_3SH	Gaseous sampling, gas chromatography	GC (Varian, CP 3800, SN: 103953)	5.2.2.2
	C_xH_y-S_z	SPA sampling + liquid extraction, gas chromatography	GC (Varian, CP 3800, SN: 101000)	5.2.2.1 and 5.2.2.2
Hydro-carbons	C_2H_4 – BTX	Gaseous sampling, gas chromatography	GC (Varian, CP 3800, SN: 103953)	5.2.2.1 and 5.2.2.2
	> BTX	SPA sampling + liquid extraction, gas chromatography	GC (Varian, CP 3800, SN: 05279)	5.2.2.1

5.2.1 Gas analysis

The composition of permanent gas components is monitored by a permanent gas analyzer (ABB Advance Optima Series)[114] consisting of two analyzer modules installed downstream of a condenser and a suction pump which enables a constant gas flow of about 26 l/h at standard conditions. The combination of two analyzer modules Uras 14 and Caldos 17 enables the quantification of O_2, CO, CO_2, CH_4 and H_2.

5.2.1.1 Non dispersive infrared absorption module

The ABB, AO2000 *Uras 14 module* (SN 3.243575.5) offers the possibility of detecting up to 4 gas components by non-dispersive infrared absorption (NDIR) in a wavelength range between 2.5-8 µm.[115] The measurement principle is based on the wavelength specific absorption of infrared light by heteroatomic gas components contained in a measurement cuvette (2). The light emitted with intensity I_0 at its source, is diminished in its intensity according to the lambert Beer law (Eq(41)) at wavelength specific absorption bands ($\varepsilon(\lambda)$) of the gas components contained in the measurement sample. A sketch of the measurement principle is shown in Figure 5-12.

$$I_1 = I_0 \cdot e^{-\varepsilon(\lambda)\cdot l\cdot c} \quad \textbf{(41)}$$

The sample gas flows continuously through the measurement cuvette (2) of length l, whilst the light is interrupted by a rotating shutter (1), such as to obtain distinct values of measurement and establish and alternating lightpath. The light beam is guided once through the sample and once through a cuvette containing N_2 (3), whereby N_2 does not absorb electromagnetic waves in the IR-range. The absorption properties of the heteroatomic molecules inside the sample lead to wavelength-specific deficiencies (I_1) in the IR-spectrum (5) proportional to the concentration (c) of that specific substance in the sample. The detectors (4) positioned at the outlet of the sample tube and reference tube, contain the desired component for analysis.[115]

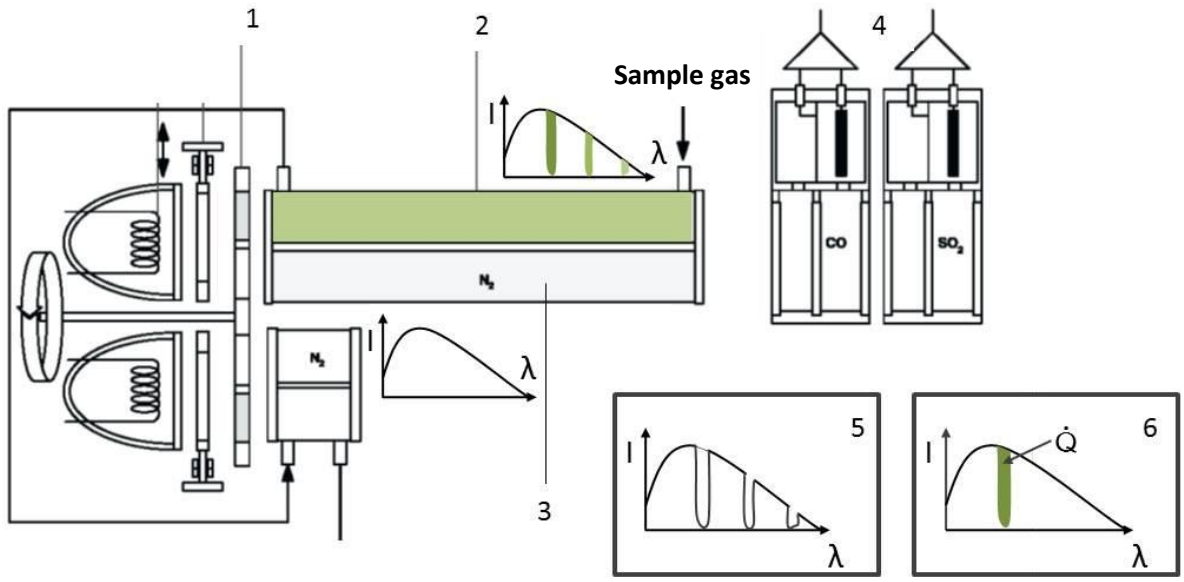

Figure 5-12: Working principle of the gas analyzer module Uras-14, applied for the detection of CO, CO_2, CH_4 and O_2 (different measuring technique)[37]

As the IR-beam reaches the detectors, the light beam that has passed through the sample exhibits deficiencies at the specific IR-absorption bands while the lightbeam that has passed through the N_2-cuvette contains the full spectra of emitted IR-waves (Figure 5-12-6). Inferentially the absorbable energy content, which is transformed into heat inside the detector, is different between the alternating lightpaths. This leads to an oscillation of pressure inside the detector whereby the amplitude is proportional to the concentration of the specific detected component in the sample. As the absorption only takes place at the component specific IR-bands two detectors can be installed in a row without a shading influence. With two parallel sampling cuvettes this leads to a maximum of four detectable substances per Uras 14 module via NDIR -measurement. The deployed Uras module is additionally equipped with an electrochemical sensor for O_2 detection.[114,115]

5.2.1.2 Thermal conductivity sensor

The ABB AO2000 *Caldos 17 module* (SN: 3.243581.5) enables the detection of H_2 due to the relevant differences in thermal conductivity between H_2 and the other permanent gases contained in the syngas mixture. It works on the principle of a wheatstone bridge with one thin-film resistor being exposed to the sample gas. The content of H_2 in the gas mainly determines its thermal conductivity that leads to an increased cooling effect on the thin film resistor with rising H_2-content in the sample. Inferentially this leads to a reduced resistance in the exposed thin film resistor. In order to maintain a specific ratio of the resistance value with a second resistor that is not exposed to the sample gas, a circuit produces a current to counter the temperature loss of the exposed resistor. This current is used as a measure for the H_2 content in the gas. The influence on heat removal of the other components contained in the gas is considered according to the measurement of the Uras 14 module and corrected arithmetically.[114]

The difference between 100% and the sum of content of the gas components mentioned is considered to be the N_2 fraction that includes about 1-2 vol% of light hydrocarbons (C_2H_2 - BTX) present in the syngas as determined by gas chromatography.

5.2.2 Gas chromatography

For the measurement of gaseous sulfur components, volatile hydrocarbons and tar analysis a total of three Varian CP-3800[116] gas chromatographs were utilized. Depending on the measurement task, the analyzers were equipped with a pulsed flame photometric detector (PFPD) or a flame photometric detector (FID). The working principle of these detectors is elucidated in more detail in sections 5.2.2.1 and 5.2.2.2.

The application of gas chromatography as a main tool of measurement is based on the flexibility and versatility of this technology, allowing the analysis of liquid and gaseous samples concerning their composition and concentration in a broad variable range of resolution. In all of the applied chromatographs the samples were evaporated prior to being charged on a capillary column for separation of the different components. The range of resolution is adjustable by a split ratio in the injector determining the fraction of sample that is charged on the column, as well as due to sensor and component specific limitations.[116]

The high surface area of the capillary column enforces intense interactions between molecules contained in the gas and the stationary phase at the inner wall of the column. These interactions increase with molecule size, whereby large molecules are strongly retained by the stationary phase and smaller molecules are able to pass the column more easily due to a constant flow of inert carrier gas as mobile phase. In all the conducted measurement applications helium (He) was used as mobile phase inside the column. With an either gradual or stepwise increase in temperature even larger molecules are released from the stationary phase of the capillary column and subsequently reach the detector as propagated by the mobile phase. The modes for column operation vary between constant flow and constant pressure inside the column.[116] In all the measurements a constant flow mode was established which is especially required for analysis via PFPD due to the necessity of stable flow ratios inside the detector.

A major benefit of the application of gas chromatography as the main analytical tool is the possibility of individually detecting numerous different components by species and concentration. This is an advantage as compared to other methods that often allow either the detection of single components (e.g. H_2S) or a nonspecific sum concentration of species containing a common representative compound (e.g. sulfur). Further details on the different specification of the conducted measurements are explained subsequently.

5.2.2.1 Tar analysis

The tar analysis discussed in the results section is based on solid phase extraction (SPA) with subsequent liquid extraction and GC-FID analysis. The principle of SPA-sampling is based on the lower dew point of tars as compared to permanent gas components and therefore precipitation of the hydrocarbons on a polar matrix of aminosilicates. For this purpose a sample volume of 96 ml is sucked through an SPA – tube in a time span of approximately 45 min under application of a syringe pump. The low sampling rate was established to compensate fluctuations in the gas composition due

to erratic changes in fuel supply. In order to obtain representative measurements of the tar content, the temperature of the gas must not fall below the dew point of tar components prior to sampling. Therefore the sampling was taken from a heated line (Syngas stream, Figure 5-1) at a temperature of 350 °C through a PTFE coated septum via a syringe. Between sampling and extraction, the samples were cooled in order to minimize evaporation of volatile tar components such as phenols. Benzene, toluene and xylole were detected by GC-measurement but not considered as tars in the analysis of results, as they usually do not condensate in syngas applications given their low dew point and the low partial pressures of these substances in the produced gas.[15] The extraction is done by flushing the SPA-sample with a total of 3.6 ml of Acetone in two subsequent extraction cycles thus producing two vials with liquid per SPA sample. The determination of tar content and composition is done by automated liquid injection of the extracted samples into a GC (CP 3800, SN: 05279)[116] equipped with an FID detector.

The liquid samples are evaporated in the injector of the GC and led through a capillary column (CP-Sil 5CB, 30 m length, 0.32 mm diameter, 0.25 µm film) for separation of the various hydrocarbons before they reach the FID-detector at a component specific retention time. The duration of the analytical method is 43 min with a starting temperature of 50 °C and an end temperature of 280 °C. The largest distinguishable components detected are fluoranthene and pyrene with a molar mass of 202.3 g/mol, and boiling points of 375 °C and 404 °C respectively. Inside the FID detector the hydrocarbons contained in the carrier gas are combusted in a hydrogen flame with a setup of the detector as shown in Figure 5-13.

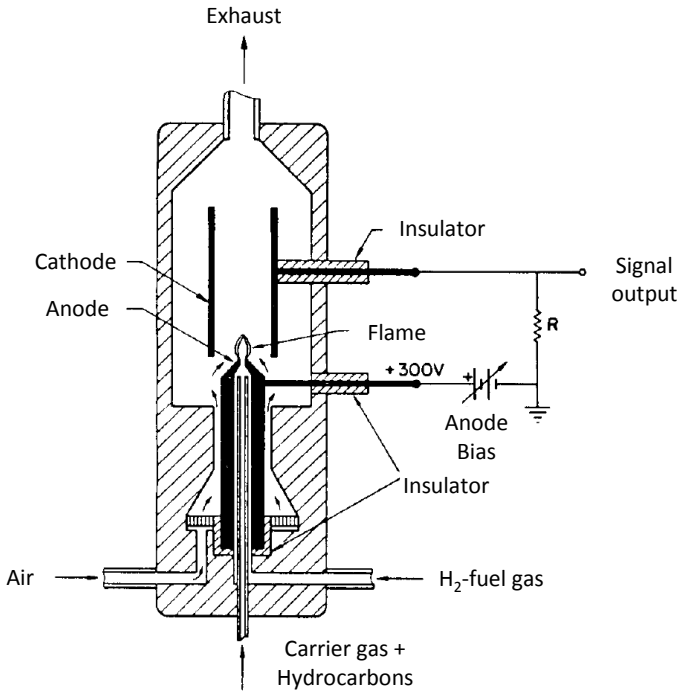

Figure 5-13: Working principle of a flame ionization detector[117]

The comparatively low gas flow of 1.5 ml/min carrier gas, containing the hydrocarbons from the sample, is mixed inside the detector with a hydrogen flow of 30 ml/min and jetted through an orifice for combustion with 300 ml/min of air. Under contact with air the CH* radicals, formed by thermal

cracking, react with atomic oxygen to partly produce ions according to the following reaction (Eq (42))[117]

$$CH^* + \frac{1}{2}O_2 \leftrightarrow HCO^+ + e^- \quad \textbf{(42)}$$

The occurring ionization produces a current between polarized electrodes of the flame tip (Anode) and the collector tube (Cathode) as depicted in Figure 5-13. The current is detected and amplified to produce a quantitative signal according to the hydrocarbon species present within the flame. The response of the FID is proportional to the number of unoxidized carbon atoms present in a hydrocarbon molecule.[117] The signal response is displayed over the duration of the analytic method to yield distinctive signal peaks at component specific residence times. The determination of the corresponding component for a specific signal peak a can be established via calibration, GC-MS detection of component fragments or literature data if available for the applied method. In order to translate the areas under the signal peak into a corresponding value of concentration, a component specific calibration with samples of known concentration is necessary.

Besides the GC-FID measurement of common hydrocarbons contained in the liquid samples, an additional step of analysis was performed on the liquid samples for the detection of sulfurous tar components with another GC (Varian CP 3800, SN: 101000) via GC-PFPD analysis. The specifics of a GC-PFPD detector are explained subsequently.

5.2.2.2 Sulfur analysis

The analysis of sulfur content and composition of sulfurous components conducted in the course of the presented work is based mainly on GC-PFPD analysis in two different devices (Table 5-3). Besides the analysis of sulfurous tar components contained in the liquid samples obtained from SPA analysis, the sulfur detection mainly focuses on gaseous sampling of a cleaned gas as shown in Figure 5-11. The detection of different gaseous components, such as H_2S, COS and CH_3SH, is performed by means of a CP-3800 gas chromatograph (SN.: 103953) equipped with a heat able valve oven as shown in Figure 5-14.

The sample gas is purged into a series of Haysep columns for TCD analysis (14-A), as well as sampling loops for FID (14-B) and PFPD (14-C) analysis. With the onset of measurement, the sample loops are flushed with helium as carrier gas and the samples are propagated to two different injectors and capillary columns accordingly as indicated in Figure 5-14. The gaseous sample directed to the FID detector (Figure 5-13) served for the analysis of light hydrocarbons from C_2H_2 to the molar weight of BTX components. The sample for sulfur analysis is injected into a Gaspro Q column (30 m length, 0.32 diameter, SN 113-4332), enabling the distinguished detection of H_2S and COS as well as CS_2 and CH_3SH without external cooling of the capillary column. The duration of chromatographic measurement is 8.6 min, starting from a temperature of 50 °C to a final temperature of 240 °C. The interval between two data points is about 12 min, including the time of measurement and reinitializing the instrument.

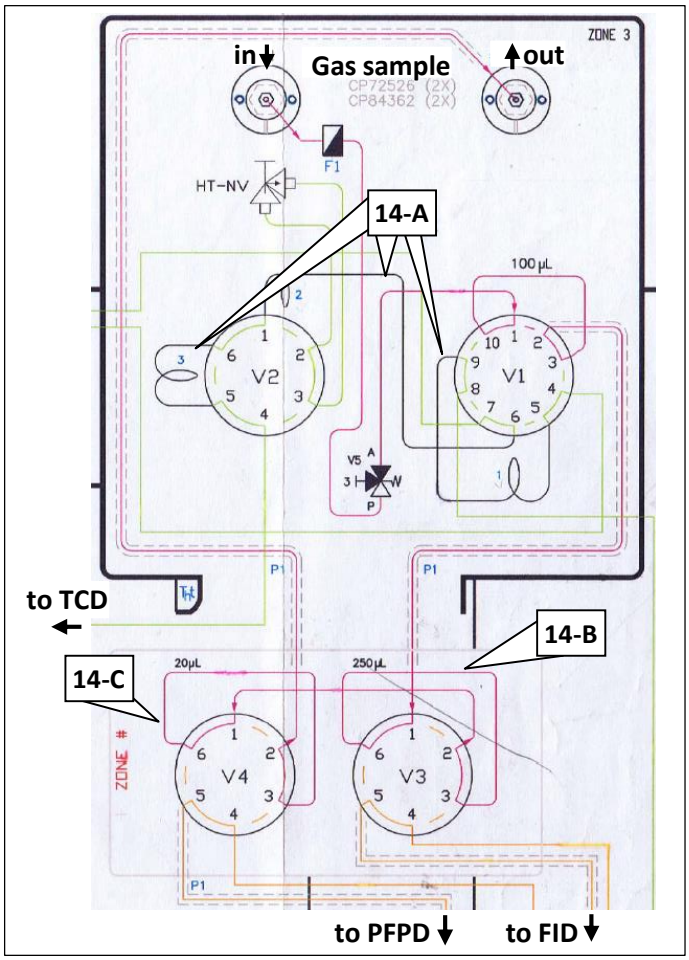

Figure 5-14: Flow chart of the sampling system of the GC (Varian, CP 3800, SN: 103953) employed for sulfur analysis[116]

After passing the capillary column for separation of components, the carrier gas containing the sulfurous components is combusted in a GC-PFPD detector following a sequence of events as shown in Figure 5-15.

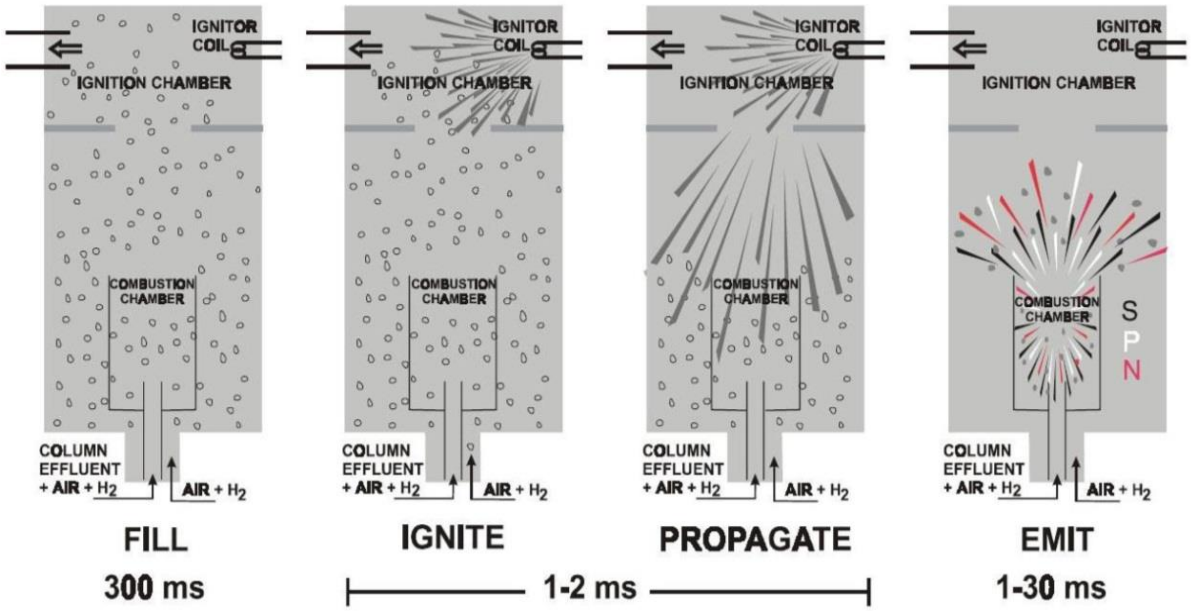

Figure 5-15: Working principle of a pulsed flame photometric detector[118]

Initially the main body and the combustion chamber of the GC-PFPD detector are filled with a combustible mixture of hydrogen and air plus a small fraction of carrier gas containing hydrocarbons and sulfurous components from the sample. At the exhaust of the main body the combustible gas mixture enters the ignition chamber with the ignitor coil. After ignition, the flame propagates into the main body and the combustion chamber of the detector. Inside the combustion chamber the luminous radicals of sulfur, phosphor and nitrogen are emitted during oxidizing reactions with air.[118] An important condition for obtaining optimum measurement results under application of a PFPD is the flow ratio between the flows into the combustion chamber and the main body of the detector. These determine the distribution of the column effluent inside the detector during propagation of the flame front, whereby the latter is ideally contained only in the combustion chamber as depicted in Figure 5-15 (Emit).[118] The described setup of the detector with the different sections of ignition chamber, main body and combustion chamber allow a pulsed combustion of gaseous column effluents due to the preceding steps of filling, ignition and propagation. On the other hand the containment of column effluents in the combustion chamber allow for a high sensitivity of the sensor, as all sulfurous compounds contained are basically ignited simultaneously in the small volume of the ignition chamber. This enables an optimization of the delay in sensor response for the selective detection of either sulfurous or in other applications phosphorous or nitrogenous luminescence as shown in Figure 5-15. In the applied setup for detection of sulfurous compounds the light emission of the combustion is detected by a photometric detector with a time offset of about 8 ms. This enables the selective detection of sulfurous compounds due to an element dependent time offset of the maximum in photoluminescence caused by the formation of radicals in the combustion process. The light emission curves of different radicals involved during combustion are shown in Figure 5-16.

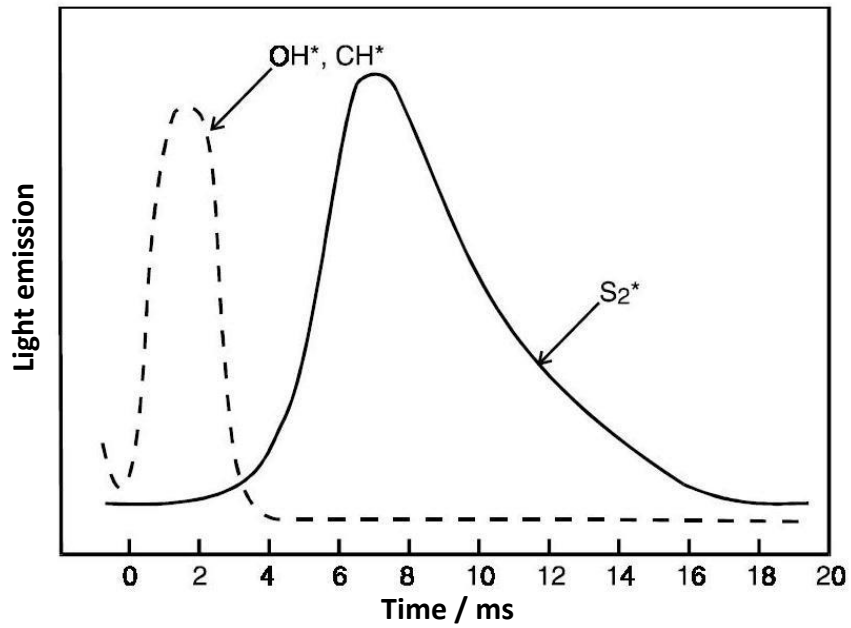

Figure 5-16: Time related peaks of light emission for specific detection of sulfur content[118]

The feature of pulsed flame inside a PFPD-detector with consecutive cycles of filling and combustion as shown in Figure 5-15 introduces the dimension of time dependence to the signal detection.[119] It therefore allows the specific detection of sulfurous components by regarding only the time of maximum light emission caused by S_2* radicals during measurement. As depicted in Figure 5-16 this allows for fading out the light emission of other radical-reactions involved in the oxidization process.[118] For the commonly low concentration of sulfurous components as compared to other hydrocarbons, this results in a major decrease of signal noise and therefore lower detection limits for sulfur measurement as compared to other methods of sulfur detection.[119] This is especially valid in comparison to the more common concept of a flame photometric detector (FPD) where the column effluents are burned in a continuous flame. The principle of detection is the same as in PFPD-analysis but once hydrocarbons are eluted from the column simultaneously with sulfur, the formation of CO_2 in the detector can cause a relevant damping of the sulfurous signal due to absorption effects. As such a simultaneous elution of sulfur and hydrocarbons cannot be prevented in the detection of sulfurous hydrocarbons a PFPD analysis can effectuate its full potential.[119] This is also valid in comparison to other measurement techniques for sulfurous components in gaseous samples, which are either selective only to single components such as colorimetric or electrochemical sensors or detect the sum of sulfurous compounds contained in a sample such as fluorescence detectors.[120] A disadvantage of PFPD-measurement is its' sensitivity towards the continuity of measurement conditions, that is discussed in section 6.5.

5.2.3 Particle characterization

The measurements for particle characterization presented in this study were externally performed at Forschungszentrum Jülich (Germany), Bioenergy 2020+ (Austria) and the Research Center Pharmaceutical Engineering "RCPE" (Austria). The applied methods are subsequently presented in a short overview.

5.2.3.1 BET – Analysis

A surface area & porosity-analyzer (TRISTAR II, Micromeritics, Aachen, Germany) was deployed for the determination of the surface area and pore properties via adsorptive measurement following the Brunauer – Emmett – Teller (BET) method. The measurement is based on the adsorption of nitrogen as adsorptive on the surface of a sample under cryogenic conditions at 77 K. The determination of the surface area is deduced from the increment of pressure in the analysis chamber corresponding to the inlet of nitrogen. The pore structure can be deduced form the hysteresis of the adsorption- and desorption isotherm. The accuracy of pressure measurement is indicated with +/- 0.1 % of the full scale.

5.2.3.2 ICP-OES

The elemental composition of different sorbent samples was analyzed by means of inductively coupled plasma - optical emission spectroscopy (Spectro Arcos SOP, Kleve, Germany).[121] Prior to ICP-OES, each sample was digested with nitric acid in a microwave assisted autoclave system (Multiwave 3000, Anton Paar). The measurements were carried out according to EN 15290 and 15297, and are based on the element specific emission of electromagnetic waves when exited in inductively coupled plasma as an energy source.

5.2.3.3 SEM-WDX

Scanning electron microscopy (SEM) in combination with wavelength-dispersive X-ray spectroscopy (WDX) was applied for magnified imaging of the different CaBa sorbents before and after use in the fluidized bed. The combined utilization of SEM and WDX-analysis allows the element specific resolution of the SEM –images by distinct excitation of known electron migrations specific to each element. For such a wavelength specific excitation the result is an element specific response over the analyzed area of an SEM image.

5.2.3.4 XRD

The investigations on crystallography of the different CaBa samples are based on X-ray diffraction (XRD) under application of the diffractometer D4 ENDEAVOR (Bruker, Billerica, USA). The method used is a focused Bragg-Brentano-geometry, common in powder diffractometry. By X-ray emission of a Cu-K-alpha electron excitement (U = 40 kV; I = 40 mA) the crystal-specific scattering is detected in dependence of the scattering angle Θ with a step width of 0.02°, and a duration of 5 seconds per step.

6 Experimental results and discussion

Based on the motivation of establishing in-situ desulfurization as a method for coarse desulfurization in biomass gasification as outlined in section 3 an evaluation of potentially suitable sorbents for sulfured capture was performed by means of thermodynamic calculation described in section 4. The results of this thermodynamic evaluation allow for a qualified and limited selection of sorbent materials, which combine features of thermal stability, chemical activity, and a low price as well as availability. With these given restrictions and based on the thermodynamic assessment, CaO-based naturally occurring materials were considered suitable for a coarse desulfurization as well as in terms of proof of concept. A more sophisticated BaO-based material also seems a viable sorbent with the potential to reduce the residual sulfur content to values below 5 ppm_v H_2S according to thermodynamic calculations. In order to verify the theoretical results from section 4.2, an experimental screening of CaO- and BaO-based in-situ desulfurization was performed under application of the experimental setup and analytical methods described above (section 5). In the following section, the applied test rig is characterized in detail and conditions of the experimental investigations are elucidated (section 6.1). Furthermore the results obtained from the experimental application of CaO- and BaO-based in-situ desulfurization are presented and discussed in detail (sections 6.2 and 6.3). In a closing chapter (section 6.4) the possibility of a combined application is investigated and process options for further innovations are discussed.

6.1 Characterization and conditions of experimental setup

The investigations of in-situ desulfurization follow a similar pattern for the different sorbents and are based and bound to the characteristics and conditions of the experimental setup. The setup described in section 5.1 is subsequently characterized under experimental conditions.

6.1.1 System characterization and boundary conditions

As described in section the gasifier is part of a test rig planned prior to the beginning of the experiments described in the presented work.[25,26,37] Therefore the main parameters of gasification were given by the previous dimensioning of the test rig and by conformity with previous results concerning beneficial gasification conditions conducted by Kienberger.[37] These include the minimum required flow of steam for fluidization of the bed material olivine (200 -300 µm) and a steam-excess-ratio of 4 in order to achieve a full conversion of char inside the gasifier. The necessity of a full conversion of char, as a requirement for stable continuous operation, also determines the lower limit of applicable reactor temperature in the range of 750 °C. This limit is given by the Boudouard reaction (Eq (3)) that requires external heat and a sufficient temperature level for the gasification of coke to gaseous CO. The upper limit of achievable temperatures is given by the maximum power input (3.5 kW) and allowable temperature of the reactor heating tubes of 950 °C. With respect to losses and limitations of heat transfer, the maximum temperature in the reactor was in the range of 780 °C initially, and later increased to around 810 °C by changes in the setup as described in section 5.1.2.1.

With the given boundary conditions of the experimental test rig, the choice of a suitable particle size of the added sorbent was based on a dimensioning calculation with respect to fluidization criteria in the investigated fluidized bed. These conditions resulted from the set values for steam and fuel mass flow of 540 and 500 g/h respectively (section 5.1.1). With the given inner diameter of the fluidized bed reactor this results in a superficial velocity of u_s = 0.084 m/s. Under consideration of the Archimedesnumber (Eq (43)) for different particle sizes

$$Ar = \frac{d_p^3}{\nu_s^2} \cdot \frac{\rho_p - \rho_s}{\rho_s} \quad \textbf{(43)}$$

the corresponding Reynoldsnumbers can be calculated for the incipient point of fluidization (45) and the onset of pneumatic discharge (47) by applicable relations.[122]

$$Re_{fl} = \frac{Ar}{1400 + 5.22 \cdot \sqrt{Ar}} \quad \textbf{(44)}$$

$$Re_{pd} = \frac{Ar}{18 + 0.61 \cdot \sqrt{Ar}} \quad \textbf{(45)}$$

With the definition of the Reynoldsnumber (Eq (47)), a minimum allowable particle diameter can be found iteratively with respect to the Reynoldsnumber at the onset of pneumatic discharge (Eqs (45) and (47)), under the condition that the superficial velocity present in the fluidized bed is below the flow velocity that would cause a pneumatic discharge of particles with a corresponding diameter d_{min}. (Eq (46))

$$u_{fl} < u_s < u_{pd} \quad \textbf{(46)}$$

$$Re_{pd} = \frac{d_{min} \cdot u_{pd}}{\nu_s} \Rightarrow d_{min} = \frac{Re_{pd} \cdot \nu_s}{u_{pd}} \; with \; u_s < u_{pd} \quad \textbf{(47)}$$

The equivalent calculation can be applied for the determination of a maximum allowable particle diameter under the condition that the superficial velocity in the fluidized bed is higher than the flow velocity required for fluidization of a particle with a diameter d_{max}.(48)

$$Re_{fl} = \frac{d_{max} \cdot u_{fl}}{\nu_s} \Rightarrow d_{max} = \frac{Re_{fl} \cdot \nu_s}{u_{fl}} \; with \; u_s > u_{fl} \quad \textbf{(48)}$$

Under application of the criteria mentioned above, the fluidizable range of particle size was determined for the different sorbent materials according to their density $\rho_p$as listed in sections 6.2 and 6.3.

6.1.2 Experimental procedure

All of the experiments conducted in the course of the presented work are based on the gasification of wood pellets as standardized fuel with homogenous properties concerning composition and gasification behavior. As elucidated in section 5.1.3 an elevation of the sulfur content was necessary in order to observe a decline in sulfur content upon the addition of the investigated sorbents for in-situ desulfurization.

A standardized operational procedure of the experiments performed in the gasification test rig (Figure 5-1) as listed below, is destined to facilitate reproduction of the obtained results:

- Calibrate fuel and steam to standard operational values of 500 g_{fuel}/h and 540 g_{steam}/h
- Setup reactor, fill with 1500 g of Olivine (or less, according to the experimental setup (Table 6-3))
- Switch on trace heating of experimental periphery with a set value of 350 °C
- Set initial startup value of reactor heating to 50°C and enter final value of 700 °C (Reactor will be heated up using a ramp of 60 °C per hour over night)
- Once reactor heating is at 700 °C enable N_2 flow of 0.5 l/min to prevent corrosion of mesh inside the steam nozzle
- Set final value of reactor heating 870 °C and temperature of steam generator to 90 °C
- Once temperatures inside the reactor are at 800 °C, set temperature of steam generator to 116 °C and open magnetic valve to allow a slow onset of fluidization
- As temperatures stabilize inside the reactor and in the freeboard under fluidized conditions, enable fuel supply and disable N_2 flow to the reactor
- Visually check correct function of the flare and check for CO emissions in the periphery of the test rig
- Approximately after one hour of experiment the conditions in the gasifier start to stabilize with a constant temperature inside the fluidized bed and fluctuating temperatures in the freeboard of the gasifier, indicating that a stationary fraction of char is present inside the fluidized bed
- At this point the addition of sulfur is started by means of CS_2 for CaO-based desulfurization and 3000 ppm_v H_2S in N_2 for BaO based experiments. (section 5.1.3)
- Subsequently start gas analysis measurement (5.2.1) and GC-measurement (5.2.2.2) after calibrating the device
- Once the measured values of H_2S content stabilize in the destined set point range, the test rig is set for the experimental investigation by addition of desulfurization sorbents or variation of parameters

A detailed sequence of the experiments performed for the characterization of calcium- and barium-based desulfurization is listed in the corresponding chapters respectively (Table 6-3, Table 6-7).

6.1.3 Experimental conditions of in-situ desulfurization

By following the experimental procedure listed in section 6.1.2 the standard experimental conditions inside the gasifier are established. These include a steam-excess-ratio of 4, a reactor temperature of 775 °C and a freeboard temperature of 825 °C. After enabling the fuel supply to the gasifier, it takes about 3 hours until the temperatures in the gasifier are stabilized, as shown in Figure 6-1. The Temperatures inside the fluidized bed (t_FB-1 and t_FB-2) are not distinguishable after starting the fluidization with steam as the spread between them is in the range of few degrees Celsius under fluidized conditions.

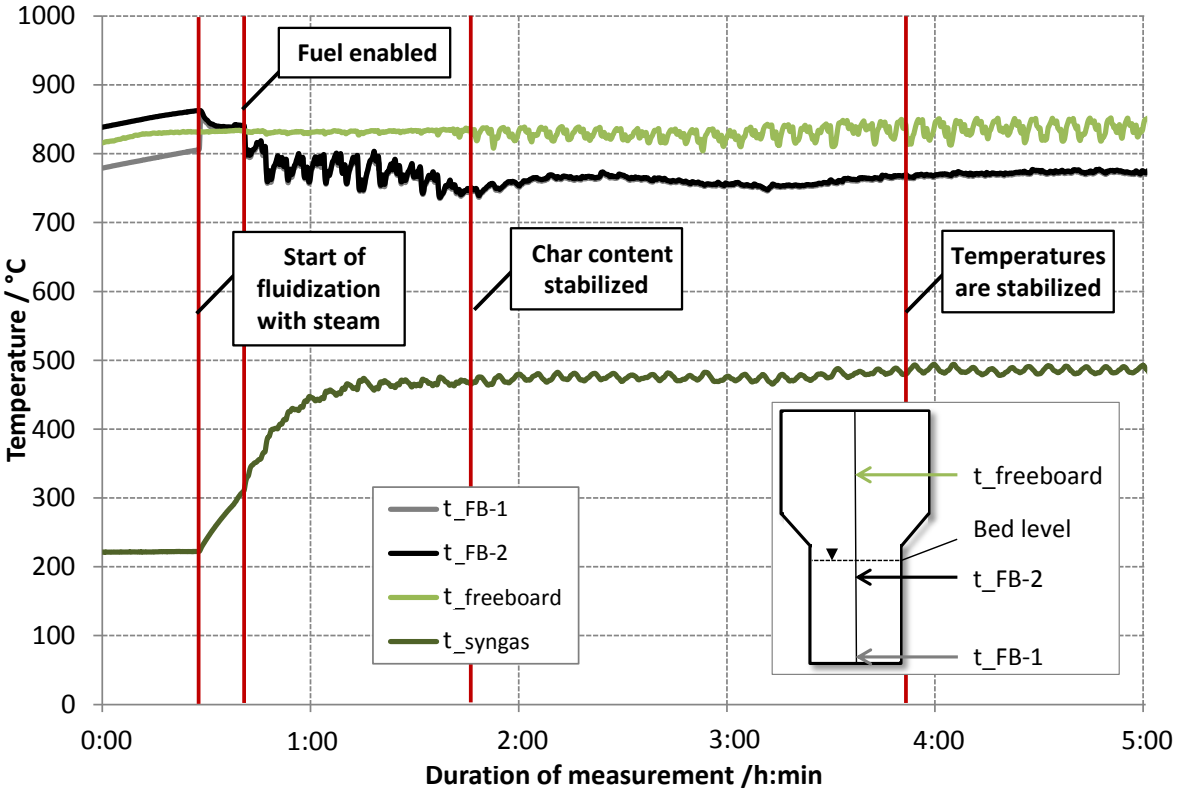

Figure 6-1: Trend of temperatures inside the reactor (t_FB-1, t_FB-2, t_freeboard) and in the product gas line (t_syngas) at the beginning of an experiment

Further it is shown in Figure 6-1 how the temperatures in the fluidized bed stabilize after a constant amount of char has accumulated inside the reactor. Once the fluidized bed is expanded due to the accumulation of char, the freeboard temperature starts to fluctuate with the frequency of the fuel supply. After the conditions in the gasifier have stabilized the composition of the produced gas is measured by means of gas analysis (GA). The results of GA measurement are shown in Figure 6-2 as an example.

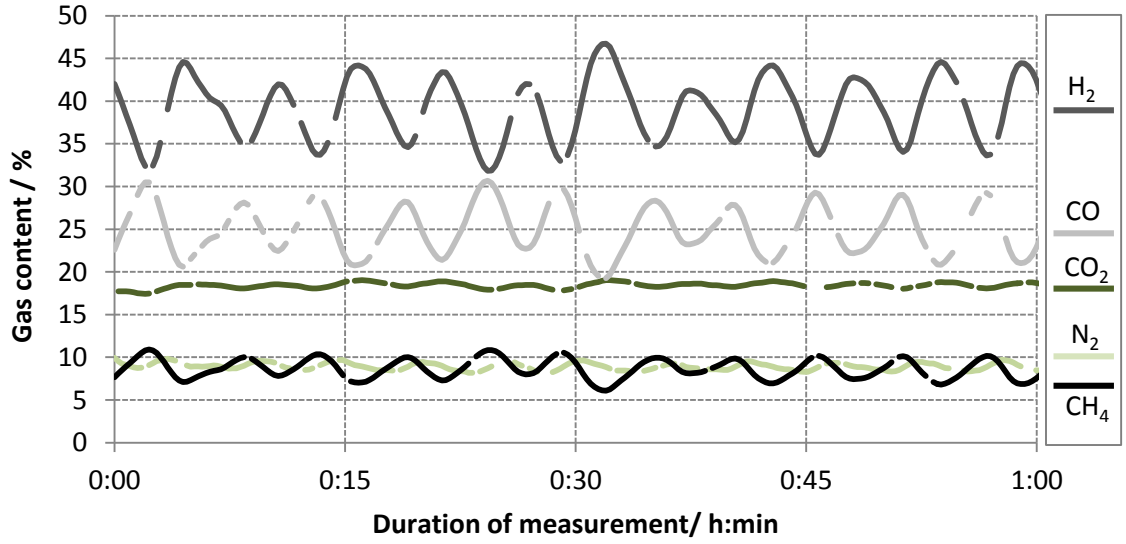

Figure 6-2: Composition of the syngas produced by gasification of wood pellets in the allothermal fluidized bed gasification test rig

The composition of the produced syngas is prone to fluctuations caused by the erratic supply of fuel to the gasifier. Mean values of the composition under standard experimental conditions are summarized in Table 6-1. The gas obtained from the experimental setup described in section 5.1.1 was enriched with sulfur in order to visualize a desulfurization effect upon the addition of an in-situ sorbent. As described in section 5.1.3 two different methods were applied for the elevation of the sulfur content depending on the intended set value of H_2S feed concentration.

For the investigation of BaO-based desulfurization under the application of CaBa, set values of H_2S content in the syngas were selected to be approximately 90 ppm_v. This represents the sulfur content derived by gasification of a lower-grade fuel such as wood residue with bark content. Under consideration of the inherent sulfur content of wood pellet derived syngas (Table 6-1), the elevation of sulfur content is in the range of 60ppm_v H_2S. The addition of sulfur was established using a bottle of mixed gas containing 3000 ppm_v H_2S in nitrogen, whereby the addition of 0.25 L/min (under standard conditions) of this gas sufficed to achieve the desired rise in H_2S content

For the experimental investigations of desulfurization with calcium based sorbents, the syngas was supposed to contain about 1400 ppm_v H_2S as to be in accordance with the simulated results presented in section 4.2. An elevation of the sulfur content was achieved by the addition of CS_2 under application of the gas manifold described in 5.1.3. The temperature at the steam inlet of the BFBG allows a full conversion of CS_2 to H_2S, which is the most stable form of gaseous sulfur under syngas atmosphere. Accordingly, no CS_2 was measured downstream of the gasifier even for long-term (60 h) experimental runs, thus taking into account saturation effects. This leads to sulfur-gas compositions with a predominant H_2S content and traces of COS, CH_3SH, and thiophenes. For both methods of sulfur injection, the deviation in composition of permanent gases in comparison to syngas derived by mere gasification of wood pellets without any addition of sulfur is negligible (Table 6-1).

Table 6-1: Comparison of different mean gas compositions for varied methods of sulfur elevation

Experimental results	H_2S, set	H_2S, measured	COS	H_2	CO_2	CO	N_2	CH_4	H_2O
	$ppm_{v,dry}$	$ppm_{v,dry}$				$\%_{,dry}$			%
Wood pellets	-	18	< DL	39.7	19.0	25.1	7.3	9.0	40
Wood -pellets + CS_2	1400	1195	59	41.0	18.4	24.2	8.5	7.9	39
Wood -pellets + H_2S	~90	85	< DL	40.6	17.9	23.6	10.8	7.3	40

While measurements of the sulfur content at the beginning of an experimental run indicated the elevation of H_2S to 1400 ppm_v by the addition of CS_2, the actual mean value of H_2S in the gas after some hours of experimental run does no longer reach the intended set value of 1400 ppm_v as shown in Table 6-1. The average sulfur content at different operating hours is depicted in Figure 6-3**.**

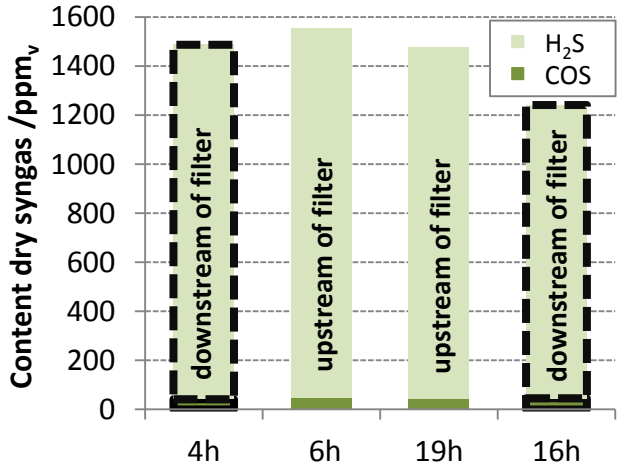

Figure 6-3: Sulfur content in the produced gas depending on the sample point and duration of measurement (Table 6-3: Experiments NS_FI#1, CaO_FI#2)

The sulfur content measured in the gas is not stable within the first hours of the experiment. This is attributed to the deposition of char in the housing of the hot gas filter and subsequent sorption of sulfur on its surface. As a result of this process, the measured H_2S content is in the range of 1500 ppm_v within the first hours of the experiment but decreases to a steady value of about 1200 ppm_v after approximately 5 hours. To confirm the assumption of adsorption of sulfur in the filter, measurements were performed with a stream of gas separated from the main gas line directly after the reactor outlet, upstream of the particle filter (Experiment NS_FI#1). The H_2S content in the gas upstream to the filter is rather constant with 1506 and 1433 ppm_v as depicted by the medium values after 6 and 19 hours of experimentation, respectively (Figure 6-3).

In order to exclude a direct influence of the adsorption of H_2S in the hot gas filter on the determined steady state value upon addition of lime, measurements have been performed under equilibrium conditions with excess addition of sorbent (Experiment CaO_FI#2). These results showed no dependency of the equilibrium value and the sampling point. This implies that the adsorption of H_2S occurs only at higher sulfur loads shown in Figure 6-3 and not under CaO-based steady state conditions of about 500 ppm_v H_2S (Figure 6-6).

The measured value for COS content is at 59 ppm_v for the medium content at all investigated sampling points and does not change with the duration of experiment or change of sampling outlet. Other gaseous sulfur components have not been detected in relevant concentrations under initial gasification conditions. After the initial decline, the content of H_2S remains constant at a value of about 1200 ppm_v and COS at about 50-60 ppm_v. The tar content in the gas was determined to be in range of 15 g/m^3_{std} by means of GC-FID measurement (section 5.2.2.1). This value is rather high compared to published results from other allothermal gasifiers (Table 2-6).[18] The slight differences with higher values for the investigated experimental test rig might be attributed to the comparatively small scale of the freeboard which usually facilitates the conversion of higher hydrocarbons to permanent gas components. Nevertheless, the experimental setup and the obtained syngas are suited to determine the effect of in-situ desulfurization on the sulfur content and the gas composition.

6.2 Calcium-based in-situ desulfurization[1]

The concept of in-situ desulfurization aims to reduce the overall effort involved in gas cleaning by introducing a process of desulfurization, which does not need an additional downstream apparatus. Suitable sorbent materials have to be stable at the elevated temperatures of gasification in the range of 800 °C (Figure 2-7) and need to be either suited for multicycle use or cheap enough for once through application. The latter criterion is met using naturally occurring CaO-based materials suitable for sulfur capture. Additionally nature derived CaO-based sorbents such as lime, limestone and dolomite are easily available and easy to handle concerning toxicology and experimental precautions. Concluding from the obtained results of simulated desulfurization equilibria, discussed in section 4.2.1.1, the application of CaO-based sorbents can only be justified in the context of coarse desulfurization. According to thermodynamic equilibrium calculations, an equilibrium of about 500 ppm_v residual H_2S can be expected for the experimental conditions present in the test rig (Figure 5-1). In order to confirm the simulated results, experiments with CaO-based in-situ sorbents were performed, based on real gasification of wood pellets with increased sulfur content. The results were obtained by application of different CaO-based sorbents and under varied process parameters in order to elucidate and quantify different influencing factors affecting the performance of in-situ desulfurization.

6.2.1 Sorbent characterization and preparation

Four different calcium-based sorbents were experimentally applied and compared for their performance in in-situ desulfurization. These include limestone and calcined lime, as well as two dolomite charges. One consisted of uncalcined dolomite and another of fully calcined dolomite the final product of the two-stage calcination reaction shown in Eq (30). The lime and limestone sorbent were obtained from a mill in Peggau, Austria. The dolomite and calcined dolomite come from the Spessart, Germany.

The dolomite and especially the fully calcined dolomite contained a high amount of powdery fines below 80 µm in diameter. For fully calcined dolomite this finest fraction sums up to almost one third of the sorbent mass as delivered. Besides that, the dolomitic sorbents were quite soft, which is a well-known detrimental property of dolomite concerning the application in a fluidized bed.[62]

Following on from the displayed conditions for stable fluidization of sorbent particles within the fluidized bed, listed in, a particle size fraction from 80 to 500 µm was found suitable for the application of lime as well as limestone, which proved to be of a similar density ρ_p after calcination. For dolomite and fully calcined dolomite a variation of the applied fraction was necessary. Comparing the particle size distribution of the dolomite sorbents with the particle size fraction of lime and limestone, a relevantly higher content of fines is present in dolomite and fully calcined dolomite as shown in Figure 6-4.

[1] Segments of this section have already been published by Husmann *et al.*[69,111]

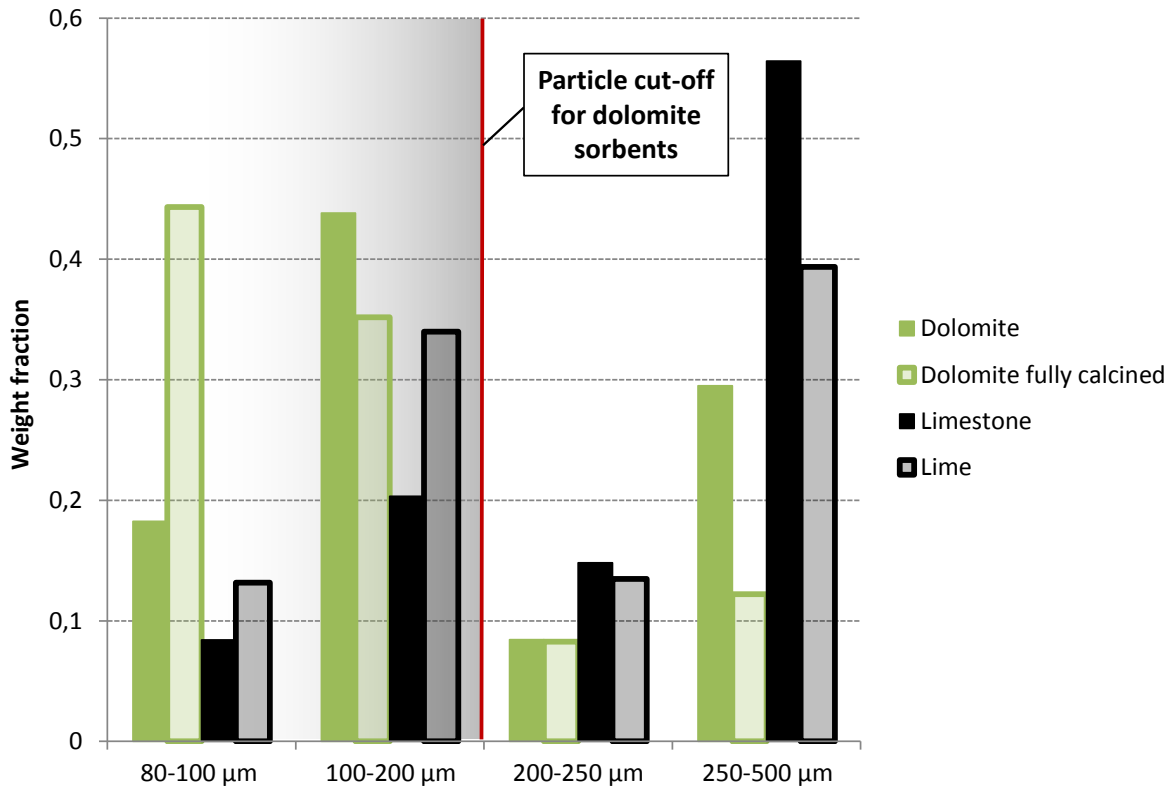

Figure 6-4: Deviation of particle size fractions in the size range of 80 to 500 µm for the different CaO-based sorbent materials

In the applied sieve fraction of limestone and lime between 80 and 500 µm a share of 56 and 39 wt% respectively is larger than 250 µm in sieving diameter. On the contrary only 8 and 13 wt% of the applied limestone and lime sorbents are between 80- 100 µm. In the equivalent particle size fraction of dolomite and fully calcined dolomite, a share of 18 and 44 wt% respectively form the sieve fraction between 80 – 100 µm and only 29 wt% of dolomite and 12 wt% of fully calcined dolomite are above 250 µm in sieving diameter. Especially under consideration of the increased grinding of the soft dolomite sorbents within the fluidized bed, an elutriation of the sorbent is to be expected. Given the lower density of dolomite samples as compared to lime and limestone, a larger particle size fraction in the range of 200(250) – 500 µm was applied for dolomitic samples as shown in Table 6-2.

Table 6-2: Particle properties of tested CaO-based materials, the differences to 100% in the elemental composition being oxygen and trace elements (SA –Surface area)

		Fully calcined dolomite	Dolomite (not calcined)	Lime	Limestone
Basic chemical composition		CaOMgO	$CaMg(CO_3)_2$	CaO	$CaCO_3$
Particle size fraction	µm	250 - 500	200 - 500	80 - 500	80 - 500
SA (BET)	m^2/g	1.82	4.34	4.87	0.65
Pore volume	cm^3/g	0.0089	0.0122	0.0179	0.0032
Pore size	nm	19.09	12.46	12.28	17.55
Water content	$wt\%_{,dry}$	7.0		9.0	
Carbon		1.7		0.7	
Al		0.2	0.4	0.1	0.1
Ba		6.3	1.5	0.0	0.0
Ca		30.7	22.4	63.5	38.9
Fe		2.1	1.4	0.1	0.1
K		0.1	0.1	< 0.1	< 0.1
Mg		14.0	9.8	0.3	0.2
Mn		1.2	0.9	< 0.1	< 0.1
S		1.6	0.3	0.1	< 0.1
Si		0.6	0.9	0.2	0.3
Sr		0.2	< 0.1	< 0.1	< 0.1

Based on the elemental analysis by ICP-OES measurements listed in Table 6-2 lime and limestone consist basically solely of CaO and $CaCO_3$ respectively. The dolomite charges contain a relevantly increased amount of minor components as compared to lime and limestone. Besides the main constituents calcium (Ca) and magnesia (Mg), barium (Ba), iron (Fe) and manganese (Mn) are also contained in relevant quantities. This offers the possibility of positive material interactions of trace elements as observed by Stemmler et al. who obtained a residual H_2S content of 50 ppm_v by application of slag lime, containing numerous trace compounds, as compared to 100 ppm_v H_2S for the application of pure CaO in fixed bed desulfurization experiments.[86] According to BET-analysis shown in Table 6-2 fully calcined dolomite proves to have less than half the surface area as compared to lime. The same accounts for the pore volume doubled in lime as compared to fully calcined dolomite with even larger pores in the latter. Another difference between lime and limestone as compared to dolomite and fully calcined dolomite is the trend of surface area between the calcined and uncalcined species. While the surface are is increased for lime as compared to limestone by a

factor of over 7, it is decreased by a factor of 2 considering fully calcined dolomite as compared to dolomite. The first, an increase of surface are during calcination, is to be expected due to the release of CO_2 as a product of the heat induced dissociation (Eqs (30)(31)).[123] The reduction of surface are in fully calcined dolomite and the low surface are of the latter compared to lime can supposedly be explained by destruction of the pore structure during grinding of the soft material and by sintering effects during the calcination itself.[82]

6.2.2 Experiments on CaO-based in-situ desulfurization

The investigation of CaO-based in-situ desulfurization constitutes the major part of the performed experiments. As stated in section 6.1.2 the sulfur content in the gas was elevated by the addition of CS_2 to values between 1200 and 1400 ppm_v H_2S.

Once a stable initial H_2S content was established in the gas, a defined amount of desulfurization sorbent was added depending on the purpose of the experiment (Table 6-3). The sorbent was added in batches with a standard interval of 10 min via the fuel inlet of the test rig (Figure 5-3 (2-D)). The standard amount of sorbent added in experiments under non sorbent-limited conditions was 5.9 g of lime per 10 min or the equivalent amount of CaO for the other CaO-based sorbents. As observed in preliminary test on in-situ desulfurization the hygroscopic sorbent formed agglomerates upon contact with the humid syngas atmosphere in the air lock of the fuel supply which prevented a defined dosage of the sorbent and led to defluidization of the bed and blockages of the fuel supply eventually. The added powder was therefore wrapped in negligible amounts of paper as shown in Figure 6-5, which proved to successfully prevent the formation of agglomerates during sorbent addition.

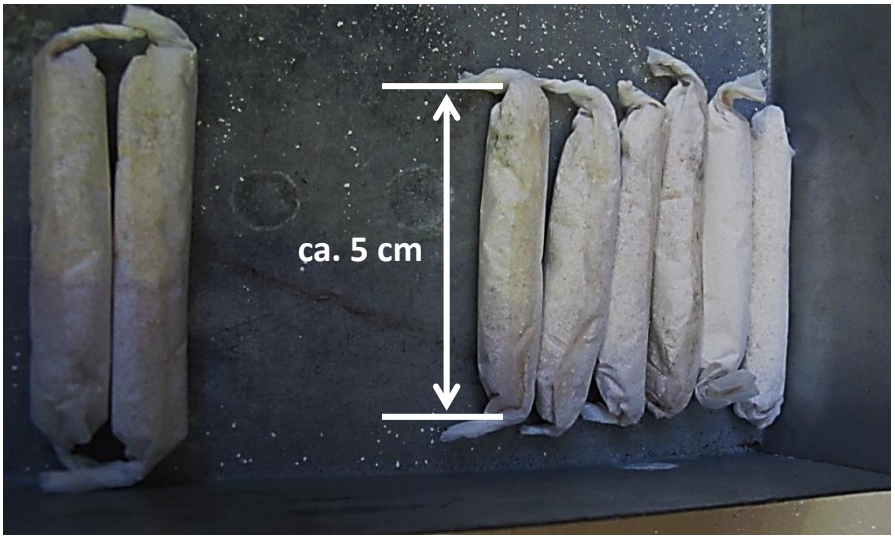

Figure 6-5: Sorbent charges wrapped in small amounts of paper to prevent agglomeration

The experiments performed for the investigation of performance of CaO-based sorbents in in-situ desulfurization are listed in Table 6-3 grouped by the different sorbent materials lime, limestone, fully calcined (f. c.) dolomite and dolomite. The conducted investigations include differences between the different sorbent materials and the influence of a variation of different gasification parameters. Some experiments without the addition of sorbent (NS_SG#1, NS_N2#1, NS_FI#1) provided important information for system characterization. The most comprehensive investigations

are based on the application of lime in order to determine the steady state equilibrium (EQ) of CaO-based desulfurization or the minimum necessary amount of sorbent and stoichiometric influence (SI). The variation of gasification parameters such as steam content (SC), temperature (TI) and residence time (RT) follows the same pattern for the different sorbents. The steam content was varied by alternating the steam inlet in the range of 410 to 680 g/h. The temperature influence was investigated by a variation of the reactor temperature from 700 to 775 °C and the influence of residence time was examined by changing the fuel and steam inlet to yield plus and minus 10 % of the standard settings. The influence of sorbent properties such as the particle size (PS) was investigated for lime and fully calcined dolomite only.

Table 6-3: Experiments with CaO-based sorbents (CaO-SS – steady state of CaO-based desulfurization, OS – over stoichiometric, excess addition of sorbent in nonspecific ratio)

	Reference #	Experimental properties	t_bed	t_free board	mass flow rate Fuel/ steam/ sorbent			total sorbent added	Initial H_2S
					g/h	g/h	g/min	g	ppm_v
Lime	NS_SG#1	Gas composition with mere gasification of pellets	775	825	500	540	-	-	18
	NS_N2#1	Determination of gas properties/variation of N_2 content	775	825	500	540	-	-	1258
	NS_FI#1	Influence of Filter on H_2S content	775	825	500	540	-	-	1445
	CaO_FI#2	Investigation steady state and influence of Filter	775	825	500	540	OS	< 200 g	CaO-SS
	CaO_EQ#1	Investigation of steady state	775	825	500	540	OS	< 200 g	1182
	CaO_RT#1	Influence of residence time	775	825	450/ 550	500/ 620	OS	< 200 g	CaO-SS
	CaO_SI#1	Investigation of stoichiometric influence			500	540	0.039	12.48	1194
	CaO_SI#2	Investigation of stoichiometric influence			500	540	0.041	15.99	1118
	CaO_SI#3	Investigation of stoichiometric influence			500	540	0.043	16.77	1096
	CaO_SI#4	Investigation of stoichiometric influence			500	540	0.047	23.97	1076
	CaO_TI#1	Influence of temperature	700-775	775	500	540	OS	< 200 g	CaO-SS
	CaO_SC#1	Influence steam content	775	825	500	410/ 680	OS	< 200 g	CaO-SS
	CaO_PS#1	Influence of particle size (80-500µm)	775	825	500	540	OS	< 200 g	701
	CaO_PS#2	Influence of particle size (100-200µm)	775	825	500	540	OS	< 200 g	718

	Reference #	Experimental properties	t_bed	t_free board	mass flow rate Fuel/ steam/ sorbent			total sorbent added	Initial H_2S
					g/h	g/h	g/min	g	ppm_v
Limestone	CaCO3_TI#1	Influence of temperature	700-775	775	500	540	OS	< 200 g	1543
	CaCO3_SC#1	Influence steam content	775	825	500	410/680	OS	< 200 g	CaO-SS
	CaCO3_RT#1	influence of residence time	775	825	450/550	500/620	OS	< 200 g	CaO-SS
	CaCO3_SI#1	Investigation of stoichiometric influence	775	825	500	540	0.21	37,8	1259
Dolomite fc	CaOMgO_TI#1	Influence of temperature	700-775	775	500	540	OS	< 200 g	CaO-EQ
	CaOMgO_SC#1	Influence steam content	775	825	500	410/680	OS	< 200 g	CaO-SS
	CaOMgO_RT#1	influence of residence time	775	825	450/550	500/620	OS	< 200 g	CaO-SS
	CaOMgO_SI#1	Investigation of stoichiometric influence	775	825	500	540	0.25	45	1193
	CaOMgO_SI#2	Investigation of stoichiometric influence	775	825	500	540	0.35	63	1104
	CaOMgO_PS#1	Influence of particle size (100-200µm)	775	825	500	540	OS	< 200 g	1361
	CaOMgO_PS#2	Influence of particle size (100-200µm)	775	825	500	540	OS	< 200 g	CaO-SS
Dolomite	CaMg(CO3)2_EQ#1	Investigation of steady state	775	825	500	540	OS	< 200 g	1214
	CaMg(CO3)2_TI#1	Influence of temperature	700-775	775	500	540	OS	< 200 g	1292
	CaMg(CO3)2_SC#1	Influence steam content	775	825	500	410/680	OS	< 200 g	CaO-SS
	CaMg(CO3)2_RT#1	influence of residence time	775	825	450/550	500/620	OS	< 200 g	CaO-SS
	CaMg(CO3)2_SI#1	Investigation of stoichiometric influence	775	825	500	540	0.45	81	1254

While some of the experiments follow the start-up procedure described above, other experimental investigations on distinctive influences of certain parameters are based on a follow up sequence of consecutively changed parameters. In order to exclude influences caused by the experimental history of an ongoing sequence, the test rig was first set to standard conditions (775 °C reactor temperature, 825 °C freeboard temperature, steam-excess-ratio 4) and the CaO-based steady state (CaO-SS) of 500 ppm_v H_2S before a new parameter change was investigated. The experiments which are part of a follow up sequence are indicated with the abbreviation “CaO-SS” as the initial value of H_2S in the gas. Furthermore experiments that are not specifically performed to elucidate the influence of sorbent

stoichiometry are indicated with the abbreviation "OS" for over stoichiometric, as the precise ratio of sorbent to sulfur was not necessarily kept constant over the whole duration of the experimental investigation.

6.2.3 Effect of CaO-based sorbents on the gas composition

With the initial conditions described in section 6.1.3 (775 °C reactor temperature, 825 °C freeboard temperature, steam-excess-ratio 4) and based on a gas with a composition as shown in Table 6-1, the effect of the addition of lime to the fluidized bed of the gasifier was investigated. The sulfur sorbent was added in a clear over-stoichiometric ratio of about 10 times more CaO than would be necessary for the sorption of sulfur down to the CaO-based steady state equilibrium. By means of a GC-PFPD the trend of all detectable gaseous sulfur components was surveyed during the addition of lime and the subsequent decline in total sulfur content as depicted in Figure 6-6.

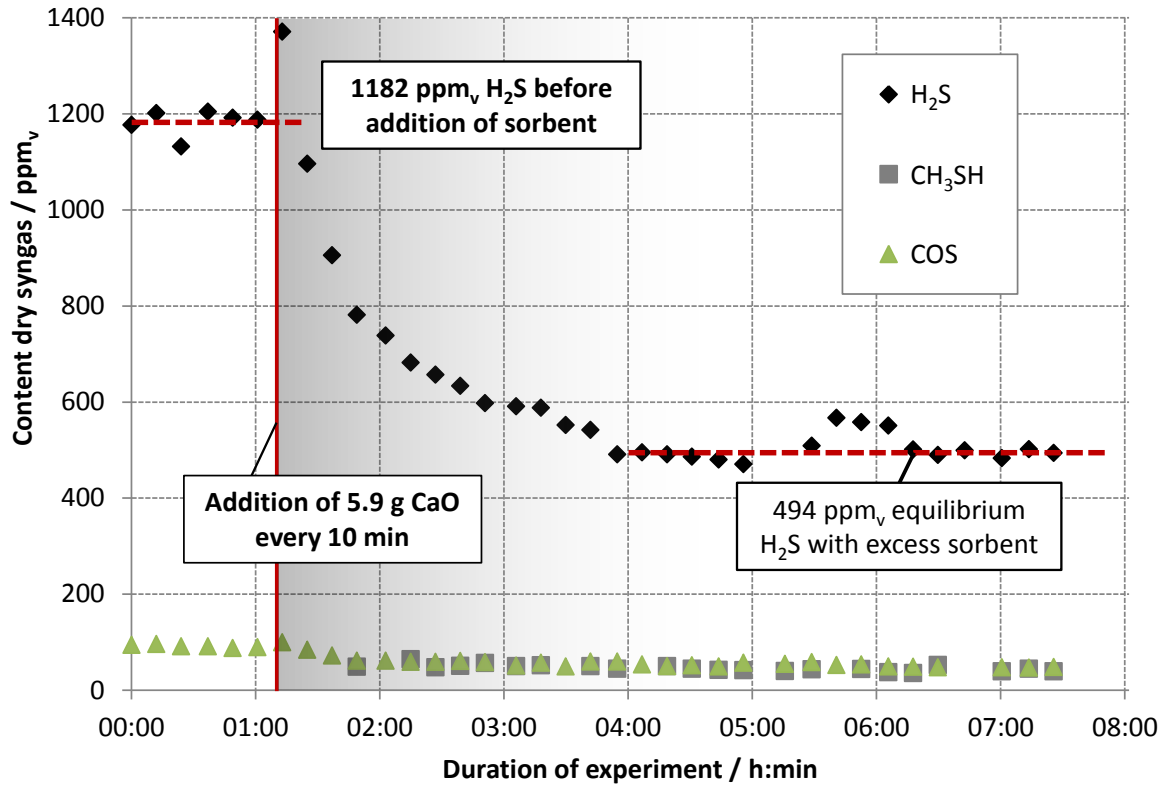

Figure 6-6: Trend of residual sulfur content upon addition of lime as desulfurization sorbent with respect to different sulfurous components, (775 °C reactor temperature, 825 °C freeboard temperature, steam-excess-ratio 4, Table 6-3: Experiment CaO_EQ#1)

As shown in Figure 6-6 H_2S is clearly the dominant sulfur component detected in the syngas. With a ratio of 20:1 as compared to COS the only other gaseous sulfur compound measured under initial conditions. The addition of lime leads to a decrease of the residual H_2S content to a value of about 500 ppm_v, equivalent to the thermodynamic equilibrium of CaO-based desulfurization (Figure 4-4) for the conditions prevailing in the gasifier, as shown in section 4.2.2. The decline of COS is in the same range of roughly 50 % as compared to the initial content thus indicating an equilibrium behavior between the different gaseous sulfur compounds. This is in accordance with other research results on in-situ desulfurization in literature.[73] After an experimental duration of about 2 hours,

Methylmercaptane (CH_3SH) is detected as third sulfurous compound in the gas. This was initially attributed to the addition of lime[111], but is most likely caused by saturation effects within the isopropanol of the impinger bottles for gas conditioning. Due to the high split rate required for H_2S detection, the content of CH_3SH is in the magnitude of the detection limit of the GC-PFPD. Compared to the H_2S contained in the gas the CH_3SH and COS concentration is lower by a factor of 10-20. As H_2S is clearly the predominant sulfurous compound and due to the different ranges of measurement between major and minor components the following investigations focus on the residual H_2S content only.

Besides the trends in sulfurous compounds the tar content and composition was analyzed before and after the addition of lime via SPA-sampling as described in section 5.2.2.1. The total tar content slightly declined upon addition of lime as desulfurization sorbent from 15.4 to 13.6 g/m^3_{std} whereby the standard deviation is in the range of 3 g/m^3_{std} for both values. A more detailed analysis containing the main tar components listed according to their molar weight is shown in Figure 6-7.

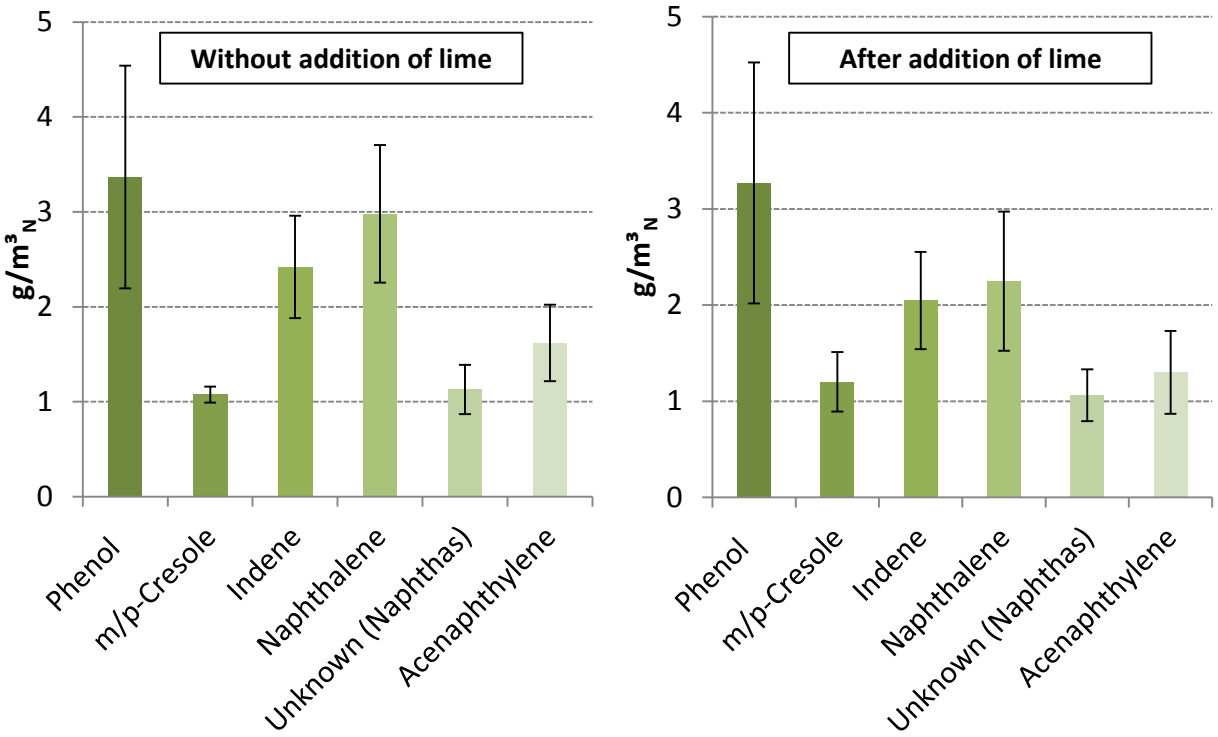

Figure 6-7: Comparison of effect of the addition of lime onto the composition and content of tar components in the gas (Without lime: mean value of 14 samples, after addition of lime: mean value of 20 samples)

The composition of tars does not relevantly change due to the addition of lime with phenol being the main component followed by naphthalene and indene independent of sorbent addition. Solely a slight decrease of heavier tars especially indene and naphthalene as compared to phenol and cresol is detected for the addition of lime. Regarding the high deviation in sampling and analysis, the determined changes in tar concentration and composition have to be considered as negligible. According to results reported in literature[41,57,62] a catalytic activity of lime and other CaO-based materials concerning the conversion of tars is demonstrated profoundly for various gasification setups. On the other hand the olivine, which was used as a bed material in the conducted experiments, has a comparable catalytic activity itself.[41,19] Concluding from the obtained results shown in Figure 6-7, the comparatively low amount of added lime in the range of 100 – 200 g as

compared to the amount of 1400-1500 g olivine as bed material has, if at all, a negligible additional catalytic effect on tar conversion. The same observation can be deduced from the results concerning the addition of dolomite and fully calcined dolomite which yield a mean tar concentration of 13.17 g/m^3_{std} based on eight measurements with a standard deviation of 1.72 g/m^3_{std}. An increased catalytic activity towards tar conversion by addition of dolomite and fully calcined dolomite to the bed material olivine, as stated by other researchers,[41,62] was therefore not observed according to the obtained results. A summary of the syngas composition and properties before and after the addition of lime is listed in Table 6-4.

Table 6-4: Comparison of syngas composition and properties before and after the addition of lime

Experimental results	H_2	CO_2	CO	N_2	CH_4	H_2S	COS	$S\text{-}C_xH_y$	Tars	H_2O
			$\%_{,dry}$				$ppm_{v,dry}$		g/m^3_{std}	%
Wood -pellets + CS_2	41.0	18.4	24.2	8.5	7.9	1195	59	13.6	15.4	39.2
Wood -pellets + CS_2 + CaO	41.8	18.8	23.2	8.5	7.5	494	36	3.7	13.6	38.5

The SPA-samples for the analysis of tar components were partly used for the determination of organic sulfurous compounds with dew points lower than that of thiophene. As shown in Table 6-4, the separate analysis of sulfurous tar components, performed by means of gas chromatography under application of PFPD-measurement (section 5.2.2.2), shows a clear influence of the addition of lime to the gasifier. A comparison concerning the content and composition of these sulfurous tars in a sulfur-enriched gas before and after the addition of lime as in-situ sorbent is depicted in Figure 6-8.

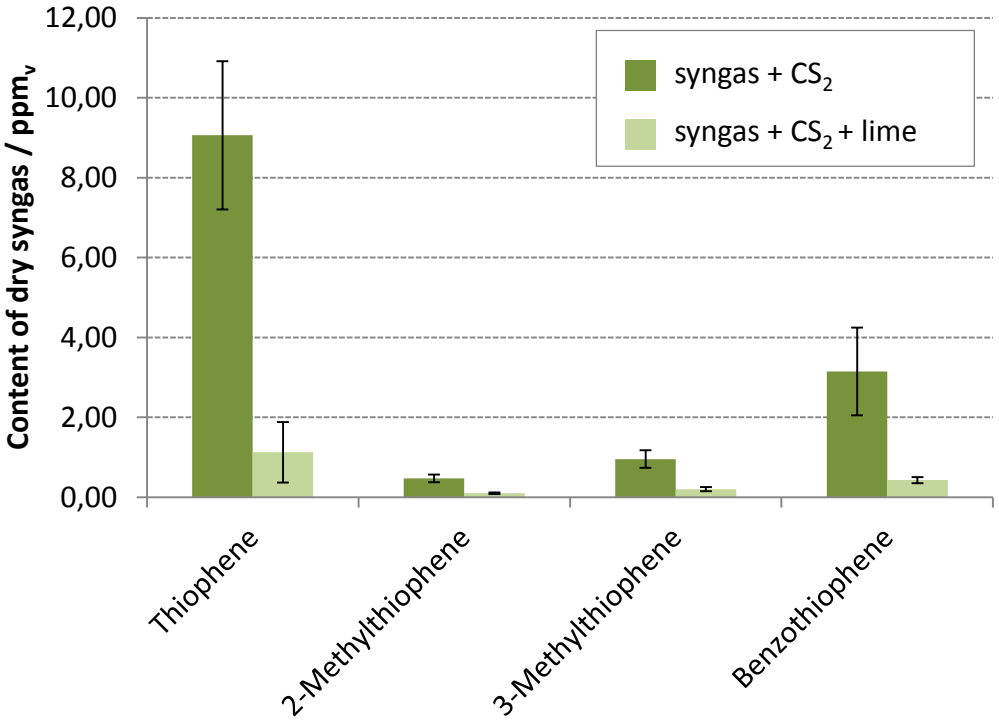

Figure 6-8: Content and composition of sulfurous tar components in the gas with respect to the effect of the addition of lime (Mean value of 6 measurements, from 2 samples each)

Thiophene is clearly the dominant sulfurous compound measured in the SPA-samples for tar analysis. Before the addition of lime, 9.1 ppm_v thiophene are contained in the gas followed by benzothiophene with 3.1 ppm_v. The addition of lime leads to a clear decline in the measured sulfurous hydrocarbons. For both, the thiophene and benzothiophene content is declined by a factor of about 8 resulting in 1.1 ppm_v and 0.43 ppm_v respectively. The sum of the detected sulfurous hydrocarbons is reduced from 13.6 to 1.9 ppm_v by the addition of lime with a corresponding decline in H_2S from about 1200 to 500 ppm_v. Thiophene contents between of 0.2 and 0.6 ppm_v were measured in studies by Zuber et al.[124] with corresponding H_2S concentrations of about 17 ppm_v. This equals a ratio between H_2S to Thiophene of about 40:1 as compared to about 130:1 for the sulfur enriched syngas presented in Table 6-1. Inferentially thiophene is of more significance in wood gasification without elevated sulfur content. On the other hand the decline in sulfurous hydrocarbons due to in-situ desulfurization is even more significant as compared to the H_2S content in the gas. This might be of relevance for downstream applications and further treatment of the gas as the organic sulfurous compounds require an additional HDS- conversion step prior to adsorptive sulfur removal.[124] The investigations on sulfurous tar components confirm H_2S as clearly predominant and representative sulfur component in the gas due to an analogy of behavior for the different sulfurous components.

6.2.4 Desulfurization steady states of different CaO-based sorbents

The calcium-based sorbents tested for in-situ desulfurization in this work vary significantly in the composition of minor elements, especially comparing lime and dolomite (Table 6-2). The theoretical thermodynamic desulfurization equilibrium for CaO in the relevant temperature range and conditions within the gasifier is depicted in Figure 4-4. Further factors influencing the desulfurization performance, such as the interaction of different metal oxides or surface related effects require experimental investigation. The results of desulfurization experiments with over-stoichiometric addition of the four different CaO-based sorbents (Figure 6-9) under standard experimental conditions (775 °C reactor temperature, 825 °C freeboard temperature, steam-excess-ratio 4) are shown in Figure 6-9. Solely the results for limestone were obtained at a lower reactor temperature of 700 °C (CaCO3_TI#1).

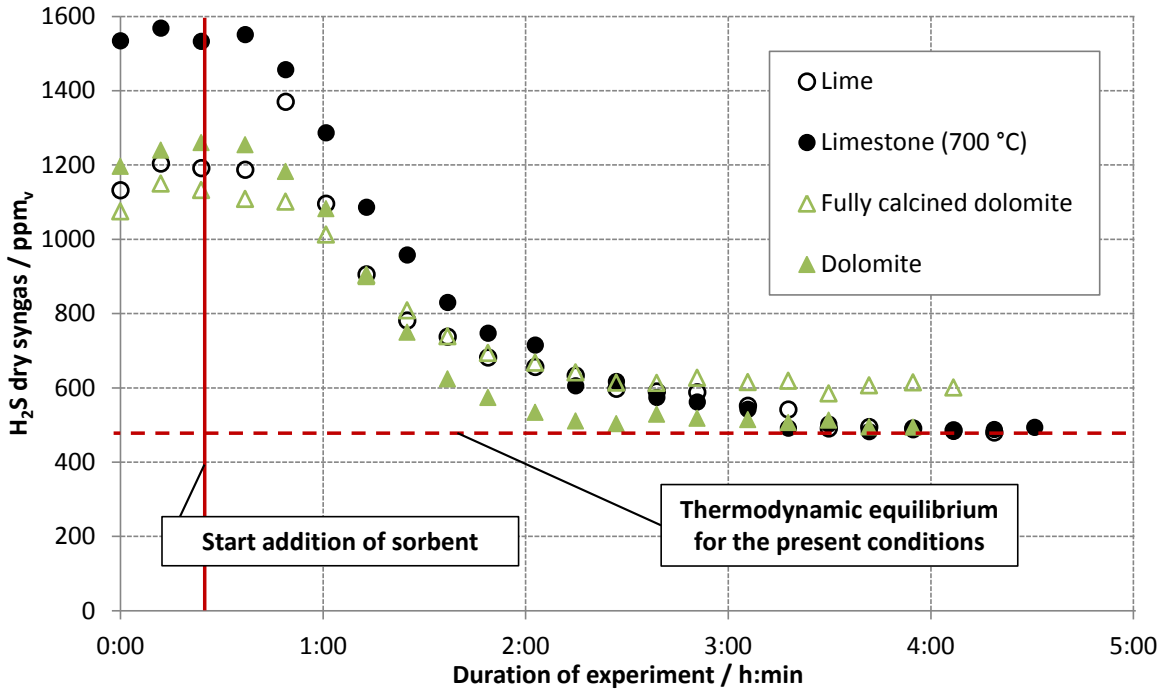

Figure 6-9: Residual H_2S content of produced gas under application of different sorbents at standard conditions (775 °C reactor temperature, 825 °C freeboard temperature, steam-excess-ratio 4, Table 6-3: Experiments CaO_EQ#1, CaCO3_TI#1, CaMg(CO3)2_EQ#1, CaOMgO_SI#2)

According to equilibrium calculations CaO exhibits the lowest thermodynamic desulfurization equilibrium compared to the trace compounds in the tested dolomite under the applied experimental conditions. Accordingly CaO should be the dominant component for desulfurization. As all of the tested sorbents (Figure 6-9) are calcium based, a steady state desulfurization value no higher than that of lime (CaO) is to be expected - with the possibility of positive material interactions of minor compounds in dolomitic sorbents. As depicted in Figure 6-9, this accounts for limestone and uncalcined dolomite with steady state desulfurization of approximately 500 ppm_v H_2S, which is exactly at the same level of desulfurization as compared to the addition of lime. Moreover this level of desulfurization is in the magnitude of thermodynamic equilibrium for the present conditions (Figure 4-4) and is in accordance with the results of other research groups.[73] Upon addition of fully calcined dolomite, the residual H_2S content is reduced from 1100 to 600 ppm_v. The unexpected behavior of fully calcined dolomite with steady state desulfurization of above 600 ppm_v may be explained by the sorbent specific structural properties. These include porosity and crystallite size caused by the industrial production process with higher temperatures in the furnace during calcination. According to BET-analysis shown in Table 6-2 fully calcined dolomite proves to have less than half the surface area as compared to lime. The same accounts for the pore volume, which is double in lime as compared to fully calcined dolomite with even larger pores in the latter. The low surface area of this sorbent in combination with the soft structure of the material, and therefore enhanced grinding upon contact with the bed material olivine, will lead to the observed inferior performance of fully calcined dolomite as compared to the other sorbents. As uncalcined dolomite and limestone are calcined in-situ upon addition to the reactor, the low initial surface area of limestone does not allow a direct conclusion about the performance as sulfur sorbent. The experiments presented in Figure 6-9 indicate a similar behavior of limestone and lime. Accordingly an increase of surface area upon in-situ calcination, can be assumed, which would be in accordance with

observations in literature.[110] The decrease of surface area comparing dolomite and fully calcined dolomite is contrary to the general expectation of an increase in porosity upon calcination due to the release of CO_2 from the crystal structure. According to the supplier, the dolomite is first calcined in a furnace at 850 - 900°C and afterwards ground to the desired particle size. This might account for sintering effects[82] and a destruction of the microstructure in the soft material by clogging of pores. A direct comparison of the analyzed samples of dolomite and fully calcined dolomite is further not valid due to the different particle size fractions of the applied sorbent. Weldon et al. also observed residual H_2S contents far above the thermodynamic equilibrium under in-situ application of dolomite and suggested an internal inhibition of the desulfurization reaction due to an elevated steam content in the particle pores.[73] This would especially account for larger particles with poor pore diffusion. As shown in section 6.2.5 this explanation is supposedly not valid for the presented results due to a positive effect of increased particle size.

6.2.5 Influence of particle size

An influencing factor that had to be examined for comparison of the sorbents used, is the influence of particle size. This is because differences in the particle size distribution in the range of 80 to 500 µm are present in the sorbent samples compared. The dolomite, and in particular the fully calcined dolomite, contains a relevantly larger fraction of fines which leads to increased discharge of sorbent particles from the fluidized bed to the filter housing if the whole fraction of 80 to 500 µm is applied. It is therefore investigated if the difference in particle size distribution has an influence on the steady state desulfurization equilibrium. Results comparing the desulfurization properties of lime and fully calcined dolomite with different particle size fractions are shown in Figure 6-10 under application of standard experimental conditions (775 °C reactor temperature, 825 °C freeboard temperature, steam-excess-ratio 4).

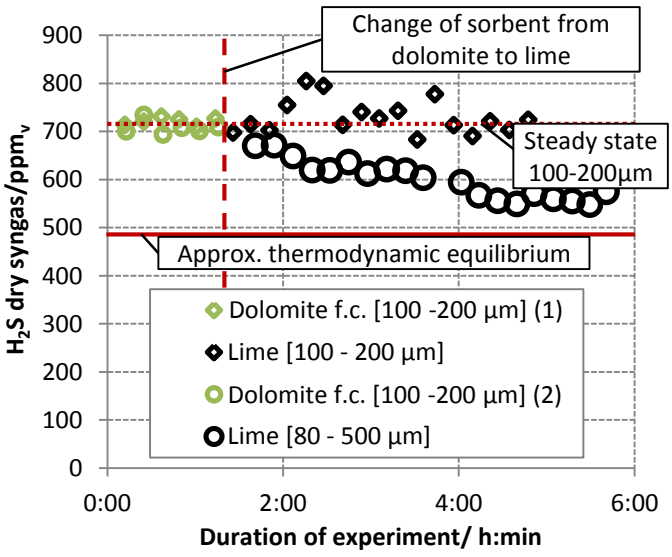

Figure 6-10: Influence of the particle size on the desulfurization equilibrium, comparing lime and fully calcined dolomite (dolomite f.c.) (Table 6-3: Experiments CaOMgO_PS#2, CaOMgO_PS#1, CaO_PS#1, CaO_PS#2)

The results of the residual H_2S content for different particle size fractions (Figure 6-10) show a good conformity for different experimental runs (diamonds and circles) with the 100 - 200 µm fraction of the fully calcined dolomite (dolomite f.c. 1 + 2). These indicate a steady state equilibrium of about

700 ppm_v H_2S for standard experimental conditions. Afterwards, the type of added sorbent was changed from fully calcined dolomite to lime, once with the identical particle size fraction of 100 to 200 µm and once with lime in the full range of 80 to 500 µm, including mainly coarse particles larger than 250 µm. The content of residual H_2S does not change when the sorbent is simply changed from fully calcined dolomite to lime under application of the 100 to 200 µm particle size fraction. However, once coarse particles are added to the system, the content of residual H_2S decreases to about 550 ppm_v as depicted in Figure 6-10. These results show that the particle size has a relevant influence on the desulfurization behavior, whereby contrary to the general expectation, larger particles improve the desulfurization efficiency for in-situ application. This is contrary to the explanation of pore diffusion effects and to previously published results for particle size influence according to TGA measurements.[83,77] The observed effects are most likely accounted for by attrition and subsequent discharge of fines from the fluidized bed. This can be controlled by the amount of fines in the filter housing. For lime and fully calcined dolomite such an increased discharge of fines was observed if only the particle size fraction from 100 to 200 µm was applied. As further shown in Figure 6-10, mainly the coarse particles that remain stable inside the fluidized bed are responsible for a low residual H_2S content under steady state conditions. As the increase of particle size leads to a decrease of the residual H_2S content, it can further be deduced that diffusion inside of the particle pores is not the limiting factor for the achieved desulfurization efficiency in the presented results. In order to establish in-situ desulfurization without limitation by the amount of sorbent prevailing in the reactor and to reduce discharge of fines from the fluidized bed only the coarse particle fraction of dolomite and fully calcined dolomite were applied as indicated in Table 6-2.

6.2.6 Influence of sorbent stoichiometry

In order to exclude sorbent availability as a limiting factor in experiments with fully calcined dolomite and to get a better understanding of the characteristics of CaO-based in-situ desulfurization, the influence of the sorbent stoichiometry was investigated. Further the variation of sorbent stoichiometry is a viable experimental procedure for the determination of sorbent conversion as described in section 6.2.10 and the investigation of a minimum necessary amount of sorbent. This is essential for an economic evaluation as described in section 7.

The investigations on the influence of amount of sorbent are based on two sets of experimental procedures. One is the effect of a varied amount of sorbent under sorbent limiting conditions. For this purpose the stoichiometric ratio of the addition of lime (introduced as γ) was increased stepwise in a series of four subsequent experiments (775 °C reactor temperature, 825 °C freeboard temperature, steam-excess-ratio 4) starting from a stoichiometric ratio of 1 (Figure 6-11, γ = 1.02) This is in clear contrast to the settings of simulation described in section 4 and the other experimental investigations on CaO-based in-situ desulfurization, where the unlimited availability of sorbent was set as a prerequisite for the experimental conditions with sorbent to sulfur ratios γ of above 10. The determination of the sorbent to sulfur ratio is based on the initial H_2S content measured in the gas prior to the addition of sorbent as compared to the molar amount of CaO added as the active component for sulfur sorption (Eq (49)).

$$\gamma = \frac{Ca}{S} = \frac{\dot{n}_{Ca}}{\dot{n}_{gas,dry} \cdot x_{H_2S_{initial}}} \quad \textbf{(49)}$$

The results for stoichiometric addition of lime are shown in Figure 6-11 and indicate a clear effect of an increase in the Ca/S ratios with respect to the achieved steady state desulfurization.

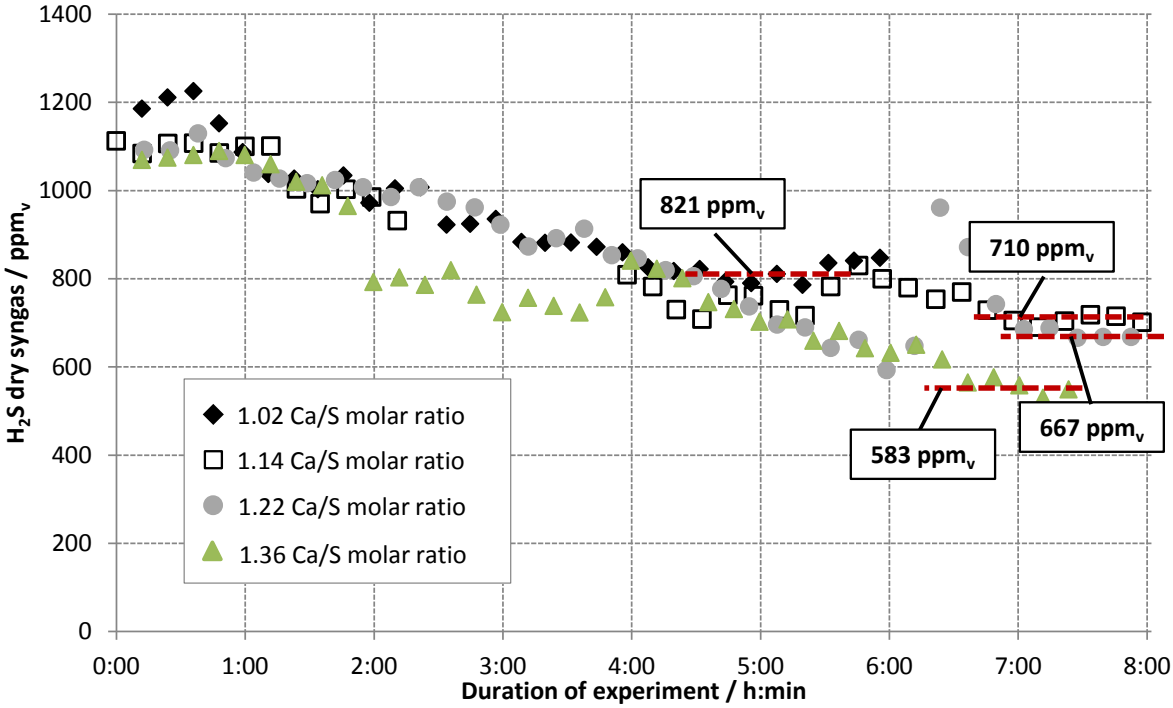

Figure 6-11: Influence of sorbent amount on the achieved steady state desulfurization for addition of lime in the range of stoichiometry (Table 6-3: Experiments CaO_SI#1 - CaO_SI#4)

The trends in residual H_2S content depicted in Figure 6-11 for different amounts of added sorbent show that even with stoichiometric addition of lime a clear desulfurization effect is observed. The addition of 1.02 moles Ca/S leads to a decline in sulfur content from 1200 ppm_v to approximately 821 ppm_v. With a further increase in the ratio of sorbent to sulfur the steady state values can be lowered. At a molar ratio of 1.36 the value of residual H_2S content reaches 583 ppm_v, which is close to the steady state value with addition of excess sorbent. Furthermore, the reduction of the residual H_2S content from 1200 ppm_v down to 583 ppm_v by the addition of 0.47 g of lime every 10 min, equaling a molar Ca/S ratio of 1.36, is a promising result for the application of in-situ desulfurization with lime. In other experimental studies on in-situ desulfurization in gasification application a Ca/S – ratio of 1.5 to 2 was established.[73] The obtained results in literature also show a tendency of lowered steady state values with increased Ca/S ratio but lack the determination of a steady state value at excess sorbent addition. The overall trend of the achieved values of residual H_2S for stoichiometric addition compared to the steady state of H_2S at excess sorbent addition is depicted in Figure 6-12.

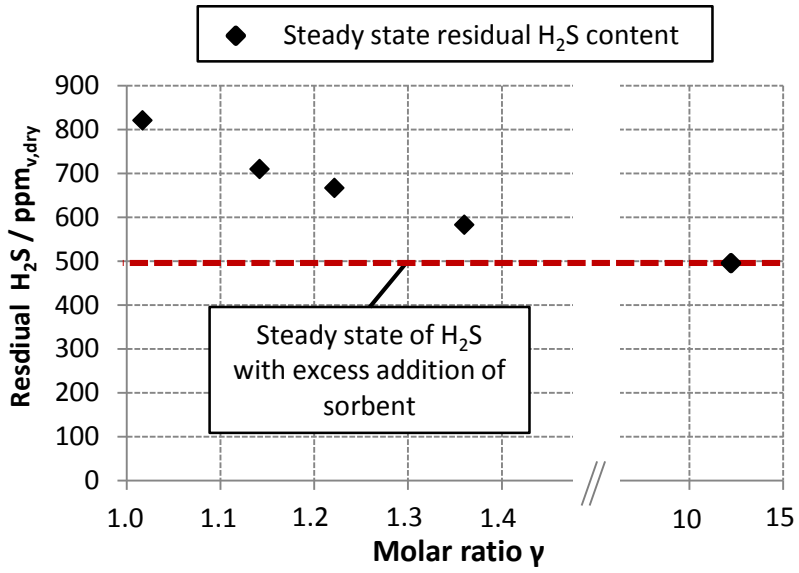

Figure 6-12: Comparison of different values of steady state desulfurization in relation to the Ca/S for addition of lime in the range of stoichiometry

Figure 6-12 shows a rather linear connection between the increase in sorbent/sulfur ratio and the achieved residual H_2S content, indicating a clear limitation of desulfurization by the available amount of sorbent in the gasifier. Inferentially a molar ratio *γ* below 1.5 is not sufficient to establish stable desulfurization conditions down to the steady state residual sulfur content under excess addition of lime.

Another set of experimental procedures aimed at the determination of the influence of stoichiometry on the desulfurization behavior of fully calcined dolomite. The experimental procedure was based on reducing the rate of over-stoichiometric addition of fully calcined dolomite. This was done in order to exclude a sorbent limitation as the reason for an increased residual H_2S content as compared to desulfurization with other CaO-based sorbents (Figure 6-9). As shown in Figure 6-12 reducing the molar ratio *γ* under sorbent limiting conditions would lead to an increase in the steady state value of desulfurization. A variation of the amount of sorbent addition was performed with molar ratios *γ* of 3.4 and 5.2 under standard experimental conditions (775 °C reactor temperature, 825 °C freeboard temperature, steam-excess-ratio 4). As shown in Figure 6-13 both experiments lead to the same steady state value of residual H_2S of 600 ppm_v. Mostly, the duration of the achieved desulfurization down to the steady state varies as a response to a varied amount of added sorbent. As shown in Figure 6-13, this duration varies between 90 min for 63 g and 30 min for 45 g of fully calcined dolomite added to the system. Further, the rise of residual H_2S content (slopes A and B) is slower, if more sorbent is contained in the fluidized bed (Figure 6-13(B)). Inferentially the achieved steady state value for in-situ desulfurization with fully calcined dolomite is not directly limited by the amount of sorbent in the reactor as shown for experiments with lime at lower *γ* ratios in the range of 1 - 1.5 (Figure 6-12).

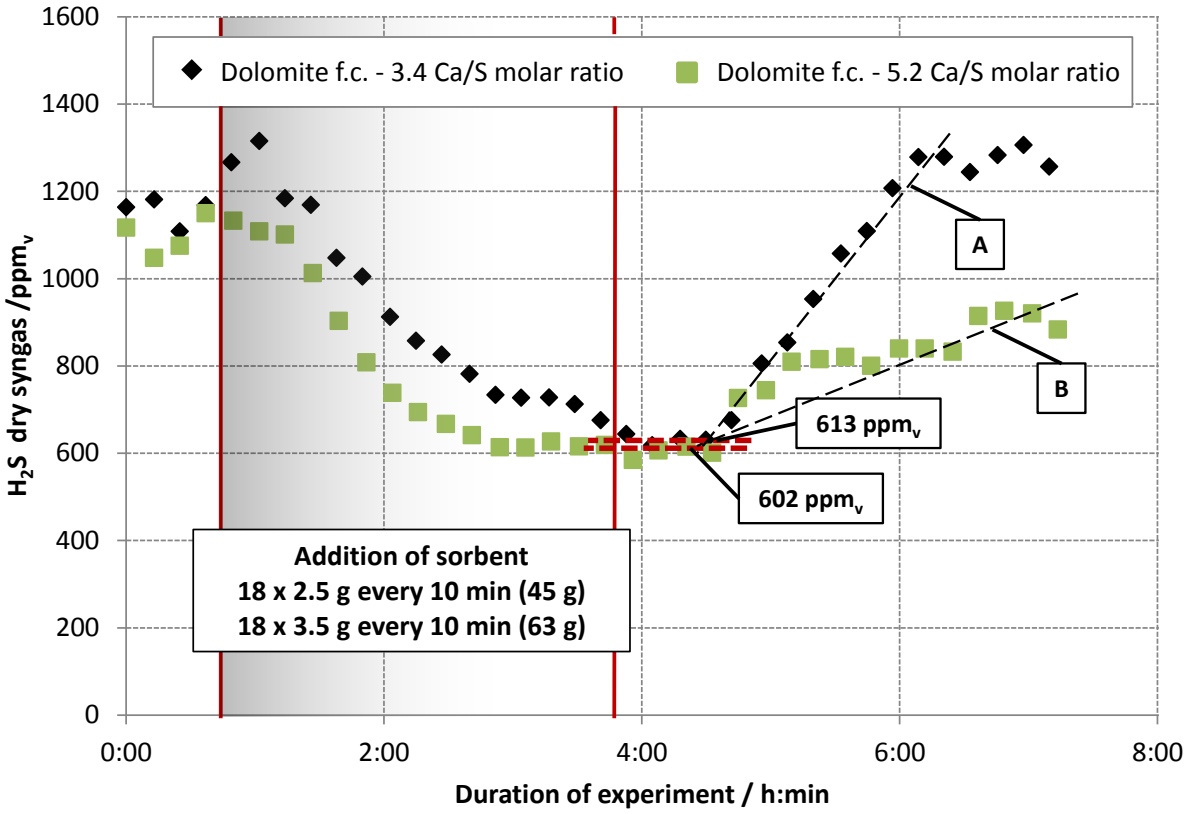

Figure 6-13: Comparison of desulfurization behavior for addition of varied amounts of fully calcined (f.c.) dolomite in the over stoichiometric range (Table 6-3: Experiments CaOMgO_SI#1, CaOMgO_SI#2)

6.2.7 Influence of residence time

In order to approve the independence of the desulfurization results from kinetic limitation, the residence time of the H_2S containing syngas with the sorbent in the fluidized bed was varied. For this purpose the inlet flows of fuel, steam and CS_2 were altered in the range of +/- 10% in relation to standard operating conditions. The degree of variation was limited due to fluidization criteria in the fluidized bed such as to obtain gas velocities above the incipient fluidization point and below the excessive pneumatic discharge of fines. The deviation in residual H_2S content after desulfurization remained below +/- 5% upon alteration of residence time and did not indicate a clear decline of the steady state value once the residence time was increased. The observed fluctuations were therefore considered as not significant regarding the numerous influencing factors in real gasification experiments. This shows that the residual H_2S content does not primarily depend on the residence time for the presented results in steady state desulfurization.

6.2.8 Influence of temperature

Thermodynamics state the influence of steam content and gasification temperature on the equilibrium of Eqs. (33) and (34) as shown in Figure 4-4. For desulfurization with CaO-based sorbents, another influencing factor concerning temperature is the equilibrium of calcination reactions (Eqs. (30) and (31)), which also depend on the partial pressure of CO_2 in the reaction atmosphere. In order to investigate the influence of temperature on the desulfurization steady state under real gasification conditions, a variation of temperature has been conducted. With the aim of also verifying the onset of calcination reactions, limestone and uncalcined dolomite have been added in the gasification

process at a temperature of 700 °C in the reactor and 775 °C in the freeboard of the reactor. The reactor temperature was increased stepwise to a level of 775 °C in the reactor at constant freeboard temperature. Steam and fuel input were kept at standard values with a steam excess ratio of 4 and sorbent added at a ratio *γ* of 10 for both experimental runs. The results are depicted in Figure 6-14.

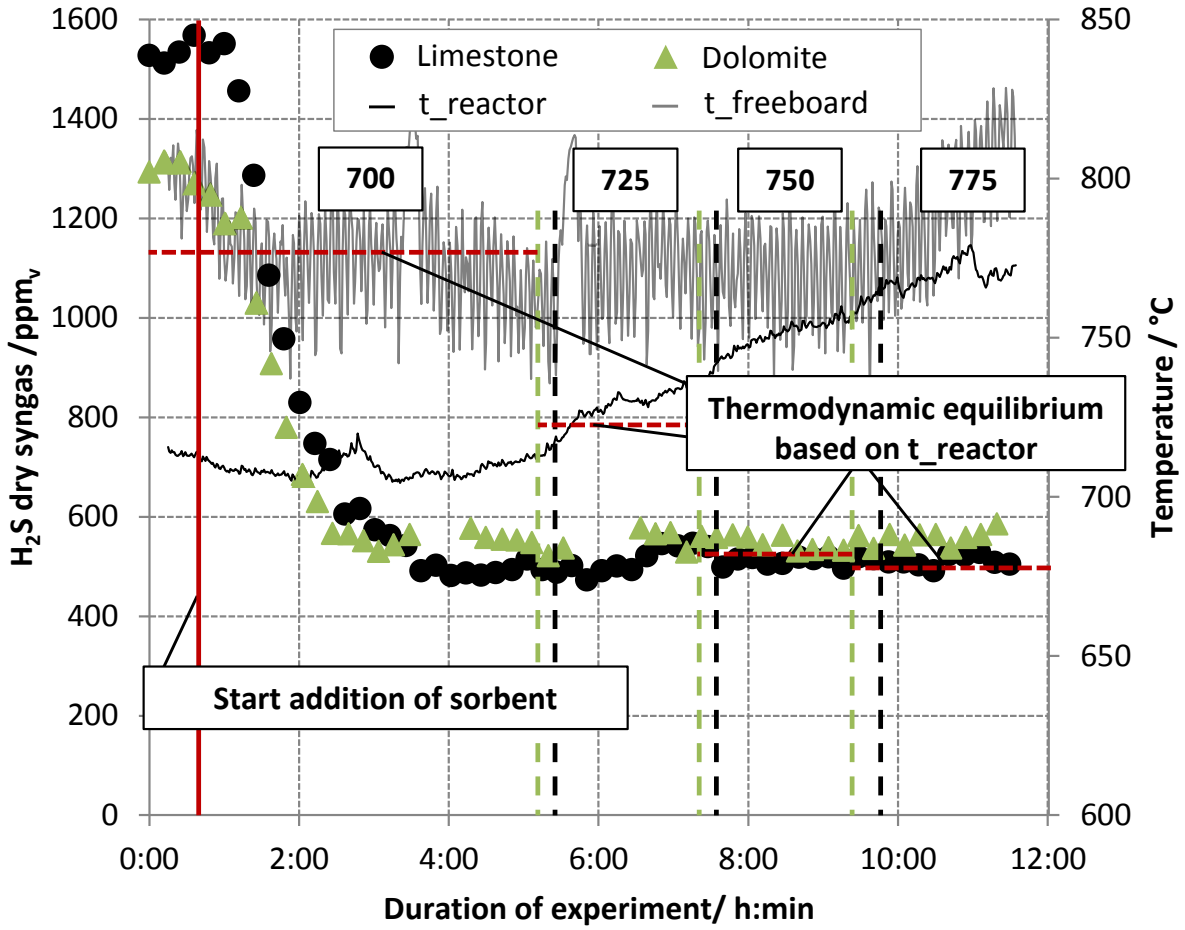

Figure 6-14: Variation of gasification temperature with a stepwise increase of the reactor temperature from 700 to 775 °C at a constant freeboard temperature of 775 °C. Temperatures are shown for the experimental run with dolomite. Thermodynamic equilibrium shown is based on equilibrium calculations (compare Figure 4-4) (Table 6-3: Experiments CaCO3_TI#1, CaMg(CO3)2_TI#1)

When sorbent is added, the residual H_2S content of the produced gas drops for both sorbents, limestone and uncalcined dolomite, to a value of about 500 to 550 ppm_v as shown in Figure 6-14. The values for dolomite are slightly higher than those for limestone. The stepwise increase of temperature did not result in any related changes of the residual H_2S content. The value of 500 ppm_v residual H_2S is below the thermodynamic equilibrium based on the reactor temperature of 700°C. The fact that the residual H_2S content is promptly reduced to a minimum value of around 500 ppm_v and remains constant upon elevation of the reactor temperature from 700 to 775 °C therefore implicates that the freeboard temperature which was kept constant at 775 °C determines the achievable level of desulfurization. Inferentially the fluidized bed is partly extended into the freeboard region. This is confirmed by the decline in freeboard temperatures upon addition of sorbent as shown in Figure 6-14. A clear separation of the zones is difficult due to the limited size of the gasification reactor, especially as the bed height changes with the amount of coke contained or the amount of added sorbent. Even for standard conditions with temperatures of 775 °C in the

reactor and 825 °C in the freeboard the measured results of the residual sulfur content prove to be in the exact same range of 500 ppm_v (Figure 6-14) whereby the equilibrium value at 825°C is above 650 ppm_v H_2S (Figure 4-4). Thus it can be stated that in a combined system consisting of different reaction zones, the effective steady state equilibrium is determined by the conditions resulting in the lowest thermodynamic equilibrium of the desulfurization reactions (Eqs (33) and (34)). The presented results therefore confirm that sulfidation is the dominant step as compared to the reverse release of H_2S from CaS[125] On the other hand it is shown in section 6.4.1 that the reverse reaction takes place if the content of H_2S in the gas is decreased. The scope of variation of temperatures was limited due to the requirements for the gasification reaction itself. It is mainly the steam reforming of tars (Eq (11)) and the Boudouard reaction (Eq (3)) that requires external heat and a sufficient temperature level for the gasification of coke to gaseous CO.

In order to maintain stable gasification conditions, it is necessary to remain above a temperature level of around 770 °C in the freeboard of the reactor. A further increase of reactor temperature was not possible due to heat-transfer limitations of the gasification reactor and material limitations within the reactor heating tubes.

While uncalcined sorbents are added to the fluidized bed, the CO_2 content of the gas increases by about 0.5 vol% with the same magnitude for dolomite and limestone. This change in the gas composition does not occur when calcined sorbents are added. The increase of the CO_2 content in the gas indicates that, for limestone and uncalcined dolomite, the onset of calcination reaction happens promptly at a temperature level of 700 °C in the reactor and 775 °C in the freeboard. It can therefore be assumed that all results presented for limestone and dolomite refer to the fully calcined state, meaning that desulfurization follows Eq (33) instead of Eq (34).

6.2.9 Influence of steam content

In addition to the temperature of the reaction environment, the steam content is also a major factor influencing the thermodynamic equilibrium due to the release of water during sulfidation of CaO (Eq (33)). The steam-excess-ratio has therefore been varied in the range of 3 to 5 (Eqs (22)-(24)). The corresponding values for steam input are 410, 540 and 680 g/h. The fuel input has been kept constant at 500 g/h with standard experimental conditions (775 °C reactor temperature, 825 °C freeboard temperature, $\gamma \sim 10$) except for the variation in steam-excess-ratio. Figure 6-15 shows the corresponding residual H_2S content for the application of lime and dolomite under steady state conditions.

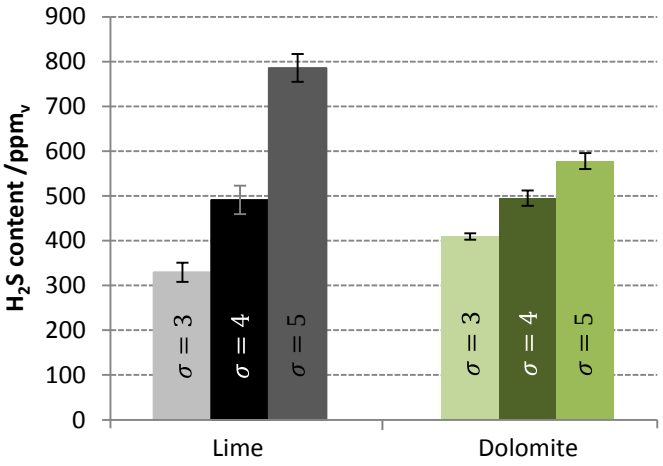

Figure 6-15: Comparison of residual H_2S content under steady state conditions for lime and dolomite upon variation of steam-excess-ratio (σ); average values of several hours of measurement for each setting (Table 6-3: Experiments CaO_SC#1, CaCO3_SC#1, CaMg(CO3)2_SC#1)

The effect of the steam content on the desulfurization in steady state operation is clearly visible for the tested sorbents. The comparison of results for lime and dolomite as shown in Figure 6-15 indicates a relevant difference between the effects of a changed steam-excess-ratio for the different sorbents. For lime, the residual H_2S content increases from 330 to 786 ppm_v and for dolomite it increases from 410 to 578 ppm_v upon elevation of the steam-excess-ratio from 3 to 5. The values for standard conditions of steam-excess-ratio 4 are roughly identical with 491 and 495 ppm_v for lime and dolomite, respectively. Further differences can be observed in the changes of gas analysis data (Figure 6-16). The trends of CO and H_2 content are shown for the increase of the steam-excess-ratio from 4 to 5, which leads to an increase of H_2 and decrease of CO due to the water-gas-shift reaction (Eq (6)) The different effect of a varied steam-excess-ratio might be explained by the functionality of the MgO in dolomite as a water-gas-shift catalyst[83]leading to a less significant change of the actual steam content upon increase of the steam inlet flow. This assumption is supported by the analysis of gas composition shown in Figure 6-16.

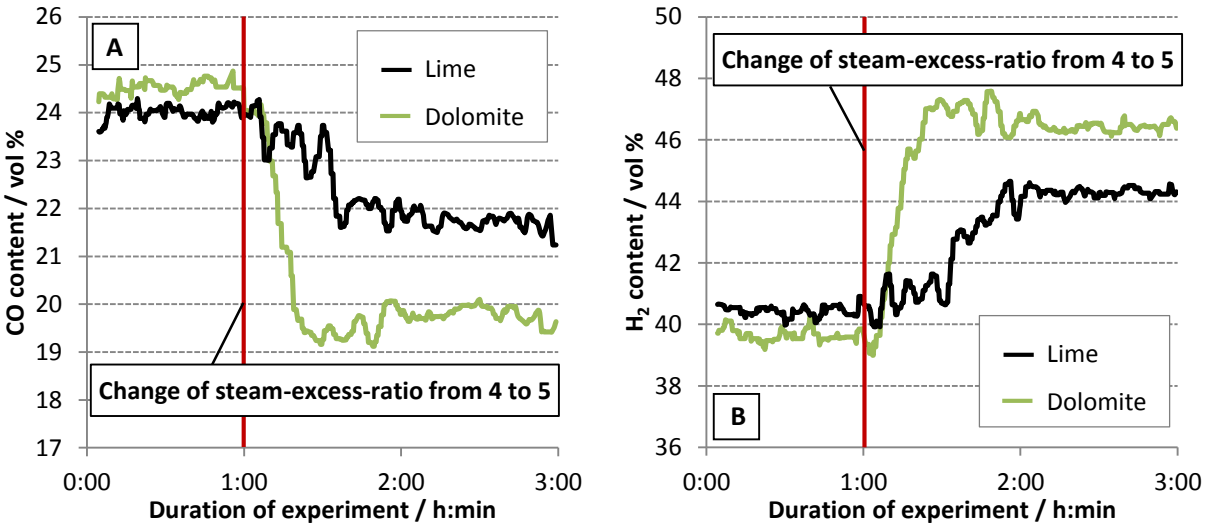

Figure 6-16: Change of gas composition upon increase of steam-excess-ratio from 4 to 5 with Figure 6-16 (A) showing CO and Figure 6-16 (B) showing H_2 gas analysis data

Part A of Figure 6-16 shows the CO-content in the gas and part B the corresponding H_2-content an hour before and two hours after increasing the steam-excess-ratio from 4 to 5. The content of CO decreases promptly once the steam inlet is increased in a fluidized bed containing dolomite and, at the same time, the H_2 content rises accordingly. For a fluidized bed containing lime, the changes in the gas composition are far less distinct. The increase of steam inlet leads to a slow onset of variation in gas composition indicating a less pronounced water-gas-shift reaction and thus a higher steam content in the syngas. This especially qualifies dolomite for the use in a syngas with high steam contents above 40 vol%. The corresponding change in volume of the produced syngas upon variation of the steam inlet is equivalent to a variation of H_2S concentration, as the amount of added CS_2 is kept constant. As long as the sorbent material is added in excess and the partial-pressure of H_2S is negligible compared to the partial-pressure of steam in the gas, such a change in H_2S concentration does effectively not influence the thermodynamic equilibrium as explained in section 4.2.1.3. This is also confirmed by experimental investigation as shown in Figure 6-14 were a higher initial H_2S content due to a lower amount of produced gas at lower temperatures (700 °C) leads to the same steady state equilibrium of 500 ppm_v as compared to standard conditions.

6.2.10 Determination of sorbent conversion

Another important aspect for the comparison of different sorbents is the amount of material needed to reduce the H_2S content to the value of steady state operation. Besides the purpose of determination of desulfurization characteristics as shown in Figure 6-11 and Figure 6-13, the need for a minimization of the amount of added sorbent is primarily economic, due to the costs of sorbent input and disposal.[126-128] Further, the addition of a defined amount of sorbent with subsequent analysis of the total reduction of H_2S in the produced gas allows for the evaluation of the fraction of CaO that is converted to CaS.

For this purpose, the addition of sorbent was limited to a reduced rate and interrupted after 3 hours of batch wise addition. At such reduced Ca/S ratios (Table 6-5) the addition of in-situ sorbents results in a spontaneous decline of residual H_2S in the gas but once the addition of sorbent is stopped, the residual H_2S content rises until it eventually reaches the initial feed concentration. This results in a temporary depletion of H_2S from the gas which can be directly related to the amount of CaO added to the gasifier and equals the number of moles of adsorbed H_2S. The moles of adsorbed H_2S were derived from the results of GC measurement. For each value of measurement, the difference between the actual value after addition of sorbent and the average value of initial H_2S content was calculated. The difference in the H_2S content ($\Delta H_2S_{initial-actual}$) multiplied by the duration of measurement $\Delta t_{measurement}$ results in an area of depletion of H_2S as depicted in Figure 6-17. The sum of all measured values then yields the total amount of H_2S adsorbed under consideration of the molar flow of dry gas ($\dot{n}_{gas,dry}$) (Eq (50)).

$$H_2S_{adsorbed} = \sum \dot{n}_{gas,dry} \cdot \Delta H_2S_{initial-actual} \cdot \Delta t_{measurement} \quad \textbf{(50)}$$

The described method for the determination of adsorbed sulfur is depicted in Figure 6-17 by the integration of the depletion of H_2S from the product gas.

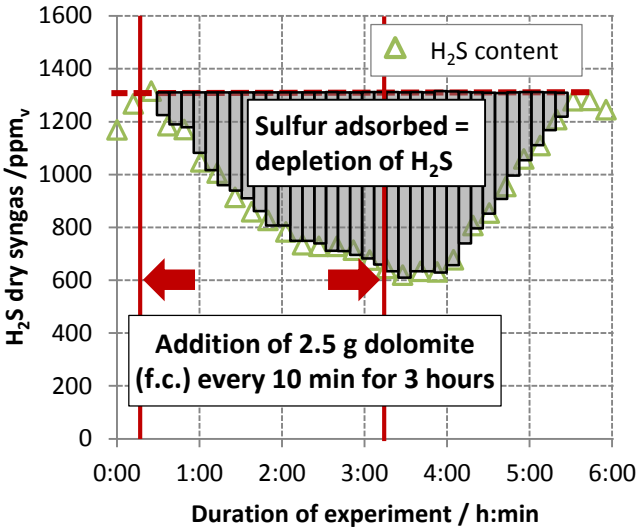

Figure 6-17: Estimate of the total amount of adsorbed sulfur by numerical integration of the desulfurization effect shown by the example of fully calcined (f.c.) dolomite (Table 6-3: Experiment CaOMgO_SI#1)

As shown in Figure 6-17, the number of moles of H_2S adsorbed is considered as the amount of total sulfur adsorbed. Consequently, a sorbent conversion (Eq. (51)) can be estimated by comparing the total moles of sulfur adsorbed to the total moles of sorbent added. For dolomite, the calculated results only refer to the content of CaO in the dolomite and thus considering that MgO passes the reactor as an inert (section 4.2.1.1). According to the desulfurization reaction (Eq. (33)), the amount of adsorbed H_2S is equal to the number of moles of CaS formed.

$$X_{CaO} = \frac{n_{CaS}}{n_{CaO}} \quad (51)$$

Based on this procedure, the conversion of CaO was estimated for the compared sorbents under application of the particle size fractions listed in Table 6-2. The addition of a coarse powder in the case of dolomite-based sorbents reduces the influence of attrition and discharge of fines for the comparatively soft material whereby the latter cannot be prevented due to the severe attrition within the fluidized bed. An overview of the obtained results for the determined sorbent conversion is shown in Table 6-5 with a comparison thereof depicted in Figure 6-18.

Table 6-5: Comparison of conversion of different sorbents

Sorbent	-	CaO				$CaCO_3$	CaOMgO		$CaMg(CO_3)_2$
H_2S equilibrium	ppm_v	821	710	667	583	536	626	611	459
CaO equivalent / min	g	0.039	0.041	0.043	0.047	0.12	0.13	0.18	0.14
Ca/S molar ratio γ	-	1.0	1.1	1.2	1.4	2.9	3.4	5.2	3.4
X_{CaO}	%	35	39	38	30	34	16	14	36

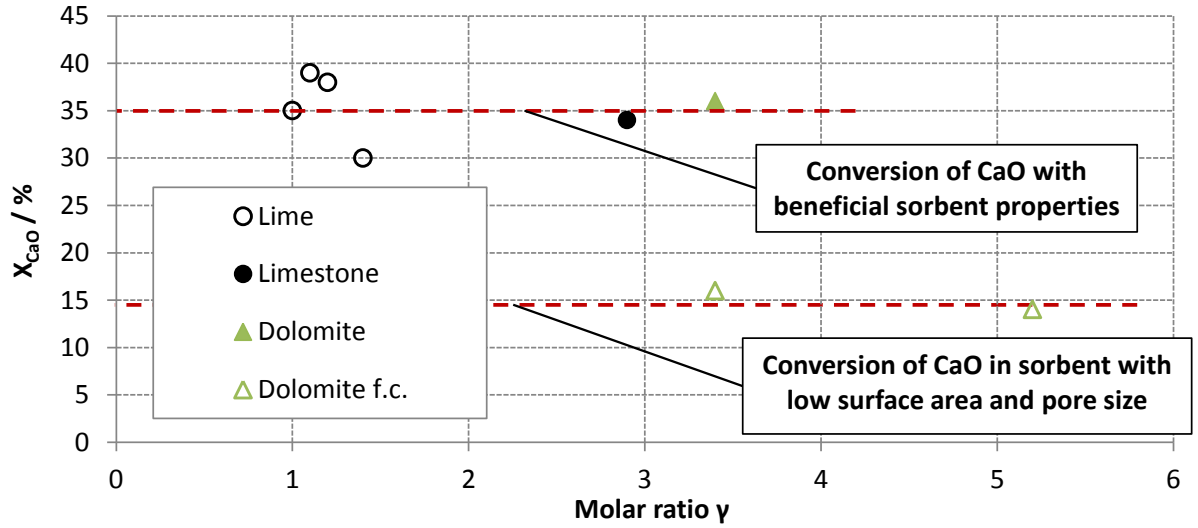

Figure 6-18: Comparison of conversion of CaO in different sorbents according to the molar ratio *y* and sorbent properties

As shown in Figure 6-18 for lime, a medium conversion of 36% has been calculated based on 4 subsequent measurements with different amounts of sorbents. (Table 6-5) Results in the same range have been obtained for limestone and dolomite (34% and 36%). These findings are in accordance with investigations by Yrias et al.[80] stating that both, dolomite and limestone, can be effective sorbents for sulfur capture once the prevailing gasification conditions allow the calcination of $CaCO_3$. The effect of sintering of the produced CaS layer was not investigated explicitly nor do the results indicate such a process e.g. by an increased conversion of dolomite as compared to lime and limestone. The widely stated benefit for the use of dolomite[80-82,129,130], a reduced sintering of the formed CaS due to the contained MgO, was therefore not confirmed in the course of the presented experimental work. Contrarily fully calcined dolomite showed conversions of 14 and 16% CaO to CaS that were found in subsequent experiments, resulting in a clearly lower conversion concerning the CaO fraction in this sorbent (Figure 6-18). This result is in accordance with the elevated steady state desulfurization shown in Figure 6-9 and the BET- measurements (Table 6-2) that indicate a significantly lower surface area of fully calcined dolomite as compared to lime. Increased discharge of the soft material in combination with a smaller active surface will account for the low conversion. The obtained results also confirm that the MgO in the dolomite does not contribute to the desulfurization and that minor elements also seem to pass the reactor as inert. This is shown by the mostly equivalent conversions of CaO to CaS in lime, limestone and dolomite. The inert behavior of minor elements reflects the obtained results for desulfurization steady states, which are identical between dolomite containing a large fraction of minor components and lime, whereby the latter consists basically solely of CaO (Table 6-2). Accordingly positive material interactions concerning the achievable steady state equilibrium of desulfurization were not observed for multicomponent dolomite in the course of the presented experiments.

This excludes the observed catalytic effect of MgO in dolomite on the progress of water-gas-shift reaction (Eq (6)). These results qualify dolomite for the use in gasification processes with steam contents above 40 vol% in the produced syngas, as the effect of the promoted water-gas-shift reaction proves to be beneficial for the achievable desulfurization equilibrium. A disadvantage of the use of dolomite is the higher amount of sorbent needed, due to the MgO content that has to be

considered as inert for desulfurization. This is especially the case with fully calcined dolomite, with an average conversion of 15% of CaO to CaS as compared to 35% for the other sorbents. Considering a CaO content of 60 wt% in the applied dolomite, about four times as much sorbent is needed for the same desulfurization effect as compared to the application of lime. In summary, the application of fully calcined dolomite seems least advisable for desulfurization purposes due to a supposed sintering during calcination. Regarding the catalytic effect of MgO on the water-gas-shift reaction, the use of dolomite which is calcined in-situ seems appropriate, especially for high steam atmosphere, whereby disposal related problems increase with the amount of sorbent needed. According to the presented results and as limestone costs less than lime, the use of limestone seems the most advisable for coarse desulfurization in biomass gasification under calcining conditions.

Under consideration of the benchmark of 100 ppm_v stated in Figure 3-1 as upper limit for the achievable residual sulfur content via in- situ desulfurization the results obtained by CaO-based desulfurization experiments shown in section 6.2 are not sufficient. The experimentally achieved steady state value of 500 ppm_v H_2S therefore confirms the calculated thermodynamic equilibrium for the conditions present in the gasifier as demonstrated in section 4.2. Only for high sulfur gasification fuels producing H_2S contents in the gas of above 1000 ppm_v the application of CaO-based in-situ desulfurization might be warranted. This applies for fuels containing sulfur in the range of 0.35 wt% and above, such as paper residue sludge and sewage sludge (Table 2-2) or equivalent admixtures of such waste materials to other types of fuel. As the achievable value of 500 ppm_v residual H_2S does not suffice a satisfactory outlet concentration of in-situ desulfurization experimental investigations were continued with other materials offering lower thermodynamic equilibrium values (Figure 4-5).

6.3 Barium based in-situ desulfurization[1]

Regarding the benchmark for lowering the residual sulfur content to values below 100 ppm_v based on in-situ desulfurization (Figure 3-1), the achievable steady state desulfurization under application of a CaO-based sorbents cannot suffice this criterion due to thermodynamic limitations. This is in clear contrast to the thermodynamic limits given by the application of a BaO-based desulfurization sorbent synthesized at Forschungszentrum (FZ) Jülich with equilibrium values below 5 ppm_v H_2S for the intended process conditions (Figure 4-5). The experimental results of the process application of this sorbent under in-situ conditions are described in the following sections.

6.3.1 Sorbent materials and preparation

The calcination temperature of barium is relevantly higher as compared to calcium with a required temperature of over 1000 °C depending on the CO_2 partial pressure.[132] As $BaCO_3$ is not favorable for desulfurization purposes the application of Barium as desulfurization sorbent is commonly not considered in the context of syngas desulfurization (Figure 2-7).[91] A recently developed BaO-based sorbent, synthesized by FZ Jülich, however proved the potential of stabilized BaO and was successfully tested in fixed bed application in a plug flow reactor with bottle-mixed simulated syngas.[86] This BaO-based "CaBa" sorbent was obtained from FZ Jülich for investigation of the desulfurization properties under experimental application in real gasification experiments with the

[1] Segments of this section have already been published by Husmann *et al.*[131]

gasifier test rig as shown in Figure 5-3. The CaBa was synthesized according to a procedure first described by Stemmler.[48] In order to produce a solid solution of BaO in CaO, a miscibility gap of these earth alkaline oxides at temperatures above 1200 °C is taken advantage of. The reactants for synthesizing the mixed phase are the carbonates $BaCO_3$ and $CaCO_3$ mixed in a molar ratio of 1:9. The mixture of powders is further ground in a mortar and mixed with distilled water to a paste. Extrudates of 2 mm in diameter and 2-4 mm in length were formed and filled into a platinum crucible. The extrudates were then heated in a muffle furnace with a ramp of 10 K per minute to an end temperature of 1600 °C. At this temperature level the carbonates are calcined and then tempered for a duration of 10 hours with the aim of producing finely dispersed reactive oxide particles.[48] Subsequently the produced solid solution of oxides is cooled to room temperature and stored under dry conditions until application. Careful handling especially with regard to exposure to humidity is necessary as the sorbent material is highly hygroscopic. With the humidity contained in the surrounding air the sorbent extrudates decompose to a fine powder within 24 hours. Samples exposed to air decompose under formation of CaOH and BaOH as also observed and analyzed in prior research.[48] Additionally a careful handling of the sorbent is necessary as all the water soluble Ba-compounds are toxic. This necessitated increased safety measures during sorbent handling and gasifier operation as explained in section 6.3.3.

A total of 943 g of the sorbent was obtained from FZ Jülich for the experiments presented herein. According to preliminary tests, sintering of the sorbent occurred under fluidized bed conditions and even by heating the sorbent in a muffle furnace to temperatures of 800 °C. As a consequence a method for further sorbent preparation was established in order to prevent sintering effects and obtain a sorbent with an appropriate particle fraction. The nomenclature used for the different charges of sorbent is “CaBa original“ for the sorbent as obtained by FZ Jülich and “CaBa pelletized” for the post treated sorbent material.

The “CaBa original” as supplied by FZ Jülich consisted of some extrudates in the original length range of 2-4 mm but mostly of a fine powder below 250µm sieve fraction. The fine fraction was not suitable for in-situ application due to elutriation from the gasifier. On the other hand even the extrudates in the coarse fraction were soft and supposedly not stable under fluidized conditions. Further treatment was therefore necessary in order to increase the particle size and hardness of the supplied powder. For this purpose the original CaBa powder was pressed to tablets of 20 g (Figure 6-19 (A)) and then baked in a muffle furnace at 800 °C for 30 min. The results were stone-like sintered blocks as shown in Figure 6-19 (B) that were subsequently crushed in a mortar (Figure 6-19 (C)). The obtained powder was then sieved to a desired particle size fraction of 250 to 1000 µm. The sorbent produced according to the procedure shown in Figure 6-19 is referred to as “CaBa, pelletized”.

Another modification that was based on preliminary tests in a muffle furnace was the combined addition of “CaBa, pelletized” with lime as separating agent in order to prevent sintering. The lime was of the same material as characterized in Table 6-2 and added with the “CaBa, pelletized” in a weight based ratio of 1:1. More details concerning the effect of the addition of lime are given in sections 6.3.4 and 6.3.5.

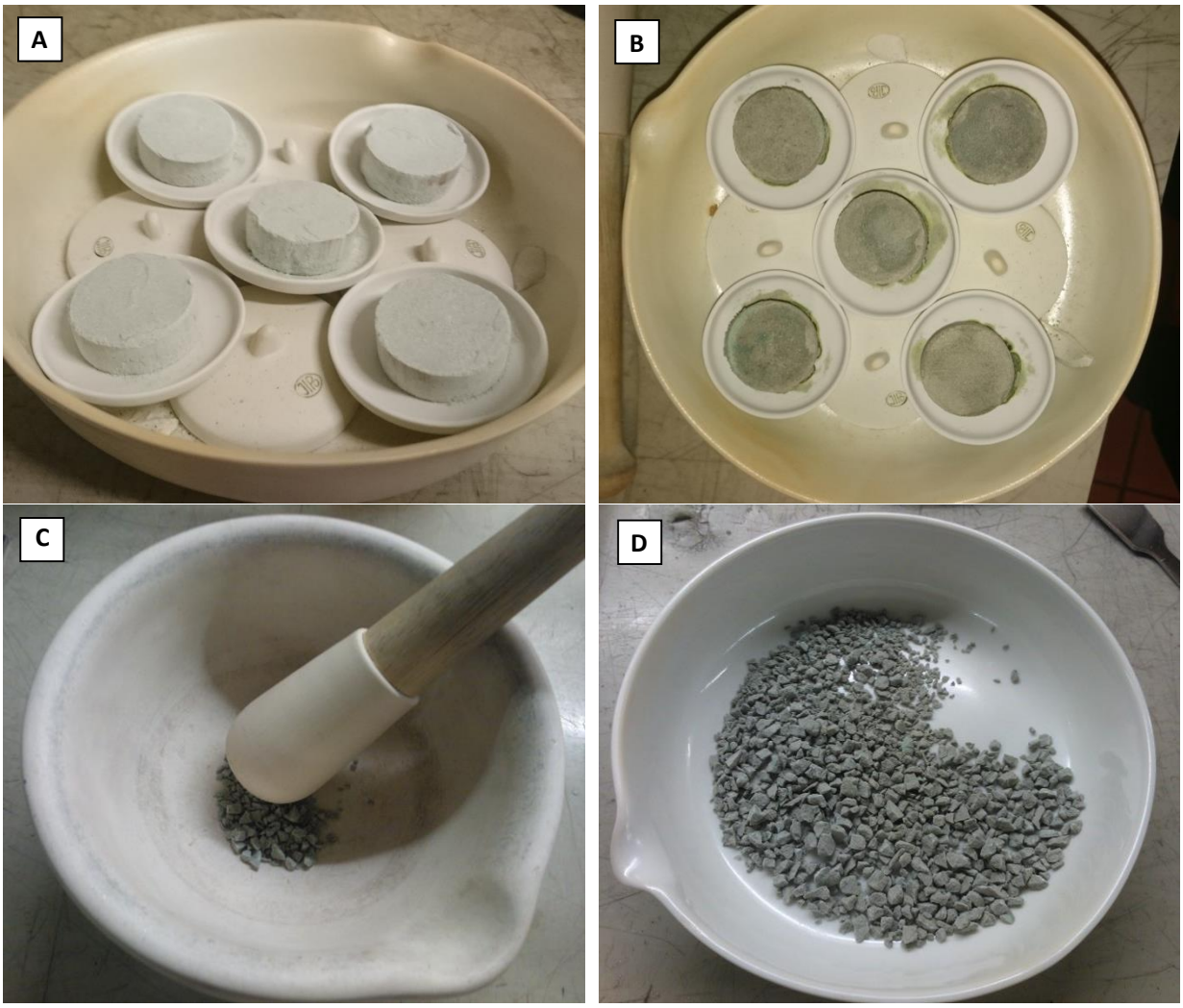

Figure 6-19: Preparation procedure of the pelletized CaBa sorbent – (A: Pressed tablets from fines of original CaBa, B: Tablets after calcining in muffle furnace, C: Grinding of the tablets in a mortar, D: prepared sorbent "CaBa-pelletized with a particle size fraction of 250 -1000 µm)

6.3.2 Sorbent characterization

For a better understanding of the functionality and structure of the CaBa sorbent, a detailed particle analysis was performed at FZ Jülich. These measurements include SEM-EDX, ICP-OES and XRD measurements as well as a BET-Surface analysis conducted by the Research Center Pharmaceutical Engineering (RCPE) in Graz. The properties of the original and the pelletized powder are shown in Table 6-6. Besides the original and pelletized CaBa sorbents, a natural lime from a mill in Peggau, Austria was applied in the course of the investigations on BaO-based desulfurization. The lime was used as a separating agent to prevent sintering of the pelletized CaBa sorbent when added in a gravimetric ratio of 1:1. The properties and elemental composition of the lime is shown in Table 6-2.

Table 6-6: Particle properties of tested BaO-based materials, the differences to 100% in the elemental composition being oxygen and trace elements

		CaBa, orig.	CaBa, pelletized	CaBa, pelletized - sulfided	Bed material after application in fluidized bed
Particle size fraction	µm	> 250	250-1000	250 - 1000	200-300
Mean particle size	µm	1150	734	-	-
ρ	g/cm³	1.7	2.0	-	-
Surface area	m²/g	0.63	0.18	0.72	-
Pore volume	m³/g	0.004	0.001	0.001	-
Pore size	nm	23.1	22.5	7.2	-
Elemental analysis					-
Ba	wt%,dry	20.4	19.0	5.50	0.57
Ca	wt%,dry	49.9	52.5	49.9	4.1
Al	wt‰,dry	0.13	0.14	0.35	0.8
Fe	wt‰,dry	0.11	0.17	0.12	30.1
K	wt‰,dry	< 0.01	< 0.01	1	3.6
Mg	wt‰,dry	2.6	2.7	2.6	274
S	wt‰,dry	0.04	0.11	13.5	0.49
Si	wt‰,dry	0.21	0.2	3.5	175

As shown in Table 6-6 by comparison between the original and the pelletized CaBa sorbent, the elementary composition of the CaBa sorbent basically does not change in the process of post treatment. Solely the sulfur content increases from 0.04 to 0.1 wt‰, which can be attributed to the impact of a chemical transfer process in the furnace due to the high affinity of BaO towards sulfur. Results from BET measurements indicate that the surface area and pore volume are relevantly decreased from 0.63 to 0.18 m²/g and 0.004 to 0.001 cm³/g, respectively, during the preparation of a coarse powder with definite particle size fraction. This goes along with an increase in the density of the pelletized sorbent from 1.7 to 2.8 g/cm³. The lower density of the original material in combination with the soft structure leads to crushing of the extrudates and excess elutriation of fines from the fluidized bed. The pelletized CaBa proved to be stable within the bed as shown by the analysis of bed material after experimental use. The pelletized CaBa after in-bed use (CaBa, pelletized -sulfided) was sorted by hand from the bed material after application as desulfurization sorbent in an experiment with 85 ppm_v H_2S feed and an exposure of 56 hours. Due to the distinctive particle size a clear separation from particles of the bed material or ash is warranted. The comparison of the pelletized CaBa before and after application in a fluidized bed shows a significant increase in surface area from 0.18 to 0.72 m²/g and a decline in pore size from 22.5 to 7.2 nm. The decline in pore size might be attributed to the closure of pores by expansion of BaO during conversion to BaS. Both

effects might also be results of the non-representative sampling of the sulfided material due to the manual sorting from the bed material. The investigated sample consisted rather of the coarse particles within the range of 250 to 1000 µm and is therefore not equivalent to the pelletized CaBa before application as in-situ sorbent.

The comparison of elemental composition between the pelletized CaBa before and after application in the fluidized bed shows some relevant changes concerning minor elements and the content of barium in the sorbent. Especially alumina, silicon and potassium are increased approximately by factors 2, 10 and 100 respectively. Most likely this can be attributed to the deposition of ash forming elements from the wood pellets (Table 4-1) used as gasification fuel. The comparison of sulfur and barium content before and after use of the pelletized CaBa in the fluidized bed shown a full conversion of BaO to BaS on the one hand and a relevant depletion of barium from the sorbent on the other hand. The full conversion can be concluded from the molar content of Ba and S in the sulfided CaBa with 0.042 mol_{Sulfur}/100g compared to 0.04 mol_{Barium}/100 g meaning that some sulfur is bound either chemisorbtive or physiosorbtive to other constituents. The leaching of barium from the sorbent is in the range of 70 % considering a Ba-content of 19 wt% before and 5.5 wt% after application in the fluidized bed. The loss of barium in the sulfided CaBa can supposedly be explained by interactions of the sorbent with the bed material in the fluidized bed showing a relevant barium content in the bed material after combined application (Table 6-6). Comparing the low amount of 62.5 g sorbent added, with the amount of 1400 g of bed material, the mass balance for barium is considered to be closed. This means that no severe elutriation of barium from the fluidized bed has to be assumed based on the data shown in Table 6-6.

6.3.2.1 SEM-EDX Analysis

In order to prevent sintering effects and obtain a suited particle size fraction of the CaBa sorbent the original material as delivered by FZ Jülich was pelletized as described in section 6.3.1. The original CaBa plus the pelletized particles in the size range of 250 to 1000 µm were analyzed using SEM-EDX (Figure 6-20 and Figure 6-21).

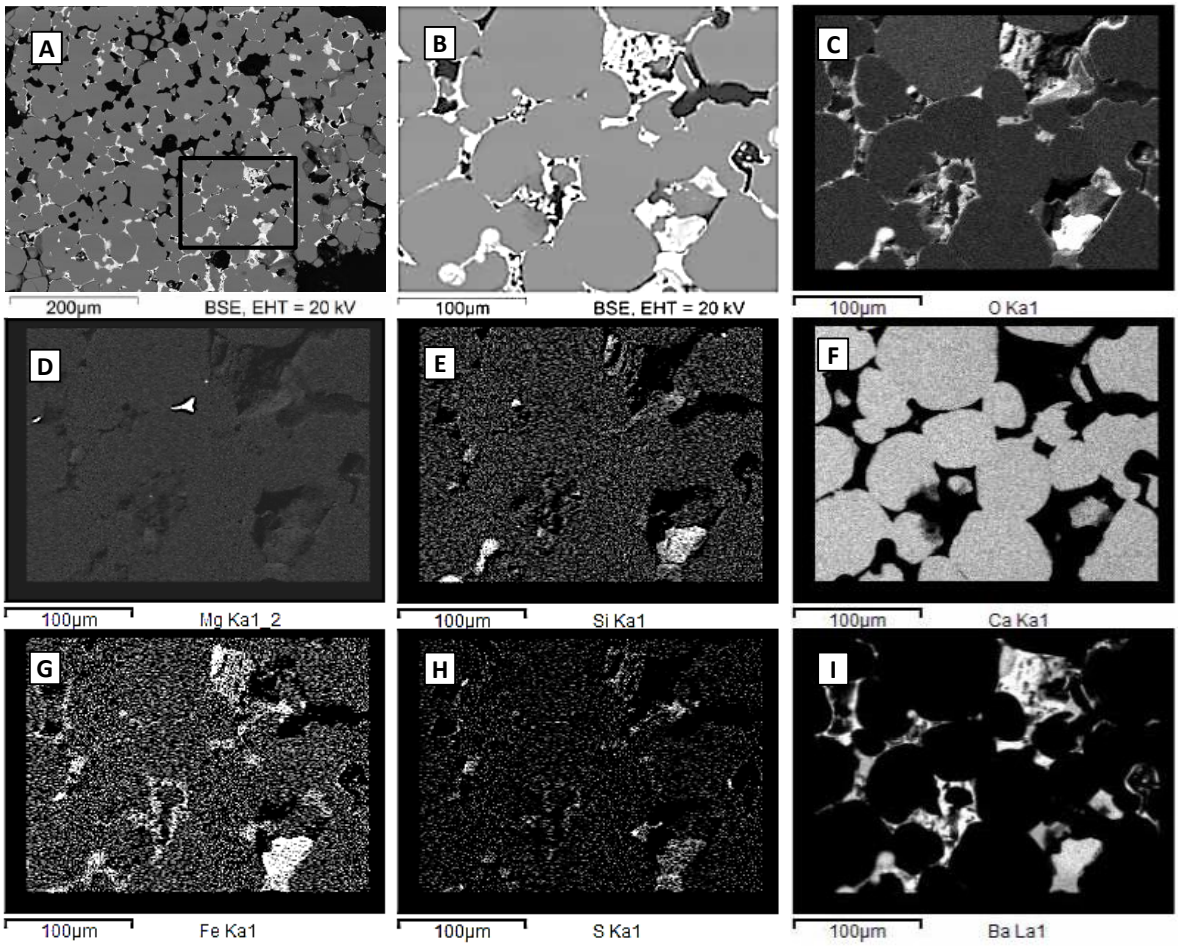

Figure 6-20: SEM (A and B) pictures of original CaBa sorbent with element sensitive EDX pictures of the magnified area (C: Oxygen, D: Magnesium, E: Silicon, F: Calcium, G: Iron, H: Sulfur, I: Barium)

From the SEM pictures with low magnitude (Figure 6-20 picture A) it can be seen that the particle-size of the original CaBa was larger as compared to the pelletized and treated material (Figure 6-21 picture A). The original material consisted of some larger extrudates of up to a few millimeters in size and mostly fines below 250 µm in diameter. Only the large fraction was applied in order to prevent pneumatic discharge of the sorbent from the fluidized bed. Further it is shown at increased magnitude, under consideration of the "Ca" EDX-responses, that the CaO-crystallites are larger and denser in the original material (Figure 6-20 picture B) as compared to the pelletized CaBa sorbent (Figure 6-21 picture B). The results of SEM-EDX measurements of both CaBa samples show sintering bridges between the CaO crystallites. The EDX reveals that the BaO is mostly contained in these sintering bridges and is not primarily embedded in a mixed solution phase with CaO, as the Ca-response appears separated from the Ba-response. (Figure 6-20 and Figure 6-21, picture I)

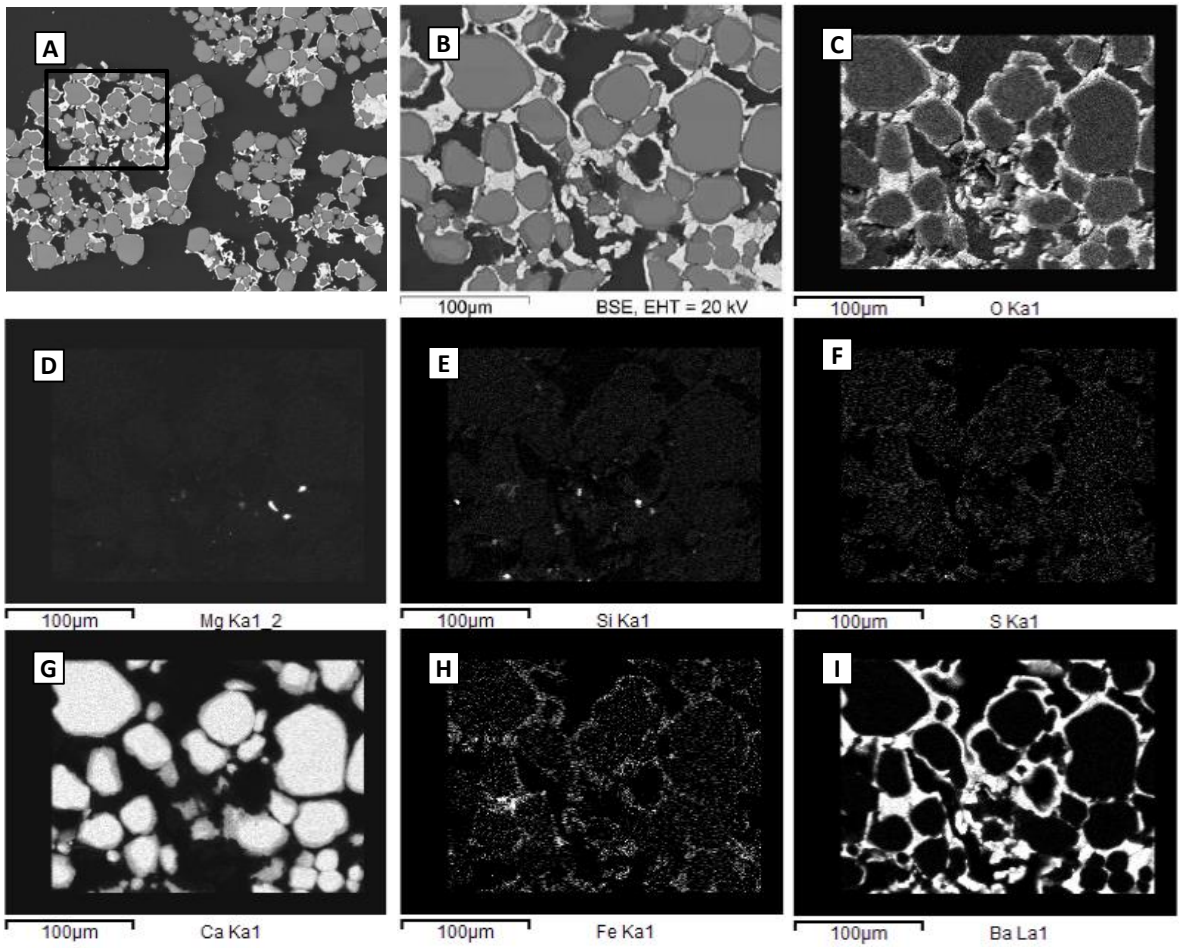

Figure 6-21: SEM (A and B) pictures of the pelletized CaBa sorbent with element sensitive EDX pictures of the magnified area (C: Oxygen, D: Magnesium, E: Silicon, F: Sulfur, G: Calcium, H: Iron, I: Barium)

The local separation of Ba and Ca gives rise to questions about the mechanism of stabilization of BaO in the CaBa sorbent. The stabilization of BaO in a solution with CaO was the mechanism supposed in previous research[48] which would prevent the carbonization to $BaCO_3$ due to a solubility gap of BaO in CaO at temperatures above 1200 °C.[133] If this was true at least a certain overlapping of the two element responses would have to occur with a stronger response of Ca than of Ba considering a miscibility of 10 mol% BaO in CaO. Clearly this is not the case according to the obtained result of particle analysis. On the other hand, stabilization in the form of BaO is confirmed by XRD-measurements (Figure 6-24) and with regard to the results of dolomite based in-situ desulfurization. Fully calcined dolomite contains 6.3 wt% Ba present as $BaCO_3$ that do not improve the desulfurization properties of this sorbent as compared to lime (Table 6-2). It is therefore confirmed that the mere presence of Ba in the CaBa sorbent does not account for the determined steady state desulfurization in range of 35 ppm_v residual H_2S (Compare to section 6.3.7). According to the EDX- analysis, it is especially the Fe-response that is congruently dispersed with the Ba-signal. A stabilizing interaction between Ba and Fe in the CaBa sorbent can only be assumed at the current stage of research. Further investigations will have to elucidate the exact mechanism of stabilization of BaO in the CaBa sorbent as a better understanding of the interactions of the contained materials will open up the path for synthesis of enhanced BaO-based sorbent materials.

The pelletized CaBa was exposed for 3 days to a syngas containing approximately 85 ppm_v H_2S in a gasification experiment conducted in the gasifier described above (CaBa_2, Table 6-7). Afterwards, the CaBa granulate was sorted and separated from the bed material to enable a particle analysis of the loaded sorbent material (Figure 6-22).

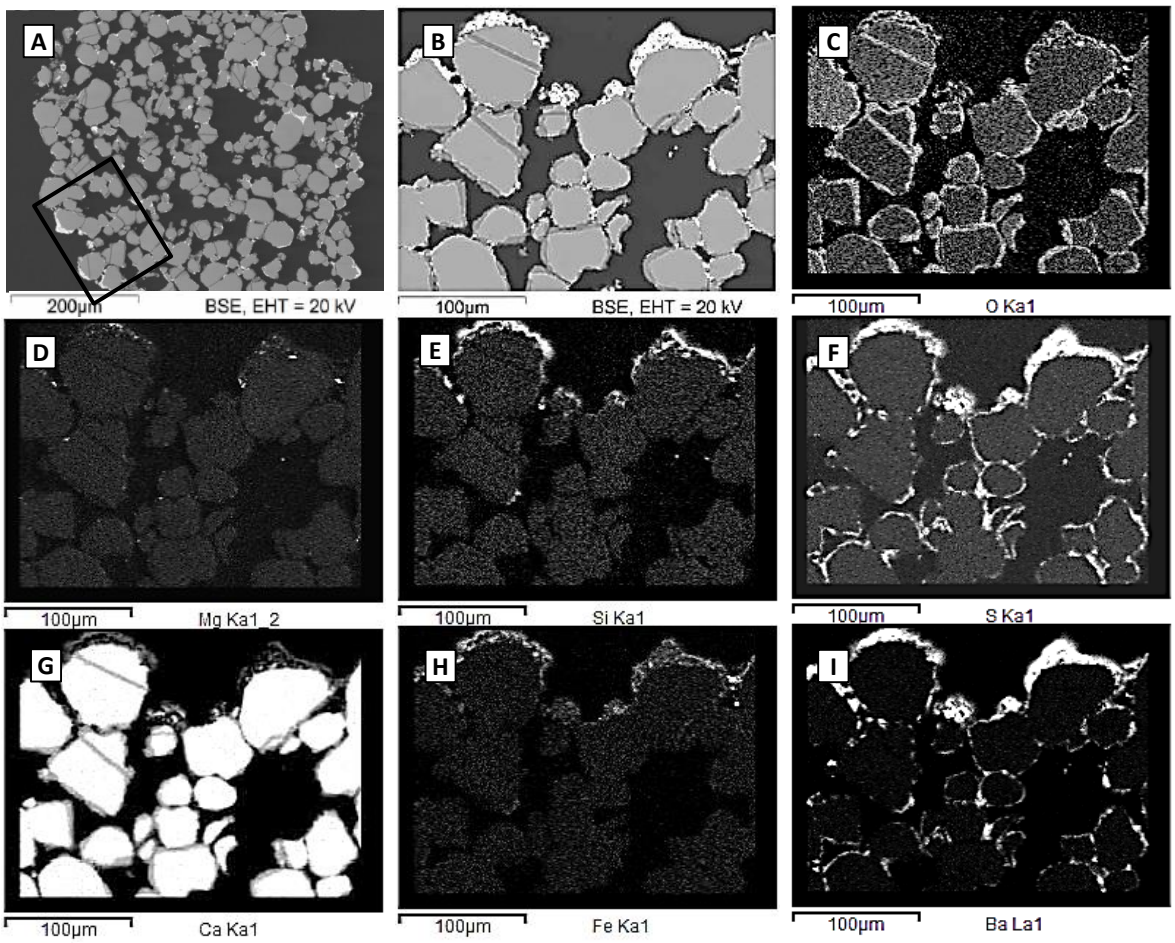

Figure 6-22: SEM (A and B) pictures of the pelletized CaBa sorbent after 56 hours of in-situ desulfurization (85 ppm_v H_2S feed); with element sensitive EDX pictures of the magnified area (C: Oxygen, D: Magnesium, E: Silicon, F: Sulfur, G: Calcium, H: Iron, I: Barium)

SEM-EDX analysis of the sulfided sorbent via confirms the stabilization of BaO in an active state by the incorporation of sulfur solely in areas with high barium content (Figure 6-22). This is especially shown by direct comparison of Figure 6-21 F and I with Figure 6-22 F and I. The first indicates a high Ba content in the sintering bridges (Figure 6-21 I) and a weak sulfur-specific response (Figure 6-21 F). For the latter (Figure 6-22 F and I) both responses are clearly visible and congruently dispersed over the analyzed area.

The SEM image after desulfurization (Figure 6-22) further indicates a certain abrasion of barium from the sorbent after application in a fluidized bed as the barium rich areas are reduced when compared to Figure 6-21. This effect is confirmed by the results of ICP-OES analysis (Table 6-6) with a decrease from about 19 wt% Ba to about 5.5 wt% Ba. This is explained by interactions with the bed material, that according to SEM-EDX results (Figure 6-23), also exhibits traces of barium after contact with the sorbent material. It is also shown that the barium is contained once again in sintering bridges between the olivine particles. Other than in the sorbent particles, the Ba-response is locally dispersed

congruently with the Ca-signal. The sintering of bed material therefore still occurs even after the addition of lime as a separating agent but is reduced to an extent that no longer affects the fluidization of the bed material in the reactor.

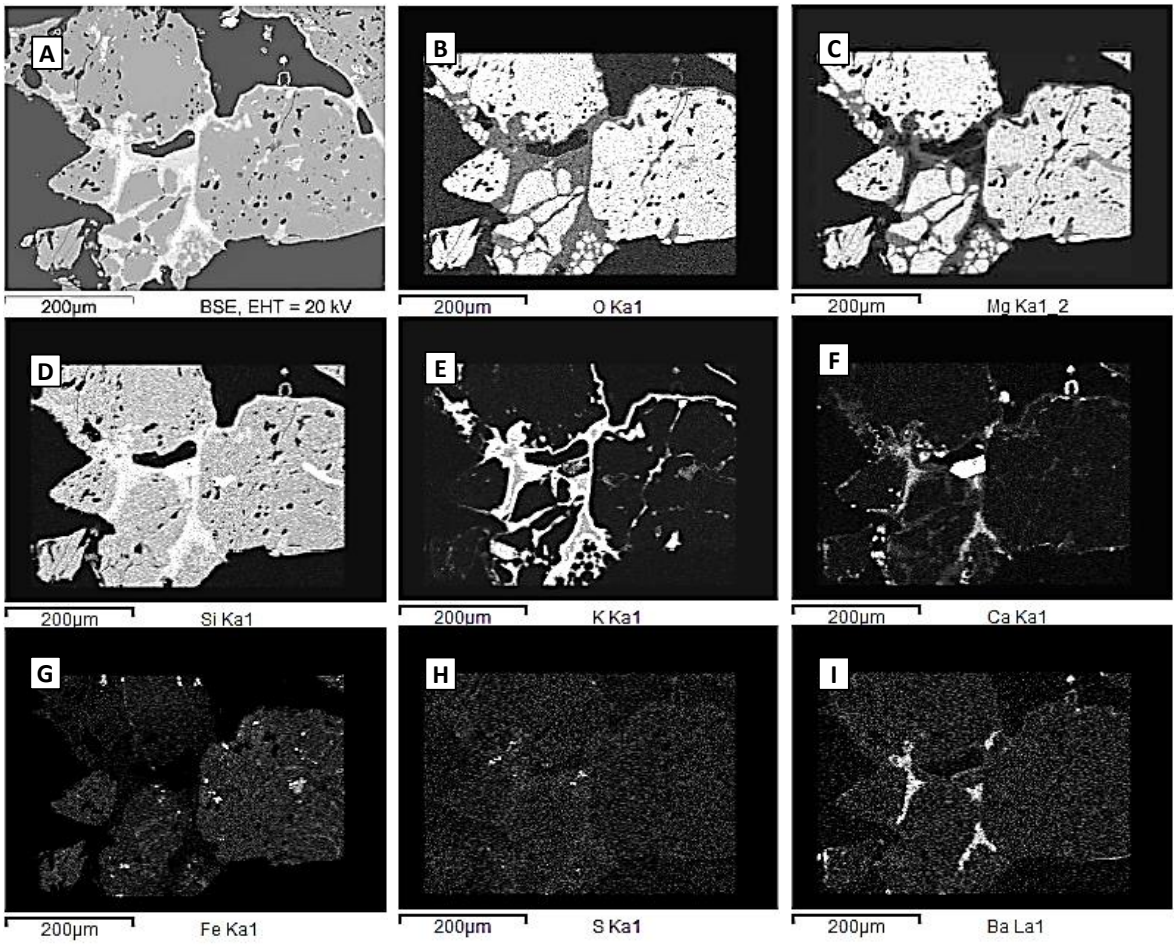

Figure 6-23: SEM (A) picture of the bed material olivine with element sensitive EDX pictures of the magnified area (B: Oxygen, C: Magnesium, D: Silicon, E: Potassium, F: Calcium, G: Iron, H: Sulfur I: Barium) after use in the fluidized bed for 56 hours of in-situ desulfurization (85 ppm_v H_2S feed)

6.3.2.2 XRD-Measurements

The functionality of barium as an active component during in-situ desulfurization is in accordance with XRD measurements (Figure 6-24). The XRD results show a prominent response for BaO and especially CaO in unsulfided sorbent samples and a clear signal for a BaS crystallite phase after the application as desulfurization sorbent. The absence of a mixed crystallite-phase of BaO and CaO in the unsulfided sorbent samples also indicates a stabilization-mechanism for BaO other than the formation of a solution phase with CaO whereby the detection limit of the XRD-measurement is in the range of 5 wt%.[48]

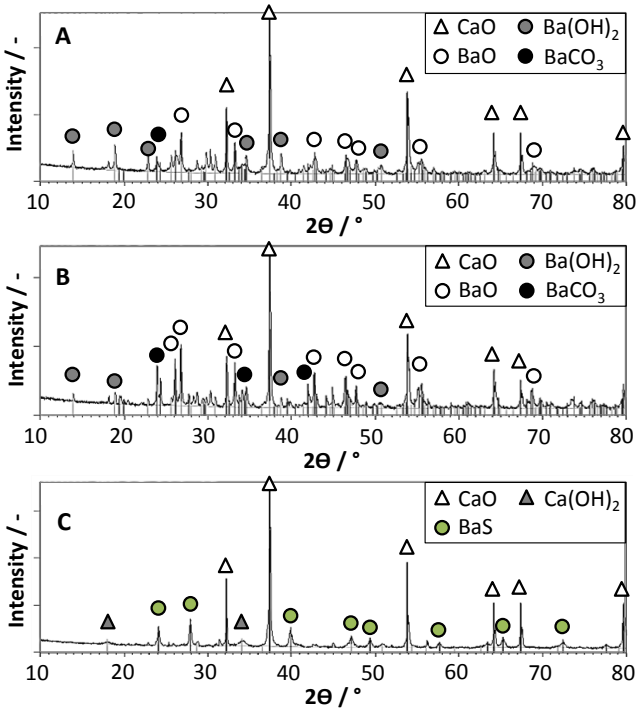

Figure 6-24: XRD results of the tested CaBa sorbent. A original, B pelletized, C sulfided (Table 6-7: CaBa_2, 56 hours in BFBG, 85 ppm_v H_2S feed)

While the unsulfided sorbent samples (A and B) contain barium in the form of BaO alongside with a certain amount of $BaCO_3$ and $Ba(OH)_2$ due to reaction with air before analysis, BaS is the only Ba-containing phase in the sorbent after desulfurization. The XRD-results therefore indicate a full conversion of BaO and other Ba-containing crystallites to BaS. This is in accordance with the ICP-OES results presented in Table 6-6. Further, the conversion of BaO to BaS can be estimated by a method presented in Section 6.2.10 according to the depletion of H_2S in the produced gas upon addition of a defined amount of sorbent. All the applied methods and measurements indicate a full conversion of BaO to BaS whereby the loss of Ba from the sorbent leads to a higher uncertainty in the determination of a conversion in comparison to a homogeneous sorbent such as lime.

6.3.3 Experimental procedure

The application of CaO-based sorbents for in-situ desulfurization yielded residual H_2S contents of about 500 ppm_v that proved to be in good accordance with thermodynamic simulations (Figure 4-4). According to named thermodynamic simulations, a desulfurization to below 5 ppm_v H_2S is feasible under application of BaO, based on the gas composition within the investigated test rig (section

4.2.1.1). Inferentially different experimental conditions are appropriate as compared to the investigation of CaO-based desulfurization. While CaO-based sorbents are suitable for coarse desulfurization only, the application of BaO on the other hand promises residual sulfur contents of a few ppm_v H_2S (Figure 4-5). Assuming a steady state value below 50 ppm_v H_2S the addition of several hundred to above 1000 ppm H_2S, as required in CaO-based experiments, would lead to an increased formation of BaS and therefore increased sorbent consumption in BaO-based experimental investigations. On the other hand such an excess addition of sulfur is supposedly not required for the determination of the BaO-based steady state value of in-situ desulfurization. Consequently the initial H_2S content in experimental investigations on the performance of CaBa was set to a lower value in the range of 85 ppm_v as compared to 1200 – 1500 ppm_v H_2S in CaO-based desulfurization experiments.

The elevation of the sulfur content by addition of CS_2 proved to be less reproducible in such low concentrations leading to increased deviations in the initial H_2S concentration of up to 25 % of the intended set value. This method of sulfur elevation was therefore inappropriate for the investigation of BaO-based in-situ desulfurization especially for experiments with the aim of calculating a sorbent conversion. As a consequence the method of sulfur supply was changed to the addition of a gas containing 3143 ppm_v H_2S in N_2 as stated in section 5.1.3. The ratio of sorbent to sulfur was maintained in a similar range as compared to the CaO-based experiments with a ratio δ as defined in Eq

$$\delta = \frac{Ba}{S} = \frac{\dot{n}_{Ba}}{\dot{n}_{gas,dry} \cdot x_{H_2S_{initial}}} \quad \textbf{(52)}$$

An overview of the experiments performed for the characterization of CaBa as sorbent in in-situ desulfurization is shown in Table 6-7.

Table 6-7: Experiments performed with BaO-based sorbents

Refer-ence #	Experimental properties	t_bed	mass flow rate		sorbent mass flow rate		total sorbent added		H_2S content syngas	molar feed ratio	
			fuel	steam	CaBa	lime	CaBa	lime	(initial)	**δ** Ba/S	**γ** Ca/S (lime)
		°C	g/h	g/h	g every 10 min		g	g	ppm_v	ppm_v	-
CaBa_1	CaBa_original, high_ADS	760	500	540	2.5	-	62.5	-	86	7.71	-
CaBa_2	CaBa_pelletized + lime, high_ADS	760	500	540	2.5	2.5	62.5	62.5	88	7.54	2211
CaBa_3	CaBa_original, low_ADS	760	500	540	0.63	-		-	75	2.23	-
CaBa_4	CaBa_pelleltized, low_ADS	760	500	540	0.63	-		-	107	1.56	-
CaBa_5	CaBa_pelletized + lime, low_ADS	760	500	540	0.63	0.63	15	15	92	1.82	508
CaBa_6	CaBa_pelletized + lime, low_ADS, high_S	760	500	540	0.63	0.63	15	15	139	1.20	336
CaBa_7	CaBa_pelletized + lime, low_ADS, high_T	810	500	540	0.63	0.63	15	15	83	2.01	563
CaBa_8	CaBa_pelleltized + lime, high_ADS, high_T, high_S	810	500	540	2.5	2.5	62.5	90	600 -> 470 (CaO-based)	1.11	467
CaBa_9	CaBa_pelletized + lime, high_ADS, high_T, high_S	810	500	540	2.5	2.5	62.5	90	350	1.90	801
CaBa_10	CaBa_pelletized + lime, low_ADS, high_T, no_S	810	500	540	0.63	0.63	15	15	22	7.60	2123

The experiments listed can be divided in different stages of investigation with the main experimental properties and the reference number (#) given as identification. The experiments differ between the amount of added sorbent of either 62.5 or 15 g CaBa (high_ads, low_ads) the type of sorbent added according to the procedure described in section 6.3.1 (CaBa-original, CaBa pelletized) plus the addition of lime as separating agent. A main process variation was the increase of reactor temperature from 760 to 810 °C (high_T). Other individual process variations concerning the set point of initial H_2S feed (high_S, no_S) vary depending on the experiment but are listed explicitly in Table 6-7. The reference numbers of the experiments are included in the captions of figures showing experimental results, such as to relate to the specific experimental conditions listed in Table 6-7.

The addition of sorbent was performed via the fuel inlet of the BFBG after a stable initial H_2S content was established in the gas and according to the procedure described in CaO-based experimental

setup (6.2.2). As discussed in section 6.3.5, the addition of lime as a separating agent proved to successfully inhibit the sintering of the added batches of CaBa sorbent. The lime was added in a weight ratio of 1:1 and mixed with the pelletized CaBa prior to the wrapping of the sorbent batches (as shown in Figure 6-5).

6.3.4 Application of original CaBa

The CaBa-sorbent was tested for its desulfurization properties as in-situ sorbent in BFBG operation. As the thermodynamic equilibrium of BaO-based desulfurization is magnitudes below that of a CaO – based equilibrium, the initial H_2S content was set to be in the range of 85 ppm_v H_2S. As a consequence of the experimental results described in section 6.2.8 showing the calcination of $CaCO_3$ even at reactor temperatures around 750 °C, the standard reactor temperature was decreased from 775 °C to 760 °C in order to ensure increased longevity of the reactor heating. On the other hand the standard setting for the freeboard temperature was increased from 825 to 840 °C to ensure a sufficient char conversion in the freeboard of the reactor. Details of the experimental procedure for investigation of the performance of CaBa as desulfurization sorbent are described in section 6.3. A first experimental application of the original CaBa, as delivered by FZ Jülich, showed a strong tendency to sintering of the batches of added sorbent. The effect of a nonhomogeneous operation of the BFBG is unambiguously shown by the spread of temperatures in the fluidized bed with its onset shortly after the addition of the original CaBa sorbent. Figure 6-25 shows the trend of temperatures at different thermocouples within the reactor. The depicted time scale is equivalent to that of following experimental results with the “0-point” of experimental duration indicated 50 minutes ahead of sorbent addition to the fluidized bed. This allows for comparison with previous experiments based on the application of CaO as shown in section 6.2 and also includes the display of initial conditions, prior to sorbent addition.

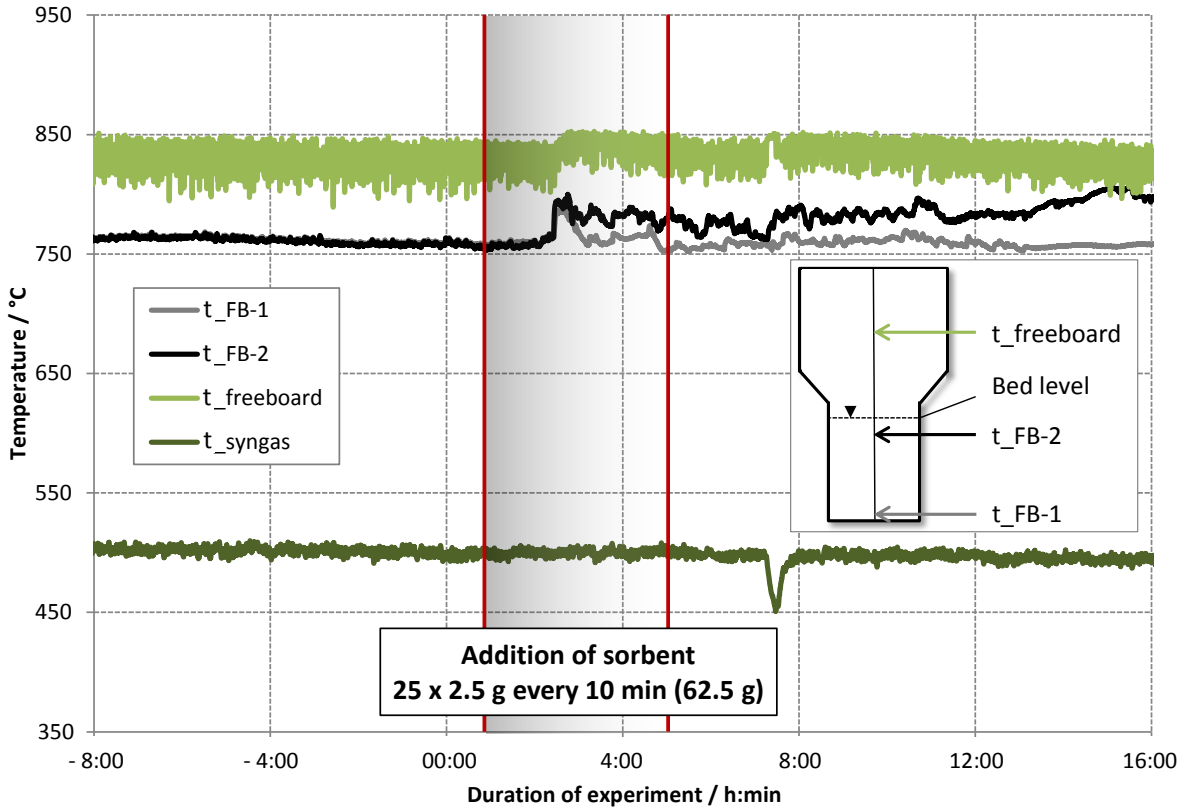

Figure 6-25: Trend of temperatures in the reactor, freeboard and product gas line upon addition of CaBa sorbent. (Ba/S ratio 7.71, Table 6-7: Experiment CaBa_1)

Under stable fluidized conditions, before the addition of sorbent, the temperatures t_FB-1 and t_FB-2 are about equal due to homogeneous mixing within the fluidized bed (Figure 6-25). The spread of temperatures in the fluidized bed occurs abruptly with its onset at about 90 minutes after the addition of original CaBa-sorbent. While the temperature above the steam inlet (t_FB-1) remains more or less constant at the initial level of about 760 °C the upper bed temperature (t_FB-2) drifts apart to values of about 800 °C. The spread of temperatures increases with time and does not vanish even within 12 hours after the addition of sorbent was stopped. The analysis of the bed material after the experiment, shown in Figure 6-26, confirmed the assumption of sintering effects due to the addition of the original CaBa sorbent.

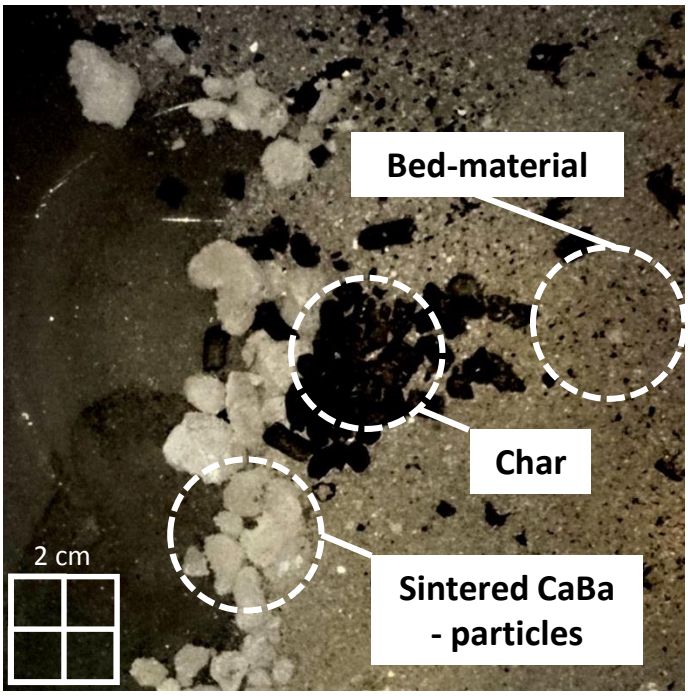

Figure 6-26: Agglomerated sorbent and bed material after an experiment with original CaBa

As a result of sintering, coarse lumps of up to a few centimeters in size formed in the fluidized bed, thus preventing a stable fluidized state. The consistency of the agglomerates, shown in Figure 6-26 together with olivine and char, was like that of soft and porous limestone with obvious incorporation of olivine into the sintered batches of added sorbent. Even though the conditions in the gasifier deteriorate once the original CaBa sorbent is added to the reactor, a desulfurization effect can be observed (Figure 6-27). As a consequence of the observed sintering effect and in order to obtain stable particles with a suitable size fraction, the sorbent was post-treated and pelletized as described in section 6.2.1.

6.3.5 Influence of sorbent treatment

An amount of 15 g of the original and the pelletized CaBa with a particle size fraction of 250-1000 µm was added to the fluidized bed in subsequent gasification experiments with approximately 85 ppm_v H_2S feed. In both cases, the addition of CaBa sorbent caused defluidization of the fluidized bed due to sintering effects. According to tests conducted in a muffle furnace (compare section 6.3.1), the addition of lime as separation agent offers a possible way to prevent sintering. Upon the addition of a combined additive composed of 50 wt% pelletized CaBa and 50 wt% lime as separating agent a detrimental effect on the fluidization conditions in the gasifier no longer occurred. Results concerning the desulfurization effect of these experiments are depicted in Figure 6-27.

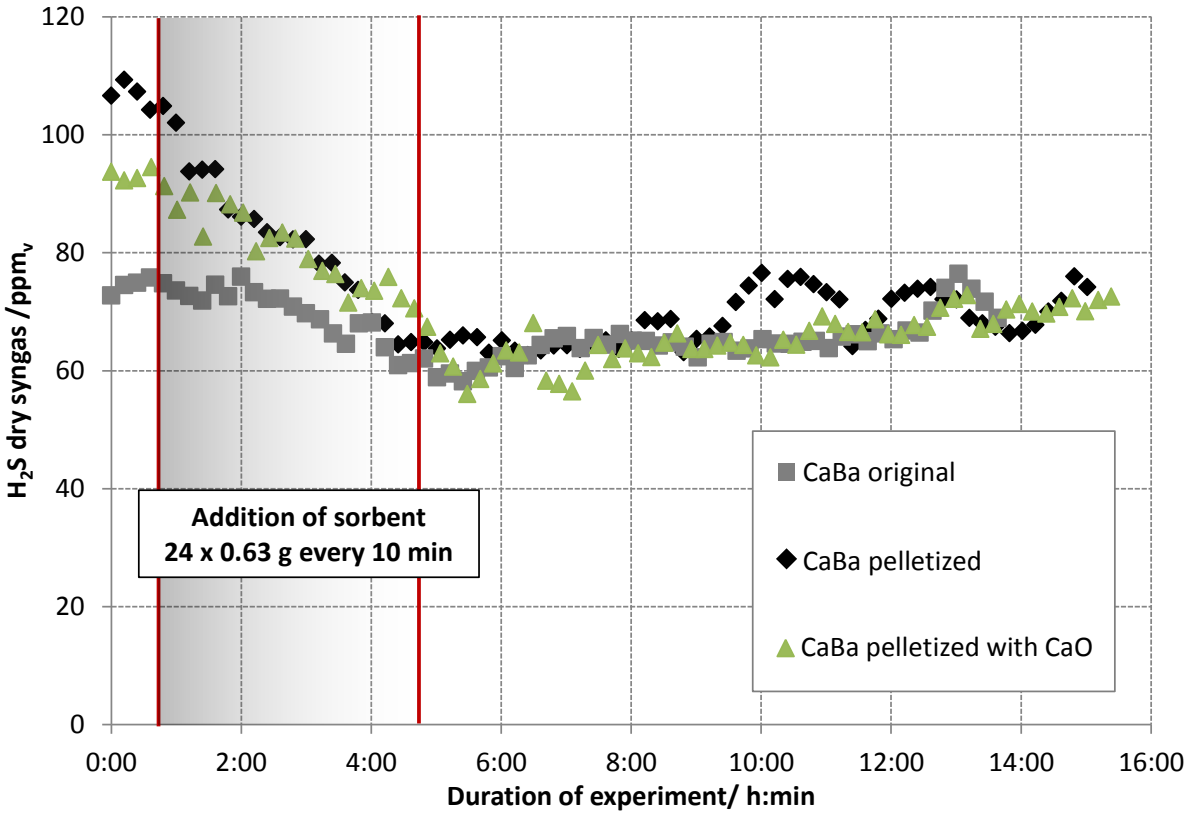

Figure 6-27: Comparison of different CaBa sorbents with an addition of 15 g CaBa each (760 °C reactor temperature, Table 6-7: Experiments CaBa_3, CaBa_4, CaBa_5)

Comparison of the desulfurization performance of different CaBa powders and additives (Figure 6-27) shows a good conformity concerning the achieved residual H_2S content with 0.63 g of CaBa added every 10 min for 4 hours resulting in a total amount of 15 g CaBa added in each experiment. A δ in the range of 1.8 was maintained for the different experimental runs. The slight increase of the values for residual H_2S over time can most likely be attributed to the inevitable elutriation of fines from the fluidized bed. The deviations in the initial H_2S feed content are caused by initial uncertainties of the sulfur supply, whereby it is shown that the desulfurization performance of the treated CaBa increased rather than deteriorated. According to the results shown in Figure 6-27 it can be deduced that the addition of lime as separating agent does not influence the desulfurization performance but prevents sintering and therefore ensures stable fluidized conditions in the reactor. As a consequence, the addition of lime as separating agent was established as standard procedure for further experiments.

6.3.6 Influence of sorbent amount and sulfur content

The addition of 15 g of the pelletized CaBa to a gasification process with an initial H_2S content of 92 ppm_v (Table 6-7) leads to a clear decline in residual H_2S of about 29 ppm_v to a mean steady state value of 63 ppm_v H_2S. This correlation was clearly demonstrated and proved to be reproducible (Figure 6-27) but is far above the thermodynamic limit concerning the achieved level of steady state desulfurization. The addition of 15 g CaBa under the described gasification conditions equals a Ba/S ratio δ of 1.82 which is in the range of sorbent addition used by other researchers at pilot scale.[73] As the achieved desulfurization effect is low as compared to the predicted limits by thermodynamics

(Figure 4-5) the value of δ was increased by a factor of about 4 to a value of 7.71 with the corresponding desulfurization results depicted in Figure 6-28.

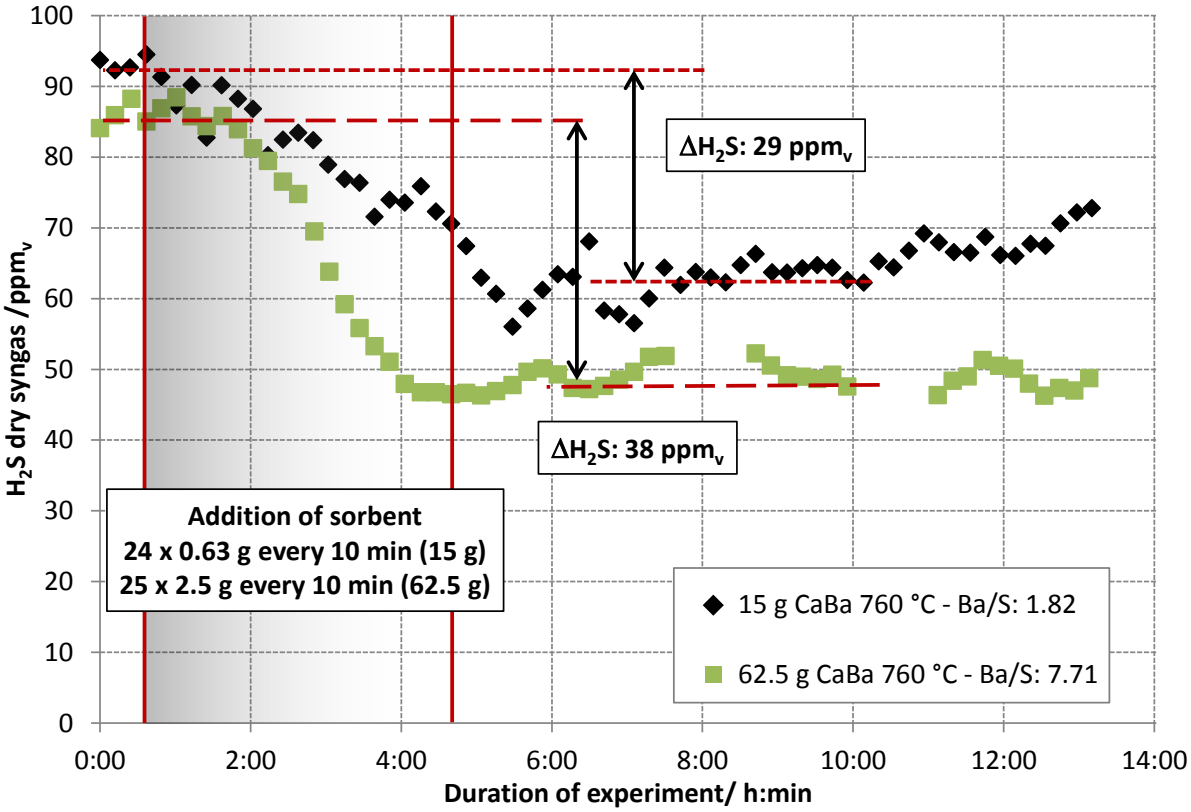

Figure 6-28: Desulfurization results upon variation of the added amount of CaBa sorbent with according Ba/S ratios (Table 6-7: Experiments CaBa_5, CaBa_1)

As shown in Figure 6-28 an increased ratio of sorbent to sulfur leads to a decrease in the steady state residual H_2S content to a mean value of about 48 ppm_v. Compared to a depletion of about 29 ppm_v H_2S for 15 g of added CaBa the increased addition of sorbent leads to a reduction in H_2S content of about 38 ppm_v.

The effects of an increased stoichiometric ratio δ in the application of the CaBa sorbent reveal clear differences in comparison to a variation of the amount of added sorbent for fully calcined dolomite (section 6.2.6). While, in dolomite-based experiments the increase of the amount of added sorbent in the over-stoichiometric regime leads to a prolonged duration of steady state desulfurization at a congruent level of residual H_2S (Figure 6-13), the behavior of BaO-based desulfurization indicates a different mechanism of limitation. In both experiments, with 15 and 62.5 g of added sorbent, the achieved residual sulfur content remains fairly constant for a period of more than 10 hours even though the addition of sorbent was stopped after 4 hours. Inferentially the observed rate of reaction does not significantly decrease over time as would be the case for a major influence of product layer or internal diffusion as rate determining steps. Further it can be deduced that the conversion does supposedly not follow a simple shrinking core model as commonly suggested for solid-gas-reactions by Levenspiel et al.[134] The shrinking core model assumes a progressing conversion of product layer surrounding a shrinking core of unreacted solid. As the available surface for reaction decreases in a spherical particle with proceeding conversion and shrinking of the unreacted core, the resistance for chemical reaction increases with progress of conversion and would lead to reduced overall rate of

reaction with time.[134] This process is not observed according to the experiments shown in Figure 6-28 as a reduced rate of the desulfurization reaction would necessarily lead to an increased residual H_2S content with the duration of the experiment and thus the progress of conversion from BaO to BaS. Due to the inhomogeneous structure of the CaBa sorbent and the BaO being contained mostly in sintering bridges between the CaO crystallites (Figure 6-21) the discrepancy to the shrinking core model seems reasonable.

Another experimental procedure in order to elucidate the mechanism of limitation is the variation of partial pressure of H_2S as gaseous reactant of the desulfurization reaction. Such a variation was performed in different experiments under addition of 15 g CaBa with an increased initial H_2S concentration (Figure 6-29).

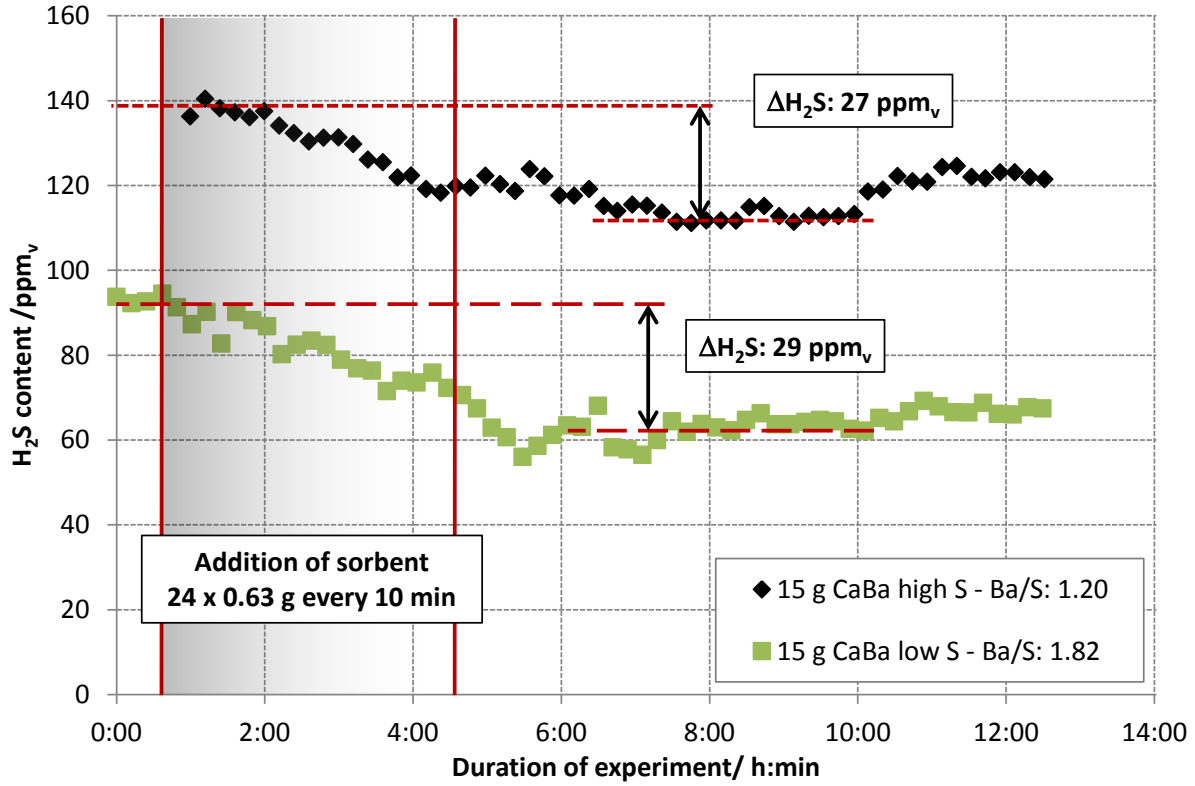

Figure 6-29: Desulfurization results upon varied partial pressure of H_2S in the gasifier by increasing the initial feed content from 85 to 140 ppm_v H_2S (Table 6-7: Experiments CaBa_5 and CaBa_6)

The results depicted in Figure 6-29 indicate the exact same desulfurization effect upon increase of H_2S inlet concentration from 92 to 139 ppm_v with 29 as compared to 27 ppm_v respectively. These results indicate a constant rate of reaction for both initial set values of H_2S partial pressure. Figure 6-30 indicates the different scenarios for the influence of partial pressure on the overall rate of reaction $-r_{A,0}$ depending on the rate determining step.

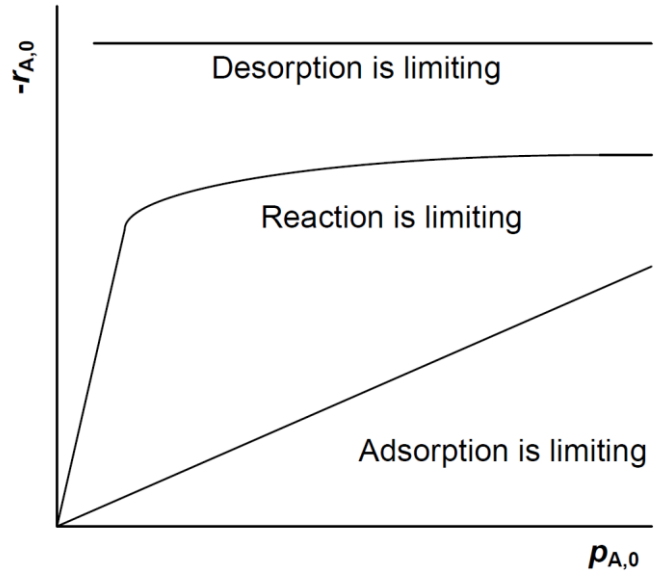

Figure 6-30: Correlation between overall speed of reaction and the partial pressure of reactant A[135]

According to Figure 6-30 an increase of the partial pressure $p_{A,0}$ of reactant "*A*" at initial conditions, would result in an increased overall speed of reaction if the adsorption of reactant on the solid surface of the catalyst or adsorbent was the limiting step. As shown by the results in Figure 6-29 the increase of partial pressure of the gaseous reactant H_2S does not increase the overall rate of reaction. Inferentially either a limitation by surface reaction or desorption of gaseous H_2O from the surface can be concluded as limiting factors on the overall rate of reaction. In order to further differentiate between a limitation by chemical reaction or physical desorption, experiments were performed under a variation of reactor temperature as the influence on the overall rate is far more pronounced for chemical limitation.[134]

6.3.7 Influence of temperature

As observed by Stemmler et al.[86], the desulfurization with CaBa solely works at temperatures well above the onset of calcination. In experiments with limestone and dolomite discussed in section 6.2.8, it was shown that CaO-based sorbents are present in the calcined form for the conditions prevailing in the BFBG. As indicated by the experimental results discussed in section 6.3.6, the influence of temperature seems to be more complex than the mere condition of application of CaBa under calcining conditions. In order to investigate the influence of temperature and verify the previously shown effect[86] of an increased performance at elevated temperature, experiments were conducted at an increased reactor temperature of 810 °C as compared to 750°C in previous BaO-based desulfurization experiments (Figure 6-31). A further elevation of the gasification temperature was not possible due to limitations of the reactor heating even after improvements in heat transfer as described in section 5.1.2. The freeboard temperature was kept constant at a level of 840 °C, such as not to vary the temperature level of steady state equilibria in the gaseous phase.

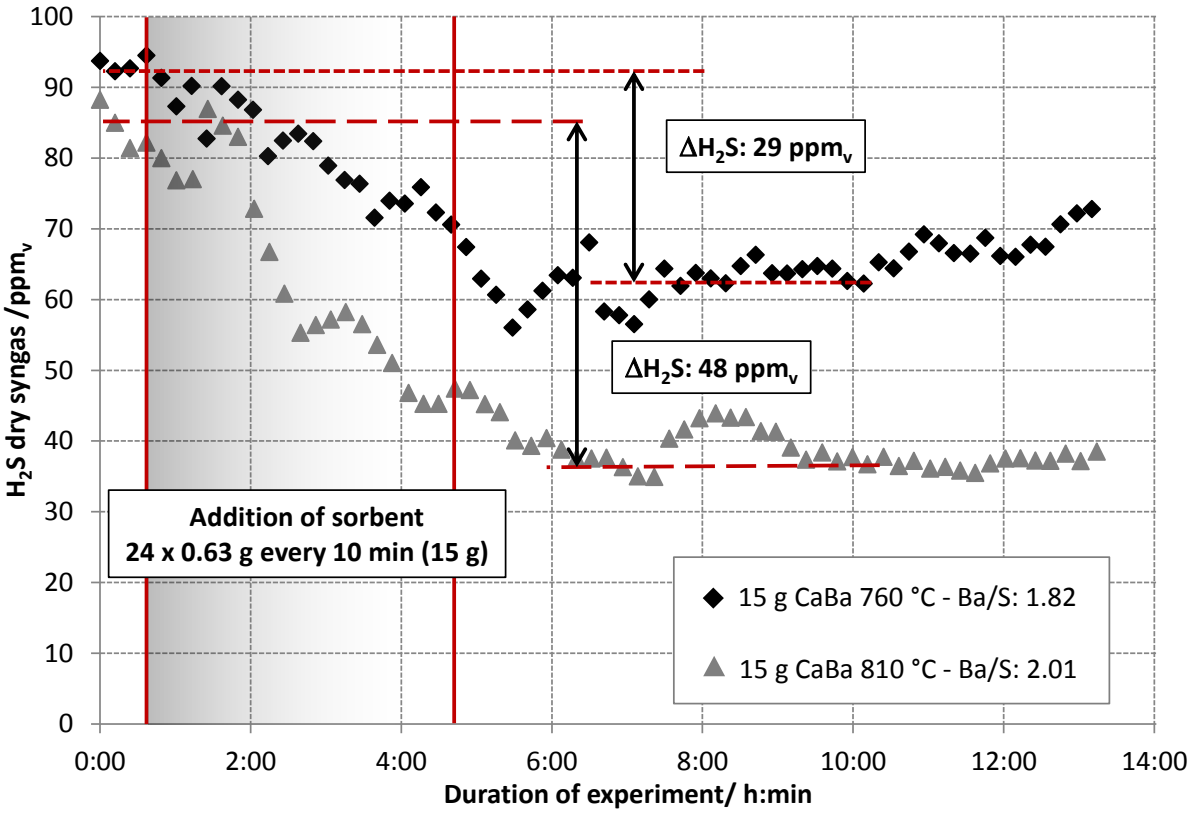

Figure 6-31: Desulfurization results upon varied gasification temperatures with according Ba/S ratios (Table 6-7: Experiments CaBa_5 and CaBa_7)

As depicted in Figure 6-31, even with an amount of 15 g of added CaBa sorbent, a significant desulfurization efficiency was achieved, due to the increase of reactor temperature by 50 K. This resulted in a decline in H_2S content by about 48 ppm_v in comparison to 29 ppm_v H_2S for the same amount of sorbent added at 760 °C. The increase of reactor temperature therefore has an even superior effect as compared to an increased amount of added sorbent. The effect of an increased reactor temperature on the observed rate of reaction is shown in Figure 6-32 by example according to Levenspiel.[134] As film diffusion is considered unlikely in the turbulent flow regime of a fluidized bed the strong influence of increase in temperature as shown in Figure 6-31 for the application BaO confirms the limitation by chemical surface reaction.

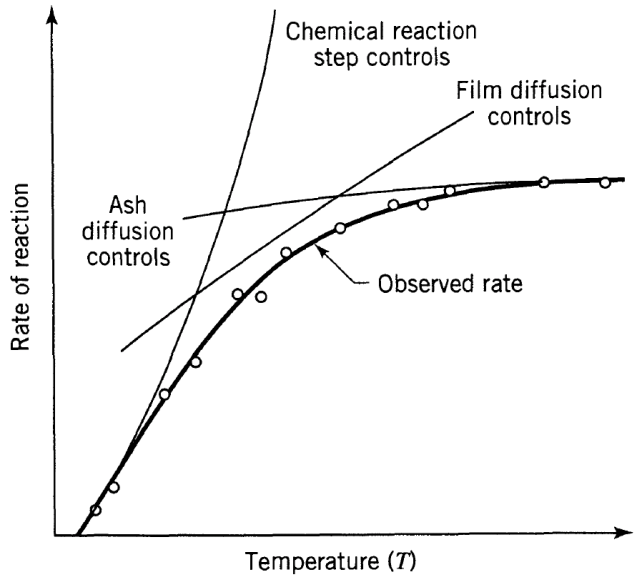

Figure 6-32: Effect of an increased reactor temperature on the observed rate of reaction[134]

The results shown in Figure 6-31 confirm the assumption of limitation by reaction kinetics for the application of the CaBa-sorbent at reactor temperatures of 760 °C. The improved performance of CaBa at increased temperatures of application is also in accordance with previous research conducted by Stemmler et al.[86] Only the reason for the observed phenomenon of limited performance at temperatures below 760 °C can be restated. A lower temperature limit for the application of CaBa is thus supposedly not given by the carbonization temperature of CaO but by the reactivity of BaO itself.

With respect to the observation of an increased rate of reaction at increased temperatures, experimental investigations were aimed at determining the desulfurization properties of CaBa at elevated H_2S contents in the syngas. For this purpose an experiment (CaBa_9) was performed at an initial H_2S content of 350 ppm_v H_2S at a reactor temperature of 810 °C (freeboard temperature 840 °C, steam-excess-ratio 4) under application of 2.5 g CaBa every 10 minutes thus equaling a δ of about 2 and a total added amount of 62.5 g. Figure 6-33 shows a comparison of the obtained results at increased H_2S content with desulfurization results starting from about 85 ppm_v H_2S at 810 °C (CaBa_7).

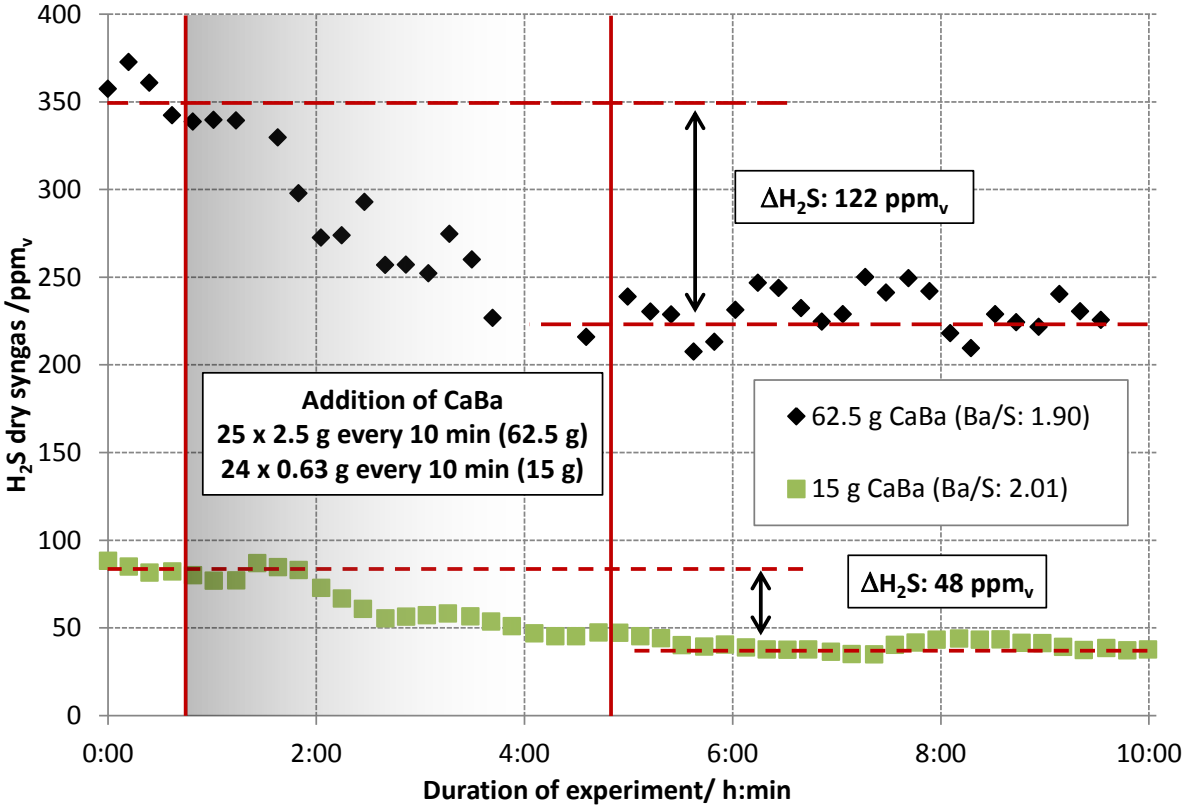

Figure 6-33: Influence of increased amounts of added sorbents with a constant molar Ba/S-ratio of about 2, at reactor temperatures of 810 °C (Table 6-7: Experiments CaBa_7 and CaBa_9))

The experimental investigation of application of CaBa for desulfurization of a syngas with an initial feed content of about 350 ppm_v H_2S resulted in an increased depletion of sulfur from the syngas in the range of 122 ppm_v H_2S (Figure 6-33). Even though the effect of desulfurization is increased as compared to application of CaBa with equal molar ratio δ at low sulfur conditions, the desulfurization is supposedly still limited by the rate of reaction, indicated by the established steady state at values of about 230 ppm_v H_2S. A final experimental confirmation of the feasibility of desulfurization from several hundred ppm_v H_2S feed to the observed steady state at 35 ppm_v under low sulfur conditions (Figure 6-31) was not possible within this work. This was due to material related limitations in further increasing the reactor temperature and also due to limitations in sorbent availability. On the other hand some conclusions for the required conditions of such an experimental investigation can be drawn from the results obtained within the conducted work. Assuming the necessity of removing H_2S from syngas with an initial content of 500 ppm_v, equaling the steady state of CaO-based desulfurization under the investigated experimental conditions, a value ΔH_2S of about 465 ppm_v would have to be removed by CaBa in order to achieve the steady state of 35 ppm_v H_2S. Further assuming a linear correlation between the temperature and the observed rate of reaction as shown in Figure 6-32 for the temperature range dominated by the chemical reaction step, an interpolation follows as shown in Figure 6-34.

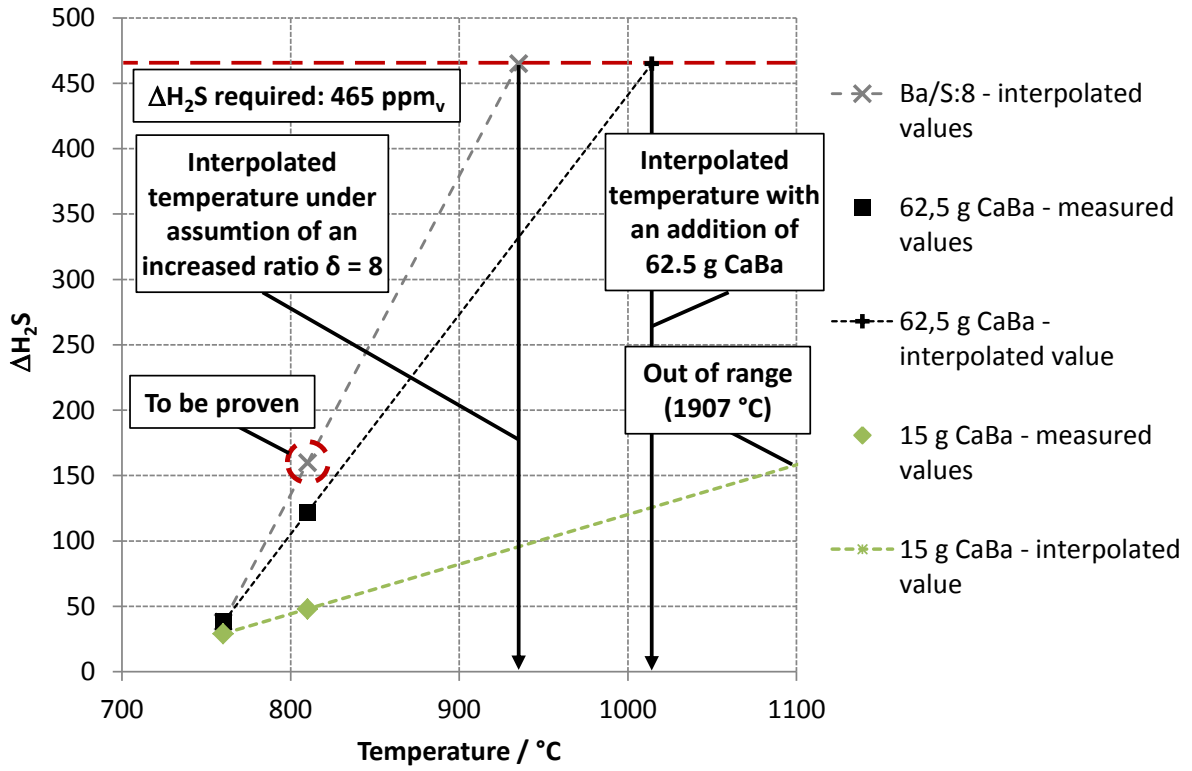

Figure 6-34: Interpolation of desulfurization results obtained by experimental investigation (Table 6-7: CaBa_1, CaBa_5, CaBa_7, CaBa_9)

Deduced from the linear interpolation of the experimentally determined values for depletion of sulfur (ΔH_2S) with an added amount of 15 g CaBa under an increase of reactor temperatures (Table 6-7: CaBa 5 and CaBa 7), the required reactor temperature for a desulfurization effect of ΔH_2S = 465 ppm_v is at about 1907 °C. This level of temperature is not realistic and out of range for allothermal fluidized bed gasification of biomass with common values in the range of 750 to 900 °C.

The effect of increased reactor temperature is more significant for the experiment CaBa 9 with an initial feed of about 350 ppm_v H_2S and an added amount of 62.5 g CaBa (δ of 2). The interpolation of the trend for experimental results of ΔH_2S under addition of 62.5 g CaBa yields a required temperature of about 1014 °C in order to achieve a desulfurization effect in the range of 465 ppm_v H_2S (Figure 6-31). This temperature level is still high compared to commonly applied conditions in biomass gasification and the interpolation is only valid under the assumption of a linear correlation between the observed rate of reaction with increased temperature. This is only the case for a continued limitation by the reaction step and minor influence of diffusion effects (Figure 6-32).

On the other hand a Ba/S ratio δ of 2 is low compared to the experimental investigations on CaO-based desulfurization. Concluded from the increased effect of desulfurization upon elevation of the molar ratio δ from 2 (CaBa_5)) to 8 (CaBa_1) at 760 °C reactor temperature, the impact of an increased δ at elevated reactor temperatures of 810 °C can be estimated whereby the assumed effect lacks experimental proof and needs to be proven. This allows once more the interpolation under assumption of a linear correlation between the reactor temperature and the observed rate of reaction according to Figure 6-32. The interpolation of the desulfurization effect at an increased ratio δ of about 8 indicates that a reactor temperature in the range of 900 - 950 °C might be a suitable

experimental setup in order to achieve a sulfur removal of 465 ppm_v H_2S under excess addition of CaBa. This temperature level is closer to a realistic scenario of application in biomass gasification. Furthermore the calculatory value of 465 ppm_v H_2S is aimed at the concept of a combined application of CaO- and BaO-based desulfurization, which is discussed subsequently in section 6.4. This value is therefore based on the steady state of CaO that is at a level of 500 ppm_v H_2S for the investigated gasification conditions. According to thermodynamic simulation (Figure 4-4) and experimental investigation (Figure 6-15) this steady state value will be lower in syngas with less steam as compared to the 40 % contained under the investigated conditions. In order to prove these assumptions further experimental work is required. These experiments will need to include the investigation of three major aspects:

1) The influence of an increased temperature, beyond the current limitation of 810 °C present in the applied experimental setup
2) The influence of an increased amount of added sorbent with a ratio δ of 8 at increased temperatures and high initial H_2S feed of about 500 ppm_v
3) The effect of a reduced steam content in the range of 20 vol% on BaO based desulfurization

In order to further elucidate the limitation mechanism in the applied CaBa sorbent, continuous measurements in a broader range of temperature, under variation of the stoichiometric ratio and particle size are needed. On the other hand the complex influences inside a real fluidized bed gasifier are not preferable for examining the surface kinetics of BaO sulfidation. As BaO is commonly not considered for desulfurization purposes, kinetic data on the desulfurization performance of BaO and especially the investigated CaBa sorbent is not available in literature. Such data would ideally have to be obtained by thermogravimetric analysis as performed by Westmoreland *et al.*[136] for the sorbents MgO, CaO, ZnO and V_2O_3. They observed a first order kinetic with respect to H_2S for all investigated sorbents and a behavior according to the Arrhenius equation with increased temperature.

6.4 Combined desulfurization with CaBa and lime

To conclude, the combined desulfurization of H_2S with lime and CaBa was investigated. As described above, lime serves as a separating agent for the application of CaBa sorbent but acts as a desulfurization sorbent itself, resulting in a steady state value of about 500 ppm_v H_2S as described in section 6.2.3. In-situ desulfurization based on lime is thus suitable as a method for coarse desulfurization whereby the application of CaBa proved to yield residual sulfur contents of 35 ppm_v H_2S (Figure 6-31) which is sufficiently low for subsequent ZnO-based desulfurization in a downstream fixed bed reactor. The combined desulfurization under application of CaBa and lime therefore offers the possibility of a coarse sulfur removal under formation of CaS from CaO and a further reduction of the residual H_2S content down to about 35 ppm_v based on the formation of BaS from BaO.

6.4.1 Experimental application of CaBa and lime

In a preliminary experiment, the combined desulfurization under application of CaBa and lime was investigated. For this purpose the initial feed content was established in the same range of 1200 ppm_v H_2S as for investigations with CaO-based sorbents discussed in section 6.2. An amount of 2.5 g of the CaBa sorbent was added every 10 minutes via the fuel inlet of the BFBG together with lime in a

weight ratio of 1:1. As the initial H_2S content was in the range of 1200 ppm_v the lime acted as a separating agent in order to prevent sintering of the CaBa sorbent but also as sorbent for coarse desulfurization down to values of around 500 ppm_v H_2S. Comparison between the desulfurization results under application of CaBa (Figure 6-28) and lime (Figure 6-7) shows a much faster decline to a steady state value for lime than for CaBa with durations of about 2 hours for the first as compared to about 4 hours for the latter. Therefore a stepwise desulfurization was assumed for the combined application of both sorbents with the BaO-based steady state value succeeding the establishment to a CaO-based steady state value for residual H_2S. The obtained results depicted in Figure 6-35 show a completely different behavior of the system as compared to the stated assumptions.

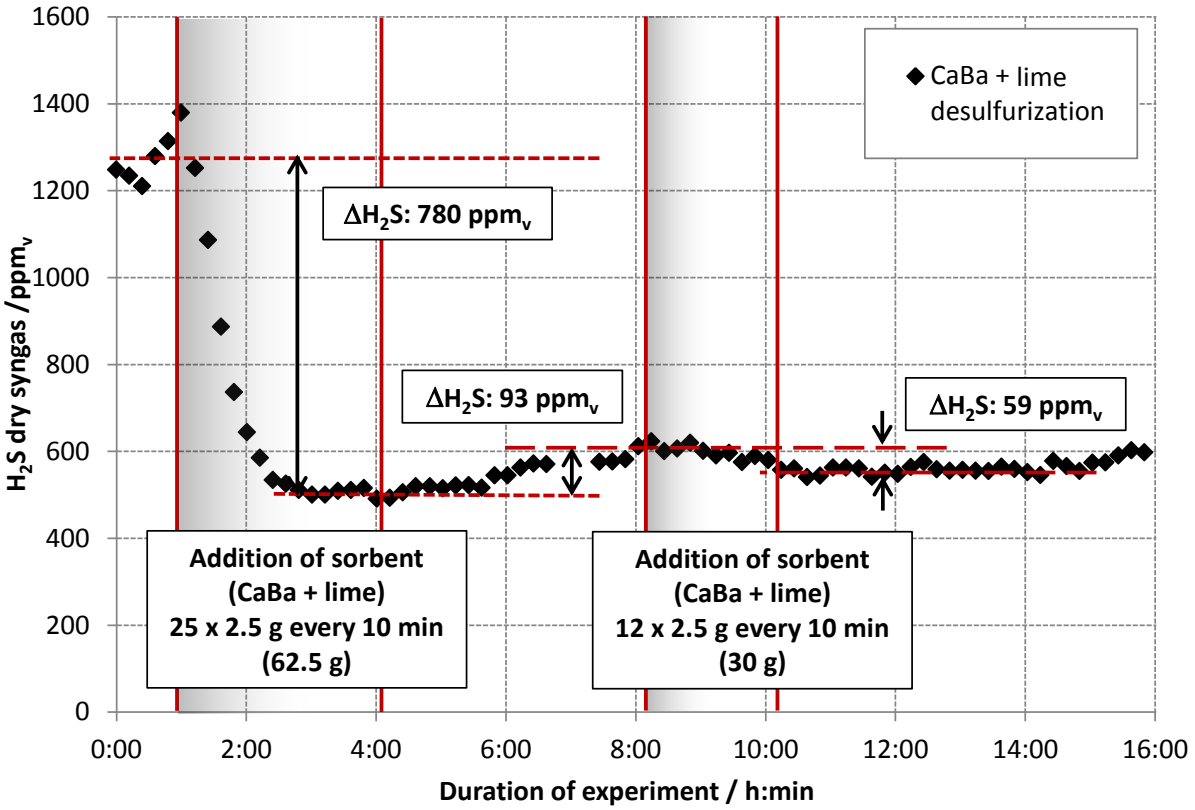

Figure 6-35: Mixed desulfurization with CaBa and lime added in a weight ratio of 1:1 (760 °C reactor temperature, 840 °C freeboard, steam-excess-ratio 4)

The results of a combined application of CaBa and lime (Figure 6-35) indicate a decline from an initial H_2S content of about 1300 ppm_v to a steady state value of about 500 ppm_v H_2S as expected for a CaO-based desulfurization at the conditions (760 °C reactor temperature, steam-excess-ratio 4, compare Figure 6-6) applied. The residual H_2S content then rises slowly to values of about 600 ppm_v instead of further declining due to a BaO-based desulfurization effect. The repeated addition of CaBa and lime leads to decline in residual H_2S of about 52 ppm_v to values around 550 ppm_v. As the CaO-based desulfurization is not clearly separable from a possible effect of the addition of CaBa the obtained results of the experiment shown in Figure 6-35 require further investigation. The experiment does show that a combined desulfurization of CaBa and lime does not yield the expected reduction of residual H_2S to values significantly below 500 ppm_v. In order to further elucidate this behavior the effects CaO- and CaBa-based desulfurization have to be investigated separately.

For this purpose an experiment was performed with H_2S addition limited to 600 ppm_v and subsequent addition of 30 g lime. This caused a decline of residual H_2S and resulted in CaO-based desulfurization steady state value of 482 ppm_v H_2S (Figure 6-36 – CaO+CaBa desulfurization). Starting from this CaO-based steady state value, 62.5 g of CaBa were added in 25 batches of 2.5 g. Lime was added as a separating agent in a weight ratio of 1:1. As shown in Figure 6-36 the resulting CaBa-based decline in residual H_2S was in the range of 44 ppm_v related to the CaO-based steady state value of 482 ppm_v. The CaBa-based desulfurization effect of 44 ppm_v H_2S under combined desulfurization of lime and CaBa and an addition of 62.5 g sorbent is therefore in the same range as the achieved desulfurization effect of 48 ppm_v H_2S with only 15 g added CaBa at an initial sulfur content of 83 ppm_v H_2S (Figure 6-31). In order to further elucidate the interaction of lime and CaBa desulfurization, the experiment was repeated with an initial value of 375 ppm_v H_2S clearly below the steady state equilibrium of CaO-based desulfurization (Figure 6-36).

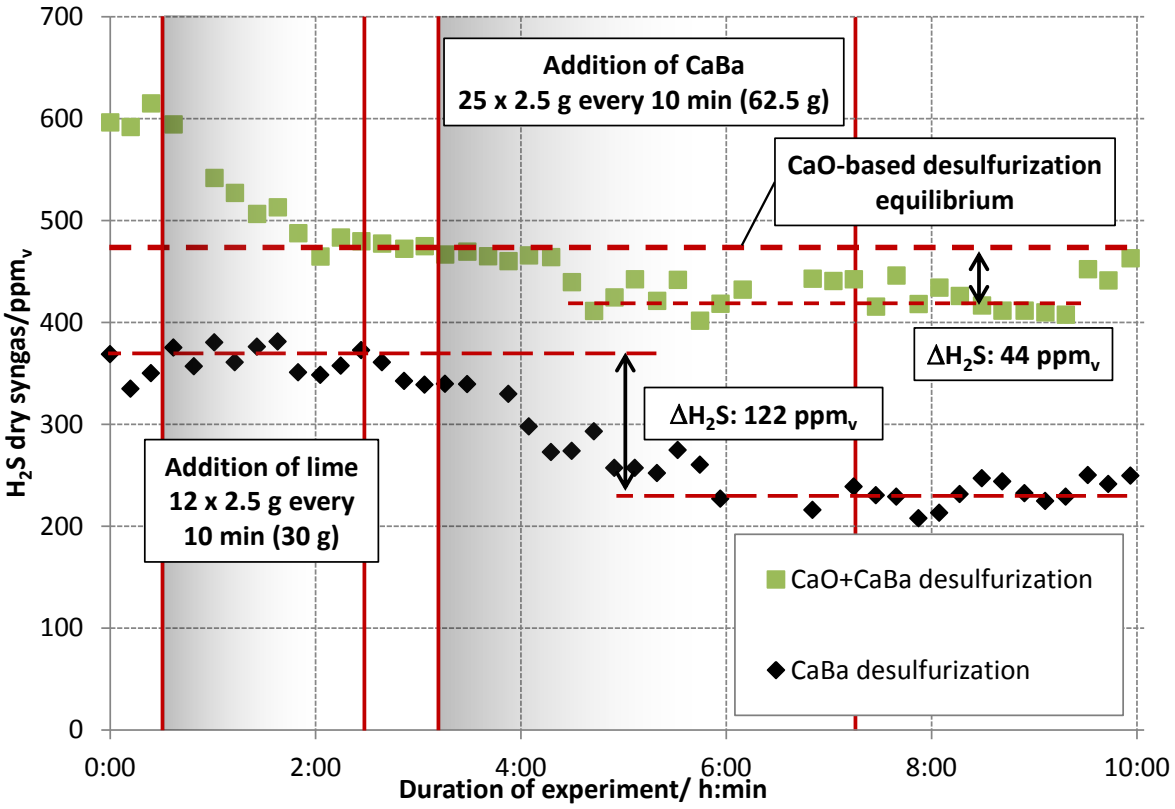

Figure 6-36: Comparison of the effect of CaBa addition starting from a CaS-H_2S equilibrium (Table 6-7: CaBa_8) and H_2S concentrations below the onset of CaS formation (Table 6-7: CaBa_9) (Both experiments: 810 °C reactor temperature, 840 °C freeboard, steam-excess-ratio 4)

At an initial feed of 375 ppm_v H_2S the addition of 30 g of lime did not result in any related decline of the H_2S content in the gas. Upon addition of 62.5 g CaBa a clear decline in the H_2S content was shown with an average of 122 ppm_v as compared to the initial feed (Figure 6-36 –CaBa desulfurization). The obtained results confirm a clear improvement of CaBa based desulfurization at increased reactor temperature compared to the results at 760 °C presented in Figure 6-28. Further it is shown that the CaO-based desulfurization does not add up with the effect of CaBa application to result in an increased combined effect of in-situ desulfurization. The results are better explained by a replacement of CaO-based desulfurization by BaO-based sulfur reduction considering a feed concentration of 600 ppm_v H_2S in the experiment with combined desulfurization effects. This was the

case if a release of sulfur from CaS would occur with the onset of BaO based desulfurization. Considering the CaO-based desulfurization as a reversible equilibrium reaction, such a release of H_2S by CaS is obvious once the content of H_2S in the gas is reduced below the equilibrium of CaO-based desulfurization. The chemical instability of CaS is known and a common hurdle in the discharge of used desulfurization sorbents due to the release of H_2S from CaS upon contact with the humidity of the air.[72] On the other hand the regeneration of CaO from CaS is, in most applications, not considered as a desirable process step as CaO is abundantly and cheaply available and therefore qualifies for single use in desulfurization with subsequent disposal.[127,128] Inferentially, research-activities are more focused on the stabilization of CaS as $CaSO_4$ for disposal than on the regeneration of CaO for multicycle application.[126]

In order to confirm the hypothesis of release of H_2S by CaS during combined desulfurization with use of CaBa and lime, the reverse reaction of desulfurization was experimentally induced by the interruption of CS_2 supply (Figure 6-37).

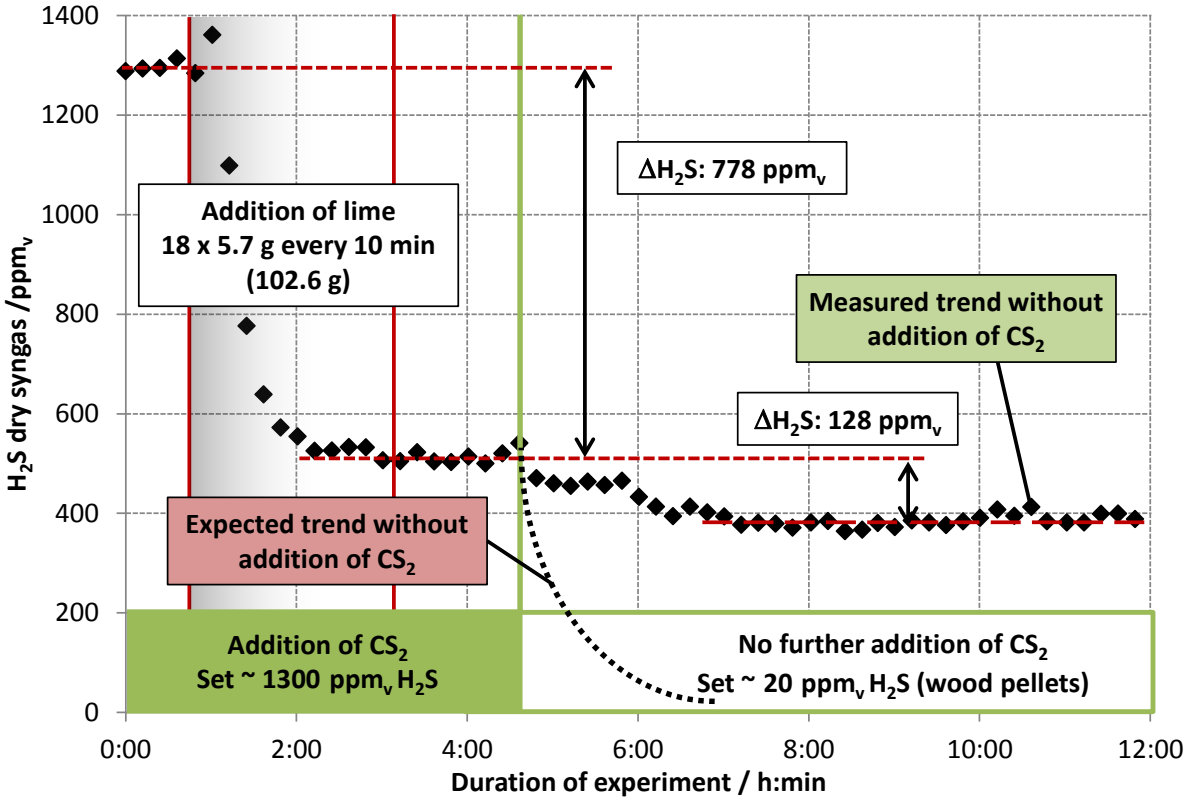

Figure 6-37: Investigation of the release of H_2S by CaS by desulfurization with lime and subsequent interruption of the CS_2 supply (760 °C reactor temperature, 840 °C freeboard, steam-excess-ratio 4)

Figure 6-37 shows a desulfurization experiment, based on the addition of lime to a continuously running gasification process with 1300 ppm_v H_2S feed. A steady state equilibrium of 500 ppm_v H_2S is established within less than 2 hours after the first addition of in-situ sorbent. This steady state value remains constant even after the addition of sorbent is stopped and while sulfur is continuously fed via supply of CS_2 equaling a set value of 1300 ppm_v H_2S. The supply of CS_2 is stopped after about 5 hours of experiment. This would usually lead to a fast decline in the residual H_2S content of over 50 ppm_v per hour as previously shown in experiments without CaS contained in the fluidized bed. As demonstrated in Figure 6-37 the CaS contained in the fluidized bed prevents such a decline of sulfur

content in the gas by continuously releasing H_2S. This leads to a new steady state H_2S content of about 400 ppm_v based on the equilibrium of sulfur release. This steady state remains stable for about 8 hours before the residual H_2S content eventually drops (not shown due to congestion in the fuel supply).

The obtained results (Figure 6-37) clearly show the reversibility of the desulfurization reaction with subsequent release of H_2S by CaS, if it is not stabilized in the process. Accordingly, with the applied experimental setup, the release of H_2S from CaS leads to a limited efficiency of the combined desulfurization of CaBa and lime with initial H_2S feed concentrations above the steady state equilibrium of CaO-based desulfurization.

6.4.2 Options for process setup

As demonstrated in section 6.4.1, the combined in-situ desulfurization by application of CaBa and lime in a single reactor vessel is not effective due to the release of H_2S from CaS once the sulfur content in the gas drops below the thermodynamic equilibrium of CaO-based desulfurization. A separation of the desulfurization steps would therefore be necessary if a combined desulfurization was pursued under the application of CaBa and lime. With the aim of simplifying the process setup by application of in-situ desulfurization, the installation of an additional heated desulfurization reactor downstream of the gasifier would be contradictory. Therefore the separation of the different desulfurization steady states of CaBa and lime within a single gasification reactor would be necessary in order to comply with the original intention of establishing in-situ desulfurization as process step for a coarse desulfurization.

This might be valid for the application in a countercurrent FICFB – reactor, especially for a new reactor design with internals, developed at Vienna University of Technology (Figure 6-38).[137]

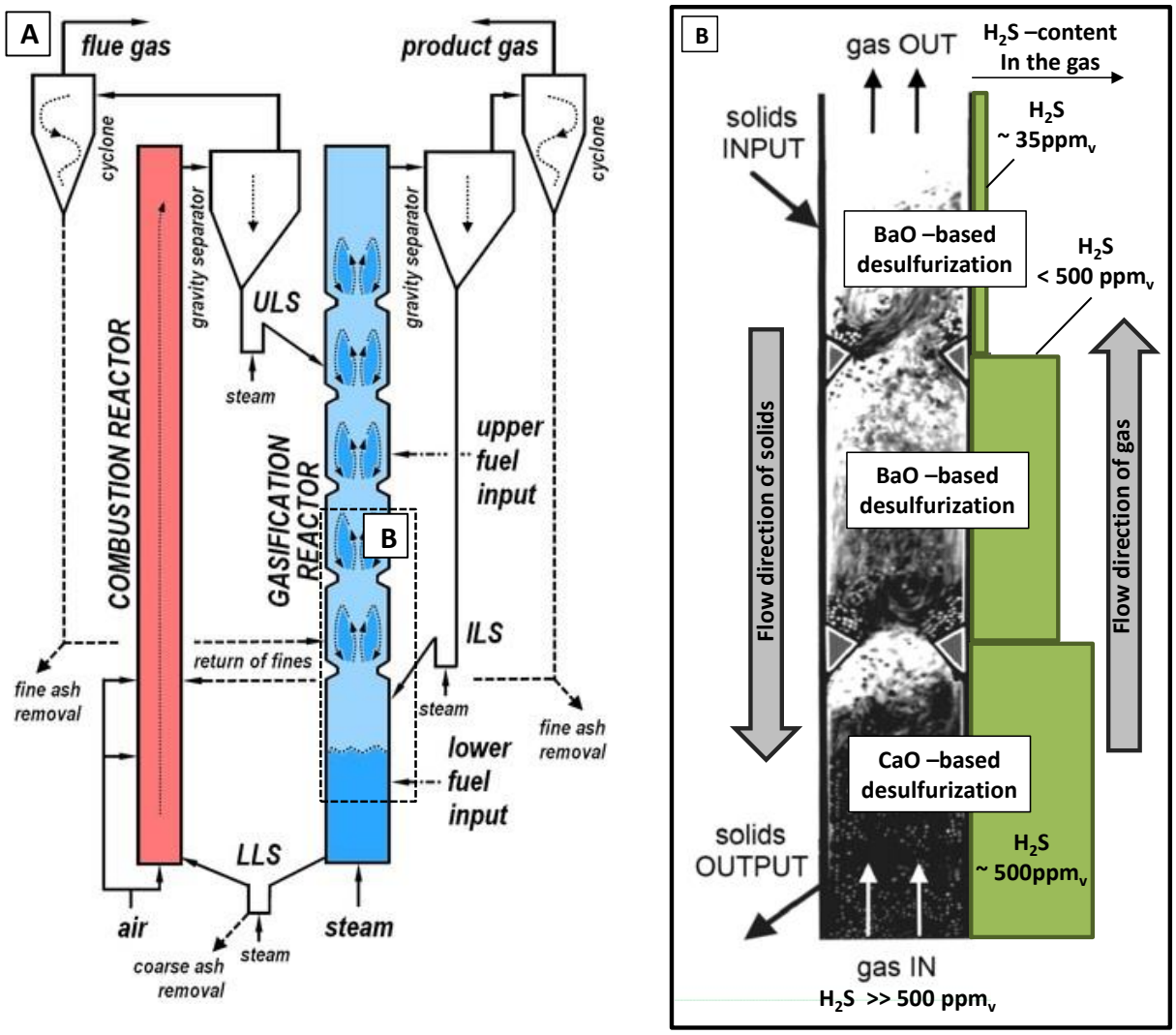

Figure 6-38: (A) Working principle of a countercurrent FICFB – reactor, developed at Vienna University of Technology[137] (B) Flow pattern inside the gasification reactor with an example of consecutive desulfurization steps

The currently developed reactor design follows the FICFB concept as described in section 2.3.2 but exhibits several improvements and additions to the basic reactor as depicted in Figure 6-38. After being heated up due to the exothermic reactions in the oxidizing atmosphere of the combustion chamber the bed material is inserted to the upper section of the fluidized bed gasifier. Other than in the standard setup, the gasification reactor does not consist of a single vessel but is composed of a sequence of overlaying gasification chambers separated by flow obstacles. The fluidization velocities are adjusted in a way that the bed material is temporarily stabilized in the separated fluidized regions and still continuously passes on to the cascade underneath. This system was originally designed for an increased tar conversion on the catalytically active surface of the bed material as it enables gas solid interactions over the full height of the gasifier.[137] This is in clear contrast to the classic design of a BFBG were the solids concentration is mainly restricted to the single vessel of the fluidized bed which allows only limited gas-solid interactions in the freeboard region of the gasifier. The countercurrent design presented in Figure 6-38 can be described as a multi-stage cascade of stirred vessels with the gas phase flowing upward and the solids downward towards the outlet at the bottom of the gasifier.[137]

The temporary stabilization of the bed material in consecutive chambers of the gasification reactor seems suitable for the separation of different gas-solid interactions at different steady state conditions in the context of in-situ desulfurization as shown in Figure 6-38 (B). As the solids flow downstream in the countercurrent gasifier, the setup allows the establishment of a low BaO-based desulfurization steady state in the upper chambers of the gasification reactor. While the BaO in the CaBa sorbent is converted to BaS, the sorbent passes on to downward sections of the gasifier with a higher content of H_2S in the gas. Once the steady state equilibrium of CaO-based desulfurization is surpassed, the CaO in lime starts to convert into CaS. Before the loaded sorbent materials are passed on to the combustion chamber, the lime is exposed to the sulfur rich gas around the fuel inlet at the bottom of the reactor. A release of sulfur from BaS or CaS can therefore be prevented, as the driving force of the desulfurization reaction always remains towards the formation of sulfides as the sulfur content in the gas does not drop below the equilibrium values of the desulfurization reactions (Eqs (33),(35)). Further this reactor setup provides the possibility of stabilization of the formed sulfides under the oxidizing conditions in the combustion reactor.[127,128] The sulfides that are formed during desulfurization in the gasifier are only stable under reducing conditions. In contact with air they decompose, which is the reason for restrictions in landfill disposal of these components.[126] The oxidizing conditions and the heat in the combustion chamber facilitate the conversion into the stable sulfates $CaSO_4$ and $BaSO_4$. Research will have to confirm that the formed sulfates are stable enough to not again decompose once they are reintroduced to the gasifier.[125] On the other hand the continuous circulation of the solids in the FICFB setup shown Figure 6-38 also exhibits the possibility of a constant removal of used sorbent materials.[137]

The easily facilitated removal of used sorbents is a general advantage of a circulating fluidized bed as compared to a stationary bubbling fluidized bed in the context of in-situ desulfurization. It can therefore be stated that for further application of in-situ desulfurization a variation of the process setup is recommendable. For the investigation of a combined in-situ desulfurization under application of CaBa and lime the gasifier setup shown in Figure 6-38 exhibits various advantages which lead to the adaption of the pursued concept for gas cleaning shown in Figure 3-1 as a motivation for the conducted work. With the experimental results obtained in sections 6.2 and 6.3, the concept for a process setup can be depicted as shown in Figure 6-39.

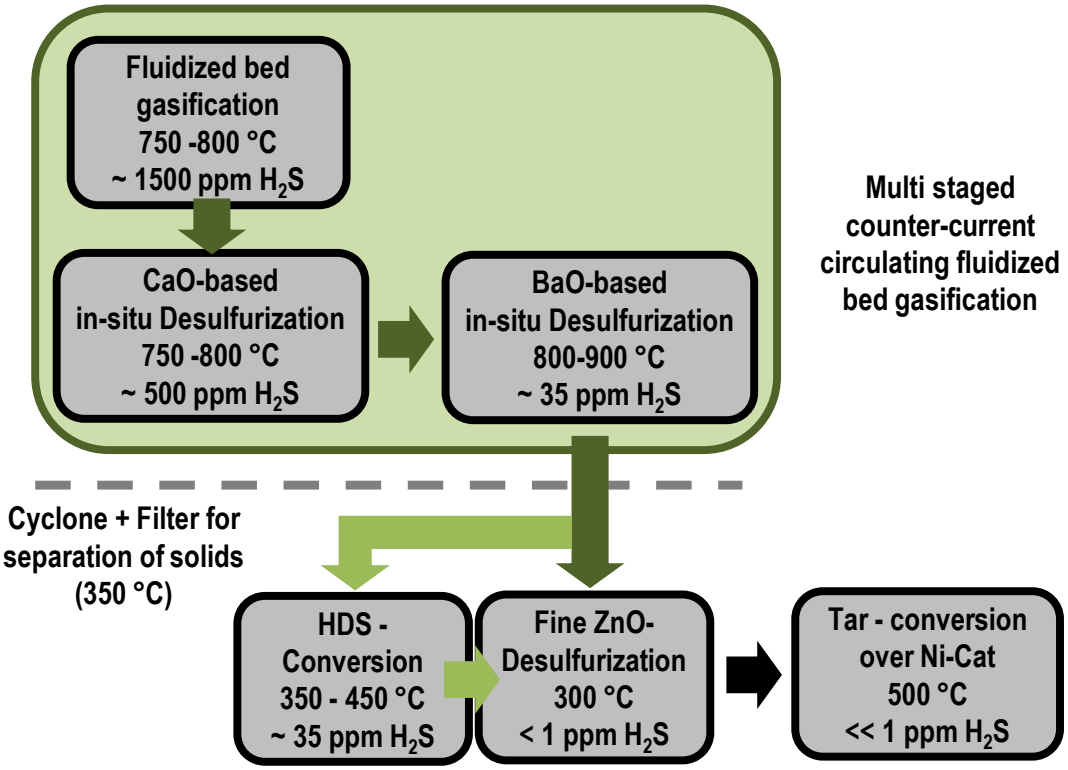

Figure 6-39: Suggested process concept with adapted setup and conditions based on the results and conclusions obtained from the presented work

Besides the easily facilitated removal of used sorbents and the possibility of establishing different steady states of desulfurization by introducing a staged setup depicted in Figure 6-38, it is also possible to establish a temperature gradient inside the gasifier as shown in the adapted concept for process setup, depicted in Figure 6-39. A setup with a staged temperature would be beneficial according to the results discussed in sections 6.2 and 6.3 with different optimum temperature ranges of CaO- and BaO-based desulfurization. In a countercurrent setup where the hot bed material is entered from the top of the reactor such a staged distribution of temperatures occurs naturally and can therefore be taken advantage of in ideally achieving the output margins of residual sulfur content as shown in Figure 6-39. Another potential synergy is given by the commonly lower steam content in FICFB gasification as compared to the conditions present during the experimental investigations.[86] This will result in lower steady state values for CaO (Figure 6-15) - and propably as well for BaO-based in-situ desulfurization.

Besides the advantages concerning in-situ desulfurization, the increased complexity of a system shown in Figure 6-38 will raise the investment cost of the gasifier setup. This increase in complexity will have to be justified by other advantages such as reduced tar content due to the increased interaction of the syngas with the catalytic particles of the fluidized bed. Furthermore the applicable size range of such gasification units will have to be established according to the market situation discussed in section 7, taking into account the increased investment costs due to the higher degree of process complexity.

6.4.3 Consideration of legal restrictions

A general drawback in considering the application of CaBa as desulfurization sorbent is the classification of BaO as toxic agent. BaO is soluble in water in concentrations of 3.5g/100 ml at 20 °C and transforms into a highly alkaline barite-solution. The corrosive character of BaO upon contact with mucous membranes limits the likelihood of swallowing relevant amounts of BaO. On the other hand even upon incorporation of a dose below 1 g severe physical effects like the paralysis of the central nerve system are to be expected.[138]Upon inhalation, the substance can cause a toxic pulmonary edema that may be lethal even after treatment. This gives reason for the low maximum allowable concentration (MAC – value) of dust load of 0.5 mg/m^3_{std} under working conditions. For the application of the BaO containing CaBa-sorbent in a fluidized bed environment with inherently high dust loads, this would give rise to the requirement of severe safety precautions concerning the discharge of dust from the system and aeration of the working environment.[138]

On the other hand the addition of only 1 wt% sorbent, respectively 15 g of CaBa to a fluidized bed containing 1500 g of olivine, sufficed to reduce the residual H_2S content by 50 ppm_v for 12 hours (Figure 6-32). Considering the BaO-content of 10 mol% in the CaBa sorbent this equals a mass of 3.5 g BaO added to the gasification process. Besides the low amount of sorbent necessary for desulfurization, especially for the application in a FICFB or comparable gasifier setup with transfer of the bed material to zones with oxidizing conditions, a stabilization of the instable BaS into $BaSO_4$ would occur. $BaSO_4$ is toxicological harmless and applied as contrast increasing agent in X-ray screening.[138] As a full conversion of BaO to BaS was observed during the experimental investigation of the CaBa sorbent, the occurrence of BaO in the fluidized bed of the gasifier would be limited and an extraction of BaO with the ash might be preventable. Further experimental investigation is required to confirm the full conversion of BaO to BaS and subsequent stabilization as $BaSO_4$ upon application of CaBa sorbent in a circulating fluidized bed.

Given the fact that the ash of fluidized bed gasifiers in biomass application contains several highly toxic components ranging from organic fractions such as polyaromatic hydrocarbons or inorganics such as chromate[139] the exposal of gasifier content to the environment has to be strictly prevented in any case even without the addition of “CaBa”. This accounts for the ash as well as for the dust load in the gas phase as the presence of over 20 vol% CO in the produced syngas, by itself prohibits the exhaust of untreated syngas into the environment and comes along with high demands concerning safety precautions. Inferentially the application of a BaO-containing desulfurization sorbent, such as CaBa, would most likely increase the cost for discharge of wastes, as considered in the economic evaluation (section 7) and eventually increase safety precautions in the process setup. On the other hand it seems not justified to generally exclude the application of a BaO-based desulfurization sorbent due to legal restrictions, considering the numerous toxic substances involved in biomass gasification, which requires strict precaution against environmental exposure anyways.

6.5 Discussion of possible sources of error

The measurements presented in the experimental section of this study are prone to numerous sources of error that shall be discussed subsequently according to their either systematic or statistical nature.

6.5.1 Systematic errors

The addition of CS_2 to the steam inlet of the reactor proved to be an efficient and reproducible method for the elevation of sulfur content in the gas, without relevantly changing the composition of permanent gases. The continuity of CS_2 supply was warranted by stable temperature and pressure conditions in the container with liquid, and controlled by gravimetric changes of the container over time on stream, as well as by the measurement of sulfur content in the gas. The temperature within the BFBG warrants an expected full conversion of CS_2 to H_2S. Accordingly no CS_2 was measured downstream of the gasifier even for long term (60 hours) experimental runs, thus taking into account saturation effects. Nevertheless the amount of CS_2 extracted from the container filled with liquid according to the gravimetric changes as compared to the calculated amount of CS_2 necessary for the achieved elevation of H_2S content were far apart. The gravimetric gap was in the range of 45 % based on the value of extracted CS_2, meaning that only a little more than half of the sulfurous compound was extracted from the container, injected to the reactor, converted to H_2S and detected by the GC. As balancing the injected sulfur was comparatively exact for the injection of H_2S into the gasifier, with less than 10 % loss, the detected values via GC-measurement were considered rather accurate. Possible explanations for the gap between measurements and gravimetric balancing would be a relevant loss of CS_2 during the startup phase of CS_2 supply, caused by extraction of droplets from the container or the sulfidation of steel parts at H_2S contents above ~1300 ppm_v. For future measurements an initial H_2S content of the syngas no higher than 1000 ppm_v and a continuous control of the gravimetric changes of the liquid container are strongly suggested.

On the other hand, it has to be stated that due to the sorptive nature of sulfurous compounds, the accuracy of a single measured value has to be considered as low because of sorption equilibria in the periphery and impinger bottles for tar and water removal. This will especially account for dynamic changes in the actual sulfur content of the produced gas, which will be detected with a delay due to such sorption and desorption effects. These effects equalize under steady state conditions. The sum of measured values does therefore reflect the behavior of the system and allows definite conclusions about the influencing factors on in-situ desulfurization in the context of biomass gasification.

Another error that is of systematic character is given by a continuous sampling of a side stream of the produced syngas for gas analysis compared to a fluctuating gas flux out of the gasifier due to a batch-wise fuel inlet. Approximately every 90 s a medium amount of 12.5 g of pellets is fed into the reactor, resulting in a total fuel mass flow of 500 g/h. This results in a fast increase in the amount of produced gas as indicated by a rise in reactor pressure of about 50 mbar in average and can be visually confirmed by the size of the flame in the exhaust flare. In contrast to this alternating flux of produced syngas, the slipstream for gas sampling remains constant. This results in an overly pronounced representation of the gas composition at low syngas flow during the conversion of char as compared to phases of high syngas flow with an increased amount of pyrolysis gas components.

6.5.2 Statistical errors

A source of error that is of statistical nature due to the unknown and complex systematic behavior that causes it, is the influence of the conversion of char in the freeboard of the gasifier. According to the Boudouard reaction (Eq (3)) it is accelerated by increased temperature and facilitated by a surplus of steam injected in the gasifier as gasification agent. An increase of temperature should therefore increase the conversion rate of char and increase the amount of gas until a new steady state equilibrium with less coke prevailing in the freeboard is established. Assuming that sulfur contained in the fuel gasifies quickly to H_2S, an increase in the amount of released gas should lead to a transitional decrease of the sulfur content until a new steady state between fuel input and char conversion is reached. According to experiments with variations in freeboard temperature, the opposite was observed leading to a sharp increase in the H_2S content upon elevation of the freeboard temperature. This implies that sulfur is adsorbed at the unconverted char in the gasifier. As the extent of sulfur release by variations of the freeboard temperature is an additional and avoidable insecurity in the evaluation of experimental results, the freeboard temperature was kept rather constant throughout the different experimental investigations performed.

A general influence of error in the performed experiments was the measurement technique for sulfur determination based on GC-PFPD analysis. The GC-PFPD-sensor is a highly sensitive tool that enables the detection of a broad range of vaporizable components containing the luminescent elements sulfur or phosphor in variable ranges. The more its sensitivity makes it a viable measurement technique for trace analysis in laboratory environments, the more it is affected by contaminants and pollutants contained in biomass derived syngas from a gasification process. Permanent calibration of the analysis device was necessary to counteract drifts in signal response due to soot formation or pressure changes due to precipitation of tars or other condensable substances in the valve oven for gas sampling. Complementary to the GC-PFPD analysis, the determined values of H_2S-content were double checked by “Dräger”-analysis. Besides calibration prior and after each experimental run and cross checking by Dräger sampling, most of the statements for system behavior are based on relative changes of the measured values. Therefore the presented results do not only rely on the absolute value of measurements but also indicate the response of the system upon change of a single parameter, as for example in case of the influence of particle size or steam content. Whenever statements are made that solely rely on the absolute value of measurement they were multiple checked, like for the different steady state behavior of fully calcined dolomite as compared to other CaO-based sorbents. As a consequence of the experiences made in the course of this work, the use of a GC PFPD as major measuring tool is clearly discouraged for application under rough conditions such as the analysis of gasifier derived syngas. As H_2S is clearly the predominant sulfurous component and represents the behavior of minor sulfur species as well (Figure 6-6 and Figure 6-8) a colorimetric or photometric measurement seems more advisable.

7 Assessment of economics

In order to evaluate the economic perspective of in-situ desulfurization the costs of this desulfurization technology has been estimated in comparison to a ZnO-based desulfurization, based on different assumptions. For this purpose, the economic models for the calculation will be explained, followed by a description of the assumptions and the resulting calculation. Finally, the results will be compared to the desulfurization costs of comparable technologies.

7.1 Background for economic evaluation

The experimental investigations on in-situ desulfurization were performed at Graz University of Technology in an experimental test rig for laboratory use, far below any scale of commercial application as described in section 5.1.1. The assessment of economics of in-situ desulfurization was therefore based on the size of a 1.3 MW allothermal gasifier as commercially produced by the company agnion.[44] This gasifier uses the Heatpipe reformer (HPR) technology (Figure 2-3) in order to produce a high quality syngas suitable for the upgrade to SNG. Compared to other commercial biomass applications the evaluated “HPR” - gasifier is in the small power range of fluidized bed biomass gasifiers.[43]

The small scale of a gasification process is beneficial concerning the supply with biomass obtained from a local catchment area which reduces the influence of transport costs on fuel and improves the ecological footprint.[37] Furthermore, the economy of numbers yields a reduction of production costs with increased repetition of a production or construction process. Such effects are enhanced for small, decentralized systems.[140] Both of these factors are thwarted by the economy of scale, which leads to reduced investment costs with increased size of the facility. In the prospect of SNG production, this leads to an increased specific cost for small scale gasification applications.[141]

In order to be profitable, the specific costs of produced SNG have to be below the market price of natural gas or the specific remuneration provided by subsidiaries for renewable technologies. A production of biomass derived SNG at the price of fossil fuels is presently not feasible.[4] The remuneration provided by subsidiaries is stated by the “Erneuerbare Energien Gesetz” (EEG) for the often published example of Germany. An evaluation of the estimated costs of production of SNG compared to the achievable remuneration according to the EEG is shown in Figure 7-1.

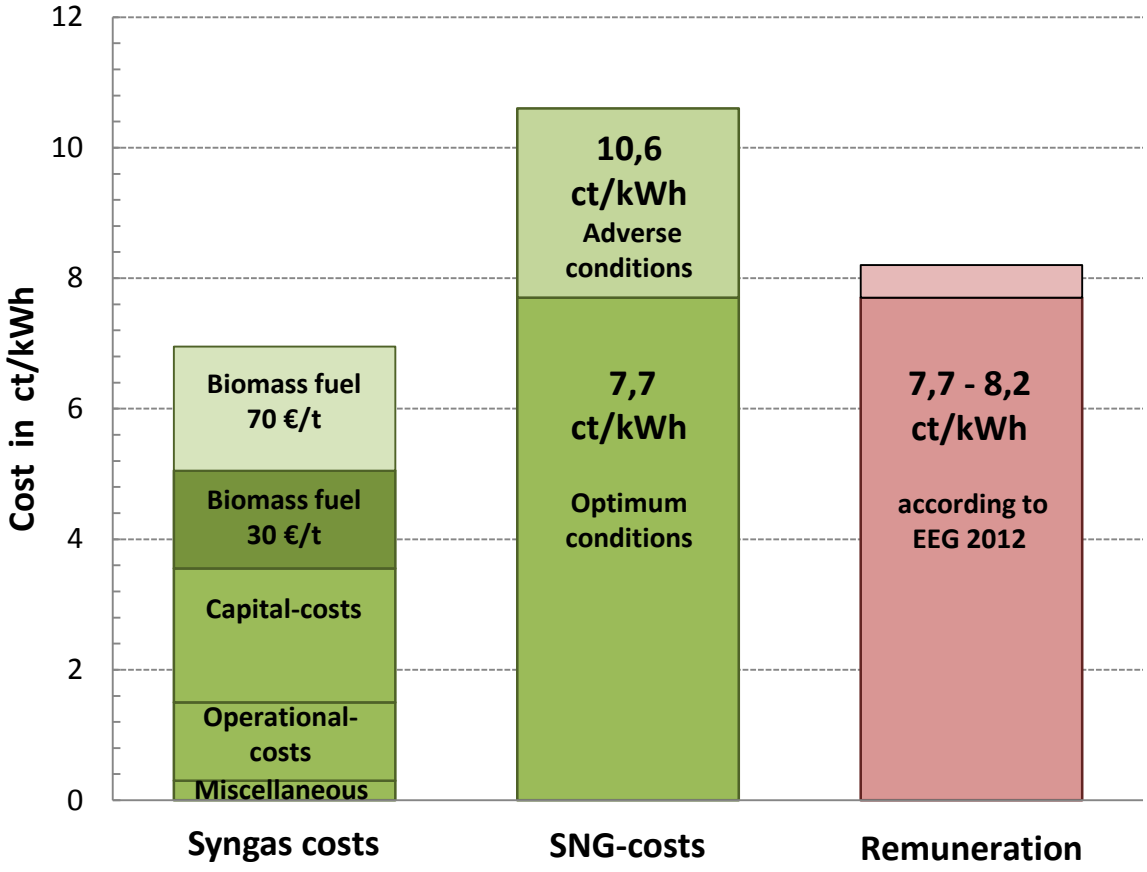

Figure 7-1: Estimate of costs for SNG-production based on the application of the heat pipe reformer technology or a comparative scale of gasification[142]

According to Karl 2006[140], the production of a tar containing syngas based on the allothermal gasification of biomass under application of the HPR technology is achievable in a cost range of 5-7 ct/kWh$_{SNG}$ depending on the required expenditure for biomass used as fuel. This estimate consists of capital costs of 2.05 ct/kWh$_{SNG}$, operational costs of 1.2 ct/kWh$_{SNG}$ and miscellaneous costs of 0.3 ct/kWh$_{SNG}$. Fuel costs are considered to be in the range of 30 to 70 € per gravimetric ton equaling 1.5 to 3.4 ct/kWh produced syngas. The conversion and purification of this raw gas into a gas with SNG-quality suitable for grid injection requires several additional process steps that increase the specific costs of the produced gas in the estimated cost range shown in Table 7-1.

Table 7-1: Estimated cost ranges for different process steps in SNG synthesis[142]

Process step in SNG-synthesis	Estimated cost range
Supply of syngas with tar content	5 - 7 ct/kWh$_{SNG}$
Desulfurization, methanation + tar removal	1.65 ct/kWh$_{SNG}$
CO_2-separation	1 - 2 ct/kWh$_{SNG}$
Overall process combined	7.7 – 10.7 ct/kWh$_{SNG}$

As described above, the supply of a raw syngas containing tar in the range of 4-8 g/m³$_{std}$[44] is feasible at costs of about 5-7 ct/kWh$_{SNG}$. An estimate on the cost evaluation of the mid temperature gas treatment described in section 2.4.2 leads to the assumption that the catalytic gas treatment consisting of a combination of sulfur removal, tar removal and methanation is feasible at a specific cost of 1.65 ct/kWh$_{SNG}$.[143] An evaluation and comparison of the available technologies for CO_2 separation leads to the conclusion that the production of a CO_2–free SNG will increase the specific cost of the produced gas by 1-2 ct/kWh$_{SNG}$. The combination of the different process steps listed in Table 7-1 leads to a final cost of the produced SNG between 7.7 and 10.7 ct/kWh depending on the assumption of optimum or adverse conditions. Even under the optimistic estimate of a total combined cost of 7.7 ct/kWh$_{SNG}$ the comparison with the subsidized remuneration for biomass derived SNG indicates only a small margin of profit. Depending on the type of biomass used as fuel and the size of the gasifier, the produced SNG for grid injection is certificated differently, leading to a bargaining margin between the gas producer and the grid operator. This leads to a specific remuneration of 7.7-8.2 ct/kWh$_{SNG}$ for the investigated type of gasifier with 1.3 MW fuel input. Inferentially a profit margin of 0.5 ct/kWh$_{SNG}$ is given under optimistic assumptions and disregarding a volatile market situation due to the requirement of subsidizing. The use of alternative and waste fuels holds the possibility of avoiding the costs for fuel input in the range of 1.5 -3.4 ct/kWh$_{SNG}$ according to Figure 7-1 or even attain a negative cost influence by discarding chargeable wastes via gasification.[7]

7.2 Economic model and fundamentals

The assessment of the profitability of an investment can be made via static or dynamic methods whereby only dynamic methods which take into account long-term effects and interest rates, prove to be suitable for the extensive and complex investments related to the energy sector. The costs related to an investment I_0 can be diverted in the capital related costs and operational costs. Both have to be compensated for by the expected income related to the investment such as to yield a positive value of the net present value, which is a common criterion for the evaluation of profitability of an investment.

The capital related costs are based on the comparison of profitability of the investment in e.g. process equipment as compared to the investment in monetary values. This criterion is assessed by the yearly capital recovery factor a_I as defined by Eq (53).[144]

$$a_I = \frac{i \cdot (1+i)^t}{(1+i)^t - 1} \quad \textbf{(53)}$$

The interest rate "*i*" is oriented at the nominal rate of return which can be expected at long term investments in monetary assets in the range of 4.5 to 6.5 %. In considerations of profitability, other factors might have to be taken into account such as risk of the investment, tax events and inflation. This results in a calculatory rate of return, the weighted average costs of capital (WACC).

The amount of depreciation required for the compensation of an investment C_{total} under consideration of a given time span and interest rate is represented by the equivalent annual costs (EAC) as defined by Eq (54).[144]

$$EAC = C_{total} \cdot a_I \quad \textbf{(54)}$$

Inferentially the EAC is the minimum amount of profit that has to be generated by the investment during the considered time *t* to return the expense made at an earlier stage.

7.3 Conditions and assumptions

The assessment of economics of in-situ desulfurization compared to the fixed bed-desulfurization based on ZnO is based on certain conditions and is prone to various assumptions. These include the technical process of HPR-gasification on which the assessment is focused and the specification of methods for calculation of the investment and operational costs as explained subsequently.

7.3.1 Technical conditions

The assessment of investment costs as part of the evaluation of economics of in-situ desulfurization is based on the process equipment required for an "HPR" gasifier at 1.3 MW scale. Concerning the assessment of operational costs another important factor besides the scale of the process is the gas composition of the produced syngas. A comparison between the syngas composition obtained by experiments performed at Graz University of Technology in the BFBG test rig shown in Figure 5-1 and the syngas produced from an agnion "HPR"-gasifier[44] is listed in Table 7-2. The assessment of operational costs is based on the gas composition obtained by the experiments performed at Graz University of Technology. This was necessary such as to rely on the experimentally determined steady state of in-situ desulfurization. The experimentally obtained results of residual H_2S mainly depend on the steam content as a major influencing factor on the equilibrium of the desulfurization reaction. The application of the experimentally determined results is further considered legitimate, as the syngas compositions compared in Table 7-2 are very similar especially concerning the steam content of 40.5 and 43.4 vol%. The similarity between the experimentally obtained syngas and the composition of an "HPR" syngas is explained by the gasification in a BFBG and similar process conditions but varies widely as compared to syngas obtained from other types of gasifiers (Table 2-6).

Table 7-2: Gas composition used for estimation of desulfurization cost (experimental) compared to the gas produced from an HPR-gasifier

Gas component		Composition	
		Experimental	HPR syngas
H_2O	vol%	40.50	43.4
H_2	vol%,dry	40.9	42.9
CO_2		18.5	21.9
CO		23.0	18.8
N_2		8.2	7.5
CH_4		7.4	8.9
C_2H_4		2	-

The composition of combustible gases contained in the syngas obtained from the BFBG test rig (Table 7-2 (Experimental)) results in a lower heating value of 3.1 kWh/m³$_{std}$ at standard conditions for the dry fraction of the gas according to (Eq (55)) or 37.2 MW/kg on a mass based calculation (Eq (56)).

$$H_{l(n)} = \sum x_i \cdot H_{l(n),i} \quad \textbf{(55)}$$

$$H_l = \sum w_i \cdot H_{l,i} \quad \textbf{(56)}$$

With a fuel input of 1.3 MW and a cold gas efficiency $\eta_{cold\ gas}$ (Eq (58)) of 0.7[42] the gasifier output of syngas equals $\dot{Q}_{syngas}$ = 912 kW or 495 m³$_{std}$/h

$$\eta_{cold\ gas} = \frac{\dot{Q}_{syngas}}{\dot{Q}_{fuel}} = \frac{H_{l,n} \cdot \dot{V}_{gas}}{H_l \cdot \dot{m}_{fuel}} \quad \textbf{(57)}$$

The syngas output from the gasifier is the relevant parameter for dimensioning the desulfurization units as the produced gas passes these process steps prior to conversion or condensation of tars and steam. Downstream of the desulfurization units, a catalytic conversion or further application of the gas is possible. In the evaluated concept a conversion and purification of the syngas is pursued at medium temperature with the aim of producing SNG. The methanation process is prone to losses of heating value due to the highly exothermic methanation reaction and slightly exothermic water gas shift reaction. This results in an efficiency of about 0.86 %[44] concerning the conversion of syngas to raw SNG according to pilot plant studies. Further considering a loss of methane during CO_2 removal in the range of 3 %[145] the final production of SNG for Grid injection is in the range of $\dot{Q}_{SNG}$ = 760 kW. This value constitutes the reference for the calculation of specific costs, as it is the relevant parameter for remuneration.

The assessment of economics of in-situ desulfurization was further based on a sulfur content of 1400 ppm$_v$ H_2S in the gas as standard value. This allows for the compatibility of results throughout the different sections of the presented work with input values of 1400 ppm$_v$ H_2S for the simulation of equilibria in section 4 and 1200 ppm$_v$ H_2S as feed content for the experimental investigation of CaO-based desulfurization equilibria in section 6.2. A sulfur content in this range represents for example a

syngas as derived by mixed gasification of wood pellets with sewage sludge. Such an elevated H_2S content clearly shows the effect of CaO-based desulfurization and therefore visualizes the costs caused by sorbent consumption within the different margins of desulfurization.

7.3.2 Assumptions concerning investment cost

ZnO desulfurization

The assessment of desulfurization costs compares the implementation of in-situ desulfurization with a process setup solely based on fixed bed downstream desulfurization with ZnO. In order to maintain this comparison as simple and accurate as possible only the relevant process steps for desulfurization are taken into account. For a desulfurization based on mid-temperature adsorption of H_2S on ZnO the required process equipment consists of a fixed bed reactor filled with ZnO, including heating, insulation and instrumentation. These parts are therefore marked in red in Figure 7-2. The gasifier and cartridge filter for particle separation are not considered in the cost evaluation as shown in Figure 7-2.

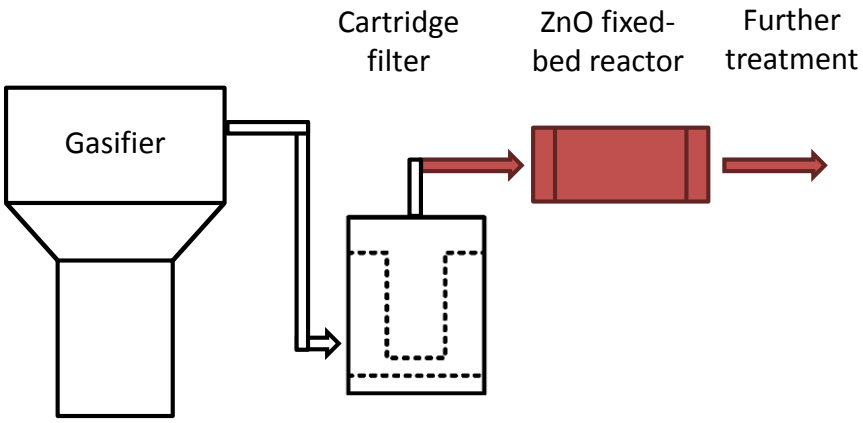

Figure 7-2: Additional equipment included in the estimate of investment costs (marked in red) for ZnO-fixed bed desulfurization

In case of the implementation of in-situ desulfurization more process steps have to be included into the estimate of investment costs. This includes the storage and supply of desulfurization sorbent materials into the gasifier. As an increased loading of solids has to be taken into account an additional separation step by means of a cyclone separator for bulk removal of solids is considered as required additional process equipment. As the implementation of in-situ desulfurization is suited only for coarse desulfurization it does not replace a downstream desulfurization in a fixed bed reactor filled with ZnO. Therefore the installation of a fixed bed reactor is still required and has to be taken into account in a comparison of desulfurization costs. The total investment costs for in-situ desulfurization consist of the sum of investment for both desulfurization steps and will always be higher than the investment costs of ZnO-desulfurization only as long as a fixed bed is needed for deep desulfurization. The required process steps for in-situ desulfurization are marked in Figure 7-3 with red color. Process steps not included in the evaluation of investment costs are indicated in black and white in the process scheme.

In-situ desulfurization

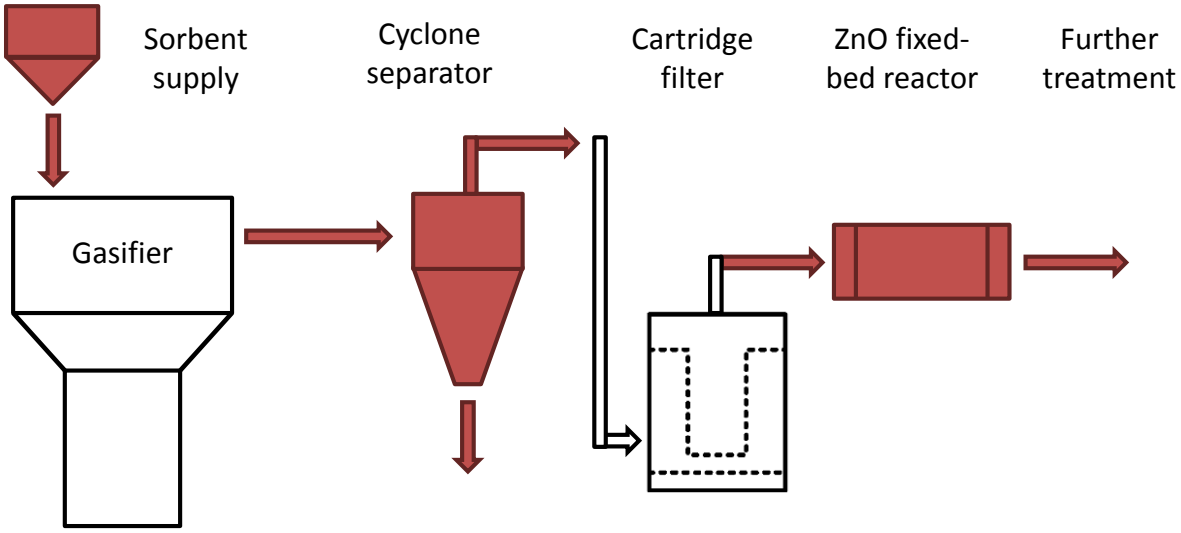

Figure 7-3: Additional equipment included in the estimate of investment costs (marked in red) for in-situ desulfurization

The installation of the equipment for the required process steps for the different desulfurization methods depicted in Figure 7-2 and Figure 7-3 results in investment costs. As the installation and commissioning of the HPR gasifier takes less than a year, the investment is considered as a single event without accumulation of interest during several years of construction. The comparison of investment costs is based on the method of net present value (section 7.2) as a dynamic calculation under consideration of an effective return of interest and an allowance for depreciation or the estimated lifetime of investment. This timespan was estimated to be in the range of 20 years due to the corrosive and abrasive conditions of application. The calculatory rate of interest –the weighted average cost of capital (WACC) – takes into account inflation, risk events and tax influence. For a general estimate the assumption of 6 % is commonly used for this value in cost calculation (section 7.2).[146] The applied values for the calculation of investment costs are summarized in Table 7-3.

Table 7-3: Amortization data for calculation of the specific investment cost (WACC –weighted average cost of capital)

Full load hours per year [h]	h_a	7500
WACC [%]	i	6
Allowance for depreciation [a]	t	20

By insertion of the calculatory values shown in Table 7-3 into Eq (53) equivalent annual capital costs can be calculated according to Eq (54). The calculation of specific costs of investment is based on the assumption that the annual capital costs have to be covered by the return on investment generated by the selling the produced SNG. The specific investment costs are therefore obtained as shown in Eq (58) by relating the annual capital costs to the accumulated output of SNG under consideration of the full load hours per year (h_a).

$$c_I = \frac{EAC}{\dot{Q}_{SNG} * h_a} \cdot 100 \quad \textbf{(58)}$$

The calculation was based on a value of h_a = 7500 full load hours per year, as this is the reference value given by the company for the operation of HPR-gasifiers. As this value is considered high for a complex and sensitive technology such as biomass gasification a variation thereof was considered in a sensitivity analysis (see Figure 7-4).

7.3.3 Conditions and assumptions for operational cost

ZnO desulfurization

Besides the investment costs for process equipment, the evaluated methods for desulfurization involve operating costs related to the amount of sulfur removed from the gas. In the case of fixed bed desulfurization with ZnO the operational costs are caused by the deactivation of ZnO by formation of ZnS and carbon deposition. According to results by Zuber et al.[64] the regeneration of used ZnO after deployment in long-term experimental application in real gasifier derived syngas did not prove possible. Therefore a regeneration of ZnS to ZnO is not considered in the cost estimate for ZnO related operational costs. The main influencing factors on the operational costs of ZnO-based desulfurization are the price of the sorbent and the achievable loading of sulfur. According to supplier information the price of a commercially available ZnO-based sorbent (BASF R5-12) is at 35 €/kg but might be reduced to 25 €/kg in case of long-term bulk purchase.[143] With respect to this supplier based prognosis the lower value of 25 €/kg was chosen as optimistic assumption for the calculation of ZnO-related consumption cost. The theoretical loading capacity of ZnO is at 40 g sulfur per 100 g ZnO. According to literature a conversion of 40 to 50 % is commonly achievable in desulfurization experiments equaling loadings of 16 – 20 wt% sulfur on ZnO-based sorbent.[92] In experimental investigations performed at Graz University of Technology with gasifier derived syngas a loading of ZnO sorbent (BASF R5-12) of 5 wt% sulfur was reached.[64] For the economic assessment presented herein the maximum loading of ZnO was assumed with 15 wt% sulfur. This value has to be considered as an optimistic assumption based on the experimental experience with the applied sorbent.[64] The discharge of used sorbent is available free of charge as it is commercially regenerated by the catalyst suppliers.

In-situ desulfurization

The estimate of operational costs of in-situ desulfurization relies on both, the acquisition of fresh sorbent and the discharge of used material. The prices of supply with naturally occurring CaO-based sorbent materials were obtained by information of suppliers as listed in Table 7-8. A market price for the newly developed CaBa sorbent is not available at the current lab scale of application. A cost of 5 €/kg is considered as a rough estimated for supply with CaBa sorbent. This takes into account the cheap ingredients $CaCO_3$ and $BaCO_3$ which are available in bulk on the one hand as well as the early non-commercial stage of development and the energy intensive production at 1600 °C on the other hand. A further discussion plus a sensitivity analysis of this assumption was performed in order to clarify the boundary conditions of economic suitability for the CaBa sorbent.

The estimated costs of sorbent discharge were based on the specific costs of ash disposal. For a common gasifier ash these are in the range of 70 € per gravimetric ton.[139] Considering the possibility of stabilization of sulfides by formation of sulfates in an oxidizing combustion zone the addition of

used sorbents to the ash would rather decrease its toxicity which warrants the assumption that a disposal would be possible at a comparable cost. A stabilization in the form of harmless and disposable sulfate is even more likely for BaS as compared to CaS but the sulfide and unconverted sorbent in the ash are toxic in the case of BaO and BaS. Therefore the costs of disposal were located in the magnitude of a more problematic ash containing for example chromate components that are also highly toxic. Such an ash doubles the cost of disposal, leading to a specific discharge cost of 140 € per gravimetric ton.[139] This value of disposal cost was assumed in the case of CaBa-sorbent.

7.4 Calculation of desulfurization costs

With the conditions and assumptions stated above the calculation of desulfurization costs is possible with regard to investment and operation specific cost.

7.4.1 Investment cost

The estimation of investment costs of a ZnO fixed bed as part of the economic evaluation of in-situ desulfurization is based on an internal study of the company agnion[143], related to the HPR gasifier as well as a process simulation of the HPR based on the tool "Ikarus" contained in ASPEN process software.[147] The company internal study is based on the installation of ZnO-fixed bed desulfurization for a side stream of 5 % from the 912 kW gasifier output. This equals a raw gas stream of 45.6 kW or a production of 39 kW SNG. The obtained investment costs (C_1) at low scale (S_1) is then transferred to the actual scale (C_2) of the investigated size of gasifier (S_2) by application of a degression parameter n according to (Eq (59)).

$$C_2 = \left(\frac{S_2}{S_1}\right)^n \cdot C_1 \qquad \textbf{(59)}$$

The exponent n is typically 0.8 to 0.9 for processes that use a lot of mechanical work or gas compression. For small-scale, highly instrumented processes, such as specialty chemical manufacture, n is in the range 0.4 to 0.5. Averaged across the whole chemical industry, n is about 0.6. The average value of 0.6 as degression factor is in accordance with data for investment cost of small to medium scale CHP-wood facilities stated in literature. Solely for the scale up of the initial filling of the reactor with adsorbent, the degression factor was assumed to be 1 as the cost estimate is already based on the condition of bulk purchase. The estimated investment costs for ZnO-based fixed bed desulfurization are listed in Table 7-4 for the two methods of cost assessment.

Table 7-4: Estimated investment costs for downstream fixed bed desulfurization with ZnO

Description	Price based on slip stream of 39 kW_{SNG}	Degression factor n	Price based on HPR (760 kW_{SNG})	Estimated price based on Icarus-calculator
Operating equipment				
ZnO BASF R5-12 (40 kg at 25 €/kg)	1000 €	1	19504 €	19504 €
Material & devices:				
reactor	5460 €	0.6	32454 €	26038 €
Pipelines:				
pipe bundle	2000 €	0.6	11888 €	9312 €
Heating & insulation				
Heating lines bundle	2000 €	0.6	11888 €	8165 €
Heat insulation package	2000 €	0.6	11888 €	4991 €
Sum material cost	**12860 €**		**91352 €**	**68010 €**
Labor	**2492 €**		**17525 €**	**12970 €**
Total sum of estimated investment cost	**14952 €**		**105147€**	**80980 €**

Based on the results of the two different routes of cost assessment, a mean value of 93064 € was taken into account for the further calculation of the specific investment costs of ZnO-based fixed bed desulfurization.

The total required investment for in-situ desulfurization consists of both, the costs for a fixed bed desulfurization reactor filled with ZnO (Table 7-4) and the additional required equipment and utilities for in-situ desulfurization such as a cyclone for separation of solids and a vibrating feeder for sorbent dosing. (Figure 7-3) The calculation of investment costs for the additional process equipment was performed analogous to the values in Table 7-4 based on an estimate for a branch stream of 39 kW_{SNG} under subsequent application of Eq (59). The degression factor was estimated to be 0.6 for all items, as the influence of scale can be assumed to be in the same range as for ZnO-based fixed bed desulfurization. The results of the calculations of investment costs for the additional utilities required for in-situ desulfurization is listed in Table 7-5.

Table 7-5: Estimated investment costs for in-situ desulfurization

Description	Price based on slip stream of 39 kW_{SNG}	Degression factor n	Price based on HPR (760 kW_{SNG})
Material & devices:			
Vibrating conveyor + Storage tank	2000	0.6	11888 €
Cyclone + Separation system	5460 €	0.6	32454 €
Pipelines:			
Pipe bundle	2000 €	0.6	11888 €
Heating & insulation			
Heating lines bundle	2000 €	0.6	11888 €
Heat insulation package	2000 €	0.6	11888 €
Sum material cost	**12860 €**		**80006 €**
Manpower	**2492 €**		**16002 €**
Total sum of estimated investment cost	**14952 €**		**96008 €**

Clearly the data shown in Table 7-4 and Table 7-5 has to be considered as a rough estimate and is prone to major insecurity. The estimated investments costs are supposedly high and might be effectively lowered as especially the required necessary equipment for in-situ desulfurization strongly depends on the gasifier setup into which the process is integrated.

With the amortization data shown in Table 7-3 for ZnO-based fixed bed desulfurization an annual capital cost of 8309 € results from Eq (54). This leads to a specific cost of investment equaling 0.142 ct/kWh_{SNG} according to Eq (58) as listed in Table 7-6. For in-situ desulfurization, the resulting values as a sum of all process steps shown in Figure 7-3 are about twice as high with a capital cost of 16679 €/a and a specific investment cost of 0.289 ct/kWh_{SNG}.

Table 7-6: Calculation of specific costs of investment for ZnO-fixed bed and in-situ desulfurization based on the cost estimates shown in Tables 7-4 and 7-5

	Specific investment costs based on Table 7-4 [ct/kWh_{SNG}]	Specific investment costs based on Table 7-5 [ct/kWh_{SNG}]	Total specific investment costs [ct/kWh_{SNG}]
ZnO – fixed bed	0.142	-	0.142
In-situ desulfurization	0.142	0.147	0.289

As the calculation of specific investment cost is based on various assumptions concerning the amortization data and the material costs, a sensitivity analysis has been performed in order to evaluate the influence of certain parameters. The required rate of return, the investment costs and the allowance for depreciation has been altered in the range of -30 to 30 % based on the original

value applied during calculation. For the full load hours a sensitivity analysis was performed in the range of -30 to +10 %, equaling 5250 and 8250 hours per year, such as to remain in a realistic margin. The resulting values for calculation of the specific costs of investment are listed in Table 7-7 for the example of in-situ desulfurization.

Table 7-7: Input values of sensitivity analysis for calculation of the specific costs of investment (WACC –weighted average cost of capital)

		-30	-20	-10	0	10	20	30
Full load hours	[h]	5250	6000	6750	7500	8250	-	-
WACC	[%]	4,2	4,8	5,4	6	6,6	7,2	7,8
Allowance for depreciation	[a]	14	16	18	20	22	24	26
Investment costs	[€]	132350	151257	170164	189071	207979	226886	245793

The corresponding sensitivity analysis based on the data listed in Table 7-7 is shown in Figure 7-4.

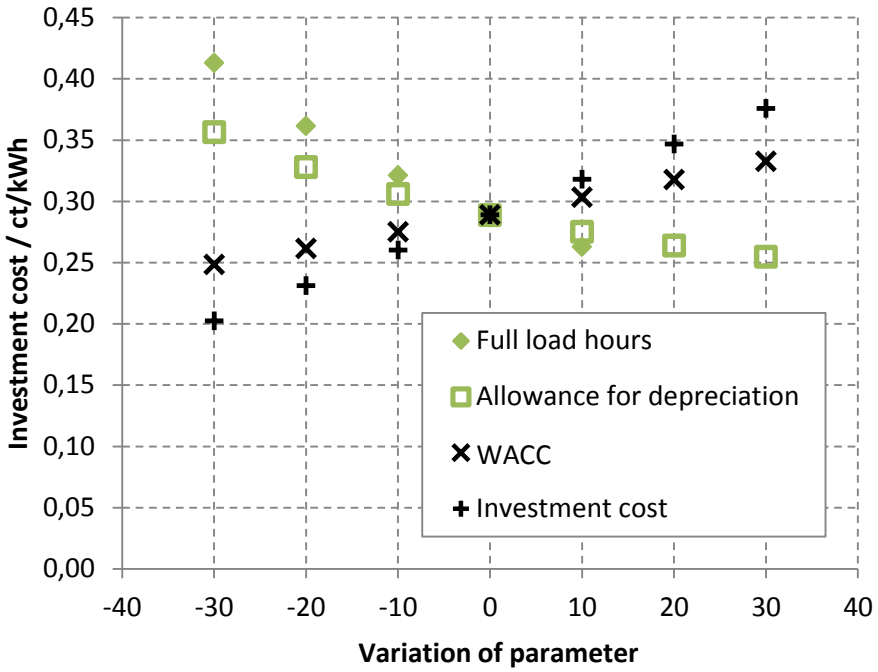

Figure 7-4: Sensitivity analysis of relevant parameters in the calculation of specific investment cost

From the sensitivity analysis shown in Figure 7-4 a major influence of the full load hours on the specific cost of investment is obvious. The optimistic estimate of 7500 hours per year might therefore lead to increased specific costs of investment under real process application. Other parameters such as the weighted average cost of capital are less pronounced in their influence on the specific investment costs. The influences are shown for the example of the specific costs of investment of in-situ desulfurization but are valid in the same way for ZnO-based fixed bed desulfurization as the method of cost assessment is equivalent for both desulfurization processes.

7.4.2 Operational costs

The calculation of operational costs is based on the specific costs of consumed sorbent per mol sulfur contained in the syngas. For this purpose the prices for sorbents are obtained by the suppliers[148] or estimated as in the case of CaBa. The cost of CaBa can only be assumed at this early stage of research with no supplying data available. The estimate of 5 €/kg is rather conservative considering the low cost of reactants $BaCO_3$ and $CaCO_3$ as discussed in more detail as part of a sensitivity analysis in section 7.5.2. Furthermore a specific price for CaBa significantly higher than 5 €/kg does exclude the application of this sorbent as in-situ desulfurization because the process would become unprofitable as compared to solely ZnO-based desulfurization. The estimate of 5 €/kg therefore is conservative based on the costs of the reactants but also marks an upper limit for economic profitability (Figure 7-7). As shown in Table 7-8 a major benefit of CaO-based sorbents for sulfur removal is their low price as bulk material.

Table 7-8: Calculation of cost for sorbent supply and disposal

		Lime	Limestone	Dolomite f. c.	Dolomite	CaBa	ZnO
Sorbent cost	€/t	100	46	110	50	5000	
	€/kg	0.1	0.046	0.11	0.05	5	25
Weight fraction active sorbent	-	1	0.56	0.53	0.30	0.23	1
$Sorbent_{(active)}$	ct/g	0.01	0.08	0.021	0.016	2.145	2.5
	ct/mol	0.6	0.5	1.2	0.9	328.9	203.5
$X_{Sorbent}$	-	0.35	0.35	0.15	0.35	1	0.38
Desulfurization cost	ct/mol_S	**1.6**	**1.3**	**7.8**	**2.6**	**329**	**534**
Ash disposal cost	€/T	70	70	70	70	140	-
	ct/g	0.007	0.007	0.007	0.007	0.014	-
Weight fraction active sorbent	-	1	1	0.53	0.53	0.23	-
$Sorbent_{(active)}$	ct/mol	0.39	0.39	0.74	0.74	9.21	-
Disposal cost	ct/mol_S	**1.12**	**1.12**	**4.96**	**2.13**	**9.21**	**-**

The weight-based specific costs of the sorbents were transformed into values based on the molar specific cost of active sorbent under consideration of the weight fraction of the active sorbent and the molar weight of the active component. For the example of dolomite, CaO is the active component for desulfurization, whereby MgO passes the reactor as an inert and CO_2 is released upon calcination (Eq (30)). This means only a fraction 0.3 g CaO are contained in 1 g of $CaMg(CO_3)_2$. With the experimentally obtained conversion of active sorbent $X_{Sorbent}$ (compare section 6.2.10), the desulfurization costs are calculated in relation to the molar amount of sulfur removed from the syngas. The same method was applied for the calculation of disposal related costs, whereby the weight fraction of active sorbent is different due to the release of CO_2 upon calcination (Eqs (30)(31)).

As stated in section 7.3.3, the disposal related costs of CaBa was assumed to be higher than for naturally occurring CaO-based sorbents. The different CaO content and conversion of CaO to CaS in the CaO-based sorbents, leads to different consumption of the sorbents resulting in clearly higher specific costs for fully calcined dolomite with 7.8 ct/mol H_2S removed from the syngas as compared to $CaCO_3$ or CaO with 1.3 and 1.6 ct/mol H_2S removed from the syngas respectively. In the case of CaBa sorbent, the molar content of 10 % BaO translates to a weight fraction of 0.23 g BaO per g sorbent as the active component. For an estimated cost of CaBa with 5 €/kg and an experimentally determined full conversion of BaO to BaS this results in a specific cost of 329 ct/mol H_2S removed from the syngas, and disposal costs of 9.21 ct/mol H_2S removed. For ZnO-based fixed bed desulfurization no operational costs have to be taken into account for disposal but the high cost of 25 €/kg for the sorbent lead to a desulfurization cost of 534 ct/mol H_2S removed from the syngas, as listed in Table 7-8.

As the application of sorbent materials is restricted by thermodynamics of the specific desulfurization reaction of the active component as discussed in section 4, the calculation of desulfurization costs is only valid under consideration of these limits of application. A desulfurization can only be obtained within a sorbent specific margin with respect to the experimentally determined limits of achievable residual H_2S content. These steady state values were determined to be in the range 500 ppm_v H_2S for CaO-based sorbents with the exception of fully calcined dolomite with 600 ppm_v residual H_2S under steady state conditions. For the application of CaBa sorbent a steady state value of 35 ppm_v H_2S was achieved. ZnO-based fixed bed desulfurization allows the desulfurization down to below 1 ppm_v residual H_2S which is considered as zero for reasons of simplification. An overview of the experimentally determined steady state equilibria as lower limits of desulfurization is listed in Table 7-9 for the considered sorbent materials.

Table 7-9: Experimentally determined residual H_2S content as the lower limit of desulfurization

		Lime	Limestone	Dolomite f. c.	Dolomite	CaBa	ZnO
$H_2S_{(ll,i)}$	ppm_v	500	500	600	500	35	~0

For the example of a gas with an initial residual H_2S content of 1400 ppm_v, equaling 0.0625 mol H_2S/m^3_{std} under consideration of the standardized gaseous molar volume $v_{m,gas}$, only 900 ppm_v can be removed by application of lime. The remaining 500 ppm_v H_2S, equaling 0.0223 mol H_2S/m^3_{std}, has to be removed by ZnO-based downstream fixed bed desulfurization. With the volumetric heating value $H_{l(n)}$ of the syngas (Eq (55)) the sulfur content above the specific limits of desulfurization for a sorbent *i,* can be transformed in a kWh_{Syngas}-based value. Multiplied with the sum of specific cost of sorbent consumption and disposal $c_{S,i}$, based on the sulfur content in the syngas, sorbent specific operational costs can be calculated according to (Eq (60))

$$c_{op\_syngas,i} = \frac{(H_2S_{residual} - H_2S_{(ll,i)})}{1000 \cdot v_{m,gas} \cdot H_{l(n)}} \cdot c_{S,i} \; ; \left[\frac{ppm_{v,H2S} - ppm_{v,H2S}}{1000 \cdot \frac{m^3_{std}}{kmol} \cdot \frac{kWh_{Syngas}}{m^3_{std}}} \cdot \frac{ct}{mol_{H2S}} \right] \quad (60)$$

The lower limit of the prior desulfurization step $H_2S_{(ll,i)}$ is then inserted as value for residual H_2S for the consecutive desulfurization step. In case of a combined in-situ desulfurization of $CaCO_3$ and CaBa with downstream fixed bed desulfurization over ZnO, three consecutive desulfurization steps were

combined leading to three different values of sorbent specific operational costs $c_{op\_syngas,i}$. The sum of these different operational costs based on the output of syngas from the gasifier is then related to the final output of SNG according to Eq (61).

$$c_{op} = \sum_{i} c_{op\_syngas,i} \cdot \frac{\dot{Q}_{syngas}}{\dot{Q}_{SNG}} \quad \textbf{(61)}$$

As the operational costs vary in dependence of the initial sulfur content and the applied combination of sorbent materials, a further analysis is conducted within the results of economic assessment for different scenarios of application.

7.5 Results of economic assessment

Besides the experimental proof of technological feasibility of in-situ desulfurization in biomass gasification for SNG-production, an economic evaluation is crucial. This has to take into account alternative technologies for desulfurization, as well as the market situation for SNG as the proposed final product of allothermal gasification of woody biomass shown in Figure 7-1. The results of this economic assessment based on different scenarios of application of in-situ desulfurization are presented subsequently.

7.5.1 Comparison of methods and sorbents for in-situ desulfurization

The approach of capturing the sulfur inside the gasifier by means of in-situ desulfurization is beneficial concerning the simplicity of apparatus design and thermal efficiency, as no additional vessel with specific temperature adjustment is required. On the other hand the conditions inside the gasifier are unfavorable according to the thermodynamic equilibrium of the desulfurization reaction as shown in section 4.2, and challenging concerning the choice of suitable sorbent materials. Under consideration of the investigated CaO- and BaO-based sorbent materials, the cost of in-situ desulfurization was estimated under the assumptions and conditions explained in sections 7.3 and 7.4. The results of this cost estimate are shown in Figure 7-5 for a combination of in-situ desulfurization with downstream ZnO-based fixed bed sulfur removal with the specific cost of desulfurization in relation to the H_2S content of the syngas.

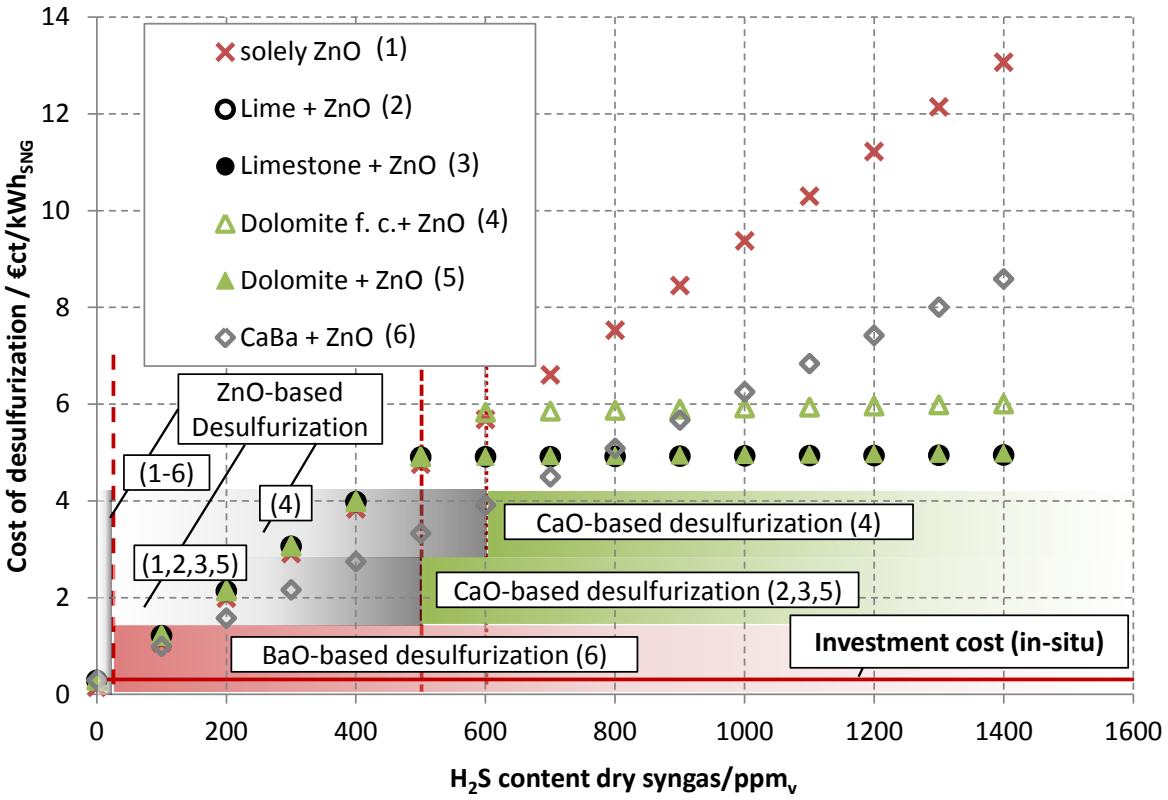

Figure 7-5: Comparison of the specific costs of desulfurization for different in-situ sorbents with the sole ZnO-based desulfurization in a downstream fixed bed. Colors mark the type of desulfurization ranges for the different experiments (marked by numbers)

With respect to the investigated process setup of in-situ desulfurization inside the fluidized bed reactor in combination with a downstream fixed bed of ZnO, Figure 7-5 shows the trend of the specific desulfurization costs for different sorbent materials. The different regimes of activity of the desulfurization sorbents are marked with specific colors and numbers to indicate the combination of materials. From the obtained data for CaO-based desulfurization depicted in Figure 7-5, it is obvious that the major impact on the specific overall costs for sulfur removal is caused by the consumption of ZnO in a downstream fixed bed desulfurization. This is shown by a near stagnation of the specific cost of desulfurization for initial H_2S-contents above the achievable desulfurization equilibrium of the CaO-based sorbent materials at 500 ppm$_v$ H_2S.

In syngas with an initial H_2S content of 1400 ppm$_v$, the share of ZnO-based desulfurization costs $c_{op\_syngas,ZnO}$ ranges from 3.85 ct/kWh$_{SNG}$ for lime, limestone and dolomite, and 4.62 ct/kWh$_{SNG}$ for fully calcined dolomite as shown in Table 7-10 and depicted Figure 7-5. The ZnO-based share of total cost is higher for fully calcined dolomite due to the increased steady state value of 600 ppm$_v$ H_2S as determined in section 6.2.4. The operational cost caused by the consumption of CaO-based in-situ sorbents listed in Table 7-10 is negligible.

Table 7-10: Calculated composition of costs for desulfurization of a syngas with 1400 ppm_v H_2S feed using different sorbent combinations according to Eqs (60) and (61)

Desulfurization sorbent (in-situ)	**i**		**Lime**	**Lime-stone**	**Dolomite f.c.**	**Dolomite**	**CaBa**	**-**
Desulfurization sorbent (fixed bed)			**ZnO**	**ZnO**	**ZnO**	**ZnO**	**ZnO**	**ZnO**
Operational cost	$c_{op\_syngas,i}$	ct/kWh$_{Syngas}$	0.04	0.03	0.15	0.06	6.65	-
	$c_{op\_syngas,ZnO}$	ct/kWh$_{Syngas}$	3.85	3.85	4.62	3.85	0.27	10.78
	c_{op}	ct/kWh$_{SNG}$	3.89	3.88	4.77	3.91	6.92	12.92
Investment cost	c_I	ct/kWh$_{SNG}$	0.29	0.29	0.29	0.29	0.29	0.14
	Combined	ct/kWh$_{SNG}$	**4.95**	**4.94**	**6.00**	**4.98**	**8.59**	**13.06**

For the desulfurization of a gas with an initial sulfur content of 1400 ppm_v H_2S the operational cost of the different CaO-based sorbents vary in the range of 0.03 ct/kWh$_{SNG}$ for limestone and 0.15 ct/kWh$_{SNG}$ for fully calcined dolomite, due to different conversion, CaO-contents, steady state equilibria and sorbent cost as elucidated in section 7.3.3. Combined with the cost of ZnO–based fixed bed desulfurization and the specific investment cost of 0.29 ct/kWh$_{SNG}$, the in-situ application of lime, limestone and dolomite results in an overall specific cost of almost 5 ct/kWh$_{SNG}$. Fully calcined dolomite results in total specific costs of 6 ct/kWh$_{SNG}$. The application of CaBa results in even higher specific costs due to the consumption of the in-situ sorbent itself. According to the experimental study discussed in section 6.3 the removal of sulfur proved possible down to a steady state equilibrium of about 35 ppm_v H_2S (Table 7-9). Therefore the ZnO –based operational cost results in a comparatively low value of 0.27 ct/kWh$_{SNG}$ as compared to the share of CaBa-based in-situ desulfurization with 6.65 ct/kWh$_{SNG}$. The high operational cost results from the assumption of the sorbent price with 5 €/kg or 5000 €/t as compared to CaO-based sorbents in the range of 50 – 100 €/t. Inferentially, the coarse desulfurization under application of CaBa as in-situ sorbent is not competitive with CaO-based sorbents under the given circumstances and assumptions made.

Compared to the application of solely ZnO-desulfurization with a total specific cost of 13.06 ct/kWh$_{SNG}$ for gas with an initial H_2S content of 1400 ppm_v the implementation of CaO-based in-situ desulfurization is advantageous. Regarding the market situation concerning the remuneration for biomass SNG as depicted in Figure 7-1, it is obvious that the combination of in-situ desulfurization with ZnO fixed-bed sulfur removal is not economically feasible under the given assumptions and conditions. Even for the application of limestone as the cheapest option for CaO-based in-situ sorbents in combination with ZnO-based fixed bed desulfurization the estimated cost for desulfurization of almost 5 ct/kWh$_{SNG}$ would annihilate the benefit of a reduced or negative cost for fuel input. This statement is especially valid considering the increased process instability and limited feasibility of gasification of wastes until the present day.[29]

A limiting factor for the application of CaO-based in-situ desulfurization in the investigated gasification process is the high steam content of about 40 vol%. The FICFB-process (Figure 2-4) does not depend on full coke conversion but on the contrary needs unconverted coke for release of exothermic heat in the combustor. Therefore it is run with lower steam to biomass ratios resulting in a syngas containing only about 17 vol% steam. This would significantly lower the thermodynamic equilibrium of in-situ desulfurization with CaO (Figure 4-4) as well as the achievable values of residual H_2S as shown by Stemmler.[48] In order to increase the applicability of economic evaluation to other types of gasifiers and gas compositions, the influence of the steam content on the cost of in-situ desulfurization was investigated. The experimentally determined steady state value of CaO-based in-situ desulfurization of 500 ppm_v H_2S coincided with the thermodynamic equilibrium of CaO as determined by simulative assessment in section 4.2. Therefore it is considered legitimate to derive the lower limits of achievable desulfurization under variation of the steam content from the results of thermodynamic assessment. An overview of the different minimum values of the equilibrium curves of H_2S in the gas phase are listed in Table 7-11 representing the expected residual H_2S content at the corresponding steam contents according to thermodynamic equilibrium calculations. The minima of the thermodynamic equilibrium curves are found at a temperature of 760 °C for the investigated gasification conditions. The position of the minimum changes according to the partial pressure of CO_2 in the syngas (Figure 4-6). Furthermore the temperature level of gasification can vary for different types of gasifiers. The obtained results showing the influence of variations in the steam content on the specific costs of desulfurization therefore have to be considered as tendencies with regard to other gasification setups.

Table 7-11: Minima of H_2S equilibrium curves for different steam contents as determined by thermodynamic equilibrium calculations

Steam content	Minimum H_2S equilibrium curve (760 °C)
Vol%	ppm_v
29	332
35	442
40	543
44	633
48	713

For sensitivity analysis concerning the steam content of the gas, the minimum values of residual H_2S for different steam contents were deviated from the thermodynamic equilibrium simulations as listed in Table 7-11 thus replacing the experimentally determined lower limit shown in Table 7-9. The economic assessment is based on limestone under consideration of limestone being the sorbent with the lowest consumption cost. The results of the cost estimate for varied steam contents are depicted in Figure 7-6 for a combination of limestone as in-situ sorbent and ZnO-fixed bed desulfurization. The strong influence of the steam-content due to the variation in thermodynamic equilibrium is clearly visible from the cost of combined desulfurization shown in Figure 7-6. For gas with an initial H_2S content of 1400 ppm_v these vary from 3.38 ct/kWh_{SNG} for a steam content of 29 vol % to 6.92 ct/kWh_{SNG} with an increased steam content of 48 vol%.

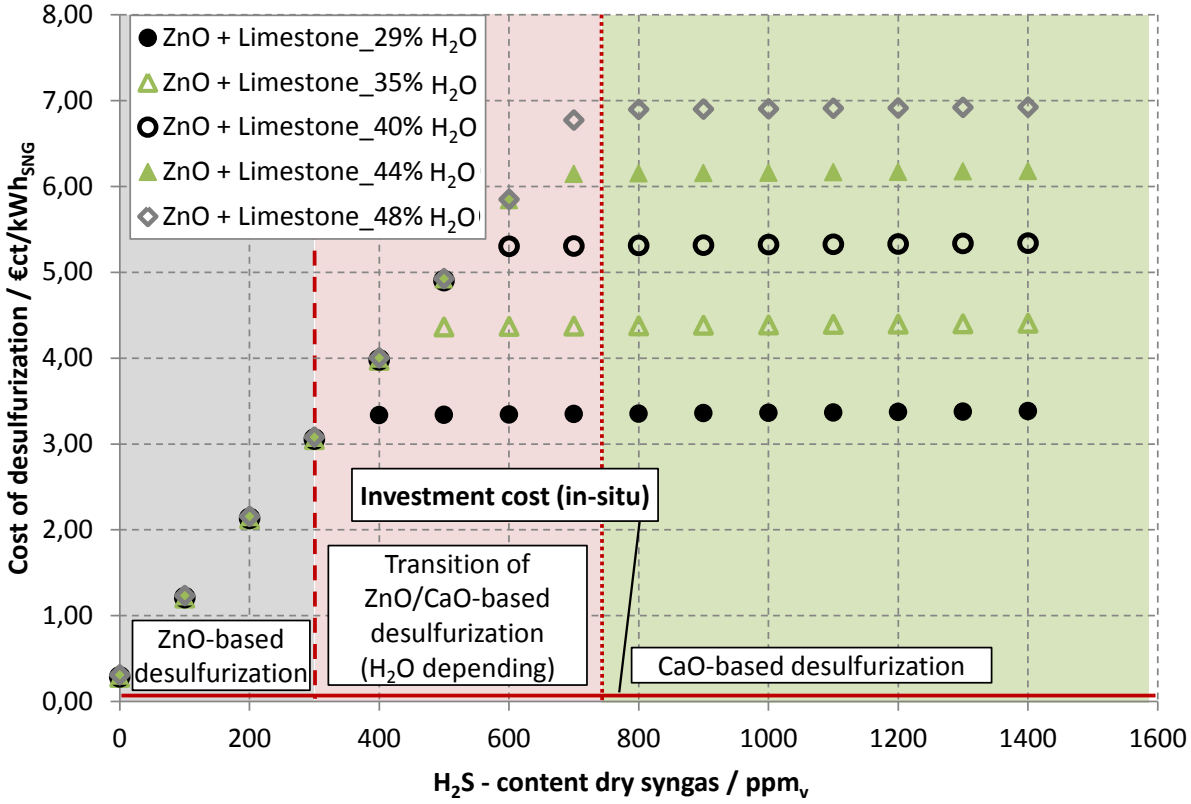

Figure 7-6: Specific costs of combined desulfurization with limestone and a downstream ZnO-fixed bed with a varied amount of steam (Background colors indicating the regimes of the specific sorbent material acting as desulfurization agent)

Considering the profit margin depicted in Figure 7-1 the resulting cost of a combined desulfurization as shown in Figure 7-6 would be too high even for a syngas with a reduced steam content of 29 vol%. Technologic alternatives for sulfur removal are based on cold gas cleaning (CGC) processes such as chemisorbtive amine scrubbing, physical absorption or biologic processes.[51] As described in section 2.4.1, the CGC comes along with the tradeoff of a reduced thermal efficiency due to several heating and cooling steps, especially considering a downstream methanation of the syngas to SNG. As the technical process equipment for CGC-sulfur removal is comparable to that of CO_2 removal, which is required prior to the grid injection of SNG, the related specific cost will also be in the same range of 1-2 ct/kWh_{SNG}. It can be concluded that for a coarse sulfur removal, under the investigated gasifier size and conditions, none of the available technologies would suffice for the demand of maintaining profitability based on the cost estimate shown in Figure 7-5. Only if a coarse sulfur removal was established at specific costs of 1 ct/kWh_{SNG} and below, an overall profit might be maintained as the use of alternative and waste fuels holds the possibility of negating the costs for fuel input.

7.5.2 Sensitivity analysis for the implementation of CaBa – sorbent

The application of the BaO-based CaBa sorbent for in-situ desulfurization is promising due to the low steady state equilibrium of residual H_2S that was achieved in desulfurization experiments (Section 6.3). In order to evaluate the opportunities and limitations connected with the implementation of this newly developed sorbent material from an economical point of view, relevant aspects and considerations are discussed subsequently.

According to the cost estimation shown in Figure 7-5 the application of CaBa is the least favorable option of the compared in-situ sorbents for coarse desulfurization. This does not take into account the option of applying CaBa for in-situ desulfurization of a gas with an initial H_2S content below 500 ppm_v H_2S. As this value indicates the lower limit of residual H_2S content of CaO-based desulfurization at 40 vol% H_2O, only the addition of CaBa can yield residual H_2S contents of 35 ppm_v and therefore exhibits a more flexible margin of application. Further the estimated cost of desulfurization with CaBa is mostly determined by the assumed price of the sorbent which is not based on economically proven data as the sorbent only exists in academic research. The assumed price of 5 €/kg does not indicate a lower limit based on the cost of substances needed for sorbent synthesis but includes the assumption of an energy intensive synthesis at lower scale of production.

The reactants needed for the synthesis of CaBa sorbent are cheaply available in bulk – trade. Limestone is available at a cost of about 46 €/t as shown in Table 7-8. The market price of $BaCO_3$ in a sufficient quality of 99.2 % ranges from 200-500 $/t[149] equaling about 181 €/t considering the cheapest offer. Regarding the initial estimate of 5000 €/t as the cost of CaBa sorbent, this would leave 4779 €/t for sorbent synthesis. Depending on the scale of production and stage of process development this specific cost might be relevantly decreased. In a sensitivity study, with results shown in Figure 7-7, various estimates for achievable production cost of the CaBa sorbent were evaluated. These range from 0.5 €/kg to 10 €/kg for the CaBa sorbent under consideration of a gas with lower initial H_2S content of 100 ppm_v as compared to the conditions investigated in Figure 7-5.

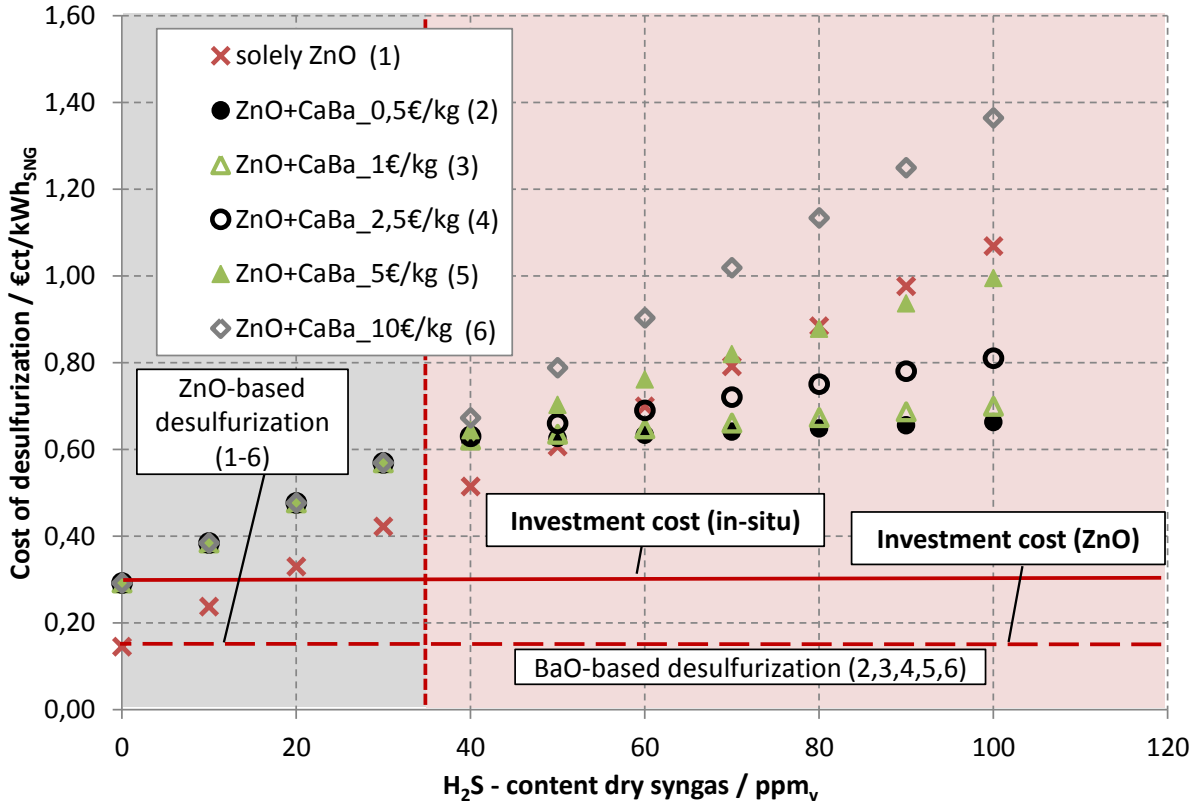

Figure 7-7: Specific costs of combined desulfurization with CaBa and a downstream ZnO-fixed bed under variation of the estimated cost for the production of CaBa sorbent (Background colors indicating the regimes of the specific sorbent material acting as desulfurization agent depending on the combination of sorbents as indicated by the numbers)

The sensitivity analysis for a varied sorbent cost depicted in Figure 7-7 shows the margin of competitiveness with downstream ZnO-desulfurization. At a specific cost for CaBa of approximately 7.5 €/kg and above, the application as in-situ sorbent is no longer profitable. If the cost for the sorbent were reduced to 1 €/kg the benefit of in-situ application as compared to solely ZnO-desulfurization can be relevant even for syngas with an initial H_2S content of only 100 ppm_v. The specific desulfurization cost of a gas with 100 ppm_v H_2S is limited to 0.7 ct/kWh_{SNG} for a combined application of CaBa at 1 €/kg and downstream ZnO-based fixed bed desulfurization as compared to 1.1 ct/kWh_{SNG} for mere fixed bed desulfurization with ZnO. The estimate of a reduced cost of CaBa sorbent of 1 €/kg seems justified for a later stage of production of the sorbent, taking into account the low cost for reactant input. An estimated sorbent price of 1 €/kg still includes more than 75 % for the synthesis and conditioning of the sorbent material regarding the availability of reactants at about 0.23 ct/kg.

Considering the motivation of the conducted work of establishing in-situ desulfurization as a cheap method for coarse desulfurization (Figure 3-1) the proof of feasibility is yet to be made, concerning the process itself and the economic profitability as well. On the other hand the performed experimental and economic analysis allows the formulation of some preconditions to which both, the feasibility of the process and the economic profitability are depending on. For the economic profitability specific costs of 1 ct/kWh_{SNG} can be derived as a benchmark value for the desulfurization of a gas with an H_2S content of 1400 ppm_v under combined application of in-situ sorbents and a downstream fixed bed of ZnO. This benchmark can be derived from the potential of reduced costs for fuel input under application of high sulfur alternative fuels (Figure 7-1). The sulfur content of above 1000 ppm_v H_2S has to be considered as an approximate range for high sulfur fuels such as mixed gasification of sewage sludge and wood pellets, whereby the value of 1400 ppm_v H_2S is used for continuity of calculation. With respect to this benchmark for economic profitability, a combination of CaO-based in-situ desulfurization and downstream ZnO-desulfurization can be excluded due to the high steady state value of CaO-based desulfurization and the resulting high share of ZnO-based desulfurization leading to combined specific costs in the range of 5 ct/kWh_{SNG}. For the application of the BaO-based sorbent CaBa, the resulting specific costs majorly depend on the costs of the sorbent itself, as shown by a sensitivity analysis in Figure 7-7. Under consideration of the formulated benchmark of 1 ct/kWh_{SNG} an upper limit can be derived for the allowable future market price of the not yet commercially available sorbent CaBa, in order to suffice the condition for desulfurization costs. Figure 7-8 shows the allowable maximum costs for CaBa in order to suffice the criterion of specific desulfurization costs of 1 ct/kWh_{SNG} for a syngas with 1400 ppm_v H_2S. Two scenarios are considered for the calculation. One is based on the application of CaBa as in-situ sorbent in combination with a downstream fixed bed of ZnO, another scenario includes the combined in-situ desulfurization under application of limestone and CaBa as depicted in Figure 6-39.

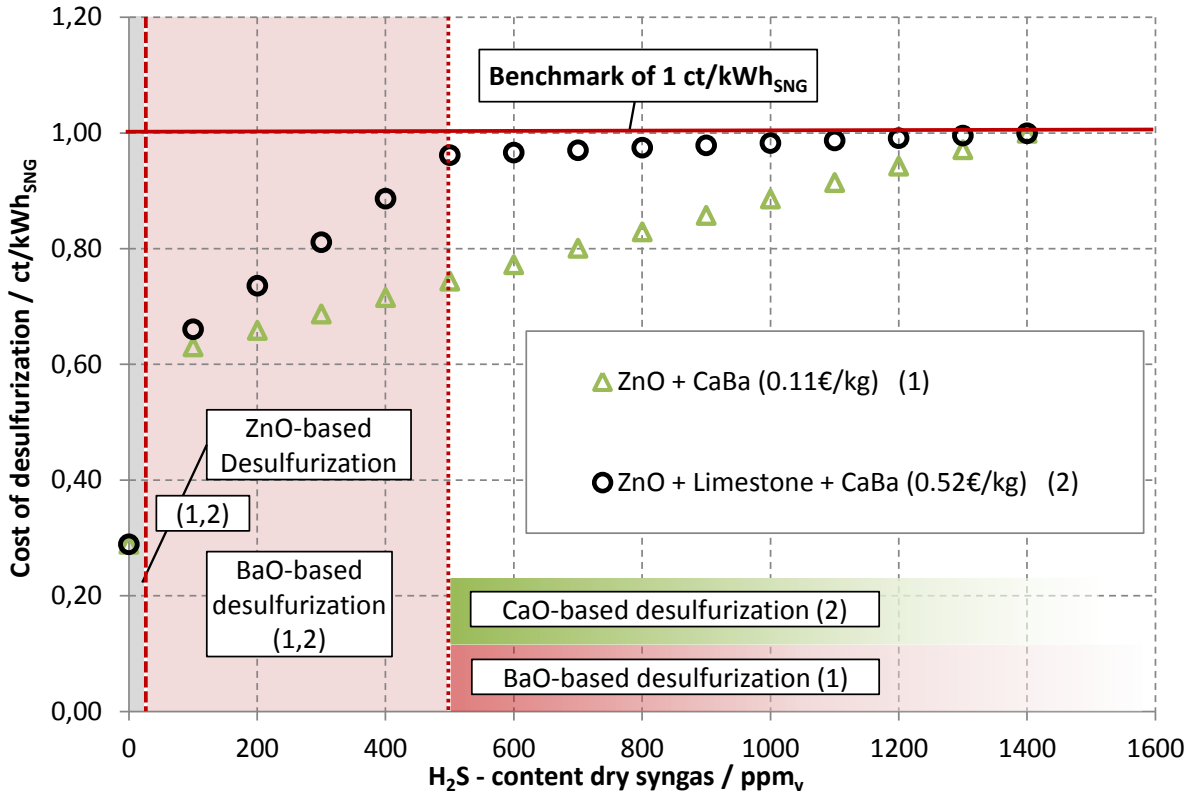

Figure 7-8: Specific cost of combined a downstream ZnO-fixed bed with in-situ desulfurization under application of CaBa, limestone and a combination of all three under an estimated cost for the production of CaBa sorbent of 1 €/kg

As shown in Figure 7-8 the mere combination of CaBa as in-situ sorbent with ZnO-based fixed bed desulfurization (Figure 7-8 (1)) would require CaBa cost of 0.11 €/kg in order to suffice the benchmark criterion for combined desulfurization costs. This can be considered nonrealistic as a market price for CaBa as it is below the material costs for synthesis of the sorbent material in the range of 0.23 €/kg even for bulk purchase. This does include the costs for synthesis under consideration of a highly energy intensive process. It can therefore be stated that the combination of CaBa and ZnO alone is not an economically viable scenario for desulfurization of a high sulfur syngas with feed contents above 1000 ppm$_v$ H_2S.

For the scenario of a combined in-situ desulfurization under application of limestone and CaBa, the desulfurization from the initial feed of 1400 ppm$_v$ to an H_2S content of 500 ppm$_v$ is CaO-based, as this value was experimentally determined to be the steady state of CaO-based desulfurization under the investigated gasification conditions (Figure 6-9). Under the investigated precondition of separating the steps of CaO- and BaO-based desulfurization (Figure 6-39) this results in a feed of 500 ppm$_v$ H_2S for the BaO-based desulfurization under application of CaBa. With respect to economic profitability under consideration of a benchmark value of 1 ct/kWh$_{SNG}$ as desulfurization costs, such a combined process is advantageous. The margin of maximum costs for the CaBa sorbent is increased to 0.52 €/kg in order to suffice the considered economic benchmark criterion. Production costs of 0.52 €/kg are at least above the costs for the raw materials and leave a margin of about 0.25 €/kg for synthesis. Given the many uncertainties contained in the performed economic assessment the resulting values clearly have to be considered as estimates only. Furthermore the considered

scenario of combined application of CaBa and limestone as sorbents for in-situ desulfurization does not include increased apparatus costs caused by the separation of the two desulfurization steps.

To sum up it can be stated that the concept of desulfurization investigated in the course of this work, an in-situ application of sorbents for coarse desulfurization combined with a downstream ZnO-based fixed bed desulfurization, is not economical for application of CaO-based sorbents as the only in-situ material. This is due to the relatively high steady state of CaO-based desulfurization in the range of 500 ppm_v under the investigated process conditions. This leads to an overproportional consumtion of ZnO as desulfurization sorbent in a downstream fixed bed and causes high specific costs of the proposed desulfurization setup. The application of CaBa as a BaO-based material is also doubtable in the context of coarse desulfurization with feed contents of 1000 ppm_v H_2S and above. The determined slow reaction rate of BaO, the release of H_2S from the CaO contained in the sorbent once the CaO-based steady state is undershot (Figure 6-37) as well as economic reasons (Figure 7-5) justify this conclusion. The combination of CaO-based and BaO-based in-situ desulfurization holds the possibility to suffice both, process and economic criteria, whereby the local separation of both desulfurization steps was shown to be a precondition. The combined application of CaBa and limestone is potentially suited to limit the specific cost for desulfurization to 1 ct/kWh_{SNG} even for a high-sulfur syngas derived from gasification of cheap waste fuels such as admixture of sewage- or paper mill sludge. The use of such alternative fuels with high sulfur loads could negate the cost of fuel input of 1.5 -3.4 ct/kWh_{SNG} according to Figure 7-1.

On the other hand the combined application of CaBa and limestone for in-situ desulfurization increases the demand for complexity of the process design as discussed in section 6.4.2 and the usage of alternative residual fuels is not yet a proven technology. An optimum is therefore to be found between the decrease of cost for fuel input, and the complexity of the gas cleaning process under consideration of the economic evaluation discussed above.

8 Conclusions and outlook[1]

The presented work aims at the implementation of in-situ desulfurization as a process step for coarse desulfurization in allothermal fluidized bed gasification of biomass. The motivation for the research is based on the necessity to increase the applicable range of gasification fuels towards waste materials in order to obtain economic competitiveness for the technology of allothermal steam gasification with the aim of SNG-production. Such waste fuels commonly contain relevantly increased amounts of sulfur and other contaminants, which can easily negate the benefit of a cheaper fuel by increased efforts for gas cleaning. This is especially valid for desulfurization under application of a downstream fixed bed of ZnO. The purpose of the presented work was to investigate the functionality of in-situ desulfurization as a process step for coarse desulfurization of a biomass derived syngas with the aim of improved economics as compared to mere ZnO-based fixed bed desulfurization. The investigations are based on a thermodynamic evaluation of potentially suitable sorbent materials as a preparation for subsequent experimental application of in-situ sorbents in a real gasification test rig, as the main focus of the presented study.

The evaluation of thermodynamic calculations on H_2S sorption, at the conditions present in the BFBG unit at Graz University of Technology, indicate that an in-situ desulfurization cannot be implemented to a sufficient extent using single metal sorbents under equilibrium conditions. According to simulated results, the residual H_2S content cannot be reduced to values below 400 ppm_v under in-situ conditions by use of single metal oxides. Even for a coarse desulfurization, depending on sorbent cost and other positive side effects, a benchmark of about 50 ppm_v H_2S needs to be reached in order to justify the implementation of in-situ desulfurization. CaO-based sorbents are beneficial concerning the low cost and stability at high temperatures, but are limited to desulfurization in the range of 500 ppm_v H_2S, according to thermodynamic calculations based on the conditions present in the BFBG at Graz University of Technology. For a solid solution sorbent “CaBa” consisting of BaO and CaO, equilibrium calculations predict a desulfurization of the syngas to a sulfur level of 2.1 ppm_v H_2S at a steam content of about 40 vol% and 800 °C. This is sufficient for further catalytic gas processing applications. As many of the influencing factors are not exactly predictable by equilibrium calculations, some mixed metal combinations, and in particular the CaBa sorbent bare a high potential to be suited for in-situ applications. Real process conditions with non-equilibrium influences are indispensable to show the limits and performance of these sorbents and allow for an evaluation according to the overall benefit as compared to mid-temperature ZnO-based fixed bed desulfurization.

Experimental investigations were thus conducted in a BFBG test rig by gasification of wood-pellets under an elevated sulfur content of approximately 1200 – 1500 ppm_v H_2S in the produced gas. The applied method of adjusting the sulfur content by injection of CS_2 enabled the investigation of in-situ desulfurization efficiency of various sorbents with a biomass derived, high sulfur and high steam content syngas. The method is advantageous as compared to the direct addition of H_2S or COS as a concentrated gas mixture of these highly toxic gases would be necessary to relevantly raise the sulfur content of the resulting syngas stream. Furthermore the method presented herein does not change

[1] Segments of this section have already been published by Husmann *et al.*[27,69,111,131]

the basic gas composition of permanent gases comparing syngas with- and without elevated sulfur content.

Experiments on in-situ desulfurization were performed under application of four different CaO-based sorbents: lime, limestone, dolomite and fully calcined dolomite. These materials are cheaply available, toxically harmless and bare the potential for coarse desulfurization. The results of the presented CaO-based experiments prooved the functionality of the test rig for the purpose of in-situ desulfurization in biomass gasification. For lime, limestone and uncalcined dolomite, a steady state value of approximately 500 ppm_v H_2S was determined, which is in accordance with the results of thermodynamic equilibrium calculations for CaO. As the achieved desulfurization by application of lime, which consists basically solely of CaO, and dolomite are in the exact same range, the residual H_2S content therefore represents the CaO-based steady state value. It was thus shown that the minor components in dolomite do not have a significant influence on the desulfurization properties under standard conditions. For fully calcined dolomite, the residual H_2S content remains at a higher level of 600 ppm_v even after over-stoichiometric addition. This is attributed to the significantly lower surface area and soft mechanical structure of this sorbent leading to a reduced rate of reaction and increased discharge from the gasifier. Concerning the gas quality, the application of lime and limestone resulted in a decline of tar concentration from 15.4 to 13.6 g/m^3_{std} and does therefore not indicate a relevantly improved tar conversion as observed in literature.

The variation of parameters for in-situ desulfurization shows the complex influences of gasification conditions on the obtained experimental results as well as differences for the sorbents compared in this experimental study. It is shown that the experimentally determined values do not behave quite like simulated values when gasification parameters are varied, especially regarding a variation in temperature. In the range of 700 to 825 °C, no influence on the steady state desulfurization was detected whereby supposedly a combined influence of freeboard and reactor temperature account for this phenomenon. The variation of the steam content in the syngas has a greater influence on the steady state desulfurization equilibrium of lime than on that of dolomite. This can be attributed to a catalytic effect of the MgO in dolomite on the water-gas-shift reaction, resulting in a smaller deviation of the actual steam content upon variation of the steam inlet flow. These results qualify dolomite for use in gasification processes with steam contents above 40 vol% in the produced syngas, as the effect of the promoted water-gas-shift reaction proves to be beneficial for the achievable desulfurization equilibrium. A disadvantage of the use of dolomite is the higher amount of sorbent needed, due to the MgO content that has to be considered as inert for desulfurization. This is especially the case with fully calcined dolomite, with an average conversion of 15% of CaO to CaS as compared to 35% for the other sorbents. Considering a CaO content of 60 wt% in the applied dolomite, approximately four times as much sorbent is needed for the same desulfurization effect as compared to the application of lime. In summary, the application of fully calcined dolomite seems least advisable for desulfurization purposes due to a supposed sintering during calcination. Regarding the catalytic effect of MgO on the water-gas-shift reaction, the use of dolomite which is calcined in-situ seems appropriate, especially for high steam atmosphere, whereby disposal related problems increase with the amount of sorbent needed. According to the presented results and as limestone costing less than lime, the use of limestone seems the most advisable for coarse desulfurization in biomass gasification under calcining conditions. The use of CaO-based sorbents for in-situ desulfurization showed the functionality for coarse desulfurization and revealed specific advantages of the compared materials. Even though the conversion and reactivity of CaO-based sorbents are

promising, the achieved equilibrium value of 500 ppm_v H_2S is too high for an efficient use as in-situ sorbents for desulfurization in biomass application.

Besides CaO-based materials commonly deployed in the in-situ desulfurization of coal derived syngas, a novel BaO-based sorbent material CaBa was investigated for the first time for its desulfurization performance under in-situ conditions in steam blown fluidized bed gasification of biomass. A desulfurization down to a few ppm_v H_2S can be possible according to equilibrium calculations for biomass derived syngas with steam contents of up to 50 vol%. As the thermodynamic desulfurization equilibrium of this sorbent material lays below 5 ppm_v H_2S and therefore more than two magnitudes below that of CaO-based in-situ materials, the initial feed value of sulfur was set to about 100 ppm_v H_2S for the experimental investigation of CaBa. Sintering of the CaBa sorbent occurred under fluidized bed conditions and had to be prevented by the addition of lime as separating agent in order to maintain stable gasification conditions. The sorption of H_2S was confirmed experimentally and was reproducible for varied amounts of added sorbent. The variation of reactor temperature indicated a limitation by reaction kinetics at a temperature level of 760 °C. Increasing temperatures to 810 °C significantly improved the desulfurization efficiency, whereby the achieved steady state equilibrium of 35 ppm_v H_2S is still far above the thermodynamic equilibrium. The stabilization of BaO in the sorbent was confirmed as desulfurization occurs by formation of BaS with no $BaCO_3$, detected according to XRD measurements. Furthermore, particle analysis (SEM-EDX) shows that the stabilization is not primarily based on the incorporation of BaO in a solution phase with CaO. A lower temperature limit of the application is thus supposedly not given by the carbonization temperature of CaO but by the reactivity of BaO itself. It is further shown by ICP-OES and SEM-EDX analysis that the content of Ba in the sorbent is decreased during in-situ application. The abrasion and transfer of Ba into sintering bridges of the bed material can account for this. According to the presented research, kinetics of the formation of BaS, limit the desulfurization efficiency of the CaBa sorbent in the range of 760 – 810 °C gasification temperature. At a temperature level of 810 °C the experimental in-situ application of CaBa in a fluidized bed gasifier resulted in a desulfurization from 85 ppm_v down to 35 ppm_v H_2S with full conversion of BaO to BaS. The desulfurization of a gas with a feed content of several 100 ppm_v H_2S down to values below 50 ppm_v was not shown within this work due to restrictions in the reactor heating regarding a further increase of gasification temperature and therefore a limited rate of reaction in the sorbent. If this limitation was averted by higher temperature of application and by further particle engineering, in order to achieve an increased surface area and fully understand the mechanism of barium stabilization, the use of CaBa for desulfurization is promising. The potential is given by the comparatively low cost of the substrate materials $CaCO_3$ and $BaCO_3$ and very low thermodynamic equilibrium of the desulfurization reaction of BaO, even for syngas with a high steam content.

As a process setup for removing high loads of sulfur down to values below the benchmark of 50 ppm_v H_2S, the combined desulfurization under application of CaBa and lime was experimentally investigated. This process setup bares the potential to ideally reduce the H_2S content in the gas from initial values of 1000 ppm_v H_2S and above down to the CaO-based steady state of about 500 ppm_v for the investigated conditions. A continuos decline in the residual H_2S content would then be effectuated by the formation of BaS in the BaO-based CaBa sorbent and result in values of about 35 ppm_v H_2S which was found to be the steady state of BaO-based desulfurization for the investigated conditions. According to experimental investigation in the BFBG test rig, the combined application of CaBa and lime did not prove to be successful for two reasons. First of all the release of

H_2S from CaS was observed once the H_2S concentration drops below the steady state desulfurization of CaO-based desulfurization. This would have to be averted by establishing a consecutive desulfurization by limestone and CaBa in separated vessels, preventing the presence of CaS in an environment with H_2S contents below the CaO-based desulfurization equilibrium. Furthermore the application of CaBa for desulfurization of a gas with several 100 ppm_v down to values below 50ppm_v H_2S was not feasible within the presented work and still needs to be proven. The demand of sorbent and conditions needed for such an application can only be deduced by interpolation of the trends observed in the conducted experiments (Figure 6-34). An application of CaBa in the temperature range of 900 to 1000 °C and under excess addition of sorbent with a Ba/S-ratio δ of 8 or above seems advisable according to the interpolation of the obtained experimental results.

With the aim of establishing in-situ desulfurization as a cheap method for coarse desulfurization as motivation for the conducted work, some further conclusions can be drawn according to the economic assessment presented in this work. The economic evaluation of in-situ desulfurization assesses the use of a combined process setup in-situ desulfurization, under application of CaBa as well as CaO-based sorbents, in combination with a downstream fixed bed of ZnO (Figure 7-3). The results are also compared to the mere application of ZnO for sulfur removal (Figure 7-2). For CaO-based sorbents the evaluation showed a disproportionately increased cost of desulfurization with increased sulfur content in the gas. This is due to the consumption of ZnO in the downstream fixed bed resulting from the high residual H_2S-content of 500 ppm_v by application of CaO-based sorbents for in-situ desulfurization. This resulted in specific cost for desulfurization of almost 5 ct/kWh_{SNG} for a syngas containing 1400 ppm_v H_2S. Under application of CaBa as in-situ sorbent the resulting specific cost is even higher with 8.5 ct/kWh_{SNG} under assumption of a sorbent cost of 5 €/kg CaBa. The motivation of establishing in-situ desulfurization is using waste fuels with a high sulfur content in order to reduce or negate the costs for fuel input. On the other hand the increased need for desulfurization must not cause a significant increase of the costs for upgrading the obtained syngas to SNG. Under consideration of the cost-share for fuel input in the range of 1.5-3.4 ct/kWh_{SNG}(Figure 7-1) the application of CaO- and BaO-based sorbents in the evaluated process setup (Figure 3-1) is not justified according to the results of economic assessment summarized above. In order to justify the increased system wear caused by application of waste fuels and also to compete with alternative technologies for desulfurization, a benchmark of 1 ct/kWh_{SNG} is stated for the specific cost of sulfur removal from a gas with 1400 ppm_v H_2S. The possibility to meet this economic criterion is given for the combined application of CaBa and limestone as in-situ sorbents, followed by a downstream ZnO-based fixed bed desulfurization under certain preconditions. First of all a separation of the CaO and BaO-based steps of in-situ desulfurization is required. This can be achieved by application in a multistaged gasifier setup as suggested in Figure 6-38. Further the residence times and temperatures have to be sufficient in order to achieve a desulfurization effect from several hundred ppm_v H_2S down to values of about 35 ppm_v upon application of CaBa. An experimental proof of feasibility was not possible within the conducted work. Finally the costs of the commercially not yet available CaBa sorbent would have to be at about 0.5 €/kg in order to meet the stated 1 ct/kWh_{SNG}.as a benchmark for the desulfurization costs of a syngas containing 1400 ppmv H_2S.

The results of the work presented herein combine the assessment of in-situ desulfurization as a process step for sulfur removal in biomass gasification from a thermodynamic, an experimental and an economic point of view. The obtained results show the feasibility of the process under gasification conditions, but also show the limits for the application of different sorbents. CaO-based in-situ

desulfurization is limited by a high steady state value of 500 ppm_v H_2S at a steam content of about 40 %. BaO-based in-situ desulfurization was investigated under application of a novel CaBa sorbent for the first time under real process conditions. A limitation was shown by kinetics of the sulfidation of BaO at temperatures in the range of 760 to 810 °C. The combined application of CaO- and BaO-based in-situ desulfurization is limited by the release of H_2S from CaS once the steady state of CaO-based desulfurization is undershot. Further experimental investigations should aim at an application of CaBa at increased gasification temperatures in the range of 900 °C and prove the feasibility of desulfurization from several hundred ppm_v down to values in the range of 35 ppm_v H_2S under application of this sorbent. Furthermore the investigation of a process design for the separation of CaO- and BaO-based in-situ desulfurization is recommended once initial H_2S contents above 1000 ppm_v are to be expected. As outlined in section 6.4.2 this could be established by a combined application of limestone and CaBa in a multistage countercurrent FICFB gasifier leading to a concept of gas cleaning as outlined in Figure 6-39. Such experimental investigations would also have to show the assumed stabilization of used sorbents by formation of sulfates in the combusting section of the gasifier. Another potential synergy is given by the commonly lower steam content in FICFB gasification as compared to the conditions during the experimental investigations presented in this work. This will probably result in lower steady state values for both, CaO- and BaO-based in-situ desulfurization. Further optimization of the CaBa sorbent as well as separate experimental investigations concerning the kinetic behavior of this sorbent, can contribute to a better understanding of the mechanism of BaO-stabilization and improvement of the desulfurization properties of CaBa. The implementation of such a combined concept for in-situ desulfurization under application of limestone and CaBa can help to bridge the exigency of economically feasible gas cleaning concepts for a syngas derived by gasification of waste fuels and residual biomass.

With the option of converting waste fuels to syngas under application of the elaborated concept of in-situ desulfurization as part of a catalytic gas cleaning concept, the potential is given for significantly reducing the production cost of SNG. The implementation of the concept of in-situ desulfurization, as developed in the presented work, can therefore be an important step for the economically competitive provision of SNG as biogeneous alternative to natural gas in a future energy system based on sustainable sources.

9 References

(1) Edenhofer, O.; Pichs-Madruga R.; Sokona Y. *RENEWABLE ENERGY SOURCES AND CLIMATE CHANGE MITIGATION: SUMMARY FOR POLICYMAKERS AND TECHNICAL SUMMARY*; SPECIAL REPORT OF THE INTERGOVERNMENTAL PANEL ON CLIMATE CHANGE; IPCC, **2012**.

(2) Edel, M; Blume, A.; Völler, K. *Zukunft Biomethan: Perspektiven und Handlungsempfehlungen für die Rolle von Biomethan im zukünftigen Energiesystem*, **2015**.

(3) Teipel, U.; Beining, R.; Adelt, M.; Vogel, A. Stand und Perspektiven der Biomassevergasung. *Chemie Ingenieur Technik* **2010**, *82*, 1941–1954, DOI: 10.1002/cite.201000119.

(4) van der Drift, A.; Biollaz, S.; Waldheim, L.; Rauch, R.; Manson-Whitton, C. *STATUS and FUTURE of bioSNG in EUROPE*; IEA-Bioenergy conference, **2012**.

(5) *Synthetic Natural Gas: From Coal, Dry Biomass, and Power-to-Gas Applications: SNG from wood - the GoBiGas project;* T.J. Schildhauer; S. Biollaz, Eds.; John Wiley & Sons, **2016**.

(6) Held, J. *Gasification- Status and technology* SGC-R-240-SE; SGC-Swedish Gas Centre, **2012**.

(7) van der Drift, A.; van Doorn, J.; Vermeulen, J. Ten residual biomass fuels for circulating fluidized-bed gasification. *Biomass and Bioenergy* **2001**, *20*, 45–56, DOI: 10.1016/S0961-9534(00)00045-3.

(8) German National Academy of Sciences Leopoldina. *Bioenergy – Chances and limits*; German National Academy of Sciences: Halle (Saale), Germany, 2012.

(9) Koch, B. *Biomass Energy Europe: Final report*; Freiburg, **2008**.

(10) Forschungs- und Technologierat Bioökonomie (BÖR). *Nachhaltige Nutzung von Bioenergie: Empfehlungen des BioÖkonomieRats*; Berlin, **2012**.

(11) Brosowski et al. *BIOMASSEPOTENZIALE VON REST- UND ABFALLSTOFFEN: Status quo in Deutschland*; NACHWACHSENDE ROHSTOFFE No. 36; Gülzow, **2015**.

(12) Fachagentur Nachwachsende Rohstoffe e. V. *BASISDATEN BIOENERGIE: DEUTSCHLAND* **2015**; FESTBRENNSTOFFE, BIOKRAFTSTOFFE, BIOGAS.

(13) Kaltschmitt, M.; Hartmann, H.; Hofbauer, H. *Energie aus Biomasse*; Springer: Heidelberg, **2009**.

(14) Milne, T.A.; Evans, R.J.; Abatzoglou, N.. *Biomass Gasifier "Tars": Their Nature, Formation, and Conversion*; NREL/TP-570-25357; National Renewable Energy Laboratory, Golden, Colorado, **1998**.

(15) Neeft, et. al. Guideline for Sampling and Analysis of Tar and Particles in Biomass. *Progress in Thermochemical Biomass Conversion* **2001**, 162–187.

(16) Strehlow, R. A. *Combustion Fundamentals: Thermochemical Tables*, 2nd edition; McGraw-Hill: New York, **1998**.

(17) Gröbl, T.; Walter, H.; Haider, M. Biomass steam gasification for production of SNG – Process design and sensitivity analysis. *Applied Energy* **2012**, *97*, 451–461, DOI: 10.1016/j.apenergy.2012.01.038.

(18) Kienberger, T.; Zuber, C.; Novosel, K.; Baumhakl, C.; Karl, J. Desulfurization and in situ tar reduction within catalytic methanation of biogenous synthesis gas. *Fuel* **2013**, *107*, 102–112, DOI: 10.1016/j.fuel.2013.01.061.

(19) Göransson, K.; Söderlind, U.; He, J.; Zhang, W. Review of syngas production via biomass DFBGs. *Renewable and Sustainable Energy Reviews* **2011**, *15*, 482–492, DOI: 10.1016/j.rser.2010.09.032.

(20) Ahrenfeldt, J.; Thomsen, T. P.; Henriksen, U.; Clausen, L. R. Biomass gasification cogeneration - A review of state of the art technology and near future perspectives. *Applied Thermal Engineering* **2013**, *50*, 1407–1417, DOI: 10.1016/j.applthermaleng.2011.12.040.

(21) Asadullah, M. Barriers of commercial power generation using biomass gasification gas: A review. *Renewable and Sustainable Energy Reviews* **2014**, *29*, 201–215, DOI: 10.1016/j.rser.2013.08.074.

(22) Erbel, C.; Mayerhofer, M.; Monkhouse, P.; Gaderer, M.; Spliethoff, H. Continuous in situ measurements of alkali species in the gasification of biomass. *Proceedings of the Combustion Institute* **2013**, *34*, 2331–2338, DOI: 10.1016/j.proci.2012.06.037.

(23) Bläsing, M.; Zini, M.; Müller, M. Influence of Feedstock on the Release of Potassium, Sodium, Chlorine, Sulfur, and Phosphorus Species during Gasification of Wood and Biomass Shells. *Energy Fuels* **2013**, *27*, 1439–1445, DOI: 10.1021/ef302093r.

(24) Marschner, H. *Mineral nutrition of higher plants*, 3rd ed; Academic Press: Amsterdam, Boston, Heidelberg, London, New York, Oxford, Paris, San Diego, San Francisco, Singapore, Sidney, Tokyo, **2012**.

(25) Plautz, D. Auswirkungen alternativer Brennstoffe in allothermen Wirbelschichtvergasern. Master Thesis, Graz University of Technology, Graz, **2013**.

(26) Binder, G. Screening von alternativen Brennstoffen für den Einsatz in einem Heatpipe-Reformer. Master Thesis, Graz University of Technology, Graz, **2012**.

(27) Husmann, M.; Hochenauer, C.; Meng, X.; Jong, W. de; Kienberger, T. Evaluation of Sorbents for High Temperature In Situ Desulfurization of Biomass-Derived Syngas. *Energy Fuels* **2014**, *28*, 2523–2534, DOI: 10.1021/ef402254x.

(28) Visser, H. J. M. *THE INFLUENCE OF FUEL COMPOSITION ON AGGLOMERATION BEHAVIOUR IN FLUIDISED - BED COMBUSTION*; ECN-C--04-054; Petten, the Netherlands, **2004**.

(29) Gatternig, B.; Karl, J. Investigations on the Mechanisms of Ash-Induced Agglomeration in Fluidized-Bed Combustion of Biomass. *Energy Fuels* **2015**, 150210154527004, DOI: 10.1021/ef502658b.

(30) Fryda, L.; Panopoulos, K.; Kakaras, E. Agglomeration in fluidised bed gasification of biomass. *Powder Technology* **2008**, *181*, 307–320, DOI: 10.1016/j.powtec.2007.05.022.

(31) Visser, H. J. M.; van Lith, S. C.; Kiel, J. H. A. Biomass Ash-Bed Material Interactions Leading to Agglomeration in FBC. *J. Energy Resour. Technol.* **2008**, *130*, 11801, DOI: 10.1115/1.2824247.

(32) Zevenhoven-Onderwater, M. et al. The ash chemistry in fluidised bed gasification of biomass fuels. Part I: predicting the chemistry of melting ashes and ash–bed material interaction. *Fuel* **2001**, *80*, 1489–1502.

(33) Zevenhoven-Onderwater, M. et al. The ash chemistry in fluidised bed gasification of biomass fuels. Part II: Ash behaviour prediction versus bench scale agglomeration tests. *Fuel* **2001**, *80*, 1503–1512.

(34) Ma, T.; Fan, C.; Hao, L.; Li, S.; Song, W.; Lin, W. Biomass-Ash-Induced Agglomeration in a Fluidized Bed. Part 1: Experimental Study on the Effects of a Gas Atmosphere. *Energy Fuels* **2016,** DOI: 10.1021/acs.energyfuels.6b00164.

(35) Ruiz, J.; Juárez, M.; Morales, M.; Muñoz, P.; Mendívil, M. Biomass gasification for electricity generation: Review of current technology barriers. *Renewable and Sustainable Energy Reviews* **2013**, *18*, 174–183, DOI: 10.1016/j.rser.2012.10.021.

(36) Zuber, C.; Binder, G.; Siddiqui, S.; Husmann, M. Possible Fuels for Usage in the Small Scale Downdraft Gasifier System E3. IBO.12.1. *Proceedings of the 24rd European Biomass Conference and Exhibition* **2016**.

(37) Kienberger T. Methanierung biogener Synthesegase mit Hinblick auf die direkte Umsetzung von höheren Kohlenwasserstoffen. Dissertation, Graz University of Technology, Graz, **2010**.

(38) van der Drift, A.; Boerrigter, H.; Coda, B.; Cieplik, M.K.; Hemmes, K. *ENTRAINED FLOW GASIFICATION OF BIOMASS: Ash behaviour, feeding issues, and system analyses*; ECN-C--04-039 ECN-C--04-039; Energy Center of the Netherlands (ECN), **2004**.

(39) Stemmler, M.; Müller, M. Chemical hot gas cleaning concept for the "CHRISGAS" process. *Biomass and Bioenergy* **2011**, *35*, S105–S115, DOI: 10.1016/j.biombioe.2011.03.044.

(40) Möller, B. Status of Bio2G and Gasification testing at GTI. http://conference.sgc.se/ckfinder/userfiles/files/2_3_%20Bjorn%20Fredriksson%20Moller.pdf (accessed August 2016).

(41) Xie, Y. R.; Shen, L. H.; Xiao, J.; Xie, D. X.; Zhu, J. Influences of Additives on Steam Gasification of Biomass. 1. Pyrolysis Procedure. *Energy Fuels* **2009**, *23*, 5199–5205, DOI: 10.1021/ef900459j.

(42) Gallmetzer, G.; Ackermann, P.; Schweiger, A.; Kienberger, T.; Gröbl, T.; Walter, H.; Zankl, M.; Kröner, M. The agnion Heatpipe-Reformer—operating experiences and evaluation of fuel conversion and syngas composition. *Biomass Conv. Bioref.* **2012**, *2*, 207–215, DOI: 10.1007/s13399-012-0046-2.

(43) Held, J. *Small and medium scale technologies for bio-SNG production*; SGC Rapport 2013:281; SGC-Swedish Gas Centre, **2013**.

(44) Kienberger, T.; Zuber, C. *AGNION'S SMALL SCALE SNG CONCEPT: Synthetic Natural Gas from Coal, Dry Biomass, and Power-to-Gas Applications;* John Wiley & Sons: Hoboken, NJ, USA, **2016**.

(45) Heatpipe-Reformer zur Holzvergasung. http://www.bioenergie-region-achental.de/gipfelprojekte/gipfelprojekte-phase-i/heatpipe-reformer/ (accessed July 20, 2016).

(46) Rauch, R. et al. *Steam gasification of biomass at CHP plant Guessing-Status of the demonstration plant*; 2nd World Conference and Technology Exhibition for Energy, Industry and Climate Protection; Rome, **2004**.

(47) Proell, T.; Rauch R.; Aichernig, C.; Hofbauer, H. Fluidized Bed Steam Gasification of Solid Biomass - Performance Characteristics of an 8 MWth Combined Heat and Power Plant. *International Journal of Chemical Reactor Engineering* **2007**, *1*, 1–21.

(48) Stemmler, M. Chemische Heißgasreinigung bei Biomassevergasungsprozessen. Dissertation, RWTH Aachen, Jülich, **2010**.

(49) van der Drift, A.; van der Meijden, C.M.; Boerrigter, H. MILENA gasification technology for high efficient SNG production from biomass. *Proceedings of the 14th European Biomass Conference and Exhibition* **2005**.

(50) van der Meijden, C.M.; Veringa, H.; Vreugdenhil, B.; van der Drift, B. Bioenergy II: Scale-Up of the Milena Biomass Gasification Process. *International Journal of Chemical Reactor Engineering* **2009**, *7*, 1542–6580.

(51) Woolcock, P. J.; Brown, R. C. A review of cleaning technologies for biomass-derived syngas. *Biomass and Bioenergy* **2013**, *52*, 54–84, DOI: 10.1016/j.biombioe.2013.02.036.

(52) *Bundes-Immissionsschutzgesetz: BImSchG*, **1974**.

(53) Colpan, O.; Dincer, I.; Hamdullahpur, F. Effect of Chemical Composition of Gases from Biomass Gasification On Solid Oxide Fuel Cell Performance. *Proceedings 2nd International Hydrogen Energy Congress and Exhibition IHEC* **2007**.

(54) Hofmann, P.; Panopoulos, K.; Aravind, P.; Siedlecki, M.; Schweiger, A.; Karl, J.; Ouweltjes, J.; Kakaras, E. Operation of solid oxide fuel cell on biomass product gas with tar levels >10 g Nm−3. *International Journal of Hydrogen Energy* **2009**, *34*, 9203–9212, DOI: 10.1016/j.ijhydene.2009.07.040.

(55) Boerrigter, H.; Calis, H. P.; Slort, D. J.; Bodenstaff, H. Gas cleaning for integrated biomass gasification (BG) and Fischer-Tropsch (FT) systems: Experimental demonstration of two BG-FT systems. *Proceedings of the 2nd World Conference and Technology Exhibition on Biomass for Energy, Industry and Climate Protection* **2004**, 51–56.

(56) Corella, J.; Toledo, J. M.; Molina, G. Performance of CaO and MgO for the hot gas clean up in gasification of a chlorine-containing (RDF) feedstock. *Bioresource Technology* **2008**, *99*, 7539–7544, DOI: 10.1016/j.biortech.2008.02.018.

(57) Delgado, J.; Aznar, M.-P.; Corella, J. Calcined Dolomite, Magnesite and Calcite for Cleaning Hot Gas from a fluidized Bed Biomass Gasifier with Steam Life and usefulness. *Ind. Eng. Chem. Res.* **1996**, *1996*, 3637–3643.

(58) Corella, J.; Aznar, M.-P.; Gil, J.; Caballero, M. A. Biomass Gasification in Fluidized Bed: Where To Locate the Dolomite To Improve Gasification? *Energy Fuels* **1999**, *13*, 1122–1127, DOI: 10.1021/ef990019r.

(59) Olivares, A.; Aznar, M. A.; Caballero, M. A.; Gil, J.; France´ s, E.; Corella, J. Biomass Gasification: Produced Gas Upgrading by In-Bed Use of Dolomite. *Ind. Eng. Chem. Res.* **1997**, *36*, 5220–5226.

(60) Orio, A.; Corella, J.; Narvaez, I. Performance of Different Dolomites on Hot Raw Gas Cleaning from Biomass Gasification with Air. *Ind. Eng. Chem. Res.* **1997**, *36*, 3800–3808.

(61) Heidenreich, S.; Foscolo, P. U. New concepts in biomass gasification. *Progress in Energy and Combustion Science* **2015**, *46*, 72–95, DOI: 10.1016/j.pecs.2014.06.002.

(62) Rapagna, S.; Jand, N.; Kiennemann, A.; Foscolo, P.U. Steam-gasication of biomass in a fluidised-bed of olivine particles. *Biomass and Bioenergy* **2000**, 187–197.

(63) Cheah, S.; Carpenter, D. L.; Magrini-Bair, K. A. Review of Mid- to High-Temperature Sulfur Sorbents for Desulfurization of Biomass- and Coal-derived Syngas. *Energy Fuels* **2009**, *23*, 5291–5307, DOI: 10.1021/ef900714q.

(64) Zuber, C.; Husmann, M.; Schroettner, H.; Hochenauer, C.; Kienberger, T. Investigation of sulfidation and regeneration of a ZnO-adsorbent used in a biomass tar removal process based on catalytic steam reforming. *Fuel* **2015**, *153*, 143–153, DOI: 10.1016/j.fuel.2015.02.110.

(65) Bu, X.; Ying, Y.; Zhang, C.; Peng, W. Research improvement in Zn-based sorbent for hot gas desulfurization. *Powder Technology* **2008**, *180*, 253–258, DOI: 10.1016/j.powtec.2007.03.039.

(66) Sasaoka, E.; Hatori, M.; Sada, N.; Uddin, M. A. Role of H 2 O in Oxidative Regeneration of ZnS Formed from High-Temperature Desulfurization ZnO Sorbent. *Ind. Eng. Chem. Res.* **2000**, *39*, 3844–3848, DOI: 10.1021/ie0004747.

(67) Lew, S.; Jothimurugesan, K.; Flytzani-Stephanopoulos, M. High-Temperature H2S Removal from Fuel Gases by Regenerable Zinc Oxide-Titanium Dioxide Sorbents. *Ind. Eng. Chem. Res.* **1989**, *28*, 535–541.

(68) Pineda, M.; Palacios, J.M.; Alonso, L.; Garcia, E.; Moliner, R. Performance of zinc oxide based sorbents for hot coal gas desulfurization in multicycle tests in a fixed-bed reactor. *Fuel* **2000**, 885–895.

(69) Husmann, M.; Zuber, C.; Maitz, V.; Kienberger, T.; Hochenauer, C. Comparison of dolomite and lime as sorbents for in-situ H2S removal with respect to gasification parameters in biomass gasification. *Fuel* **2016**, *181*, 131–138, DOI: 10.1016/j.fuel.2016.04.124.

(70) Franco, A.; Diaz, A. R. The future challenges for "clean coal technologies": Joining efficiency increase and pollutant emission control. *Energy* **2009**, *34*, 348–354, DOI: 10.1016/j.energy.2008.09.012.

(71) Zevenhoven, R.; Kilpinen, P. *Control of pollutants in flue gases and fuel gases*; Report TKK - ENY - 4; Espoo/Turku, Finland, **2002**.

(72) Abbasian, J.; Rehmat, A.; Leppin, D.; Banerjee, D. D. Desulfurization of Fuels with Calcium-based Sorbents. *Fuel Processing Technology* **1990**, 1–15.

(73) Weldon, J.; Haldipur, G. B.; Lewandowski, D.A.; Smith, K.J. Advanced Coal Gasification with Calcium Based Sorbents. *Am. Chem. Div. Fuel Chem.* **1986**, 244–252.

(74) Robin, A. M.; Wu, J. C.; Kassman, J. S. Integration and testing of hot desulfurization and the Texaco coal gasification process for power generation. *American Chemical Society Fuel Chemistry Division Preprints* **1990**, *35*, 188–195.

(75) Ben-Slimane, R.; Hepworth, M. T. Desulfurization of Hot Coal-Derived Fuel Gases with Manganese-Based Regenerable Sorbents. 1. Loading (Sulfidation) Tests. *Energy Fuels* **1994**, *8*, 1175–1183.

(76) Zheng, L.; Furinsky, E. Comparison of Shell, Texaco, BGL and KRW gasifiers as part of IGCC plant computer simulations. *Energy Conversion and Management* **2005**, *46*, 1767–1779, DOI: 10.1016/j.enconman.2004.09.004.

(77) Diego, L. F. de; García-Labiano, F.; Adánez, J. Factors Affecting the H 2 S Reaction with Noncalcined Limestones and Half-Calcined Dolomites. *Energy Fuels* **1999**, *13*, 146–153, DOI: 10.1021/ef980145f.

(78) García-Labiano, F.; Adánez, J.; Abad, A.; de Diego, L. F.; Gayán, P. Effect of Pressure on the Sulfidation of Calcined Calcium-Based Sorbents. *Energy Fuels* **2004**, *18*, 761–769, DOI: 10.1021/ef0301708.

(79) Efthimiadis, E. A.; Sotirchos, S. V. Sulfidation of limestone-derived calcines. *Ind. Eng. Chem. Res.* **1992**, *31*, 2311–2321, DOI: 10.1021/ie00010a009.

(80) Yrjas, K. P.; Zevenhoven, C. A. P.; Hupa, M. M. Hydrogen Sulfide Capture by Limestone and Dolomite at Elevated Pressure. 1. Sorbent Performance. *Ind. Eng. Chem. Res.* **1996**, *35*, 176–183.

(81) Yrjas, P.; Iisa, K.; Hupa, M. Limestone and dolomite as sulfur absorbents under pressurized gasification conditions. *Fuel* **1996**, *75*, 89–95, DOI: 10.1016/0016-2361(95)00204-9.

(82) Ruth, L. A.; Squires, A. M.; Graff, R. A. Desulfurization of fuels with half-calcined dolomite. First kinetic data. *Environ. Sci. Technol.* **1972**, *6*, 1009–1014, DOI: 10.1021/es60071a004.

(83) Álvarez-Rodríguez, R.; Clemente-Jul, C. Hot gas desulphurisation with dolomite sorbent in coal gasification. *Fuel* **2008**, *87*, 3513–3521, DOI: 10.1016/j.fuel.2008.07.010.

(84) Diego, L. F. de; Abad, A.; García-Labiano, F.; Adánez, J.; Gayán, P. Simultaneous Calcination and Sulfidation of Calcium-Based Sorbents. *Ind. Eng. Chem. Res.* **2004**, *43*, 3261–3269, DOI: 10.1021/ie0308238.

(85) Sun, P.; Grace, J. R.; Lim, C. J.; Anthony, E. J. Co-capture of H 2 S and CO 2 in a Pressurized-Gasifier-Based Process. *Energy Fuels* **2007**, *21*, 836–844, DOI: 10.1021/ef0605100.

(86) Stemmler, M.; Tamburro, A.; Müller, M. Laboratory investigations on chemical hot gas cleaning of inorganic trace elements for the "UNIQUE" process. *Fuel* **2013**, *108*, 31–36, DOI: 10.1016/j.fuel.2011.05.027.

(87) Cheah, S.; Parent, Y. O.; Jablonski, W. S.; Vinzant, T.; Olstad, J. L. Manganese and ceria sorbents for high temperature sulfur removal from biomass-derived syngas – The impact of steam on capacity and sorption mode. *Fuel* **2012**, *97*, 612–620, DOI: 10.1016/j.fuel.2012.03.007.

(88) Bakker, W. J.; Kapteijn, F.; Moulijn, J. A. A high capacity manganese-based sorbent for regenerative high temperature desulfurization with direct sulfur production. *Chemical Engineering Journal* **2003**, *96*, 223–235, DOI: 10.1016/j.cej.2003.08.022.

(89) Bale, C.; Bélisle, E.; Chartrand, P.; Decterov, S.; Eriksson, G.; Hack, K.; Jung, I.-H.; Kang, Y.-B.; Melançon, J.; Pelton, A. *et al.* FactSage thermochemical software and databases — recent developments. *Calphad* **2009**, *33*, 295–311, DOI: 10.1016/j.calphad.2008.09.009.

(90) Bale, C. W.; Chartrand, P.; Degterov, S. A.; Eriksson, G.; Hack, K.; Mahfoud, R. B.; Melancon, J.; Pelton, A. D.; Petersen, S. FactSage Thermochemical Software and Databases. *Calphad* **2002**, *2*, 189–228.

(91) Westmoreland, P. R.; Harrison, D. P. Evaluation of Candidate Solids for High-Temperature Desulfurisation of Low-Btu Gases. *Environmental Science and Technology* **1976**, *10*, 659–661.

(92) Meng, X.; Jong, W. de; Pal, R.; Verkooijen, A. H. In bed and downstream hot gas desulphurization during solid fuel gasification: A review. *Fuel Processing Technology* **2010**, *91*, 964–981, DOI: 10.1016/j.fuproc.2010.02.005.

(93) Torres, W.; Pansare, S. S.; Goodwin, J. G. Hot Gas Removal of Tars, Ammonia, and Hydrogen Sulfide from Biomass Gasification Gas. *Catalysis Reviews* **2007**, *49*, 407–456, DOI: 10.1080/01614940701375134.

(94) Ben-Slimane, R.; Hepworth, M. T. Desulfurization of Hot Coal-Derived Fuel Gases with Manganese-Based Regenerable Sorbents. 2. Regeneration and Multicycle Tests. *Energy Fuels* **1994**, *8*.

(95) Ben-Slimane, R.; Hepworth, M. T. Desulfurization of Hot Coal-Derived Fuel Gases with Manganese-Based Regenerable Sorbents. 3. Fixed-Bed Testing. *Energy Fuels* **1995**, *9*, 372–378.

(96) Alonso, L.; Palacios, J. M. A TEM and XRD Study of the Structural Changes Involved in Manganese-Based Regenerable Sorbents for Hot Coal Gas Desulfurization. *Chemistry of Materials* **2002**, *14*, 225–231, DOI: 10.1021/cm011130p.

(97) Abbasian, J.; Slimane, R. B. A regenerable copper-based sorbent for H2S removal from coal gases. *Ind. Eng. Chem. Res.* **1998**, 2775–2782.

(98) Jalan, V. *Studies Involving High-Temperature Desulfurization/Regeneration Reactions of Metal Oxides for Fuel Cell Development: Final Report No. DOE/MC/16021-1486;* **1983**.

(99) Sick, G.; Schwerdtfeger, K. Hot desulfurization of coal gas with copper. *Metallurgical Transactions B* **1987**, *18*, 603–609, DOI: 10.1007/BF02654274.

(100) Patrick, V.; Gavalas, G. R.; Flytzani-Stephanopoulos, M.; Jothimurugesan, K. High-Temperature Sulfidation-Regeneration of Cuo-Al2O3 Sorbents. *Ind. Eng. Chem. Process Des. Dev.* **1989**, 931–940.

(101) Li, Z.; Flytzani-Stephanopoulos, M. Cu-Cr-O and Cu-Ce-O Regenerable Oxide Sorbents for Hot Gas Desulfurization. *Ind. Eng. Chem. Res.* **1997**, *1*, 187–196.

(102) Yasyerli, S.; Dogu, G.; Ar, I.; Dogu, T. Activities of Copper Oxide and Cu−V and Cu−Mo Mixed Oxides for H 2 S Removal in the Presence and Absence of Hydrogen and Predictions of a Deactivation Model. *Ind. Eng. Chem. Res.* **2001**, *40*, 5206–5214, DOI: 10.1021/ie0010621.

(103) Gasper-Galvin, L. D.; Atimay, A. T.; Gupta, R. P. Zeolite-Supported Metal Oxide Sorbents for Hot-Gas Desulfurization. *Ind. Eng. Chem. Res.* **1998**, 4157–4166.

(104) Kobayashi, M.; Flytzani-Stephanopoulos, M. Reduction and Sulfidation Kinetics of Cerium Oxide and Cu-Modified Cerium Oxide. *Ind. Eng. Chem. Res.* **2002**, *41*, 3115–3123, DOI: 10.1021/ie010815w.

(105) Zevenhoven, C. A. P.; Yrjas, K. P.; Hupa, M. M. Hydrogen Sulfide Capture by Limestone and Dolomite at Elevated Pressure. 2. Sorbent Particle Conversion Modeling. *Ind. Eng. Chem. Res.* **1996**, 943–949.

(106) Meng, X.; Jong, W. de; Verkooijen, A. Thermodynamic analysis and kinetics model of H 2 S sorption using different sorbents. *Environ. Prog. Sustainable Energy* **2009**, *28*, 360–371, DOI: 10.1002/ep.10386.

(107) Husmann, M.; Zuber, C.; Kienberger, T.; Hochenauer, C. Evaluation and Application of in Situ Desulfurization as Coarse Desulfurization Step in a Catalytic Gas Cleaning Process. 2DV.1.35. *Proceedings of the 23rd European Biomass Conference and Exhibition* **2015**.

(108) Kyotani, T. Kawashima H.; Tomita, A.; Palmer, A.; Furimsky E. Removal of H2S from hot gas in the presence of Cu-containing sorbents. *Fuel* **1989**, 74–79.

(109) Stanmore, B. R.; Gilot, P. Review—calcination and carbonation of limestone during thermal cycling for CO2 sequestration. *Fuel Processing Technology* **2005**, *86*, 1707–1743, DOI: 10.1016/j.fuproc.2005.01.023.

(110) Fenouil, L. A.; Towler, G. P.; Lynn, S. Removal of H2S from Coal using Limestone: Kinetic Considerations. *Ind. Eng. Chem. Res.* **1994**, *1994*, 265–272.

(111) Husmann, M.; Kienberger, T.; Zuber, C.; Jong, W. de; Hochenauer, C. Application of CaO Sorbent for the Implementation and Characterization of an in Situ Desulfurization Steam-Blown Bubbling Fluidized-Bed Test Rig for Biomass Gasification. *Ind. Eng. Chem. Res.* **2015**, *54*, 5759–5768, DOI: 10.1021/acs.iecr.5b00593.

(112) Yu, J.; Chang, L.; Xie, W.; Wang, D. Correlation of H2S and COS in the hot coal gas stream and its importance for high temperature desulfurization. *Korean J. Chem. Eng.* **2011**, *28*, 1054–1057, DOI: 10.1007/s11814-010-0482-2.

(113) WaddingtonG.; Smith, J. C.; Williamson K. D.; Scott D. W. Carbon disulfide as a reference substance for vapor-flow calorimetry. *J. Phys. Chem.* **1961**, *66*, 1074–1077.

(114) *Advance Optima AO2000 Series: Continuous gas analyzers*. Data sheet; ABB, Ed., **2013**.

(115) ABB. Advance Optima -- Leistungsstark in der Messtechnik Infrarot-Analysatormodul Uras 14. https://library.e.abb.com/public/5519eeaf687b9051c1256e8b002e298c/s_dwa_02.pdf (accessed July 21, 2016).

(116) *CP - 3800 GC: Operators Manual;* Varian Inc., Ed.; Walnut Creek, **2004**.

(117) Cool, A. T.; Goldsmith E. John. Laser-enhanced flame ionization detector. *APPLIED OPTICS* **1987**, *26*, 3542–3551.

(118) *Pulsed Flame Photometric Detector (PFPD) for CP-3800: Operators Manual;* Varian Inc., Ed.; Walnut Creek, **2004**.

(119) Amirav, A.; Jing, H. Pulsed Flame Photometer Detector for Gas Chromatography. *Analytical Chemistry* **1995**, 3305–3318.

(120) Pongratz, G. Measurement and removal of sulfurous components in synthesisgas. Bachelor thesis, Graz University of Technology, Graz, Austria, **2014**.

(121) Spectro. Spectro Arcos: ICP-OES analyzers. http://www.spectro.com/-/media/ametekspectro/documents/brochure/spectro_arcos_brochure_eng_rev1_web0.pdf (accessed July 27, 2016).

(122) Michel, W. *Wirbelschichttechnik in der Energiewirtschaft*; Dt. Verlag für Grundstoffindustrie: Leipzig, **1992**.

(123) P. Sun; J. R. Grace; C. J. Lim; E. J. Anthony. The Effect of CaO Sintering on Cyclic CO2 Capture in Energy Systems. *AIChE J* **2007**, *53*, 2432–2442.

(124) Zuber, C.; Hochenauer, C.; Kienberger, T. Test of a hydrodesulfurization catalyst in a biomass tar removal process with catalytic steam reforming. *Applied Catalysis B: Environmental* **2014**, *156-157*, 62–71, DOI: 10.1016/j.apcatb.2014.03.005.

(125) Jagtap, S. B.; Wheelock, T. D. Regeneration of Sulfided Calcium-Based Sorbents by a Cyclic Process. *Energy Fuels* **1996**, *10*, 821–827, DOI: 10.1021/ef950156y.

(126) *Land application for Dry Flue Gas Desulfurization By-Products: Phase 3;* Ohio Agricultural Research and Development Center, Ed., **1999**.

(127) Abbasian, J.; Rehmat, A.; Banerjee, D. D. Sulfation of partially sulfided calcium-based sorbents. *Ind. Eng. Chem. Res.* **1991**, *30*, 1990–1994, DOI: 10.1021/ie00056a049.

(128) Álvarez-Rodríguez, R.; Clemente-Jul, C. Oxidation of the sulphurised dolomite produced in the desulphurisation of the gasification gases. *Fuel* **2009**, *88*, 2507–2519, DOI: 10.1016/j.fuel.2008.11.035.

(129) Fenouil, L. A.; Scott, L. Study of Calcium-Based Sorbents for High-Temperature H2S Removal. 1. Kinetics of H2S Sorption by Uncalcined Limestone. *Ind. Eng. Chem. Res.* **1995**, *34*, 2324–2333.

(130) Borgwardt, R. H. Reaction of H2S and Sulfur with Limestone Particles. *Ind. Eng. Chem. Process Des. Dev.* **1984**, *1904*, 742–748.

(131) Husmann, M.; Müller, M.; Zuber, C.; Kienberger, T.; Maitz, V.; Hochenauer, C. Application of BaO-Based Sulfur Sorbent for in Situ Desulfurization of Biomass-Derived Syngas. *Energy Fuels* **2016**, *30*, 6458–6466, DOI: 10.1021/acs.energyfuels.6b00957.

(132) McKee, D. W. Catalytic effects of alkaline earth carbonates in the carbon-carbon dioxide reaction. *Fuel* **1980**, *59*, 308–315.

(133) Van der Kemp, W. J. M.; Blok, J. G.; van der Linde, P. R.; Oonk, H. A. J.; Schuijff, A.; Verdonk, M. L. Binary alkaline earth oxide mixtures: estimation of the excess thermodynamic properties and calculation of the phase diagrams. *Calphad 1994, 18,* **1994**, 255–267.

(134) Levenspiel, O. *Chemical Reaction Engineering*, Third Edition; John Wiley & Sons, Inc.: New York, **1999**.

(135) Siebenhofer, M. Chemical reaction engineering, Graz University of Technology, **2015**.

(136) Westmoreland, P. R.; Gibson, B. J.; Harrison, D. P. Comparative Kinetics of High-Temperature Reaction Between H2S and Selected Metal Oxides. *Environmental Science 8 Technology* **1977**, 488–492.

(137) Schmid, J.; Müller, S.; Kolbitsch, M.; Tesch, W.; Hofbauer, H. G-volution II - Next Generation "DualFluid" Biomass Gasifier: Final Report. https://www.ffg.at/getdownload.php?id=4828 (accessed June 2016).

(138) *Metall Vergiftungen: Diagnostik und Therapie*. Kompendium der klinischen Toxikologie; Daunderer, M., Ed., 140th ed.; Hamburg: Ecomed, **1984**.

(139) Rauch, R. *Discharge of waste material at Oberwart and Güssing*. Telefone; Graz, Austria, 2016.

(140) Jürgen Karl. *Dezentrale Energiesysteme: Neue Technologien am liberalisierten Energiemarkt*, 2nd Edition; Oldenbourg Wissenschaftsverlag: München, **2006**.

(141) Eltrop, L.; et al. *Erzeugung und Nutzung biogener Gase in Baden-Württemberg: Projekt Cluster I „Systemanalyse"*, **2013**.

(142) Husmann, M. *Darstellung der Biogaspreisgestehung: Nachtrag zur Marktuntersuchung zu bestehenden Verfahren der CO2-Abscheidung - Internal Report*, **2012**.

(143) Kienberger, T.; Schweiger, A. *Kostenkalkulation Methanierung: Internal Report*, **2011**.

(144) Daniel W. Halpin; Bolivar A. Senior. *Financial Management and Accounting Fundamentals for Construction*; John Wiley & Sons: Hoboken, NJ, USA, **2009**.

(145) Husmann, M. *Marktuntersuchung zu bestehenden Verfahren der CO2-Abscheidung: Internal Report*, **2012**.

(146) Giesecke, J.; Heimerl, S.; Mosonyi, E. *Wasserkraftanlagen: Planung, Bau und Betrieb*; Springer-Verlag: Berlin Heidelberg, **2014**.

(147) Fraubaum, M. *FFG-Projekt „InnoGasClean": Projectmeeting*; Graz, 2016.

(148) Englert, G. *Supply cost of CaO-based sorbent material*. Telefone; Graz, 2016.

(149) Imarcgroup. Barium Carbonate Market and Mass Balance: Industry Trends, Prices, Manufacturing Process, Applications, Raw Materials, Manufacturers, Regional Breakup. http://www.imarcgroup.com/barium-carbonate-market (accessed February 23, 2017).